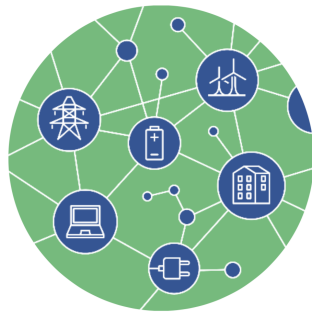




OPTIMAL SYSTEM-MIX OF FLEXIBILITY
SOLUTIONS FOR EUROPEAN ELECTRICITY

Analysis of the synchronisation capabilities of BESS power converters

D3.3



Contact: www.osmose-h2020.eu



The project has received funding from the European Union's Horizon 2020 research and innovation programme under grant agreement No 773406

Document properties

Project information

Programme	Optimal System-Mix Of Flexibility Solutions For European Electricity
Project Acronym	OSMOSE
Grant agreement	773406
Number of the Deliverable	D3.3
WP/Task related	T3.6

Document information

Document Name	Analysis of the synchronisation capabilities of BESS power converters
Date of Delivery	
Status and version	
Number of Pages	155

Responsible

Responsible	Markel Zubiaga Lazkano (markel.zubiaga@ingeteam.com)
Authors	Markel Zubiaga Lazkano, Juan Jose Valera (Ingeteam R&D, Bilbao, Spain), Carmen Cardozo, Thibault Prevost, Guillaume Denis, Yannick Vernay (RTE, La Défense, France), Yihui Zuo, Antonio Zecchino, Zhao Yuan, Rachid Cherkaoui, Mario Paolone (Distributed Electrical Systems Laboratory, EPFL, Lausanne, Switzerland),
Reviewers	Alberto Escalera (REE, Spain), Lucas Orrù (Terna, Italy)
Approver	Nathalie Grisey (RTE, France)

Dissemination level

Type (distribution level)	PU Public
	CO — full consortium, Confidential, only for members of the consortium (including the Commission Services)
	CO — some partners, Confidential, only for some partners (list of partners to be defined)

Review history

Version	Date	Reviewer	Comment
V0	December 7, 2021	EPFL	draft for internal WP 3 review
V1	December 17, 2021	Steering Committee	For review
V2	March 1, 2022		Public release

Table of content

List of Figures	5
List of Acronyms	13
1. Introduction	15
1.1. Problem formulation and reminder of the OSMOSE WP3 objectives	15
1.2. Outline and scope of this deliverable	16
2. Defining grid forming capability and synchronisation services	16
2.1. Synchronisation mechanisms	17
2.2. Reminder of the differences between a grid following and grid forming VSC	20
2.3. Inconsistencies between self-synchronisation and grid codes presently in force	28
2.4. Definition of grid forming capability	31
2.5. System services and technical capabilities in grid codes	38
2.6. Recommendations for grid code implementation	44
3. Implementing grid forming capability on off-the-shelf equipment	46
3.1. RTE-Ingteam demonstrator description	46
3.2. Technical specifications	48
3.3. Control design	52
3.4. High-level control design	59
3.5. Performance validation	62
4. Testing grid forming capability: RTE-Ingteam demonstrator	65
4.1. Test bench description	65
4.2. Experimental results on synchronisation services	67
4.3. Grid forming converter robustness	70
4.4. Experimental results on classic services	72
4.5. Discussion	74
5. Performance assessment of synchronisation service on RTS	77
5.1. EPFL IEEE-39 bus RTS test bench description and study cases	77
5.2. Characterisation of the synchronisation service	79
5.3. Evaluation of the synchronisation service effectiveness	80
5.4. Evaluation of the synchronisation service robustness	84
6. Providing a synchronisation service with ESS: EPFL demonstrator	86
6.1. Upgrading the control of EPFL BESS	86
6.2. EPFL demo: experimental results on grid connected demonstrator	89
7. Conclusion	95
8. Bibliography	96
A. Traditional ancillary services	104
A.1. Frequency regulation.	104
A.2. Voltage regulation	105

B. RTE-Ingeteam Demo: models	106
B.1. Test system and power elements model description	106
B.2. AC/DC converter control models	107
C. RTE-Ingeteam Demo: further details on control design	109
C.1. Known control modules	109
C.2. Grid forming control settings	110
C.3. High level control logic	111
D. RTE-Ingeteam Demo: simulations for control validation	117
D.1. Synchronisation	117
D.2. Reference tracking	117
D.3. Synchronisation services to grid disturbances	119
D.4. Robustness to grid distortion	122
D.5. DC side control performance	124
E. RTE-Ingeteam Demo: FAT test bench detailed description	129
E.1. Grid emulator capabilities	129
E.2. Recorded signals	130
E.3. Calculated signals	131
E.4. Initial test matrices	131
F. RTE-Ingeteam Demo: model validation from FAT records	134
F.1. Model approximations with respect to the real equipement	136
F.2. Validation method	136
F.3. Results	137
G. RTE-Ingeteam Demo incident: information and lessons learned	150
G.1. Course of events	150
G.2. Direct consequence and incident management	151
G.3. Subsequent actions	152
G.4. Technical analysis	153
G.5. Some other learnings on BESS security as critical factor	154
H. EPFL RTS model: Battery pack model parameters	155

List of Figures

0.1. Photo of the two GFM demonstrators deployed by the OSMOSE WP3 partners	10
0.2. Scope of the main original contributions of the WP3 of OSMOSE	11
0.3. Types of GFM as a function of the synchronisation services they are able to provide	11
2.1. Test system for control design: VSC connected to an infinite bus	17
2.2. Structure of the synchronous reference frame phase-locked loop (SRF-PLL)	18
2.3. Example of a VSC control with an active power synchronisation mechanism	19
2.4. VSC response to a 5° phase jump - different SCR	21
2.5. VSC response to a 5° phase jump - reactive power	21
2.6. VSC response to a 10 % grid voltage step	22
2.7. PS converter current for a three-phase fault	24
2.8. PS reactive and active current during a three-phase fault	24
2.9. 1 Hz/s RoCoF for 1 second	25
2.10. SCR reduction (line opening)	26
2.11. FRT profile	27
2.12. FRT profile applied to type PPM in France.	29
2.13. Fast fault current injection requirements in french CNC implementation	29
2.14. SCR reduction (line opening) - Grid forming stabilises grid following VSC	30
2.15. VSC response to a 60° phase jump	35
2.16. 3% of grid voltage permanent unbalance	36
2.17. Terminal voltage	37
2.18. New and traditional frequency regulation services	38
2.19. Synchronisation services act before traditional ancillary and new stability services	41
2.20. Defining synchronisation services as new non-frequency ancillary services	43
2.21. SCP margins in the France network for a 2035 scenario	45
3.1. RTE-Ingteam demonstrator diagram	46
3.2. RTE-Ingteam demonstrator connection in the Castelet substation	48
3.3. Low and Over Voltage Right-Through capability requirements	50
3.4. Active power related services - time scales	51
3.5. Power sharing functional requirements	51
3.6. State of charge control functional requirements	52
3.7. Synchronisation process results obtained in Matlab-Simulink	54
3.8. Droop control implemented at the grid forming control	56
3.9. Simplified system droop configurations	56
3.10. Simulation results for a frequency set point variation ($\Delta\omega$) of 0.013 with a $m_p = 0.01$	57
3.11. Simulation results for a frequency set point variation ($\Delta\omega$) of 0.005 with a $m_p = 0.01$	57
3.12. High level control structure	59
3.13. SoC controls limits	61
3.14. High level HESS control strategy	61

3.15. Local frequency controller (Matlab-Simulink model)	62
3.16. VSC response to a 5° phase jump - different operating points	63
3.17. VSC response to a 10° phase jump - different inertia settings	64
4.1. Main scheme of the Ingeteam test bench to validate OSMOSE demonstrato	65
4.2. Test bench impedance spectre for inductive connection impedance from 50uH to 800uH.	66
4.3. Experimental environment	66
4.4. Grid connection ($V_g=1.05$ p.u. $E_{set} = 1$ p.u.)	68
4.5. Islanding after breaker opening	68
4.6. 5° phase jump	68
4.7. 5° phase jump ($H = 5$ s) - degraded modes	69
4.8. Inertial response: Grid frequency deviation	69
4.9. System strength: Grid voltage deviation	70
4.10. Symmetric fault ride through capability ($H = 2$ s)	71
4.11. 50% Type C fault for 400 ms	71
4.12. OVRT test	71
4.13. 10% of 5th harmonic distortion on the grid voltage	72
4.14. -70 kW active power ramp ($H = 2$ s, with different n_q)	72
4.15. 70 kW active power step ($H = 2$ s)	72
4.16. 5% Step on voltage set point ($H = 2$ s)	73
4.17. 5% Step on voltage set point ($H = 2$ s) - Impact on DC side	73
4.18. 80 kvar with different ramps for $n_q = 0.01$ ($H = 2$ s)	74
4.19. Step the frequency set point ($H = 2$ s) - Impact on DC side	74
5.1. Simulation framework.	78
5.2. Diagram of 39-bus low-inertia power systems (The presence of the BESS at bus 17 is taken into account in grid).	79
5.3. Power converter Controls.	81
5.4. System frequency and BESS active power.	82
5.5. Computed rRoCoF time series.	83
5.6. Cumulative density function (CDF) of rRoCoF.	83
5.7. Frequency, power injections and grid voltage at bus 17 in Config. II-BESS for <i>Case 1</i>	85
5.8. Frequency, power injections and grid voltage at bus 17 in Config. II-BESS for <i>Case 2</i>	85
6.1. BESS converter PQ capability curves as function of v_t^{AC} and v_t^{DC}	86
6.2. 1 month historical data of frequency and phase-to-phase voltage at the BESS PCC at 21 kV, acquired via PMUs installed at the EPFL MV network. The dashed lines represent the limits of $\mu_{fpm} 3.3\sigma_f$ and $\mu_V \pm 1\sigma_V$ for frequency and voltage measurements, respectively.	88
6.3. Converter P-f and Q-V droops	90
6.4. Experimental setup of the EPFL campus MV grid hosting the utility-scale 720kVA/500 kWh BESS.	91
6.5. Ad-hoc installation of the adopted PMU inside the BESS container.	91

6.6. Experimental test results using the EPFL BESS converter in grid-following mode with 1.44 MW/Hz droop.	92
6.7. Experimental test results using the EPFL BESS converter in grid-forming mode with 1.44 MW/Hz droop.	93
6.8. Cumulative distribution function of the rRoCoF [Hz/s/kW] for the two experimental tests.	94
6.9. Cumulative distribution function of the rPADD [deg/kW] for the two experimental tests.	94
A.1. Evolution of BESS certified in France to provided FCR since 2020	105
B.1. Matlab-simulink test system model	106
B.2. Matlab-simulink converter model with simplified DC side	106
B.3. Matlab-simulink complete DC side model	107
B.4. Matlab-simulink grid forming control model	108
B.5. Matlab-simulink transient grid forming control model	108
C.1. Inner controls transfer function	110
C.2. SoC regulation enable signal logic implemented in Matlab-Simulink	112
C.3. SoC set point logic implemented in Matlab-Simulink	113
C.4. SoC regulation	113
C.5. Battery and UC SoC control implemented in Matlab-Simulink	114
C.6. SoC output selection logic	115
C.7. User configuration display blocks implemented in Matlab-Simulink	116
C.8. Parameter initialisation cases to configure system. Grid services related case (left) and ESS configuration related case (right)	116
D.1. Voltage and current during the synchronisation at converter terminals	117
D.2. Active and reactive power evolution for a voltage set point variation	117
D.3. Three phase voltage and current for a voltage set point variation	118
D.4. Grid forming equipment measured frequency and internal frequency	118
D.5. Active and reactive power evolution for a frequency set point variation	118
D.6. Active and reactive power for a 30 degrees grid phase jump	119
D.7. Three phase voltage and current for a 30 degrees grid phase jump at converter terminals	119
D.8. Active and reactive power for a grid voltage variation	120
D.9. Three phase voltage and current for a grid voltage variation	120
D.10.Active and reactive power evolution for a grid frequency variation	120
D.11.Three phase voltage and current for a grid frequency variation	121
D.12.Active and reactive power evolution for a 90% 3-phase fault at the virtual grid	121
D.13.Three phase voltage and current for a 90% 3-phase fault at grid and converter terminals	121
D.14.Active and reactive power for a 70% type C fault	122
D.15.Three phase voltage and current for a 70% type C fault at grid and converter terminals	122
D.16.Three phase voltage and current for a 10% voltage unbalance, VG and GF terminals .	122
D.17.Active and reactive power when connected to a grid with a 5% of 5th harmonic component	123

D.18. Voltage and current at grid forming equipment and the virtual grid when connected to a grid with a 5% of 5h harmonic component	123
D.19. Active and reactive power when connected to a grid with a 5% of 7th harmonic component	123
D.20. Voltage and current at grid forming equipment and the virtual grid when connected to a grid with a 5% of 7h harmonic component	123
D.21. Injected active power for transient grid forming by device with HESS configuration. UCs (blue), AC side converter (red) and battery (green)	124
D.22. Battery SoC evolution for transient grid forming in HESS configuration	124
D.23. UC SoC evolution for transient grid forming in HESS configuration	125
D.24. Injected active power by device with HESS configuration for external set point. UCs (blue), AC side converter (red) and battery (green)	125
D.25. SoC evolution for external set point in HESS configuration	126
D.26. Injected active power by device with HESS configuration for external set point. UCs (blue), AC side converter (red) and battery (green)	126
D.27. SoC evolution for for active power external set point - Only batteries	127
D.28. Injected active and reactive power by AC side converter for active power external set point - Only Battery. Operation SoC limit reached	127
D.29. Battery SoC evolution for active power external set point - Only Battery. Operation SoC limit reached.	127
D.30. Injected active and reactive power by AC side converter for active power external set point - Only Battery. Hysteresis SoC control limit reached	128
D.31. Hysteresis SoC control limit reached for active power external set point - Only batteries	128
D.32. Active power external set point only UCs ESS configuration	128
E.1. Overview of the web client to command the grid emulator	130
F.1. Estimated quantities from measured three phase currents (IRST) and two-phase line-line voltage (VRST) for Type A fault (50%, 700ms).	137
F.2. Maximum and measured positive sequence error values at a Type A fault (50%, 700ms) for each period according to TR4 FGW standard, limits for Type 1 PGU	138
F.3. Maximum and measured positive sequence error values at a Type A fault (50%, 700ms) for each period according to TR4 FGW standard, limits for Type 2 PGU	138
F.4. Estimated reactive Power for Type A fault (50%, 700ms) simulation and measurements. Focus on the beginning of the fault	138
F.5. Registered values at the CCU (converter control unit) and simulated internal control values for a Type A fault (50%, 700ms).	139
F.6. Estimated quantities from measured three phase currents (IRST) and two-phase line-line voltage (VRST) for Type A fault (70%, 500ms).	139
F.7. Maximum and measured positive sequence error values at a Type A fault (70%, 500ms) for each period according to TR4 FGW standard, limits for Type 1 PGU	140
F.8. Maximum and measured positive sequence error values at a Type A fault (70%, 500ms) for each period according to TR4 FGW standard, limits for Type 2 PGU	140
F.9. Registered values at the CCU (converter control unit) and simulated internal control values for a Type A fault (70%, 500ms).	140

F.10. Estimated PS quantities from measured three phase currents (IRST) and two-phase line-line voltage (VRST) for Type C fault (50%, 400ms).	141
F.11. Maximum and measured positive sequence error values at a Type C fault (50%, 400ms) for each period according to TR4 FGW standard, limits for Type 1 PGU	141
F.12. Maximum and measured positive sequence error values at a Type C fault (50%, 400ms) for each period according to TR4 FGW standard, limits for Type 2 PGU	141
F.13. Estimated NS quantities from measured three phase currents (IRST) and two-phase line-line voltage (VRST) for Type C fault (50%, 400ms).	142
F.14. Maximum and measured negative sequence error values at a Type C fault (50%, 400ms) for each period according to TR4 FGW standard, limits for Type 1 PGU	142
F.15. Maximum and measured negative sequence error values at a Type A fault (50%, 400ms) for each period according to TR4 FGW standard, limits for Type 2 PGU	142
F.16. Focus on the estimated active and reactive current for Type C fault (50%, 400ms) simulation and measurements.	143
F.17. Registered values at the CCU (converter control unit) and simulated internal control values for a Type C fault (50%, 400ms).	143
F.18. Estimated PS quantities from measured three phase currents (IRST) and two-phase line-line voltage (VRST) for Type A fault (100%, 300ms).	144
F.19. Estimated NS quantities from measured three phase currents (IRST) and two-phase line-line voltage (VRST) for Type A fault (100%, 300ms).	144
F.20. Registered values at the CCU (converter control unit) and simulated internal control values for a Type C fault (100%, 300ms).	144
F.21. Estimated quantities from measured three phase currents (IRST) and two-phase line-line voltage (VRST) for Type A fault (50%, 700ms).	145
F.22. Maximum and measured positive sequence error values at a phase jump (5°) for each period according to TR4 FGW standard, limits for Type 1 PGU	145
F.23. Maximum and measured positive sequence error values at a phase jump (5°) for each period according to TR4 FGW standard, limits for Type 2 PGU	145
F.24. Registered values at the CCU (converter control unit) and simulated internal control values for for a grid voltage phase-jump (5°).	146
F.25. Registered values at the CCU (converter control unit) and simulated internal control values for a grid voltage step (5%).	147
F.26. Registered values at the CCU (converter control unit) and simulated internal control values for a grid voltage step (10%).	147
F.27. Registered values at the CCU (converter control unit) and simulated internal control values for active power set point ramp variation.	148
F.28. DC side Registered values at the CCU (converter control unit) and simulated internal control values for active power set point.	148
F.29. Active power injected by each ESS for an active power step - Different weight factors.	149
G.1. Aerial view RTE Castelet substation	150
G.2. RTE–Ingeteam demonstrator photos in the substation	151
G.3. Firefighter operation (left), crane manoeuvre (centre), burned container next day (right)	152
G.4. Initial state of the system and last action before alarms triggering	154

Executive Summary

The WP3 of the OSMOSE project gathered RTE (*Réseau de Transport d'Electricité*), EPFL (*École Polytechnique Fédérale de Lausanne*) and Ingeteam R&D to demonstrate:

- the technical feasibility to provide grid forming (GFM) capability of commercially available power-electronics interfaced energy storage systems (ESS);
- that this solution can be industrially deployed without converter oversizing, and
- that its contribution to power system stability can be quantified by means of external measurements without a detailed knowledge of specific low-level controls.

For this purpose, 2 demonstrators were deployed (see Fig. 0.1):

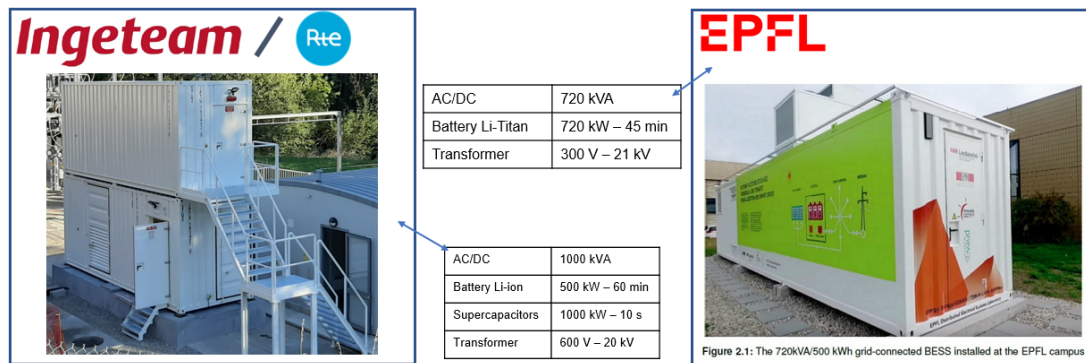


Figure 0.1: Photo of the two GFM demonstrators deployed by the OSMOSE WP3 partners

- On the left: Ingeteam implemented a GFM control proposed in the WP3 of the MIGRATE H2020 project on the voltage source converter (VSC) interfacing a hybrid ESS (HESS) to the grid. The 1 MVA fully containerised solution was specifically built for the OSMOSE project using off-the-shelf equipment and connected to a 20 kV feeder in a RTE substation. It included four lithium-ion battery racks (0.5 MVA 60 min) and six ultra-capacitor (UC) racks (for a total of 1MW-10s).
- On the right: the EPFL demonstrator quantified that the provision of synchronisation services (inertial response) superposed to traditional ancillary services (e.g. voltage and frequency regulation) and dispatch tracking can effectively reduce local frequency variations. This was achieved with a pre-existing battery ESS (BESS) composed by a 720kVA/560kWh Lithium Titanate Oxide BESS, connected to a 20 kV feeder of the EPFL Campus.

The work carried out in the WP3 of the OSMOSE H2020 project included four stages:

1. First, a technical specification phase of the demonstrators including the required monitoring infrastructure. This stage has been discussed in the deliverable D3.2.
2. Second, a modelling and simulation phase for control design and performance assessment purposes was carried out for both demonstrators. It included DC/DC and AC/DC VSC on the RTE-Ingeteam side, while the EPFL focused on adapting the multi-service optimisation framework proposed in deliverable D3.1 to the GFM mode of their BESS.
3. Third, after the proposed controls were implemented, the demonstrators entered the testing, installation and operational phases. RTE and Ingeteam performed factory acceptance tests (FAT) using a power hardware in the loop (PHIL) platform available at Ingeteam power laboratory facilities. An incident during commissioning prevented RTE-Ingeteam demonstrator to be ultimately put into service. On EPFL side, the BESS demonstrator was successfully operated in both grid connected and GFM mode and was used to validate the multi-service provision originally scheduled to be carried out on the RTE-Ingeteam demonstrator.

- Finally, results were assessed through key performance indicators (KPI) and scaled-up using a real-time simulation benchmark released open source by EPFL and referring to a modified low-inertia IEEE 39-bus network.

The contribution from WP3 are listed below and their scope is illustrated in Fig. 0.2.

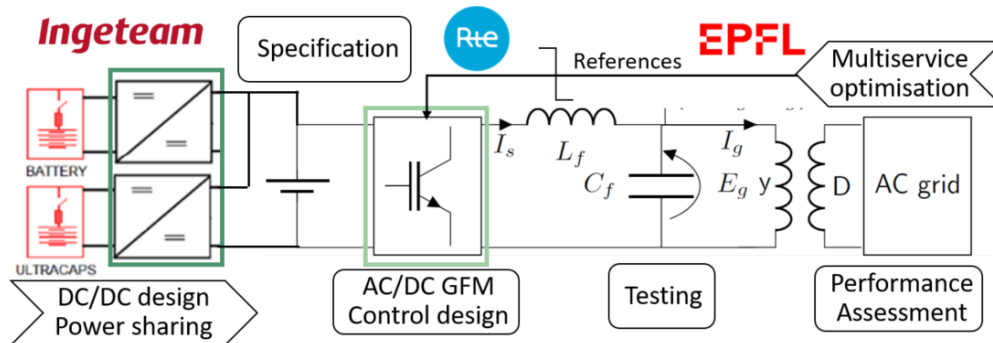


Figure 0.2: Scope of the main original contributions of the WP3 of OSMOSE

- Specification.** Functional specifications from the state of the art have been translated into technical requirements such that grid forming has been successfully defined as set of technical capabilities which is suitable for grid code implementation: *a grid forming unit shall, within its rated power and current, be capable of self-synchronise, stand-alone and provide synchronisation services* which includes synchronising power, system strength, fault current and inertial response. Therefore, a GFM unit, by definition, does not rely on grid conditions to synchronise (it can operate at a wide range of short-circuit ratios and inertia levels) and will help others to maintain synchronism under stressful conditions, while still complying with the general requirements applying to the specific technology. It must be noted that no overload or capacity reservation is associated to the GFM capability, neither the provision of traditional ancillary services such as primary voltage and frequency regulation. Moreover, depending on the subset of synchronisation services that a given unit can provide, we propose to classify them in 4 types as illustrated in Fig. 0.3, such that a synchronous machine is, by construction, a type 4 GFM unit. In this work we consider GFM VSC interfaced ESS that fall in the type 3 category.

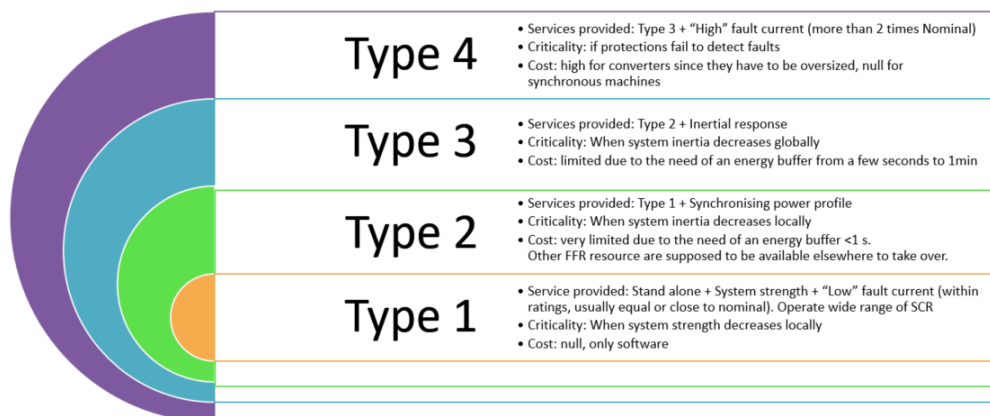


Figure 0.3: Types of GFM as a function of the synchronisation services they are able to provide

- Experimental validation that type 3 GFM capability can be provided with off-the-shelf MVA scale VSC interfacing ESS:** a) without oversizing, b) while still providing traditional ancillary services on top of synchronisation ones and c) remaining robust to grid disturbances. Results are shared for both factory testing (RTE-Ingeteam) and grid connected operation (EPFL).

3. **Testing GFM capability compliance form external measurements.** Transient fault recorder (TFR) data obtained during the RTE-Ingteam FAT confirmed that the instantaneous active and reactive power injection during phase jump, frequency ramps and voltage steps events can unequivocally discriminate GFM from grid following units in high power industrial application. This has been stated in the literature from simulation results and small laboratory scale mock-ups and requested in emerging grid codes such as GC0137 by National Grid and standards such as the German FNN, but to the best of our knowledge this is the first time MVA scale VSC experimental results for a wide range of tests are published. Stand-alone, live connection and energisation tests were considered. Challenges regarding large phase jump withstand capability, fault-ride-through (FRT) profiles, grid unbalances and harmonic distortion in control design have also been highlighted, together with open questions regarding unintended islanding.
4. **Performance assessment of synchronisation services form external measurements.** EPFL proposed KPI using accurate PMUs (i.e., with a Total Vector Error of 0.0X%) to capture the local effects of BESS providing synchronisation and frequency regulation services. They are based on the cumulative density function of the Relative Rate-of-Change of Frequency (rRoCoF) and the Relative Phase Angle Difference Deviation (rPADD): rRoCoF is computed during hourly transient at night when the presumption of the dispatchable feeder has minor variations, while rPADD quantifies the change in the phase-to-neutral voltage angle difference on different nodes with respect to the case with null delivered active power. They allow to differentiate GFM from grid following units.
5. **AC/DC control design.** The selected grid forming control robustness has been improved to behave properly in different grid conditions including permanent unbalance and asymmetrical faults. As an example, the TVI current limitation strategy was enhanced to include a negative sequence component to deal with unbalanced faults which has been published in open access. In addition, frequency regulation and synchronisation services have been successfully decoupled at the AC/DC converter level (transient grid forming).
6. **DC/DC control design.** This hybrid architecture in the RTE-Ingteam demonstrator enabled to test different strategies of DC power sharing, especially to put the burden of fast transients on the UC and therefore smoothing the battery power output. The battery is meant to provide energy intensive ancillary and flexibility services. Hence, the decoupling of the balancing (frequency regulation) and synchronisation services can be also achieved at device level.
7. **Multi-service optimisation.** EPFL proposed a framework for day-a-head to real-time control of multiservice BESS, from synchronisation services to more traditional ancillary services such as frequency containment reserve (FCR) taking into account the unit's operational constraints.
8. **Scale-up of results.** Assessment of the frequency performance of low-inertia IEEE 39-bus benchmark network demonstrates that a GFM BESS outperforms a grid-following one in improving the frequency containment thanks to the provision of immediate inertial response

These results can benefit TSOs and Entso-e in the specification of the grid forming capability. As a consequence, on RTE side, future work focuses on the implementation of connection requirements and fine tune compliance criteria and procedure as well as on the design of the suitable mechanisms for the provision of synchronisation services and their monitoring. Finally, system needs for different scenarios in the years to come must be assessed in order to define global and local prescription of synchronisation services. However, minimal GFM capacity must be installed in the system with enough anticipation through connection requirements in order to avoid scarcity risk in operation that might jeopardise power system security. Original equipment manufacturers (OEM) and academy can build upon public results to enhance robustness of grid forming control and real-time multi-service optimisation of energy systems. Experimental demonstration of GFM capability of other technologies than BESS such as VRES, HVDC and FACTS shall continue until industrial deployment is achieved.

List of Acronyms

aFRR	automatic Frequency Restoration Reserve
AS	Ancillary Service
BESS	Battery Energy Storage System
CART	<i>Contrat d'accès au réseau de transport</i>
CDF	Cumulative Distribution Function
CNC	Connection Network Code
DC	Dynamic Containment
DM	Dynamic Moderation
DSOGI	Dual Second Order Generalised Integrator
DTR	<i>Documentation Technique de Référence</i>
DUT	Device Under Test
EMTP	Electromagnetic Transients Program
EFR	Enhanced Frequency Response
ESS	Energy Storage System
EU	European Union
FACTS	Flexible Alternating Current Transmission Systems
FAT	Factory Acceptance Test
FCR	Frequency Containment Reserve
FFR	Fast Frequency Response
FLL	Frequency Locked Loop
FRR	Frequency Restoration Reserve
FRT	Fault Ride Through
FSM	Frequency Sensitive Mode
HESS	Hybrid Energy Storage System
HMI	Human Machine Interface
HVDC	High Voltage Direct Current
IBR	Inverter Based Resources
IFD	Integral Frequency Deviation
IGBT	Isolated-Gate Bipolar Transistor
KPI	Key Performance Indicator
LFDD	Low Frequency Demand Disconnection
LVRT	Low Voltage Ride Through
LFSM	Limited Frequency Sensitive Mode
LQR	Linear–quadratic regulator
NS	Negative Sequence
OVRT	Over Voltage Ride Through
PCC	Point of Common Coupling
PCS	Power Conversion System
PFR	Primary Frequency Regulation

PI	Proportional Integral
PLC	Programmable Logic Controller
PLL	Phase-Locked Loop
PMU	Phasor Measurement Unit
POI	Point of Interconnection
PPM	Power Park Modules
PS	Positive Sequence
PV	Photo Voltaic
RGCE	Regional Group Continental Europe
RMS	Root Mean Square
RoCoF	Rate of Change of Frequency
rPADD	relative Phase Angle Difference Deviation
rRoCoF	relative Rate-of-Change-of-Frequency
RTS	Real-Time Simulation
SG	Synchronous Generator
SM	Synchronous Machine
SCP	Short-Circuit Power
SCR	Short-Circuit Ratio
SoC	State of Charge
SRF	Synchronous Reference Frame
SVR	Secondary Voltage Regulation
TFR	Transient Fault Recorder
THD	Total Harmonic Distortion
TVI	Threshold Virtual Impedance
UC	Ultra Capacitor
VSC	Voltage Source Converter
VSM	Virtual Synchronous Machine
WPP	Wind Power Plant

1. Introduction

With respect to conventional generation, the term synchronisation generally refers to the process of coupling a synchronous machine (SM) to an (alternating) grid, which is usually performed by automatic systems to limit transients. Once connected to the grid, in normal operation, synchronous generators (SGs) naturally remain synchronised thanks to the well-known synchronising torque inherently provided by such units [1]. Then, close attention is given to the loss of synchronism phenomenon following large disturbances, which is formulated as a stability problem: the short-term rotor angle or transient stability in the power system literature [2]. If the SG cannot transfer the power provided by the primary source into the grid, the rotor accelerates. After a certain time, its angle reaches a critical value beyond which it cannot return to its previous equilibrium point after fault clearance. Although another stable equilibrium might be close (a multiple of 2π electrical radians to be precise, after one or a few pole slips), in general, the generator might be tripped by protection systems in order to prevent equipment damage but also phenomenon propagation due to the large power oscillations generated in the process. Faults must then be cleared fast enough, and operational rules, such as limiting the unit active and/or reactive power output in some conditions, can be implemented to limit this risk when facing plausible contingencies.

Synchronisation of grid-connected power converters is achieved, maintained and, regained after disturbances by control actions in order to ensure independent active and reactive power reference tracking. The most widespread way of synchronising and keeping converters synchronised to the main grid consists in *locking* the reference rotating frame of the converter control, usually the d -axis, at the grid voltage (or more often the converter terminal voltage) by tracking its phase. For this reason, the converters relying on this principle are referred to as grid following. The phase-locked loop (PLL) is the module in charge of this task [3] and specific strategies might be implemented to optimise its behaviour during and after large disturbances to comply with grid connection requirements in terms of performance, fault ride through (FRT), and power recovery. The loss of synchronism of power electronic interfaced resources (usually referred to as inverter-based resources, IBRs) has been thoroughly studied, but as a control interaction problem by the power electronic community [4,5] since their capability to remain synchronised in practice depends on the PLL design but is also affected by the inner (current) loops and even outer loops such as the reactive power control in weak grids [6] (see section 2.2.4). Therefore, converter grid-synchronisation stability analysis differs from the rotor angle stability of SGs and has been recently categorised by the power system community as part of the slow interaction converter-driven stability problem [7]. Indeed, for IBRs, the image of a rotor angle drifting is less suited, but the result is similar as the incapability of the control system to track the grid voltage phase generates inaccurate dq -axis current references that would ultimately lead to unacceptable power oscillations and the installation disconnection by protection systems.

1.1. Problem formulation and reminder of the OSMOSE WP3 objectives

In this work we propose to define synchronisation services as the set of responses required to ensure that grid-connected devices remain synchronised to the power system even after being submitted to large disturbances. Within this framework, **a grid forming unit, by definition, shall be capable of self-synchronise and providing synchronisation services**: it does not rely on grid conditions to synchronise and will help others to maintain synchronism, while still complying with other general requirements applying to the technology. Accordingly, a SG is by construction a grid forming unit.

OSMOSE WP3 includes two grid forming demonstrators: one is based on an existing MW-class battery energy storage systems (BESS) connected to the medium voltage network of the EPFL campus, and the other is a hybrid ESS (HESS) built by Ingeteam and connected to the RTE grid to show that:

- grid forming capability can be provided with off-the-shelf converters interfacing ESS to the grid,
- implemented grid forming controls can be robust against grid distortion and disturbances,
- supercapacitors can be used to smooth BESS power output in a hybrid ESS configuration, and
- synchronisation services can be added on top of other regulation services in a multi-service optimisation framework and their performance can be assessed from measurements.

This deliverable brings proof of the technical feasibility of implementing grid forming controls to provide synchronisation services with ESS without converter over-sizing, and shares insights on modelling, testing and monitoring of grid forming units for compliance and performance assessment.

1.2. Outline and scope of this deliverable

Chapter 2 first discusses some of the main concepts and functionalities associated to grid forming controls. Then, Chapter 3 presents the specification and design of the RTE-Ingteam demonstrator to achieve grid forming capability, while Chapter 4 shares the experience gained during the factory acceptance tests (FAT). Afterwards, Chapter 5 recalls key performance indicators (KPI) proposed in [8] and validates them in a real-time simulation (RTS) setup before showing grid-connected experimental results obtained at EPFL site in Chapter 6. Finally, conclusions are drawn in Chapter 7. Before moving forward, five underlying hypotheses within this work must be kept in mind:

Hypothesis 1. *We focus on voltage source converter (VSC) technology (transistor-based).*

Hypothesis 2. *We consider ESS applications, so the availability of the DC side energy can be easily ensured by the slower state of charge (SoC) controller. We acknowledge that this is an open question for other applications such as power park modules (PPM) including photo voltaic (PV) and wind plants (WPP), flexible alternating current transmission systems (FACTS) and high voltage direct current (HVDC) interconnectors, which is currently being addressed by academia and industry.*

Hypothesis 3. *We do not consider any over-sizing or hardware upgrade, but only software (control) modifications. Therefore, the current and set point limitations will be discussed in detail. Specific measurement equipment might, however, be required for performance assessment purposes.*

Hypothesis 4. *The impact of the provision of synchronisation services on the primary source components is not investigated. Therefore, when we say that grid forming capability can be achieved with off-the-shelf equipment without over-cost we mean capital cost. It is acknowledged that concerns exist about the eventual live span reduction of certain infrastructure due to anticipated gear tear potentially caused by the fast transient power requested by the grid forming functionality. However, to the best of our knowledge, no technical proof has been yet published on this matter.*

Hypothesis 5. *When defining services no hypothesis is made on their provision which in principle can be market-based or mandatory. An in-depth discussion on suitable mechanisms for synchronisation services procurement is out of the scope of this work, but the technical background is provided.*

Finally, the term black start refers to both, a technical capability on one side, but it is also a service. It implies much more than grid forming capability as it requires the unit to self-energise (automatic startup of the auxiliary loads), to start a blacked-out grid and maintain its operation for a specific time. It, therefore, requires storage or an available primary source and several additional control layers, in addition to a self-synchronisation mechanism. Constant voltage and frequency (V/f) controls have been typically used to provide this capability with HVDC systems [9]. The possibility to provide black start services with a WPP using grid forming controls, such as the virtual synchronous machine (VSM), has been recently proved [10], but this topic is also out of the scope of this work.

2. Defining grid forming capability and synchronisation services

This chapter is organised as follows:

- Section 2.1 briefly recalls inverter-based resources (IBR) synchronisation mechanisms. We distinguish classical grid-synchronisation (phase-locked loop or PLL-based) from self-synchronisation ones, that include the majority of the grid forming controls currently proposed in the literature.
- Section 2.2 illustrates the main differences between these two synchronisation mechanisms in terms of performance and stability. We focus on the understanding of the voltage source behaviour that is often associated to grid forming sources.
- Section 2.3 discusses the challenges and opportunities of self-synchronisation mechanism with respect to grid connection requirements in force in the European Union (EU) based on the current versions of the connection network codes (CNC) [11, 12].
- Section 2.4 presents a state-of-the-art of the definition of the grid forming capability based on available grid codes, standards and guidelines as an introduction to the technical requirements considered in this work. We insist in the difference between technical capabilities requested for grid connection that might or not imply response deployment, and a service provision.
- Section 2.5 provides a definition of synchronisation services, which is built upon existing ancillary services: traditional frequency and voltage regulation, but also emerging ones such as the fast frequency response (FFR). It will be shown that these ancillary services are often accompanied, at least in EU, by some CNC requirements. The opposite is not necessarily true: several connection requirements, such as withstand capabilities, are not associated to services.
- Finally, section 2.6 concludes with some recommendation on grid forming capability implementation on grid codes.

For the purpose of illustration, this Chapter includes time-domain simulation results obtained with a Matlab-Simulink grid forming model developed in the control design phase of the RTE-Ingteam demo (see Chapter 3) mainly in no load condition (zero initial power). The test system corresponds to the test bench used during the factory acceptance tests (FAT, see Chapter 4) shown in Fig. 2.1, where the electrical parameters of the output filter of the device under test (DUT) are Z_{filter} and C_{filter} . In the model we consider a step-up transformer (Z_{TR}), a line (Z_{Line}) and the grid short circuit impedance (Z_{SC}), but in practice, during the tests, the connection impedance was given by the output filter of the virtual grid (see Appendix E). The model description is provided in Appendix B.

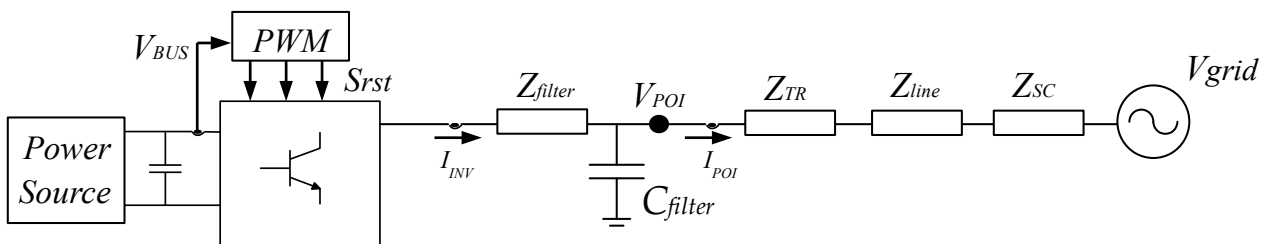


Figure 2.1: Test system for control design: VSC connected to an infinite bus

2.1. Synchronisation mechanisms

Section 2.1.1 first recalls the principle of classic PLL grid-synchronisation of VSCs and then section 2.1.2 quickly describes some self-synchronisation mechanisms.

2.1.1. Grid-synchronisation

As aforementioned, grid following converters synchronise to the grid through the PLL that tracks the grid frequency and imposes it to the converter [13]. However, depending on the specific application, different implementations exist. In three phase AC power systems, synchronous reference frame phase-locked loop (SRF-PLL) has been extensively used and will be considered in this chapter for comparison purposes. As depicted in Fig. 2.2 taken from [14], the basic idea is to use a proportional-integral (PI) controller that tracks the q-axis voltage component to zero in order to estimate the system frequency and ultimately provide the angle of the converter dq reference frame.

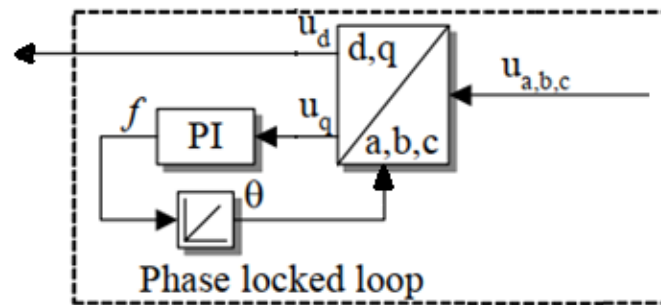


Figure 2.2: Structure of the synchronous reference frame phase-locked loop (SRF-PLL)

However, it is acknowledged that more complex structures have emerged in the last decade to overcome some limitations, mainly related to power quality issues [15] and dynamic performances in case of large grid transients [16]. We can quote for instance the Frequency Locked Loop (FLL) that can provide better performance in abnormal grid condition as they are less sensitive to phase angle jumps [17], the Dual Second Order Generalized Integrator (DSOGI) [18] or their combination (DSOGI-FLL) [19]. A literature review on grid-synchronisation methods is out of the scope of this work. The interested reader is referred to [3, 20] for more information. In spite of all those improvements, these mechanisms still need a reference signal coming from the grid to synchronise and remain prone to instability in weak grids [21].

2.1.2. Self-synchronisation

Grid leading or V/f controlled converters, more suited for standalone operation, have been known for a long time mainly within the framework of specific applications such as:

- Uninterruptible power supply (UPS).
- Islanded mode in microgrids, offshore platforms and HVDC for system restoration.

Initially, they considered fixed frequency and voltage references and are neither meant to share the load with other sources nor to synchronise with them, at least not without telecommunication [22]. In the more general case, grid forming controls include a synchronisation loop that enables the parallel operation of converters without directly relying on a fast and accurate grid voltage measurement. Therefore, they are capable of operating and sharing power when embedded in a meshed system whose generation, load and grid topology is unknown and changing.

Inspired by the synchronisation mechanism of synchronous machines (SM), the active power signal has been naturally privileged for self-synchronisation purposes based on its coupling with the voltage phases [23]. In the general case, more sophisticated formulations take into account the dynamic cross-coupling with the AC voltage amplitude [24, 25]. Finally, a reactive power synchronisation method has been recently proposed to overcome the need of firm DC side energy [26].

(Active) Power synchronisation. An internal synchronisation mechanism was proposed in [23] to avoid PLL instability (see section 2.2.4) in VSC-HVDC systems connected to weak grid and provide voltage support. The proposed synchronisation law boils down to a power-frequency (P-f) droop such that the converter frequency is set to $\omega_c = \omega^* + K_p(P^* - P_m)$, where P^* and ω^* are respectively the active power and frequency references, P_m is the measured injected active power at the converter point of interconnection (POI) and K_p is the controller gain. Then, the converter frequency ω_c is integrated once to get the phase of the converter voltage θ_c used in the rotating frame transformation as illustrated Fig. 2.3. Synchronverters [27] and virtual synchronous machine (VSM) [28] controls privileged a double integration to mimic the behaviour of conventional synchronous generators (SGs): instead on using the P-f droop to directly compute ω_c , its value is obtained by integrating the active power (or torque) error:

$$K_s \dot{\omega}_c = P^* - P_m + K_\omega(\omega^* - \omega_c) - K_d(\omega_c - \omega_g), \quad (2.1)$$

where K_s determines the inertial response as its equivalence to two times the inertia constant of a SM ($2H$) can be shown by matching this control law to the swing equation ($2H\dot{\omega} = P_{mech} - P_{elec} - D(\omega - \omega_g)$). The static frequency droop is given by K_ω (equivalent to $-1/K_p$ in steady state in the initial droop equation) and a damping term (K_d) can be added if the grid frequency, ω_g , is known.

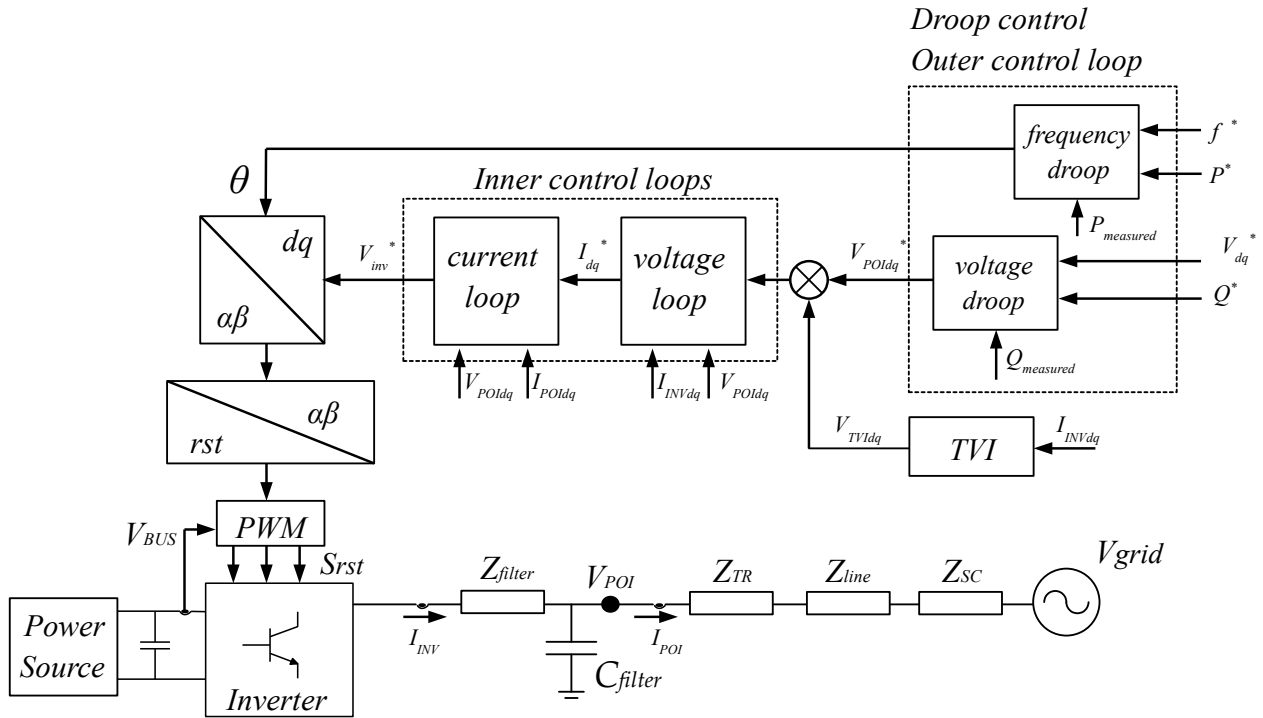


Figure 2.3: Example of a VSC control with an active power synchronisation mechanism

Active power synchronisation mechanisms endow VSC converters with certain properties that will be further discussed in the next section and that make them fall in the category of grid forming sources. The list of grid forming controls based on different variants of equation (2.1) is incessantly growing. A updated literature review on the topic is out of the scope of this work and the reader is referred to [20, 29, 30] for details.

In general, main grid forming controls proposed in literature rely on an active power synchronisation principle [31] and the synchronisation function cannot be dissociated from the active power control.

However outer loops can still be designed to update the active power and/or frequency references in order to achieve specific control objectives in different time frames. For instance, if ω^* is set to the system nominal frequency and the droop gain is not zero ($K_\omega > 0$), on top of grid forming capability, the device would be also providing a well-known ancillary service: primary frequency regulation (PFR, see Appendix A). The term "transient grid forming" was previously proposed in [8,22] to explicitly refer to the provision of grid forming capability without participating to PFR services. Again, depending on the desired strategy, this behaviour can be achieved through different control implementations, acting on the droop value, the frequency or the power reference [32,33].

Other solutions proposed in the literature to provide grid forming capability include the Angle droop control [34]. This type of control has the advantage of being fast and bringing the frequency back to nominal value after an event. Nevertheless, it relies on communication and lacks of backwards compatibility with traditional balancing mechanism based on global static frequency deviation.

Reactive power synchronisation. A different strategy to synchronise converters without PLL nor acting on the active power is proposed in [26]. It must be noted that it is not said that this solution is a grid forming control. As for all emerging synchronisation mechanisms, its overall performance requires further investigation before claiming that they can endow a VSC with grid forming capability.

2.2. Reminder of the differences between a grid following and grid forming VSC

The absence of a PLL for synchronisation purposes, or in a more general way, the non reliance on the fast and accurate grid voltage measurement, is a necessary but not a sufficient condition to claim grid forming capability. Moreover, its fundamental definition as a stiff voltage source is a necessary starting point for control design but again not sufficient specification in an industrial environment. Indeed, the specification, or even the knowledge, of the exact synchronisation loop implementation as a discrimination criterion between grid forming and grid following sources may result impractical [22]. The provision of grid forming capability must be verified by the compliance with well-defined technical requirements that can be specified in terms of active and reactive power injection as the scientific community seems to have reached a consensus that the unit response time is expected to unequivocally indicate if this capability is being provided¹.

2.2.1. Synchronising power

Synchronising power is defined here as the response of a grid-connected unit to a phase jump. In this section we compare the active and reactive power dynamic behaviour of a grid following and a grid forming VSC for a small angle disturbance (5 degrees). For the latter, we consider the specific control implemented in the RTE-Ingteam demonstrator, which is based on the filtered droop synchronisation method proposed in the MIGRATE H2020 project [31] and recalled in Chapter 3.

It must be noted that, as its name indicates, a VSC is in principle a voltage source, so at the very first instants (below a few milliseconds) that follow the grid disturbance, its modulated voltage magnitude and phase remain constant, and the power exchanged with the grid varies immediately. Then, the control strategy impacts the dynamics of the recovery of the reference power at different time frames.

¹"The reaction of the VSM to a grid fault is a consequence of the emulated behaviour of voltage source behind reactance, which results in a near to instantaneous injection of reactive power without the need for identification of the voltage phasor. On the contrary, state-of-the-art grid connected converters adopting PLLs or similar synchronisation techniques, do introduce an unavoidable delay, due to the necessity for an accurate estimation of amplitude and phase of the instantaneous grid voltage for the proper injection of the required amount of current." [35]

Active power behaviour. As shown in Fig. 2.4, the peak value of the synchronising power depends on the system impedance, defined by the short circuit ratio (SCR²) and the disturbance amplitude, here θ_g which represents the grid voltage angle. The rise time is quite fast, and as the settling time, it depends on the connection impedance (electromagnetic dynamic of the current in the inductances). Finally, the active power returns to its references, here zero, according to the dynamics of the synchronisation mechanism (control law and parameters, refer to section 3.5 for more details):

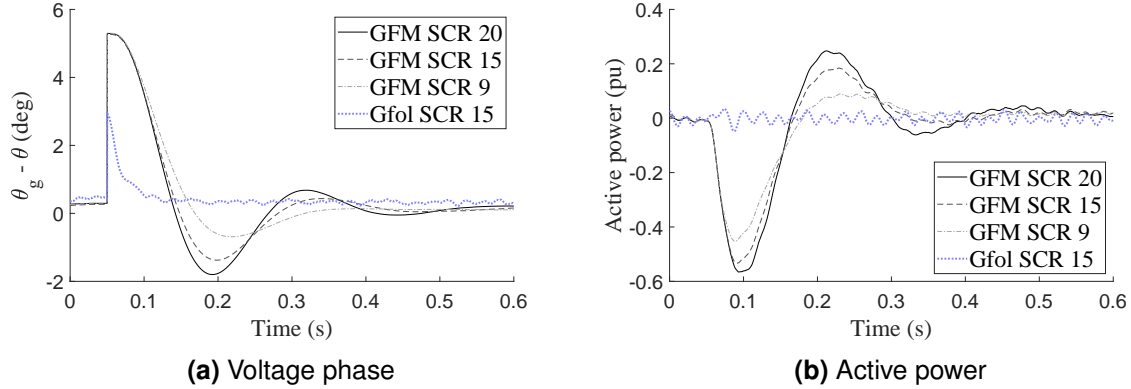


Figure 2.4: VSC response to a 5° phase jump - different SCR

- A grid forming VSC with an active power synchronisation mechanism can be tuned to reproduce the larger decay rate of the SM since its internal voltage phase is computed as a function of the injected power and imposed frequency (if a droop term is considered) error with respect to the references. Fig. 2.4 shows that in the proposed benchmark, the power goes back to zero in less than 200 ms in the three simulated scenarios. The damping varies with the SCR.
- The PLL of the grid following VSC tracks the grid phase really quickly so the current control keeps the power to the reference within the first milliseconds. The initial response is curtailed.

Reactive power behaviour. The synchronisation mechanism also affects the reactive power injection following a grid phase jump as shown in Fig. 2.5.

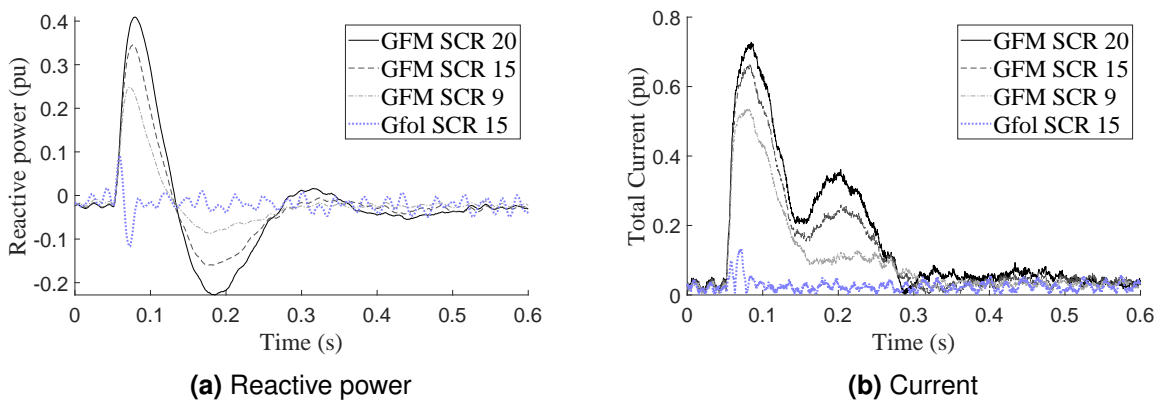


Figure 2.5: VSC response to a 5° phase jump - reactive power

²Ratio of fault current multiplied by the nominal voltage (in MVA) at a particular location to the VSC capacity (here in MVA). In this work, the point of control is the converter terminals (POI at the secondary side of the low-voltage transformer), while the SCR value represents the grid impedance at the point of common coupling (PCC), i.e. at the primary side of the transformer. From the control point of view the total SCR (adding the transformer impedance, here 6.2%) is lower.

The fast tracking of the grid phase provided by the PLL leads to almost no impact on the reactive power injection, while a transient is observed when considering a grid forming control. The total positive sequence (PS) current extracted from the converter is also shown.

2.2.2. Voltage source behaviour, current limitation and power quality

Figure 2.6 shows the voltage and reactive power variations at the VSC terminal (POI), following a grid voltage drop of 10% considering three different control strategies:

- Case 1: the grid forming control considered in this work, which includes inner voltage and current loops with damping resistors as proposed in [31] (detailed in Chapter 3).
- Case 2: the same control but without the inner control loops shown in Fig. 2.3, while keeping the damping resistors so the VSC modulated voltage reference is kept (almost) constant. This simulation is equivalent to a constant electromotive force (emf) test in a SM.
- Case 3: a grid supporting control, which is a grid following (PLL-based synchronisation mechanism) with an outer voltage control loop (instead of regulating the reactive power).

We consider identical initial operating points, output filter and connection impedance (here the aggregation of the transformer, AC line and grid short circuit impedance as shown in Fig. 2.3). In addition, the reactive power droop is set to zero ($V_{POI} = V^* + n_q(Q^* - Q_m)$ with $n_q = 0$), which matches the requirements generally applied to classical automatic voltage regulator (AVR) of a SG.

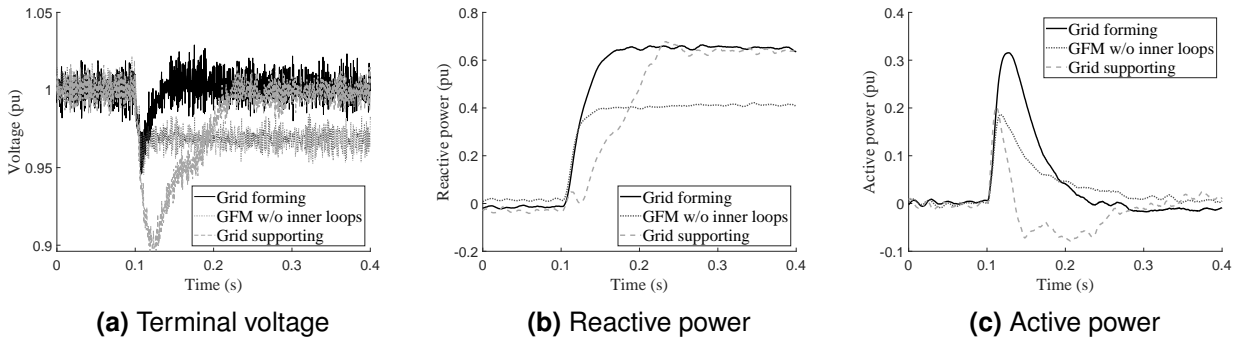


Figure 2.6: VSC response to a 10 % grid voltage step

We observe that:

- At the very first instants the voltage initially drops accordingly to the connection impedance (system SCR, line and transformer) and internal physical impedance (output filter), and therefore there is no difference between the 3 cases in the voltage behaviour at the DUT terminals.
- After a few milliseconds, the DUT terminal voltage stabilises around 0.96 p.u. in case 2.
- In case 1, the inner control loops compensate the output filter voltage drop and regulate the terminal voltage to the reference value (1 p.u.), with relatively fast dynamics. For the selected benchmark, the steady state is reached in less than 50 ms. A response time that is much faster than the one provided by classical AVR of SG whose terminal voltage at the transient time scale (around 100 ms) is mainly defined by the electromagnetic design and characterised by the transient impedance (X'_d) [36].
- In both cases 1 and 2, the grid forming control provides immediate reactive power.
- A grid supporting control is also able to compensate output filter voltage drop quite fast, here within 100 ms and therefore it regulates the terminal voltage (at POI) even faster than a SG³.

³A large power park module (PPM) controlling voltage at PCC uses an outer loop which explains larger response times.

The difference lays in the first cycles, since the initial control objective is to maintain the current, the voltage drops further, before starting to increase as ordered by the outer loop and there is a delay in the reactive power injection. It is because of this behaviour that grid following converters are often assimilated to current sources although VSC are by definition voltage sources.

In short, at high frequencies the impedance of a VSC corresponds to its output filter and, in principle it is independent of the control strategy, similarly to the sub-transient impedance (X_d'') in a SM [36]. Its value for a VSC is in general much lower than for a SM. The transient impedance (around 100ms) of a SM is also defined by construction, while it can be brought to zero in a VSC by control settings. In between, during the first cycles, the impedance seen by the system also depends of the outer control loops and the synchronisation mechanism, hence it might be hard to determine it analytically. Moreover, the damping resistors and feed-forwards terms of inner loops also affects the sub-cycle transient response. Therefore, methods for estimating or directly measuring the frequency dependent impedance profile of VSCs have gained attention in the literature [37]. Roughly speaking, from the voltage control viewpoint, a low internal impedance is desired to limit the fluctuations at the converter terminal, so it can be seen as a measure of the voltage source property, but also the VSC contribution to the system strength (see section 2.5.2.4) and reveals the limitations of grid following converters in this regard. However, it must be kept in mind that the main function of the VSC internal physical impedance is filtering harmonics and limiting the current dynamics for controllability purposes.

Current limit. Compared to a SM that can support several times their rated current, power electronics devices can only hold small over currents (20–40%) for a very short period (few ms) as manufacturers generally consider some margin in the IGBT current capability at the design stage.

However, for large voltage differences (amplitude or phase) between both sources, the grid and the converter, the current can be higher than the device nominal value. Therefore, power converters need to be protected against any event leading to over currents such as phase shifts, but also short circuits or large load connection. Hence, we recall here, that independently of the synchronisation and current limitation mechanism, the characterisation of the voltage amplitude sensitivity to current variations within current capability (system strength) and the fault current contribution must be dissociated when dealing with power electronic devices [38]. The latter must be always limited to its maximal current.

In grid following converter it is possible to limit the current simply by adding a saturation to the cascaded PI inner control loops. Instead, for grid forming converters, different strategies have been proposed in the literature [39, 40], as the solution to the problem is less straightforward [41, 42]. Indeed, applying the same strategy as the one used in grid following controls to grid forming ones may lead to fast oscillation on AC voltage as shown in III.2 Current Saturation of [31]. Other authors have proposed to switch the control to a PLL-based current control during grid faults in order to keep the synchronism with the system while still limiting the current [23]. The main drawback of this method is the need for fault detection and triggering conditions setting that might lead to complex algorithms, as well as the threshold effect and the additional disturbances it creates when switching controls.

Recently, some concepts based on a Threshold Virtual Impedance (TVI) have been proposed for current limiting purposes and will be privileged in this work [43, 44]. The idea is to implement a control structure capable of emulating the effect of a physical impedance when the current exceeds a pre-selected trigger value. The TVI limits the converter output current by virtually increasing the impedance between the converter and the grid, using a control algorithm. In short, a TVI is basically an additional voltage difference, proportional to the amount of current injected by the converter. So, by applying this voltage difference at the output, the behaviour of the system will be similar to a voltage source in series with a variable impedance, so the voltage source behaviour is to some extent preserved during faults (even if the voltage reference is changed by the control). The control dependency of the internal VSC impedance that would in principle be used in a conventional short

circuit power (SCP) calculation becomes evident. Figure 2.7 compares the response of the selected grid forming control to a grid following one in case of a three-phase fault in a no load case (zero initial power and reactive power). The first point to be noted is that at the very first instants, in both cases, the VSC injects high current and in this case the hard blocking protection⁴ (set to 1.45 p.u.) leads to an abrupt current curtailment. Secondly, when using TVI limitation strategy, the current injected by the grid forming VSC depends on the voltage dip and for solid faults it might be slightly larger. Indeed, TVI relays in two thresholds: one for the activation, here 1 p.u. and another for the actual maximal allowed current, here 1.2 p.u., while the grid following VSC was limited to 1 p.u. at all times.

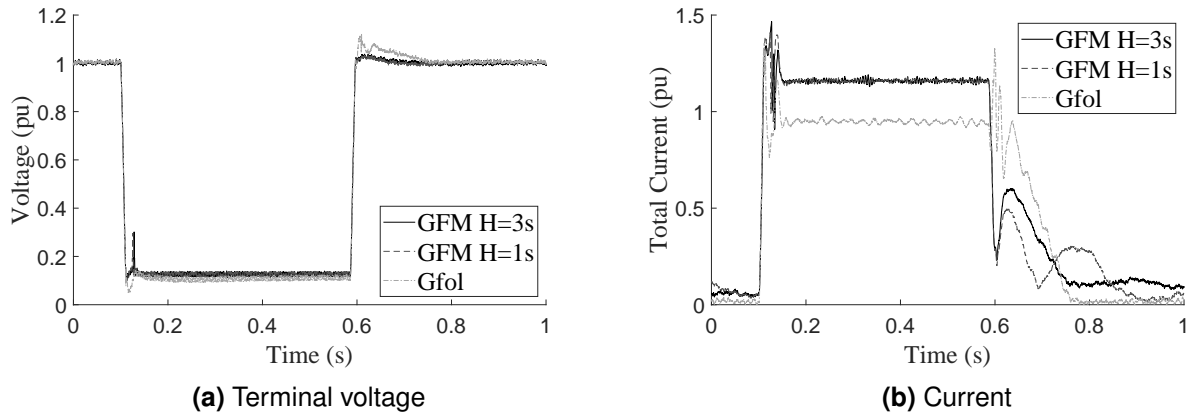


Figure 2.7: PS converter current for a three-phase fault

It is also worth highlighting that the resynchronisation time might take longer for a grid forming VSC and it is more sensitive to the operating conditions and control parameters. However, the over voltage at fault clear may be reduced. In this section we have carefully selected an ideal case to illustrate that in specific conditions a grid supporting and a grid forming VSC might exhibit a similar reactive current behaviour when limitations are reached (see Chapter 3 for an in-depth discussion). Indeed, grid following converters generally include a fast reactive current injection function to comply with grid connection requirements (see section 2.3.3), activated during large voltage variations, that acts directly on the inner current loops to accelerate the response⁵. Finally, a grid forming VSC will inject some active current when the fault is also composed of resistive elements.

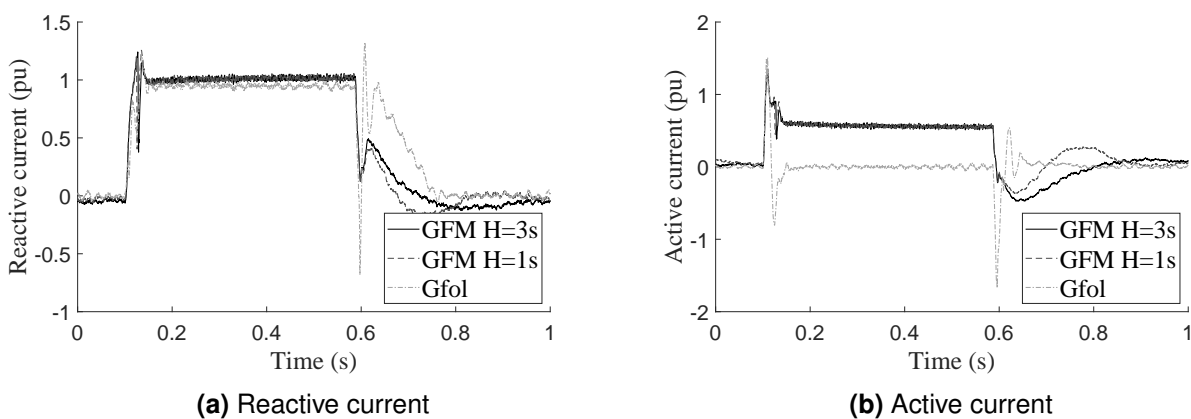


Figure 2.8: PS reactive and active current during a three-phase fault

⁴Hard blocking is a mode where the IGBT are not triggered, instantaneously stopping current flow to protect them against over current, the setting of this mode and the current capability specific to this project will be explained in section 3.3.2.2

⁵In practice, sequence separation, which has been neglected here, might lead to some delay in the initial current injection.

2.2.3. Inertial response and energy constraints

In addition to the availability of some current headroom, the provision of synchronisation services by grid forming units following grid disturbances requires a minimal DC side energy. In [22] T_{GF} is defined as the "surviving period" within which **grid forming units are expected to ensure the reachability of a new stable equilibrium point**. This often implies the injection of active power until electrical transients vanish and other flexibility levers such as balancing services, based on the observation of the system can be deployed. Proposed bounds for T_{GF} are 1 to 10 seconds [22].

Figure 2.9 presents the DUT response following a frequency variation of constant Rate of Change of the Frequency (RoCoF) of 1 Hz/s⁶ to show that, depending on the specific implementation of the converter control, other grid disturbances, such as a frequency variation sustained for a certain time, may attempt to extract larger amounts of energy from the converter.

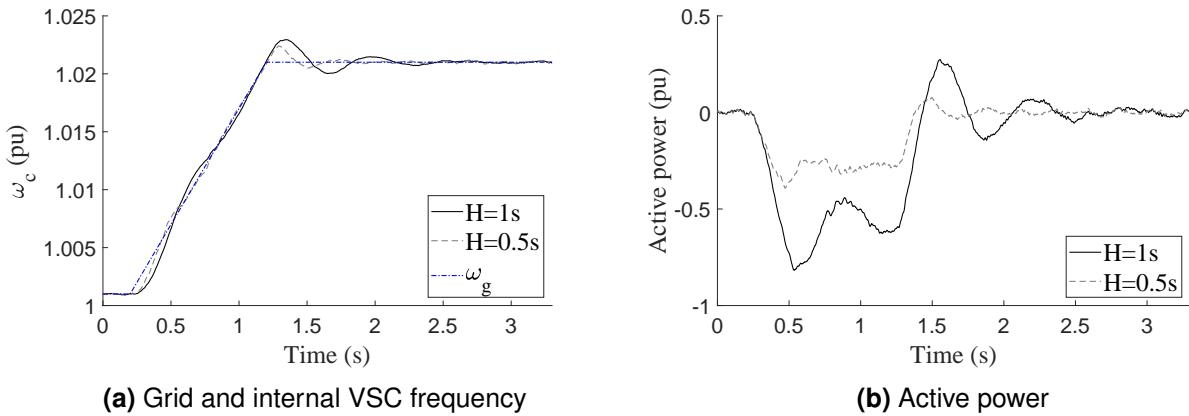


Figure 2.9: 1 Hz/s RoCoF for 1 second

- A grid forming unit can emulate the inertial response of a SM as shown in [36] if enough energy is available but not all active power self-synchronisation mechanisms provide such a response (e.g. the droop control), and even if they do, the active power beyond a certain time horizon could be limited to respect the installation energy constraints. Even if not considered in this work, in practice DC voltage control strategies could take over to limit the device contribution. Here the DUT does not provide PFR so the power goes back to zero. In this project, this is achieved by setting the converter frequency reference as the filtered VSC frequency (with a time constant of 100 ms as proposed in [36]) but other strategies can be implemented. In this test the energy contribution is settable with an equivalent inertia constant parameter (H) that has also an impact on the damping. With additional work on the control design this behaviour should be improved, but for the purposes of illustration we chose to keep the natural response.
- A grid following unit providing synthetic inertia (with enough available energy) is using the measured grid frequency from its PLL, therefore, there are some inherent delays before starting changing its active power output (around 300 ms in OSMOSE WP5 demo [45], section 5.3). For grid following units, this should be considered rather as a short-term frequency control.

The definition of synthetic inertia might be submitted to debate and in general the term is found not suited for IBR (see section 2.5.1.1). Nonetheless, in this work we consider the specification proposed in [12] (art. 14), this is: "a rapid adjustment of the active power injected to or withdrawn from the AC network in response to frequency changes, activated in low and/or high frequency regimes, in order to limit the rate of change of the frequency".

⁶For this test the grid frequency ramp is filtered to limit the discontinuity.

As a consequence, a grid forming source is **not necessarily** more capable of providing energy than a grid following one. However, if a given (grid following) unit claims the capability of providing synthetic inertia, with *rapid* allowing for delays associated to the frequency measurement, then upgrading the VSC control to provide grid forming capability should enhance the response to a "synchronous-like inertia" that starts injecting active power immediately after the frequency changes (no measurement needed). In short, grid forming controls inject an undelayed active power response to frequency changes that limits the initial RoCoF, but a minimal grid forming capability could be defined within the installation energy limits and without necessarily including a synchronous inertia emulation. After a short period of time (the survival time T_{GF}), grid forming units could reduce their active power contribution and be replaced by other resources **willing** to provide fast response services (e.g. FFR).

2.2.4. Stability considerations for inverter based resources

Intrinsic stability limits of different synchronisation mechanisms have been reported in the literature. In some cases, mitigation strategies have been proposed and were adopted in this work. Without pretending to provide an exhaustive list, we enumerate here some of them, as they constitute a relevant background for the observed behaviour in the demonstrator and contribute to our discussion on the compatibility of different synchronisation mechanisms with existing grid code and standard requirements and the definition of the grid forming capability provided in the next sections 2.3 and 2.4.

Limits of PLL based grid-synchronisation mechanisms in weak grids. In short, FRT requirements, or more specifically, power recovery specifications, impose relatively fast dynamics on the PLL and current loops. It is now widely acknowledged that stability limits of the converter control can be significantly tightened in weak networks, mainly related to the PLL behaviour, as the voltage at the connection point is significantly affected by the injected current [46]. Figure 2.10⁷ illustrates this issue following a line opening that lead to a SCR reduction from 20 to 3⁸ as discussed in [47].

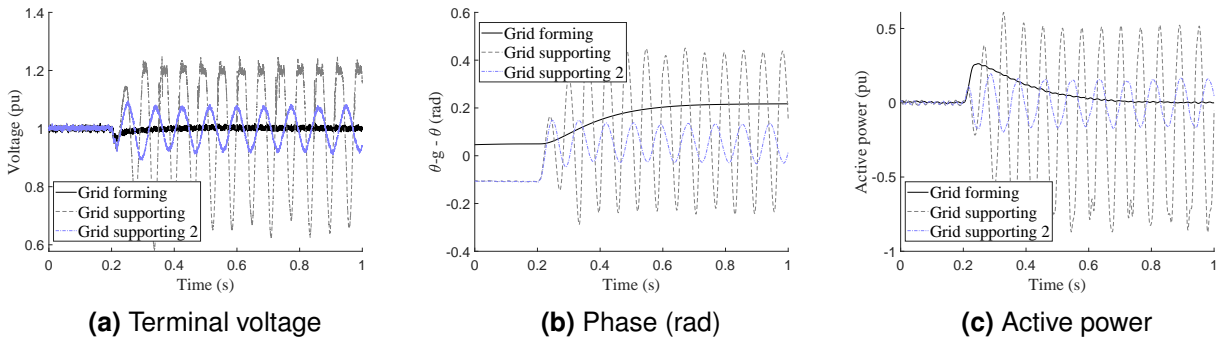


Figure 2.10: SCR reduction (line opening)

A common way of tackling this issue in transmission system applications consists in slowing down the PLL to filter voltage variation and reduce power oscillations [48]. The improvement is illustrated in blue (grid supporting 2). However, this might not always be enough and in general it implies that the resynchronisation transient, in which power references are not tracked, takes longer: a suitable trade-off between stability and performance becomes challenging to achieve with grid following converter at low SCR [49].

⁷ θ is the phase used in the park transform: we take the internal converter angle in the grid forming case, and the PLL output in the grid following case which explains the offset.

⁸It is recalled that the SCR defines here only the power system impedance while the total connection impedance, seen at the converter terminals is higher because it includes also the transformer (6.2% in the benchmark).

In principle and from the control design perspective, this problem can be addressed by an exogenous or an endogenous approach, i.e.:

- As it has usually been done in strong grid-connected applications, we can specify required conditions at POI to ensure converter proper functioning in terms of stability and performance: a minimal SCR [50], but also a maximal RoCoF [22]. These system properties would need to be then ensured by other devices: the providers of synchronisation services, today SGs.
- Or we can develop internal or self-synchronisation mechanisms that do not rely on the grid voltage phase and frequency measurements as previously discussed in section 2.1.2.

In the first case the burden of IBR integration is carried by the system, while in the second case the newcomers are requested to adapt. It has been highlighted that the optimal solution that minimises the whole system cost might be some place in the middle [51]. In this work, we focus on the **minimal requirement that could be applied to off-the-shelf IBR to progress on their immunity with low to no impact on the installation design**, only on its control, hence without additional (capital) cost.

Small signal stability and damping of self-synchronisation mechanisms. Changing the synchronisation mechanism does not make VSC immune to interaction risks with the grid, as well as with other power sources connected nearby [42, 52]. This phenomenon remains highly dependent on the impedance characteristic of the control [53] and should be thoroughly assessed for all grid connected VSC for the whole range of setpoint and possible SCR, whether they are grid forming or grid following. The risk of interaction of the current control with the network for some operating points when using a droop based grid forming control has been illustrated in [54]. In general, grid forming converters tend to be more robust to uncertainties in the plant when connected to a grid with higher impedance (lower SCR) [5]. In [55], the authors have shown that the control tuning using Linear–quadratic regulator (LQR) methods allows to have a better active/reactive power de-coupling while ensuring a proper current limitation during transients. Control tuning in this project is discussed in Appendix C (section C.2).

Transient stability and active power synchronisation. Droop and VSM type controls introduce a linear relationship between the frequency and the power mismatch. Therefore the internal angle drifts when the power cannot be delivered to the grid as illustrated in Fig. 2.11 when applying a typical FRT profile at the converter terminals (without any counter-measure implemented). To avoid this drift and increase the duration of the fault that the converter can withstand, the droop gain can be adjusted during the fault to lessen the angle variation and therefore improve the stability [43]. Other methods adjust the current angle reference during the transient (while respecting the current limitation) [44, 56] or multiply the power reference by the voltage as done in some grid following controls.

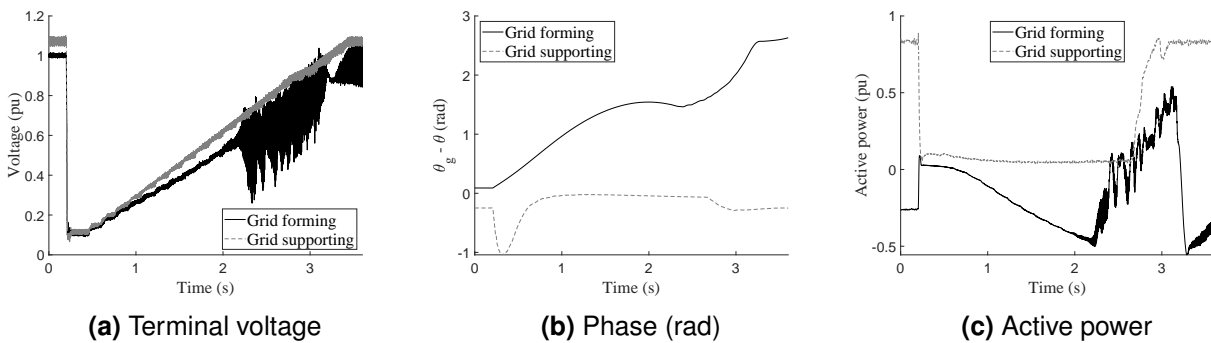


Figure 2.11: FRT profile

2.3. Inconsistencies between self-synchronisation and grid codes presently in force

In order to ensure power system security, a set of requirements have been implemented in different grid connection codes. At the EU level, coordination is achieved through CNCs: Requirements for Generators (RfG) [11] and for High Voltage Direct Current (HVDC) systems [12], which are then implemented at national level. In France, this information is available in the *Documentation Technique de Référence* (DTR) [57].

In the following we will use the term "general requirements" to refer to the technical specifications that apply to all Power Park Modules (PPM) and HVDC systems according to the current versions of the CNCs, but please note that for historical reasons they have been conceived for grid following VSC. As a consequence, in this section we discuss the challenges and opportunities provided by self-synchronisation regarding a sub-set of those general grid-connection requirements. The French implementation will be considered as a reference for non-exhaustive articles.

2.3.1. RoCoF withstand capability and loss of mains protection

According to RfG (art. 13-1-b), a PPM "shall be capable of staying connected to the network and operate at rates of change of frequency up to a value specified by the relevant transmission system operators (TSO), unless disconnection was triggered by rate-of-change-of-frequency-type loss of mains protection". Self-synchronisation mechanisms bring challenges regarding the last point as they would smooth the frequency gradient. Indeed, many loss of main protections rely on RoCoF measurement (especially on distribution grids) [58]. As discussed before, a grid forming unit generates the voltage wave form without relying on the grid voltage measurement, so it will initially maintain its phase and frequency and inject instantaneous power to limit the RoCoF, making state-of-the-art islanding detection mechanisms ineffective. This is a major drawback for DSO that will need to implement new detection mechanism to discriminate islanded and grid connected situation or change the operational rules to allow their grid to operate stably even when islanded.

Regarding withstand capability, (art. 12) of the HVDC CNC [12] set the thresholds in an exhaustive manner to $-2,5$ and $+2,5$ Hz/s and the observation window is set to 1 seconds⁹. In general, when a power electronic converter reaches hardware limits, such as current thresholds, it is first expected to stably withstand the disturbance, within predefined time-dependent profiles. If the disturbance vanishes within the profile, some performance requirements might apply during the fault and recovery process, but this might not yet be systematically done as for this requirement. As aforementioned and as a consequence of the inertial response requirement, a grid forming unit will inject high power following frequency changes that could imply reaching current limitation depending on the initial operating point and control settings, but stable operation must be always achieved.

2.3.2. FRT profile

Figure 2.12a shows the FRT profile applied to type B and C PPM in France, which include units from 1MW and upward that are connected to the network below 110kV¹⁰, while Fig. 2.12b depicts the FRT requirements for units connected to the 110kV network and above. As discussed in section 2.2.4, grid forming controls based on the active power synchronisation might encounter some challenges to ensure compliance with different FRT requirements in all possible operating conditions. Suitable solutions as the one mentioned in section 2.2.4 should received more attention in the future.

⁹"measured at any point in time as an average of the RoCoF for the previous 1 s" [12]

¹⁰limits between type can be found here: <https://eepublicdownloads.entsoe.eu/clean-documents/cnc-active-library/France/rfg-bilan-de-consultation-publique-seuils-abcd-vfinal.pdf>

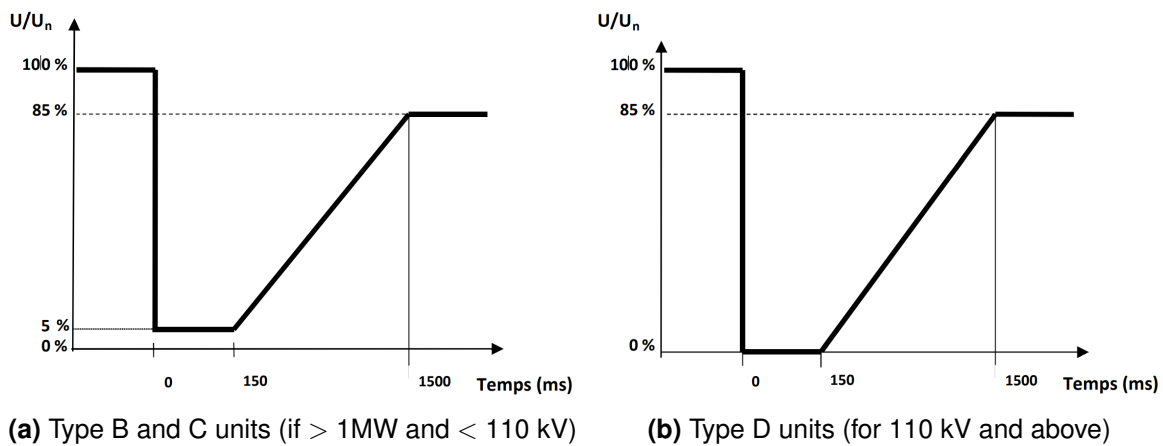


Figure 2.12: FRT profile applied to type PPM in France.

2.3.3. Short circuit contribution during faults or Fast fault current injection

The first term is used in (art. 19) of HVDC CNC [12] and the second in (art. 20-2-b)-(i)) of RfG [11] to describe a non-mandatory and non-exhaustive requirement applied to PPM from type B. It only concerns the capability of providing fast current at the connection point in case of symmetrical faults. All performance requirements, such as the operating ranges, the characteristic, the timing and the accuracy of the response, and the behaviour in asymmetrical faults are specified at national level by the relevant TSO. A grid forming unit does in principle comply with such a generic requirement, however, this might be no longer the case when we consider more detailed national implementations.

In France for instance a droop characteristic between the reactive current and the voltage is imposed for type B, C and D PPM and HVDC systems as illustrated in Fig. 2.13a and according to the 50549 standard [59]. Regarding the response time, PPM must inject fast (within 60 ms [60]) **reactive** current as illustrated in fig. 2.13b in case of voltage dips (or over voltages). Indeed, in France, reactive current priority is required for HVDC systems in accordance to art. 23 of the HVDC (resp. 21-3-e) of RfG).

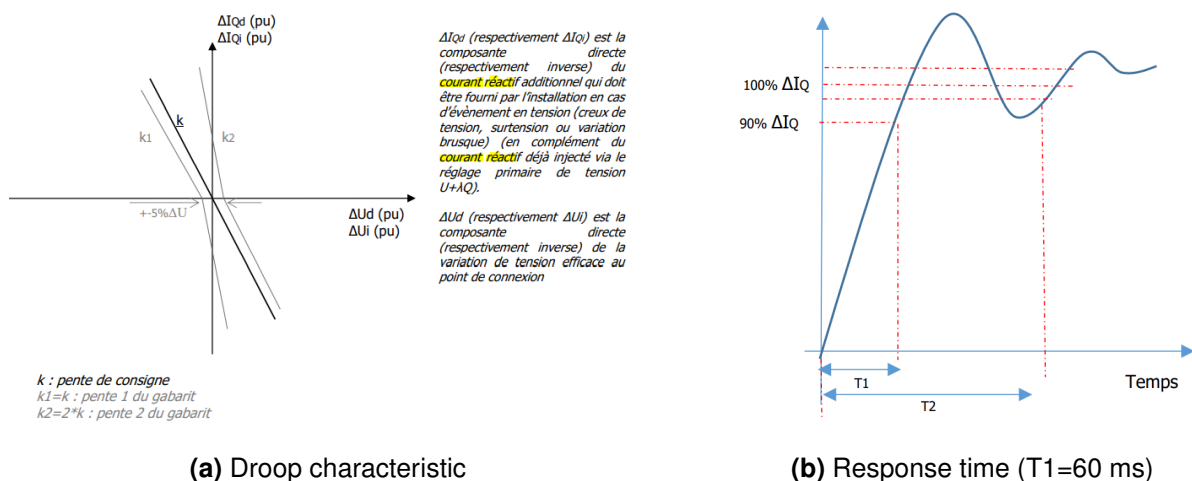


Figure 2.13: Fast fault current injection requirements in french CNC implementation

However, as shown in Fig. 2.7 and in consistence with section 2.2.1, active power synchronisation mechanisms may inject immediate active power following grid disturbance and control action may not be able (neither expected) to enforce prioritisation rules at this time scale (first cycles up to 100 ms).

For inductive faults, the active power contribution eventually caused by an initial phase jump will naturally die out and the active/reactive current share will depend on the system and grid impedance. For longer voltage dips, active or reactive power priority could be implemented as a control-based adjustment but would take action after some delay associated to the control bandwidth.

2.3.4. Power recovery after faults

Article 26 in HVDC CNC [12] (resp. art 20-3-b) in RfG [11]) allows TSO to specify active power recovery behaviour after fault. In France, HVDC systems must restore active power to 90% of its pre-fault value in 150 ms (rise time) and stabilise in a 5% band around it (settling time) in 200 ms [61]. Requirements are less constraining for PPM in France as it is only requested to restore its active power as fast as possible, but not least that 90% of its pre fault value in 2 s after the voltage at PCC has returned to a value above 0.85 p.u. [60, 62]. Grid following converters can comply with this requirements, most of the time, without major challenges but for grid forming controls, especially those including inertial response, the settling time of the active power recovery after fault might depend on the control settings selected to potentially comply with other requirements (inertia). However, they will still ramp up power rapidly which, in this regard, is the most critical feature to ensure system stability.

2.3.5. Island operation

In RfG, (art. 15-5-b), units from type C are requested to *take part in* island operation as long as the voltage and frequency remain in the limits defined in the code, if required by the relevant TSO. In France, the PPM are requested to provide results for an island test in which a SM is included (*Fiche I 10 : Réseau Séparé*, in Chapter 8 of the DTR [63]). In such a case, units should be able to operate in Frequency Sensitive Mode (FSM) (as long as they have energy available), which is associated to primary frequency control (see Appendix A).

However, according to our initial definition, a grid forming unit has the capability to self-synchronise and help other to stably operate at extremely low SCR, but more precisely independently of grid conditions. In fact, they are capable of *standalone* which brings new opportunities for island operation. They do not only allow the IBR to take part in a island, they actually *enable* its survival for a short time (that should be defined by TSO), in order to provide the voltage and frequency signals to other grid-connected devices providing regulation services. This is illustrated in Fig. 2.14 where the test shown in Fig. 2.10 is repeated (SCR reduction from 20 to 3). This time the two VSC, a grid forming and the grid following one, are connected in parallel at POI, which now lead to a stable line opening. However, this behaviour requires an adaptation of the operational rules to ensure that the network has been designed to be operated without the connection to the main grid.

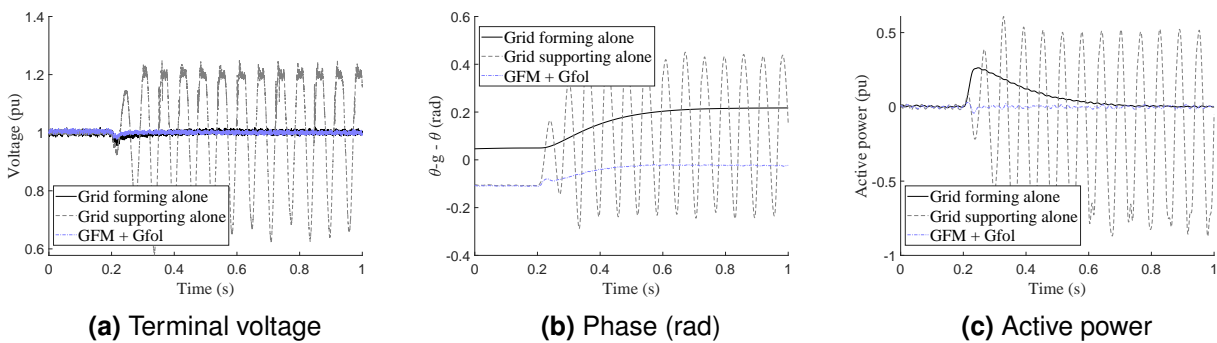


Figure 2.14: SCR reduction (line opening) - Grid forming stabilises grid following VSC

2.4. Definition of grid forming capability

We first present in section 2.4.1 a state-of-the-art on the definition of the grid forming capability. Then, section 2.4.2 summarises the minimal set of technical requirements that in this work define different types of grid forming units before listing the technologies that can provide this capability in section 2.4.3. Finally, section 2.4.4 concludes with a discussion regarding a sub-set of features that have been recently associated to grid forming units, but we think that they should be moved to the category of general requirements (as those discussed in section 2.3) and be applied to all grid-connected converters, independently of their synchronisation mechanism (including grid following).

2.4.1. state-of-the-art

In this section we elaborate on the evolution of the definition of the grid forming capability since the functional approach proposed in the MIGRATE H2020 project [22], followed by the Entsoe view published in the HPOPEIPS report and position paper [64], to close with the recently approved GB grid forming code GC0137 [65] and the German FNN guideline [66].

2.4.1.1. MIGRATE h2020 project

In 2019, a high level definition of the grid forming function was proposed in [22] such that a grid forming unit shall:

- behave as a voltage source,
- be synchronised with other grid forming sources,
- operate in standalone after seamless islanding,
- smartly limit the output current magnitude (meaning preserving a voltage source behaviour and preferably avoiding control switch during voltage dips for instance), and
- be compatible with all devices connected presently on the power system, especially SM and grid following converters.

2.4.1.2. Entsoe HPOPEIPS report and position paper

In 2020 Entsoe published a paper dealing with the High Penetration of Power Electronic Interfaced Power Sources (HPOPEIPS) [64]. According to this work, 7 properties define a grid forming unit:

- Creates system voltage (does not rely on being provided with firm clean voltage).
- Contributes to Fault Level (Positive and Negative Sequence within first cycle).
- Contributes to Total System Inertia (limited by energy storage capacity).
- Supports system survival to allow effective operation of Low Frequency Demand Disconnection (LFDD) for rare system splits.
- Controls act to prevent adverse control system interactions.
- Acts as a sink to counter harmonics & inter-harmonics in system voltage.
- Acts as a sink to counter unbalance in system voltage.

While the MIGRATE definition focuses on capabilities regarding standalone and synchronisation, the Entsoe reports adds a response deployment dimension. Some responses are more challenging to provide than others. The concepts proposed in this Chapter are inspired by this approach, but restrain the *grid forming capability* to the first points and we define *synchronisation services* as the set of responses provided by the grid forming units without any hypothesis on the provision mechanism.

2.4.1.3. GC0137: Minimum Specification Required for Provision of GB Grid Forming (GBGF) Capability

On January 31st 2022 the GB Office of Gas and Electricity Markets (OFGEM) approved the GC0137 code after more than 2 years of discussion with stakeholders [65]. Formerly known as the Virtual Synchronous Machine/VSM Capability grid code, the document defines a non-mandatory technical specification for grid forming units that we will allow ourselves to rephrase as follows. It shall:

- comprise an internal voltage source (IVS) and reactance¹¹,
- remain synchronised with the system¹² and maintain a load angle between 0 and 90 degrees,
- be capable of supplying:
 - Phase Jump Active Power¹³,
 - RoCoF response power¹⁴ which includes Real Inertia Power¹⁵,
 - Damping Active Power¹⁶,
 - Control Based¹⁷ Real Power (including Control Based Real Droop Power¹⁸ which is FFR),
 - Control Based Reactive Power,
 - Voltage Jump Reactive Power¹⁹,
 - Fast Fault Current Injection²⁰.

According to GC0137, Control Based changes have a bandwidth limited to 5 Hz (“to avoid AC System resonance problems”), while Phase Jump Active Power and Real Inertia Power “can have frequency components to over 1000 Hz”. Another point worth noticing is that a unit designed with black start capability is then required to provide grid forming capability and an exclusion is defined to the fast fault current injection requirement applied to grid following units. In addition, a minimum Phase Jump Angle Limit, for the unit to remain “in linear control without current limiting”, of 5 degrees is recommended and a 60 degrees Phase Jump Angle Withstand capability is specified. The RoCoF response power is assessed for 1Hz/s while withstand capability is requested up to 2 Hz/s. Finally, “the cumulative energy delivered” is defined “for a 1Hz/s System Frequency fall from 52 Hz to 47 Hz” in MWs, but also an inertia constant value (H) must be declared by the service provider.

Before continuing, we would like to highlight a subtlety, one well known by specialists, but seldom noticed by experts from other fields involved in the development and deployment of this new technology. From the specification viewpoint, it is common practice to differentiate capabilities from services, and focus only in the former ones, such that a grid forming unit does not provide a set of responses, it is just **capable** of supplying them which is generally assessed in very specific conditions and typically defined as grid connection requirements (mandatory or not) or as part of a certification procedure. The implications of this important difference will be discussed in the remainder of this Chapter.

¹¹the impedance between the IVS and the system can only have real physical values. Virtual impedance, is not permitted.

¹²the frequency of rotation of the Internal Voltage Source is the same as the System Frequency for normal operation.

¹³an inherent capability to respond naturally, within less than 5 ms, to changes in the phase between the IVS and PCC.

¹⁴Phase-Based Real Inertia Power plus the Control-Based Real Droop Power supplied when subject to a system RoCoF.

¹⁵an inherent capability to respond naturally, within less than 5 ms, to changes in the system phase and frequency.

¹⁶an inherent capability to respond naturally, within less than 5 ms, to system oscillations.

¹⁷refer to changes in the positive phase sequence Root Mean Square (RMS) Active Power or Reactive Power produced at fundamental System Frequency by controlled means (be it manual or automatic).

¹⁸similar to Primary Response but with a response time to achieve Maximum or Registered Capacity within 1 second.

¹⁹instantaneous reactive power to a step or ramp change in the difference between the IVS and PCC voltage magnitudes.

²⁰reactive current that starts to rise in less than 5 ms when the voltage falls below 90% of its nominal value. Deployment up to 1 p.u. must be completed before 30 ms.

2.4.1.4. FNN Guideline: Grid forming behaviour of HVDC systems and PPMs

The German FNN institute has recently published a new guideline that complements the VDE-AR-N-4131 norm about dynamic frequency/active power behaviour and dynamic voltage control without reactive current specification [66]. It basically consists in a conformity verification procedure for grid forming units that includes methods for specifying the reference behaviour, tests' description (networks and scenarios) as well as validation criteria. The term "undelayed" is privileged to characterise the immediate response of grid forming units and a "network-stabilising behaviour" is expected, which means that its response must "counteract" network changes. The proposed tests cover:

- phase angle steps of 10 and 30 degrees.
- linear frequency change with 2 Hz/s RoCoF during 0.5 seconds,
- voltage magnitude step of 5% and 10% within normal operational ranges,
- grid distortion: presence of negative sequence (2% unbalance in one phase), harmonics (including ranks 2, 5, 7, 19 and 31) and low frequency subharmonics (at 5, 10 and 15.9 Hz),
- changes in the network impedance, leading to SCR reductions from 20 to 5, 2 and 1, and
- islanding in an active network, with only load or including another grid forming converter.

Conformity verification is then based on time varying reference "envelopes" that can be applied to instantaneous value signals giving especial attention to the initial behaviour up to the first peak. These signals can be obtained from on field measurements, but also electromagnetic transient (EMT) or hardware in the loop (HIL) simulations, and they could include recalculated quantities to be determined over a certain time period, such as the active and reactive power [66]. Conformity proof includes the delivery of a technical report and a digital model of the installation and benchmarks.

2.4.2. OSMOSE WP3 definition of grid forming capability

In this work, we consider that *a grid forming unit shall, within its rated power and current, be capable of self-synchronise, standalone and provide synchronisation services*, which includes synchronising power, system strength, fault current and inertial response (further discussed in section 2.5.2).

Therefore, we define grid forming capability as a set of technical requirements listed below that precisely describe the expected response in terms of current, active and reactive power output following specific events. These requirements should be harmonised at EU level in CNC leaving a certain degree of flexibility for national implementation to deal with system dependent needs, in the same way that the short circuit current contribution during faults has been specified (see section 2.3.3).

It must be noted that the capability of providing synchronisation services is not directly subjected to an over current requirement. Current limitation strategies can be implemented to ensure that the expected response is only provided up to the device maximal current making the best use of the available headroom capacity, as it is currently requested for the fast fault current contribution.

1. **Standalone.** If requested and in coordination with the relevant system operator, the unit shall be capable of participating in island operation after the loss of the main grid, whether the island is passive or active and even if no other grid forming source is left (so with or without SM).
2. **Synchronising active power.** The unit shall be capable of providing an immediate²¹ active power output following a phase jump in consistency with the definition proposed in section 2.2.1. The relevant system operator can set constraints on the speed of the active power reference tracking recovery. This can be achieved through a time-dependent profile as proposed in FNN [66] or at least a lower bound on the return time (T_{sp}), which can be seen as a sort of minimal sustain time of the response, which can be related to the notion of 5 Hz bandwidth limit on the controlled power proposed in [65]. An upper bound for T_{sp} could be agreed at EU level.

²¹Immediate means subcycle. A 5 ms maximal response time threshold could be adopted as proposed in GC0137 [65]

3. **Inertial response.** The unit shall be capable of providing an immediate active power output following a frequency ramp (constant RoCoF) or profile (piece-wise linear RoCoF function). The relevant system operator can set constraints on the expected contribution for predefined values of RoCoF, through a fixed, settable or minimal inertia constant value (H), or in a more general way a profile specifying the power output (ΔP per RoCoF) as a function of the time. Again, a minimal sustain time (T_{ir}) should be specified and can be limited by an upper bound agreed at EU level in coordination with frequency regulation services (see section 2.5.1.2).
4. **System strength.** The unit shall be capable of providing an immediate reactive power output following a grid voltage variation. A frequency-dependent impedance characteristic of the system shall demonstrate low transient and sub-transient impedance in the linear operation domain (no current limit reached). The relevant system operator should be able to set thresholds for impedance values at specific frequency ranges which must take into account physical components between the converter and PCC (filters, valve reactors, transformer, etc.).
5. **Fault current.** This requirement defines the expected behaviour in current limitation mode. As a consequence of the voltage source behaviour the unit shall be capable of providing:
 - a) an immediate current output within the installation capabilities following voltage dips.
 - b) The active/reactive current share during the first instants of the fault shall depend on the system impedance seen from the unit (not on a "control-based" action as defined in [65]).
 - c) During asymmetrical voltage dips, prioritisation between positive and negative sequence can be defined by the relevant system operator.

Therefore, a grid forming unit, by definition, does not rely on grid conditions to synchronise (it can operate at a wide range of short-circuit ratios and inertia levels) and it is capable of helping others to maintain synchronism under stressful conditions by providing synchronisation services, but it must still complying with the general requirements applying to the specific technology. Finally, depending on the subset of synchronisation services that a specify technology is capable of providing, we propose to classify grid forming units in 4 types:

- Type 1 grid forming unit: is capable to standalone and provide system strength and fault current around nominal value ($I_n \leq I_{fault} < 2I_n$ where I_{fault} is the declared maximal current).
- Type 2 grid forming unit: is capable to standalone and provide system strength, fault current around nominal value ($I_n \leq I_{fault} < 2I_n$) and synchronising power complying with specific requirements (T_{sp} or more detailed profile).
- Type 3 grid forming unit: is capable to standalone and provide system strength, fault current around nominal value ($I_n \leq I_{fault} < 2I_n$), synchronising power and inertial response complying with specific requirement (T_{sp} , H and T_{ir} or more detailed profiles).
- Type 4 grid forming unit: is capable to standalone and provide system strength, synchronising power and inertial response complying with specific requirement (T_{sp} , H and T_{ir} or more detailed profiles), and high fault current ($I_{fault} \geq NI_n$, with $N \geq 2$).

2.4.3. Technologies able to provide grid forming capability

A SM is, by construction, a type 4 grid forming unit and most of the technologies connected to the grid through VSCs can provide grid forming capability as long as they have a *small* energy buffer that allows the active power to deviates from its setpoint. For type 1 grid forming units *small* accounts for a few tens of ms [67], while type 2 units are expected to sustain the active power response for a few hundreds of ms. Type 3 grid forming capability requires energy to be available for a few seconds. ESS as the ones considered in this project fall in the type 3 category which was previously demonstrated in [68]. Moreover, WPP can also provide type 3 grid forming capability under certain conditions as demonstrated in [69]. In the short-term, HVDC and FACTS are the most suitable candidates to develop different types of grid forming capability as they are in general TSO owned [64].

2.4.4. Beyond grid forming capability: new VSC general requirements

Before concluding this section, we highlight some technical requirements that have been recently associated to the grid forming capability but we recommend that they are assessed and applied to all VSC independently of their synchronisation mechanisms. They include:

Phase jump withstand capability. Similarly to what has been done for the RoCoF withstand capability described in the section 2.3.1, a phase jump withstand capability could be specified. Although phase jump tests have gained interest with the emergence of grid forming controls, in principle there is no reason to exclude grid following converters from this requirement. VSCs presently connected to the grid provide large phase jump withstand capability, however to the best of our knowledge, this is not specified at European level. As an example, in France, withstand capability for a line disconnection in a specific test is required to SGs in the national implementation of the grid code (*Fiche 13 : Stabilité sur Report de Charge*, in Chapter 8 of the DTR [63]). The P2800/D6.0 standard draft requires that: "The IBR plant shall ride through for PS phase angle changes within a sub-cycle-to-cycle time frame of the applicable voltage of less than or equal to 30 electrical degrees" [70]. It must be noted that this value might be higher than the maximum phase difference defined in circuit breakers to allow line closing as they must cover for unplanned line opening. For illustrative purpose, Fig. 2.15 shows the selected benchmark response for a 60° phase jump (as proposed in [65]) leading to current saturation. Here, the initial current limitation before the activation of the TVI is managed by the hard blocking protection, but different solutions can be used to protect converters in extreme conditions. In general, grid following VSC faces less challenges to recover quickly power reference tracking.

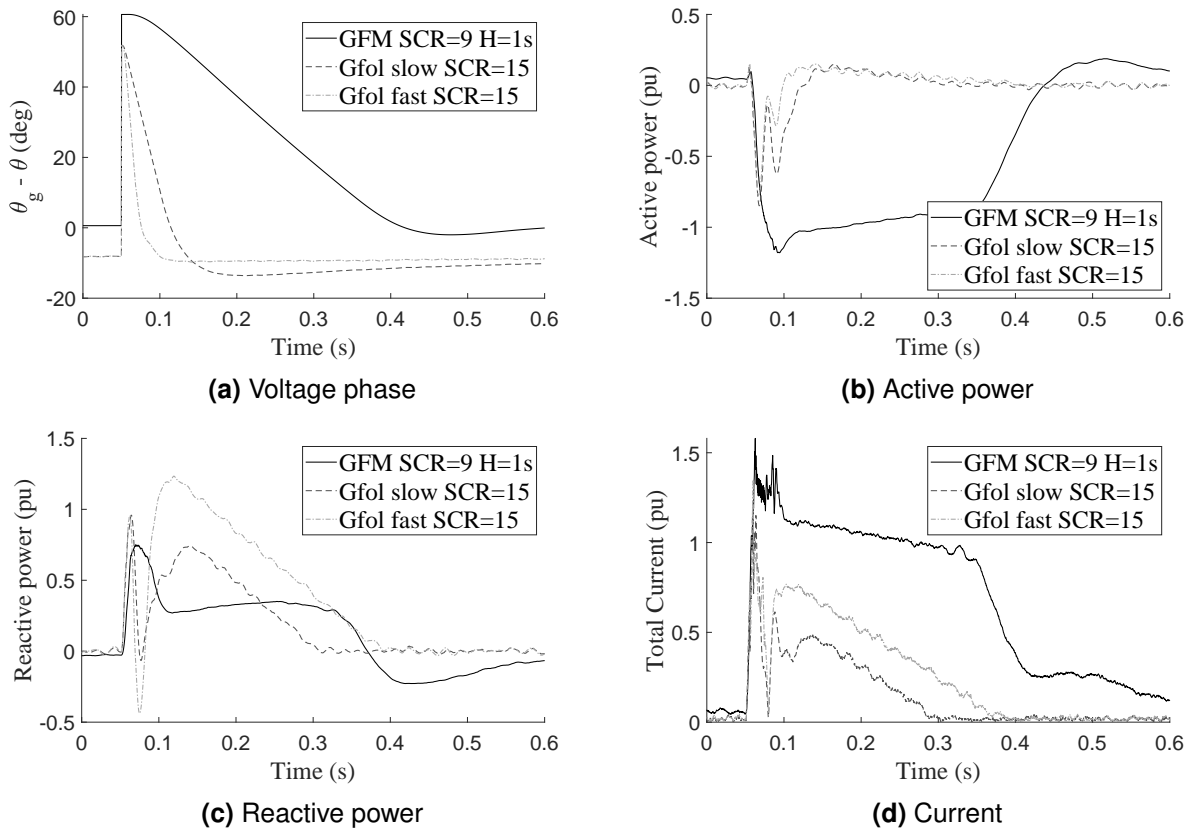


Figure 2.15: VSC response to a 60° phase jump²²

²²In this simulation we consider $m_p = 0.015$ and $t_{fp} = 30$ ms, which gives an equivalent inertia $t_{eq} = 1$ s.

Power oscillations and damping. This feature is partially covered by art. 29 in the HVDC code [12] which includes a procedure to investigate possible adverse interactions between the new installation and the grid, and constraint the owner to provide mitigation measures for connection. In RfG, art. 20.3.b also refer to “adequate” damping of active power oscillations [11]. In this regard, the GB grid forming code (GC0137 [65]) adds “the damping shall be judged to be adequate if the corresponding Active Power response to a disturbance decays within two cycles of oscillation” and requests the submission of “a Network Frequency Perturbation (NFP) Plot and Nicholls chart (or equivalent)”.

It must be noted that in the HVDC code, art. 29 is about intrinsic system damping, while art. 30 on power oscillation damping (POD, resp. power system stabilizer, PSS, in RfG) and 31 on SSR (sub-synchronous resonance) are about dedicated, outer, controllers. As discussed in section 2.2.4, some grid forming controls might exhibit low damping at lower frequency and proper tuning of inner loops might need further investigation. Other loops to provide additional damping to inter-area modes for instance (< 2 Hz) can be added to IBR independently of their synchronisation mechanism. In this sens, GC0137 includes the Defined Damping Active Power to compensate for 1Hz grid oscillations [65].

In addition, regarding current limitation, GC0137 indicates that the plant “shall be designed to ensure a smooth transition between voltage control mode and FRT mode in order to prevent the risk of instability” and that the “owners are required to both advise and agree with The Company the control strategy” [65]. Finally, in the future, some requirements might also be defined in terms of the active injection of controlled oscillating power with the growing concern on forced oscillations [71].

Negative sequence. In France HVDC system are simply requested to remain connected and stable for a maximum negative sequence component of 2% of the AC voltage at the PCC (either continuous or short term basis). Injection limits are defined in the harmonic requirements.

Now, when we say that a grid forming unit (SM or a VSC) behaves as a voltage source, we usually mean a PS and fundamental frequency only voltage source. As a consequence, it has been said that a grid forming unit is expected to naturally contribute to power quality through the absorption of harmonic and unbalanced currents [22].

However, as discussed in section 2.2.2, while the frequency dependent impedance of a synchronous machine beyond a few hertz is given by construction [72], for a VSC it will depend on the control bandwidth (around 100-150 Hz for the applications considered in this work).

Figure 2.16 shows the voltage amplitude and reactive power of a VSC when submitted to 3% of grid voltage permanent unbalance to illustrate that the synchronisation mechanism has low impact on the capability of the converter to counter 100 Hz voltage oscillations.

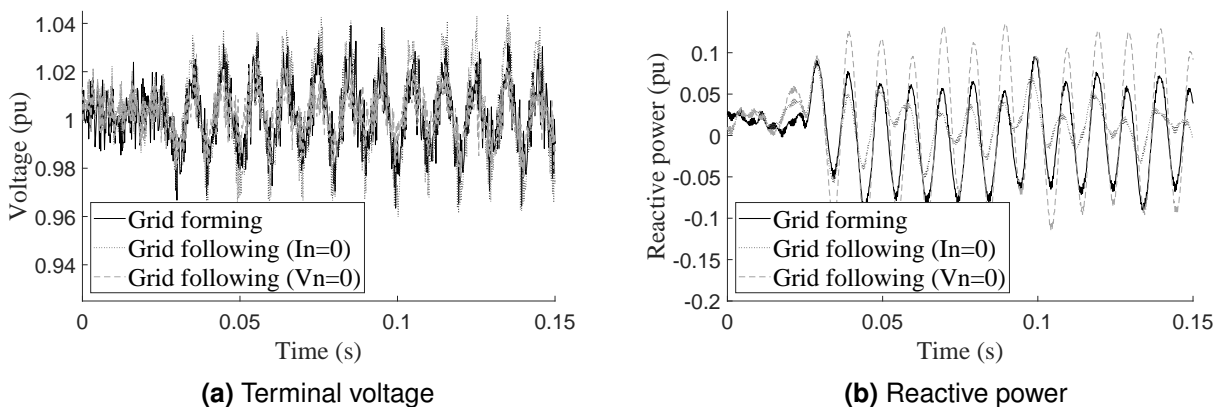


Figure 2.16: 3% of grid voltage permanent unbalance

We compare three scenarios:

- Case 1: a grid forming control without any specific NS compensation strategy.
- A grid following control with two different strategies regarding the negative sequence (NS):
 - Case 2: without any NS control ($V_n = 0$), and
 - Case 3: with a NS current compensation loop ($I_n = 0$).

Although slightly difficult to appreciate in the proposed illustration, a VSC with a classic grid forming control (case 1) behaves similarly to a grid following converter in the same conditions (case 2). They both can reduce voltage unbalance depending on the system impedance and control bandwidth when compared to NS current compensation techniques (case 3). The value of the DUT internal NS impedance can be adapted with control independently of the synchronisation mechanism. This is, Z_{inv} in Fig. 2.17 can be very high to reduce the NS current as done in Case 3, but it can also be set to zero by imposing a PS voltage only at POI. If no compensation strategy is considered (case 2), Z_{inv} depends on the PS control and the filter impedance. Bounds of this value could be defined for any VSC, which roughly speaking implies requesting a passive behaviour.

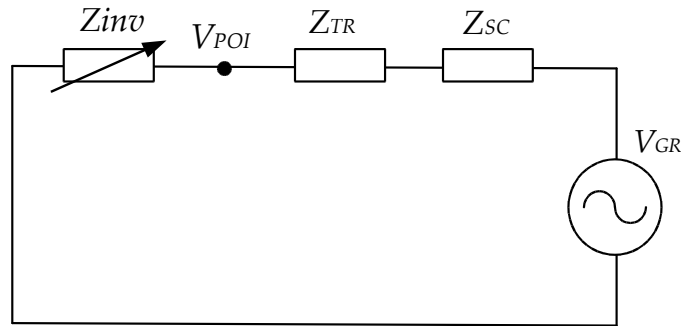


Figure 2.17: Terminal voltage

However, the limited current capability of the power electronic devices also implies that prioritisation strategies are required regarding fundamental, NS and harmonic currents even in steady state, which can be achieved by dedicated outer controllers that could limit the distortion on the current by acting in the voltage if necessarily.

Harmonics. The only reference to the topic at EU level is made in art. 34 of HVDC code to establish that TSO must provide to the owner a grid model for control design. Then, injection limits are defined at national level. We could however highlight that at high frequency, beyond the control bandwidth, the converter behaviour at its terminal is dominated by the physical components so should not differ much from a grid following. In France, IBR must withstand the presence of grid voltage background harmonic, without injecting adverse harmonic, which is already challenging to ensure in the general case. Non contractual harmonic voltage thresholds are indicated in the technical appendices of the CART (*Transmission Network Access Contract, or Contrat d'Accès au Réseau de Transport*) and producers must comply with current emission limits established as a function of the installation nominal power (limited to 5% of the system SCP), the nominal voltage (U_n) and given coefficient (K_n) between ranks 2 and 40, according to eq. (2.2) in order to limit total harmonic distortion (THD).

$$I_n = K_n \frac{S}{\sqrt{3}U_n}. \quad (2.2)$$

2.5. System services and technical capabilities in grid codes

With the deregulation of the electricity sector, the responsibility of power system security was left to TSO, even though the main resources to ensure it belong to the producers. Hence, in addition to grid connection requirements regarding the dynamic behaviour of the installations when submitted to disturbances, ancillary services²³ were defined, standardised and contractualised in order to maintain the voltage, in amplitude and frequency, within acceptable limits around the nominal values. We refer to the frequency and voltage regulation services, but we could also quote system restoration.

However, stable system operation relies on other underlying properties of power sources that were taken for granted until IBR started to replace SM. As an extension of the previous approach, the definition of new services, sometimes referred to as stability services, as a consequence of the formulation of new system needs has been widely discussed in the literature, and even deployed in some countries [51, 74, 75]. After defining grid forming as a set of technical capabilities that enable the provision of synchronisation services in section 2.4.2, we now focus on the definition of the latter.

Synchronisation services can be seen as a subset of the new stability services, the ones related to the synchronisation of generating units, with a direct impact on the angle stability and represented by the grey area in Fig. 2.18. In this section, we propose to formalise them within the framework of traditional and emergent regulation services, but also some CNC requirements. To this end, Appendix A briefly recalls how traditional ancillary services such as the Frequency Containment Reserve (FCR), the Frequency Restoration Reserve (aFRR) and the Replacement Reserve (RR), are today ensured. Then, section 2.5.1 comments on new services that have recently emerged in countries with high share of IBR, such as the FFR [75], but also other non-frequency ancillary services²⁴ [73].

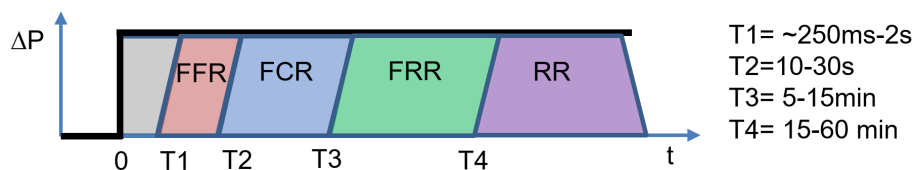


Figure 2.18: New and traditional frequency regulation services

We insist on the differentiated scope of the following three stages:

- technical capabilities related to ancillary services as defined in CNC,
- services provision rules which often detail further the expected dynamic performances and entail capacity reservation,
- certification and performance control.

Indeed, the required amount and specific performance of each service might be system dependent, including local considerations within a given network. However, the description of the technical capability to provide such a service can and should be more generic to enable coordination through standardisation and specification in grid codes applying to wide areas such as European CNC.

Although an evaluation of the system needs and an in-depth assessment of suitable procurement mechanisms are out of the scope of this work, we do hope to provide some technical background to inform decision-making on those topics as will be discussed in section 2.6. Moreover, Chapters 5 and 6 define KPI for the quantification of synchronisation services in order to bring light on the challenges and possibilities in terms of performance control of grid forming units.

²³“ancillary service means a service necessary for the operation of a transmission or distribution system, including balancing and non-frequency ancillary services, but not including congestion management” [73]

²⁴“non-frequency ancillary service means a service used by a transmission system operator or distribution system operator for steady state voltage control, fast reactive current injections, inertia for local grid stability, short-circuit current, black start capability and island operation capability” [73]

2.5.1. New stability services

Taking advantage of the speed of action of IBR, new stability services basically add a faster layer to the existing ancillary services to achieve tighter frequency and voltage control.

2.5.1.1. Synthetic Inertia

More than a requirement or a service, synthetic inertia was conceived as a specific technical solution, i.e. a control law attempting to reproduce inertial response of a SM by computing an active power modulation as a function of the filtered frequency or RoCoF. As a consequence, it is poorly suited to service and technical capability specification. Moreover, the delays associated to the frequency measurement lead to an unsuccessful inertia emulation. Therefore, some operators consider **synthetic inertia as a form of FFR** [76]. Its specificity has been defined in the literature as a function of the implemented control such that if the control for providing FFR is proportional to RoCoF it will be called Inertia-Based Fast Frequency Response [77]. As discussed before, we should avoid using control laws as a discrimination criteria between services. Still, we consider synthetic inertia here separately from FFR as an article was initially dedicated to it in EU CNC and this solution is investigated in WP 4 and 5 demonstrators within the framework of the OSMOSE project [45].

Technical capabilities in CNC. As indicated in section 2.2.3, article 14 of the 2016 HVDC CNC [12] defines synthetic inertia as a non-mandatory non-exhaustive requirement at the EU level, which is not included in the current CNC French implementation. Depending on the performances specified at national level, this capability can be provided indistinctly by grid forming and grid following units, or rather exclusively by former ones. This is similarly to the case of the fault current injection.

Service rules in other countries. Hydroquebec has been requiring synthetic inertia from wind plant for several years [78], mainly consisting in a power boost for a few second following a frequency drop that is not required in case of over frequency. ONS from Brazil is another example [75].

2.5.1.2. Fast frequency response

In a more general way, the decline of the synchronous inertia with the integration of IBR can be compensated, to some extent, by the faster deployment of active power reserves. Several definitions of the FFR exist and in this work we consider the one proposed by AEMO in [79]: "Any type of rapid active power increase or decrease by generation or load, in a time frame of less than two seconds, to correct supply-demand imbalances and assist with managing frequency".

Technical capabilities in CNC. FFR has not yet been defined in EU CNC, but the overlap with the current specification of synthetic inertia might need to be handled.

Service rules in other countries. National Grid (NG), ERCOT, EirGrid, PJM, Amprion and CEN have defined services for the provision of FFR. Following enhanced frequency response (EFR) 2016 tender with 200 MW of batteries, NG designed two new FFR products with an activation time of 1 second but different frequency delivery ranges [80]:

- dynamic containment (DC), and
- dynamic moderation (DM).

Eirgrid's FFR service requires an activation within 2 seconds, while ERCOT fastest product is as quick as 250 ms. Depending on the services, the sustain times are also variables, more than 8s for EirGrid, 5 min for CEN and 15 min for ERCOT [75]. Depending on the TSO the service might be symmetrical or mostly dedicated to over-frequency as for Amprion [75].

However, attention must be paid to the fact that some assets are connected to the distribution network and constraints might exist on the minimal activation time to ensure the good performance of existing anti-islanding mechanisms. In France, for instance, distribution system operators (DSO) do not allow FCR suppliers connected to their grid to start deploying the response before 1.5 seconds [81] which might prevent them to participate to the provision of future FFR services.

Service provision in other countries. Eirgrid, NG and ERCOT procure FFR through the energy market. They use strong criteria for qualifying and assessing the performance of a resource. Part of PJM's FFR service remuneration relies on the performance of the resource including its dynamics.

Performance control. SCADA measurements might be insufficient to monitor FFR services. In MIGRATE WP2, Wide Area Monitoring System (WAMS) were proposed [82]. In this work, phasor measurement unit (PMU) will be considered (see Chapters 5 and 6). For NG, DC is a day-ahead auction (£ per MW per hour) controlled both on operational metering data sent every second to the SO and on hourly performance monitoring files that contains data sampled at 50 ms [83].

EirGrid assesses the performance of its DS3 FFR service on relevant incidents (frequency below 49.7 Hz or above 50.3 Hz), evaluating both the active power delivery in terms of level and dynamics (tolerance of 10% of the expected power at each sample point) and the energy loss in the period [T+10s : T+20s] (the energy provided during time [T : T+10s] has to be greater than the energy lost in [T+10s : T+20s]) [84]. Data has to be sampled at 20 ms or less with an accuracy of 2ms maximum for the time of synchronisation of the measurements [85]. Payment on a period is based on a calculation of the available FFR volume of this same period [86].

2.5.1.3. Dynamic voltage support

Analogously, a faster voltage support service has been proposed in some countries to cope this time with the decline of SCP. The dynamic reactive response product proposed by EirGrid can be quoted as an example. It is defined as "the ability of a unit when connected to deliver a reactive current response for voltage dips in excess of 30% that would achieve at least a reactive power in Mvar of 31% of the registered capacity at nominal voltage. The reactive current response shall be supplied with a rise time no greater than 40 ms and a settling time no greater than 300 ms" [87]. This kind of service generally includes extra capacity (PQU diagrams beyond minimal CNC requirements.)

2.5.1.4. Providers of new stability services

IBR such as WPP, PV and ESS are particularly adapted to FFR and fast reactive power response services. In the first case, we can also add demand side response and some resources are more suited to sustain the service for a longer time than others [79]. In South Australia, AEMO requires all generation connected after July 2017 to provide inertia or fast frequency response as specified in [88]. In addition, IBR can provide fast voltage regulation at near-nominal voltage, but produce little or no additional short circuit current above the nominal value during a low voltage condition.

2.5.2. Definition of synchronisation services

The creation of new services might in some cases lead to a redefinition of the existing ones as illustrated in Fig. 2.19, but synchronisation services remain necessary at all times to fill the gap between 0 and the time when traditional and new ancillary services are deployed (grey zone), i.e. they concern the transient and sub-transient regimes. We have previously referred to them as voltage amplitude and frequency smoothing services, and they can be related to inertia and system strength contribution [89]. On top of it, we add the notion of synchronising or phase jump power that has been receiving increasing attention [51]. Corresponding technical capabilities are not yet defined in EU CNC but they should soon appear with the definition of the grid forming capability accordingly to considerations discussed in section 2.4.2. Some of them might in fact imply service deployment (as for the fault current injection), or not (as FSM mode requirement for PPM, see Appendix A).

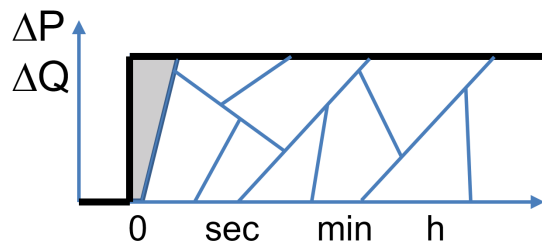


Figure 2.19: Synchronisation services act before traditional ancillary and new stability services

2.5.2.1. Inertial response

In addition to ensuring frequency regulation some TSOs monitor system inertia at different time horizons and define minimal requirements. A consensus has not been reached in the literature on whether the known synchronous, electrical or true inertia should be considered as a frequency regulation service or not [51]. In this work and in accordance with [73], we have made the choice to separate them because the initial RoCoF must be contained locally. Having enough inertia is a prerequisite for deploying balancing services on other devices. An adequate geographical distribution of the inertia is needed to ensure that the frequency remains measurable for regulation but also protection purposes, and to improve system stability by slowing down the propagation of electromechanical waves following a severe transient. It must be noted that inertial response cannot be provided by grid following sources and it is hence directly linked to the VSC synchronisation mechanism.

In terms of provision, different approaches exist. For instance, in case of an inertia shortfall AEMO directly advises asset owners. On the other hand, EirGrid has designed a dedicated service in the market, the SIR (Synchronous Inertial Response) [75]. The idea is to remunerate the inertia contribution to the system with a mechanism that promotes assets with a high ratio (Kinetic Energy/Minimal Power). It is a way to moderate the impact of the synchronous generators started especially for the provision of inertia on the overall electricity price. NG through its stability pathfinder project launched a tender process to provide inertia in the system [90], which is now open to IBR (GBGF-I plants).

According to the classification of grid forming units proposed in section 2.4.2, type 3 and 4 units can naturally²⁵ but continuous operation in grid forming should be further investigated. provide inertial response, within the installation capability, available headroom and energy. Different mechanism could be investigated in the future for capacity and energy reservation to face any scarcity risk in specific periods. However, enough installed capacity must be ensured with anticipation through CNC requirements as currently done with critical services such as (L)FSM.

²⁵A rotating machine cannot be prevented from providing inertial response if synchronously connected to the grid. A VSC interfaced BESS can provide inertial response through control settings without extra cost.

2.5.2.2. Fault current

As discussed in section 2.3.3, fast fault current injection, within the installation capability, is already part of EU CNC, and it is mandatory in many countries. In France, this requirement applies to generating units type B, C and D. As aforementioned, grid forming units just respond faster than grid following ones, to which a small delay (40-60s) could remain authorised justified by the technical incapability of such units to provide immediate response. In addition, reactive power prioritisation might be initially not possible (neither desirable) for grid forming units and should not be requested. In general, no continuous monitoring is performed on this kind of mandatory services, but they are carefully validated during the connection procedure. If deviations are detected in operation following the analysis of specific events, corrective actions can be requested to ensure return to compliance.

2.5.2.3. Synchronising power

Analogously, a technical requirement specifying synchronising power is likely to imply service deployment, within the installation capability and available headroom. It can be naturally provided by grid forming units type 2, 3 and 4. Justified by technical incapability due to the intrinsic lack of the required energy buffer, type 1 units could be exempted from providing this service. Then, dedicated provision mechanisms for synchronisation services could eventually ensure power and current capacity reservation. Event-driven performance assessment could be conducted following line switching.

2.5.2.4. System strength

According to some sources, such as MIGRATE D2.1 [38], from the system perspective, the system strength measures the “stiffness” of the grid, related to the impedance from a bus to the rest of the system, during non-fault conditions. It can be quantified by:

- System Impedance (in Ohms or per unit),
- System Strength (in MVA). It is at a selected bus, inversely proportional to the impedance from the bus into the grid.

From the sources perspective, it characterises its capability to “resist” to voltage amplitude fluctuations in response to changes in active and reactive loading. Provided that the modulated voltage is kept constant and the converter current remains below its maximum value, its contribution to system strength is then related to the equivalent impedance, which includes the filter and transformer [22].

However, in other references, such as AEMO²⁶, the system strength, characterises the voltage behaviour at a given location in the power system when facing small and large disturbances, so including current limitation mode, but also the steady state. As explained in section 2.2.2, in this work system strength relates to having a low internal impedance and must be separated from the behaviour in current limitation, but also from the services provided in steady state (primary and secondary voltage control in France, or other modes such as constant power factor or reactive power control).

All types of grid forming units defined in this work (from 1 to 4 according to section 2.4.2) can provide system strength, within the installation capability and available headroom. In France, the provision of system strength could be considered mandatory for grid forming generation units larger than 50 MW as they are already obliged to provide primary voltage control. Other mechanism could be foreseen to encourage the transient operation beyond the nominal reactive power capacity limits in force in CNC such that system strength contribution is available even at maximum steady state reactive power.

²⁶“It is the capability of the system to control and stabilise voltage both after a disturbance and in steady state operation. It is proportional to the fault level. A certain amount of system strength is required to allow voltage to remain stable and stay within a certain range, to ensure a stable operation of IBR and generator control systems, to avoid commutation failure in HVDC and to allow protection equipment to work correctly.” [91]

2.5.2.5. Needs and providers of synchronisation services

Sufficient inertial response is necessary at all times to smooth frequency variations and allow for its measurement by any type of unit that could presently provide market-based balancing services such as grid following units or loads, but also by more critical protection systems such as FRT of IBR and LFDD. A threshold of 2Hz/sec has been proposed in [22], which allows frequency to be accurately measured in a reasonable time frame. System strength (low impedance) is required for power quality and to limit stability risk in classical VSC or HVDC-LCC (line commutated converter, thyristor based) commutation failure, since a grid following IBR detecting an inaccurate voltage phase angle after a fault might inject current incorrectly and thus amplify the instability (see section 2.2.4). Hence, regions with a large number of IBR connected in grid following might require higher levels of system strength. Natural providers of synchronisation services are SM. Some investments in synchronous condensers can allow to maintain a certain level of inertia and strength in the system, but also fault current. Nevertheless other measures can be taken like committing additional generation units (ERCOT, CEN) or limiting the size of the largest contingency (EirGrid, Hydro Quebec, Nordic) [75]. It has been shown that grid forming controls allow IBR to emulate the synchronising power, inertial response and system strength of a SM if the current limit is not reached, and can therefore participate in the provision of synchronisation services, unlike the resources controlled in grid following which at best are able to provide Inertia-Based Fast Frequency Response (IB-FFR also called synthetic inertia).

Moreover, it has been proved that inertial response can be provided from the kinetic energy stored in wind turbines, at least at high wind speed [69]. In more constrained scenarios, the IBR contribution could be significantly reduced to almost zero or curtailed in case of energy unavailability (low wind or depleted storage) or current limitation. For HVDC system, only one side could provide inertial response while drawing the energy from the other side. The relevance of this response in embedded HVDC systems remains to be further investigated.

UK stability pathfinder project aims to bring stability services from the market in UK electrical grid in the near future including inertia, voltage control and short-circuit capability [90].

2.5.3. Synchronisation services as non-frequency ancillary services

EU Directive 2019/944 on common rules for the internal market for electricity and amending Directive 2012/27/EU [73] defined non-frequency ancillary services including steady state voltage control, fast reactive current injections, inertia for local grid stability, short-circuit current, black start capability and island operation capability (in yellow). In this work, we propose to add the synchronisation services (in blue) to this list but taking into account the different time scales involved and splitting voltage control in normal and current limitation conditions, within and beyond nominal rating (see Fig. 2.20).

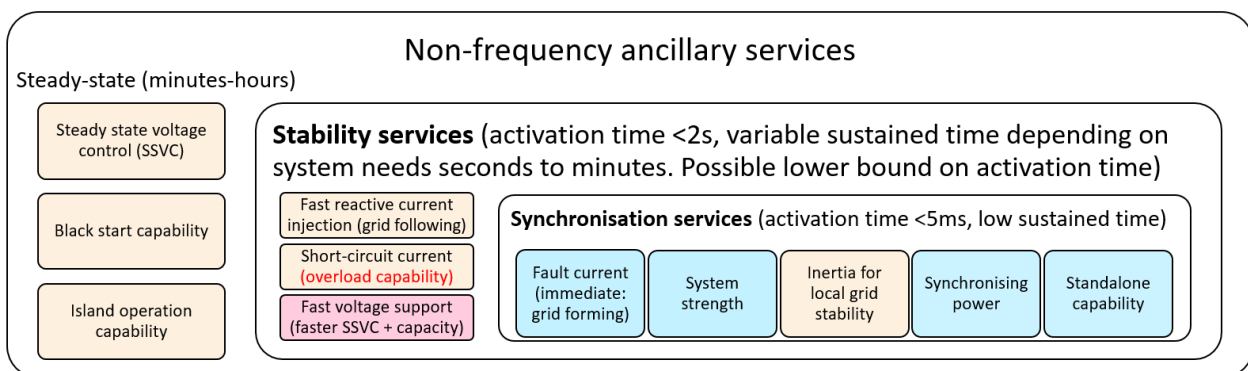


Figure 2.20: Defining synchronisation services as new non-frequency ancillary services

2.6. Recommendations for grid code implementation

2.6.1. Defining grid forming capability as a connection requirement

First of all, we would like to emphasise that marked-based services and mandatory capability provision in grid connection requirements are not necessarily exclusive notions:

- on the one hand, some connection requirements do imply obligation to deploy a specific response, such as the fast fault current injection, LFSM-O, POD or even primary voltage control;
- on the other hand, the mandatory provision of FSM capability does not imply any obligation to participate to PFR services. It just facilitates certification and ensures that enough capacity is installed and available at all times independently of the scheduled energy mix.

According to [73] TSO (and DSO) "shall procure the non-frequency ancillary services needed for its system in accordance with transparent, non-discriminatory and market-based procedures, **unless the regulatory authority has assessed that the market-based provision of non-frequency ancillary services is economically not efficient and has granted a derogation**. In particular, the regulatory framework shall promote the uptake of energy efficiency measures, where such services cost-effectively alleviate the need to upgrade or replace electricity capacity and support the efficient and secure operation of the transmission system". Indeed, as illustrated in section 2.5.2, market-based mechanisms to procure ancillary services implies much more than just technical capabilities. In addition to revenue streams, they usually lead to contracting and performance control (with the associated infrastructure deployment²⁷), and often penalties. The suitable approach for stability services provision should be the result of a cost benefit analysis including all these features.

In general, the services listed in the first category (mandatory in at least some national implementations of CNC) are known to have no significant impact in the installation design and operation (and therefore low to no cost). In addition, at least two technical drivers have led in the past to the enforcement of some non-frequency ancillary services provision as grid connection requirements:

- Criticality: scarcity would jeopardise power system security.
- Need for geographical distribution: while the frequency is said to be a global variable (at the time scale of balancing services), the voltage is not. At the same time, grid topology, AC power flow calculations and network constraints are difficult to take into account in market-based mechanisms. Without them, some regions might be dangerously deprived of ancillary services which would lead to system collapse following plausible disturbances. Hence, a scattered distribution of resources is statistically achieved by enforcing mandatory provision to a category of assets. If this measure is not enough, then TSO must install dedicated devices.

In this Chapter we have demonstrated that the synchronisation services fulfil both of these conditions: they are critical for stability and must be provided locally. Therefore, the deployment of enough grid forming capability should be ensured through grid connection requirements and harmonised at EU level through CNC [92]. We insist that no overload or capacity reservation is in principle associated to the grid forming capability, neither the provision of traditional ancillary services such as primary voltage and frequency regulation, which must be decoupled. Finally, depending on the category of the unit, only a subset of synchronising services shall be provided. All grid forming units shall contribute to the system strength and fault current but type 1 units are exempted from providing synchronising power. Moreover, many existing grid forming controls include a settable parameter to configure the inertial response, such that the technical capability of providing say 5 MWs/MVA in specific conditions does necessarily mean at this stage that the unit must continuously operate with this value.

²⁷For example, GC0137 requests a 1 MHz resolution for Grid Forming Plant tests. In addition, a Grid Forming Plant "shall be equipped with a facility to accurately record the following parameters at a rate of 10 ms: system frequency with a high immunity to grid phase jumps, RoCoF, Grid Phase Jump" [65] for performance monitoring.

2.6.2. Deployment trajectory

Now that four types of grid forming capabilities have been clearly defined through a set of technical specification and the technologies that are able to provide them have been identified, the next question is: which one of them **should** be required to provide grid forming capability? Although the evaluation of system needs is a subject for future work, we advance some recommendations to **progress on the IBR immunity with low to no impact on the installation design and to limit the need for dedicated devices to fulfil stability needs**. For the purpose of illustration, Fig 2.21 shows system strength "margins"²⁸ in the French network considering a given 2035 scenario [94] to show that under conservative hypotheses, low short-circuit levels might appear in spread locations.

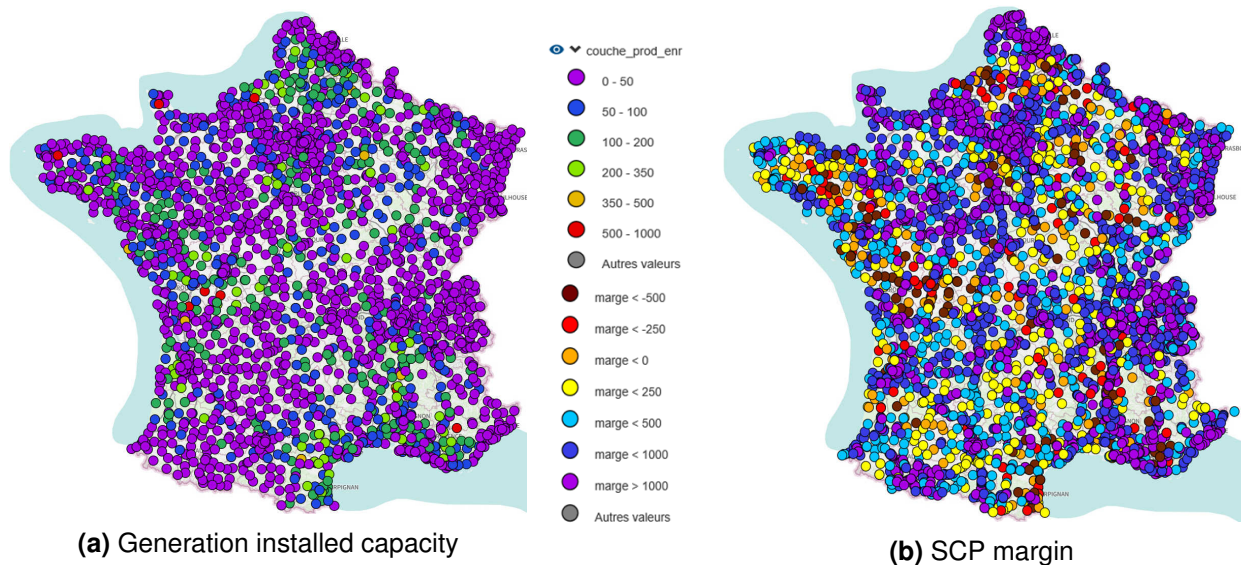


Figure 2.21: SCP margins in the France network for a 2035 scenario

1. Type 1 grid forming capability (sometimes referred to as "only AC voltage source" to exclude constraints in terms of active power injection), should be required from all new type C and D PPM and HVDC systems as soon as possible to face local decline of system strength.
2. Type 2 grid forming capability should be required from units naturally presenting a small energy buffer (between, a few hundreds of ms and 1s) in the same category. Some incentive mechanism could be deployed to upgrade type 1 grid forming units into type 2.
3. Type 3 grid forming capability should be required from ESS. As demonstrated in this project, it is technically feasible to provide this capability with off-the-shelf equipment without converter oversizing or the installation of additional devices. In addition, deliverable D3.4 [95] shows that the provision of inertial response on top of frequency regulation (FCR and FFR) and other flexibility services (schedule tracking) using the remaining non-allocated capacity has no impact on the main revenue streams. Finally, Type C and D WPP could also be requested to demonstrate type 3 grid forming capability, even if they operate at near-zero inertia at a first stage, leaving the possibility to review the operational agreement in the future if a system inertia decline proves to jeopardise power system security, which can be limited to specific periods of time.
4. Type 4 grid forming capability is already naturally provided by SG, including transient overload (current) capacity which might still be required to face fault current shortfall in some locations.

²⁸A way to compute the hosting capability of a node in terms of system strength in a meshed network with several IBR, consists in subtracting the SCP "consumed" by the connected VSCs, based on their minimal SCR (MSCR, here supposed equal to 5), to the system available fault level, i.e. the SCP without those units [93]. The SCP at each node for the different cases has been determined using RTE short-circuit calculation tool.

3. Implementing grid forming capability on off-the-shelf equipment

In this Chapter, we first recall the demonstrator description and objectives in section 3.1 while the main technical specifications defining the control design are presented in section 3.2. Then, section 3.3 explains the selected grid forming control and shares experience on its implementation in off-the-shelf equipment. Afterwards, section 3.4 provides the high level control design details and section 3.5 concludes discussing the expected behaviour of the installation for different control setting and operational points based on simulation results. Further details are included in Appendix C.

3.1. RTE-Ingteam demonstrator description

RTE-Ingteam demonstrator consisted in a 1 MVA rated power fully containerised hybrid energy storage system (HESS) as showed in Fig. 3.1, which included:

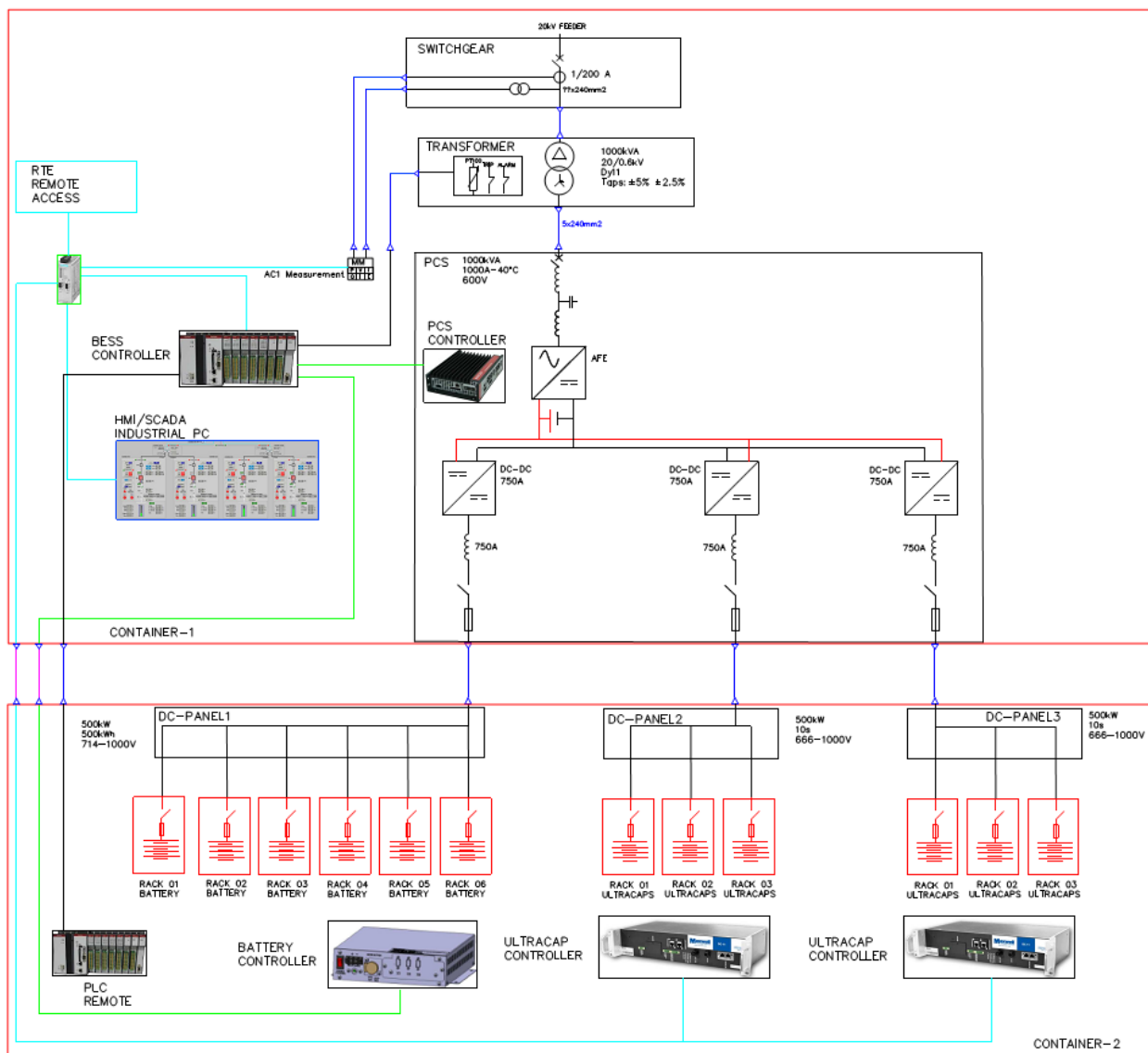


Figure 3.1: RTE-Ingteam demonstrator diagram

- four lithium iron phosphate (LFP, for *lithium ferrophosphate*) battery racks (0.5 MVA 60 min),
- two times three ultra-capacitor (UC) racks for a total of 1MW-10s,
- 3 x 500 kW DC/DC converters,
- 1 MVA low voltage (600V) AC/DC converter (with a grid forming control),
- 1 MVA 0.6/20 kV transformer (Dy11, with a short-circuit impedance of 6.2%),
- a medium voltage switchgear cubicle,
- converter water cooling and climate system,
- control and protection system,
- telecommunication and remote access,
- a human-machine interface (HMI) and monitoring system.

The installation design was decided in the beginning of the project as a trade-off between ESS size and cost while being able to test the provision of grid forming capability taking into account different configurations of the DC side:

- In a classical multi-service battery ESS (BESS) setting, similar to the one considered in the EPFL campus (see Chapter 6). The objective is to assess the different impacts of the provision of synchronisation services by a grid forming unit on top of more classical ones. The results on this regard will be discussed in deliverable D3.4 [95] only for EPFL demonstrator since RTE-Ingteam demonstrator could not ultimately be operated grid-connected (see Appendix G).
- In a synchronous condenser-like setting, where UC are used as the only source of energy to provide synchronising power and inertial response. Any other energy intensive services, including primary frequency regulation (PFR), are excluded.
- In a multi-device setting. This time the BESS is seen as a primary energy source that could represent any other resource providing exclusively active power to the system or also balancing services, such as a PV or WPP. In either case, the synchronisation services are provided by the UC. In this demo, power sharing law between devices is in-built in the local DC controller as they share the same AC/DC converter. It cannot be modified through a master controller as it is proposed in OSMOSE WP 4 where each device has its own interface.

The HESS was installed at the 20 kV bus bar of the Castelet substation, in the south of France, which as shown in Fig. 3.2 includes:

- a 63 kV line to Aix Les Thermes substation,
- a 63 kV line to Tarascon-Ussat substation,
- a 10 MVA 63/20 kV transformer dedicated to a power hydro generation unit,
- a 20 MVA 63/20 kV transformer for the power supply of an industrial consumer with underground cable, where the demonstrator was connected.

Transient fault recorders (TFR) were installed at the 20 kV feeder and at the medium voltage switchgear cubicle to isolate the contribution of the demonstrator. In addition, the power conversion system (PCS) included a TFR at converter side. In order to analyse the impact of the system on the grid, special attention must be paid to the synchronisation of the different measurement units.

Reminder of the RTE-Ingteam demo objectives. This Chapter brings proof of the technical feasibility and economic viability of providing grid forming capabilities with a commercial HESS by:

- Validating the performances of one possible implementation of a grid forming control and a current limitation strategies in an off-the-shelf AC/DC converter. In this project we chose the filtered droop approach with Threshold Virtual Impedance (TVI) as they have been already tested in a laboratory environment within the framework of the MIGRATE project [31].

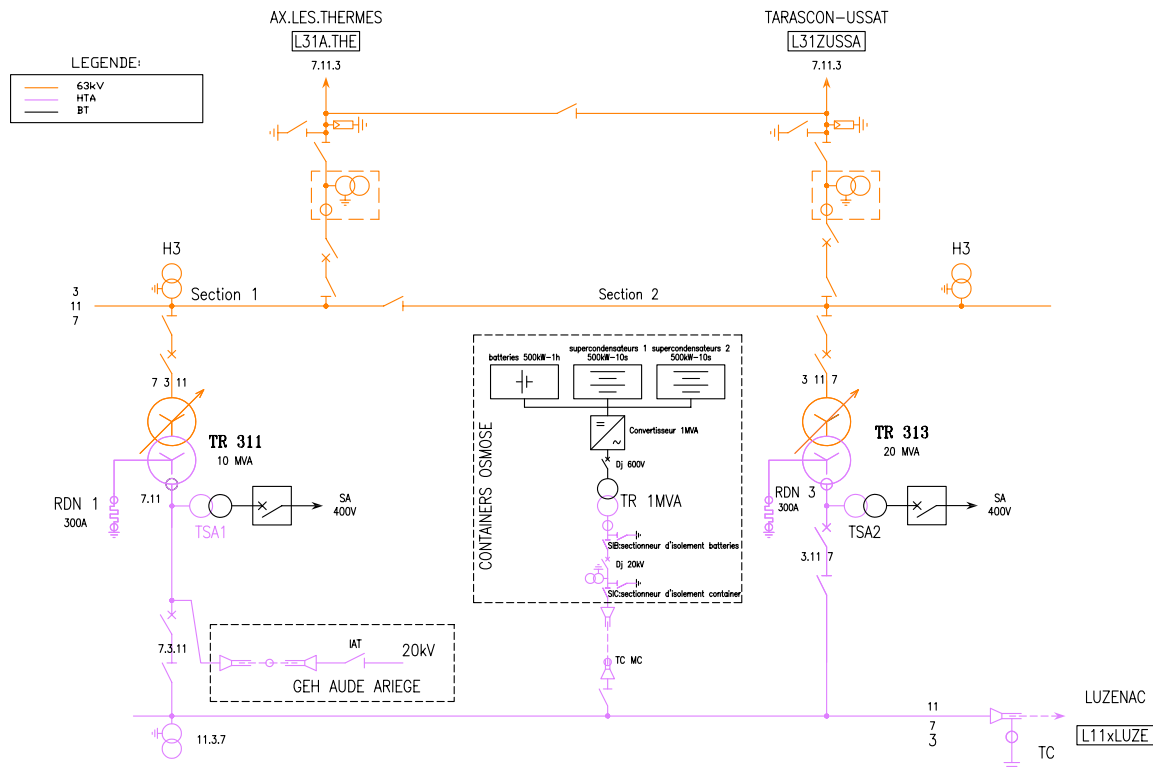


Figure 3.2: RTE-Ingteam demonstrator connection in the Castelet substation

- Assessing the capability of the AC/DC grid forming converter to provide balancing and flexibility services, such as primary frequency control or peak shaving on top of synchronisation services.
- Ensuring stable association of the grid forming function with different DC side energy management strategies between the UC and the BESS, as well as the possibility to affect one specific AC service to a dedicated DC storage device. The idea is to allocate power intensive synchronisation services to the UC while the battery provides the long term ones.
- Testing the robustness of the developed controls when facing permanent unbalance, harmonics distortion and transient grid disturbances, including asymmetrical faults.

Contributions. To achieve those goals, we have published the following innovative solutions:

- Adapting the AC/DC converter grid forming control with additional constraints from the hardware limitation and from unbalance conditions of the targeted grid [96].
- Managing the DC side power sharing with DC/DC advanced controls associated to the active parallel hybrid connection of the different storage technologies (UC and batteries) [97].
- Conducting a performance assessment in a grid connected EMT benchmark [98].
- Proposing and performing a compliance validation procedure for the grid forming capability [99].

3.2. Technical specifications

In this section, we summarise the main requirements applied to the HESS and that were added to the technical specification package regarding the provision of the grid forming capability in a multi-service and multi-device framework. It is recalled that no oversizing is considered for this purposes and all the performance compliance criteria are defined up to the system capabilities in terms of converter current and DC side energy which are considered as a fixed input at the stage of control design [8].

3.2.1. Grid forming capability specification

As introduced in Chapter 2, we defined grid forming as the technical capability to self-synchronise and provide synchronisation services, and therefore it was verified by the compliance to the set of requirements defined in section 2.4.2 and recalled here, while highlighting project specific features:

1. **Standalone.** In this project, this capability must be proved during factory acceptance tests (FAT, see Chapter 4) but is not meant to be used in operation. The installation is requested to shutdown when the system operator open the 20 kV breaker inside the switchgear cubicle. Moreover, it shall be possible to energise the system from either the DC side or the AC side. Both options must be tested, but only energisation from the AC side is used in normal operation due to the specification of the undervoltage protection settings (that would for example prevent the HESS from soft starting as the voltage ramp up would be too slow).
2. **Synchronising active power.** The immediate active power following a grid voltage phase variation must be defined by the connection impedance and the disturbance size, but should be limited to the converter current capability.
3. **Inertial response.** The dynamic of the immediate active power injection following a grid frequency variation and of the recovery of the initial active power set point must be settable. Here, we consider two parameters: the transient grid forming time constant (T_{GF}) and the equivalent inertia constant H in MWs/MVA, as a function of the droop (m_p) and the active power filter (T_f).
4. **System strength.** The system must behave as if it has low transient and sub-transient impedance and immediately start to inject or absorb reactive power following a grid voltage amplitude variation.
5. **Fault current.** In case of voltage dips, immediate current must be provided according to the system impedance and limited to the off-the-shelf converter capabilities (no oversizing). During asymmetrical voltage dips leading to current limitation, it shall be possible to naturally prioritise the negative sequence current. Other prioritisation settings were investigated in this project and represent one of the main original contributions of this work [96].

Other project requirements, beyond grid forming capability in the sense that they could be applied to grid-synchronised VSC (PLL-based grid following) as discussed in section 2.4.4, included:

6. **Phase jump withstand capability** of at least 60° in accordance with [65].
7. **Adequate damping** in all performed tests.
8. **Permanent unbalance (NS):** within current capability, the converter voltage should be positive sequence (PS) only such that the unit contribute to reduce unbalance in the system voltage. As a consequence, it supplies unbalanced current to the load.
9. **Harmonic distortion.** In presence of grid voltage harmonic distortion the converter shall first remain connected. Then, it must absorb harmonic current to reduce the voltage distortion, up to its capability and while keeping the level of harmonic current within specified limits to comply with existing requirements in terms of harmonic current emission. More sophisticated active filtering strategies could be proposed to better fit the specific needs of a given location, but this topic lays out of the scope of the project.

Moreover, additional requirements are applied to the demonstrator and verified during FAT based on present requirements for the connection of non synchronous energy storage systems (ESS) in France [100]. They are consistent with latest recommendations for IBR at European level which suggest an alignment with other CNC in accordance to [101].

10. **Active power reference tracking.** CNCs do not enforce explicit requirements on reference tracking. Expected dynamic performances are comparable to current ESS or PPM grid connected applications, which are generally below 500 ms, with limited overshoot and settable ramp.

11. **Voltage regulation services.** The system must receive a voltage reference U_{ref} with a settable reactive power droop λ such that $U_{ref} = U + \lambda Q$, where U is the voltage measured at the point of interconnection (POI, converter terminals and secondary side of the transformer) and Q the injected reactive power. This is in fact not compliant with grid connection requirements since in general the voltage must be controlled at the point of common coupling (PCC, the primary side of the transformer), but an exception was made for the demonstration. In terms of dynamic performances, we consider requirements applied to HVDC systems in France: a settling time for the primary voltage control below 2 seconds (so faster than the traditional voltage regulation).
12. **Frequency regulation services.** The system must be able to participate to:
- Primary frequency regulation as enforced in continental Europe: a settable droop K_{FCR} , a response time below 30 seconds for any K_{FCR} , and an activation time below 500 ms.
 - Fast frequency response (FFR) with settable droop K_{FFR} and a response time below 2 seconds as defined in section 2.5.1.2.
13. **Low Voltage Ride Through capability.** The HESS shall have a LVRT capability with the phase-to-phase AC network positive sequence voltage drop profile reported in Fig. 3.3a, i.e. it shall withstand at least this voltage drop profile and continue stable operation without blocking, tripping or give rise to abnormal situations or alarms during symmetrical and asymmetrical faults. Moreover, the converter shall be able to withstand reclosing on permanent faults, symmetrical or asymmetrical, close to the HESS. In addition to the non-blocking, or non-tripping capability of the converter, the HESS protection system shall be coordinated for the same capability and shall be set to the widest possible technical capability of the HESS. For any fault outside the FRT capability the Contractor shall inform the Employer about:
- the blocking conditions (profile),
 - the deblocking conditions (voltage, duration),
 - the tripping conditions, and
 - the reclosing conditions (minimum elapsed time after tripping occurrence).
14. **Overvoltage ride through capability (OVRT).** The requested profile is shown in Fig. 3.3b

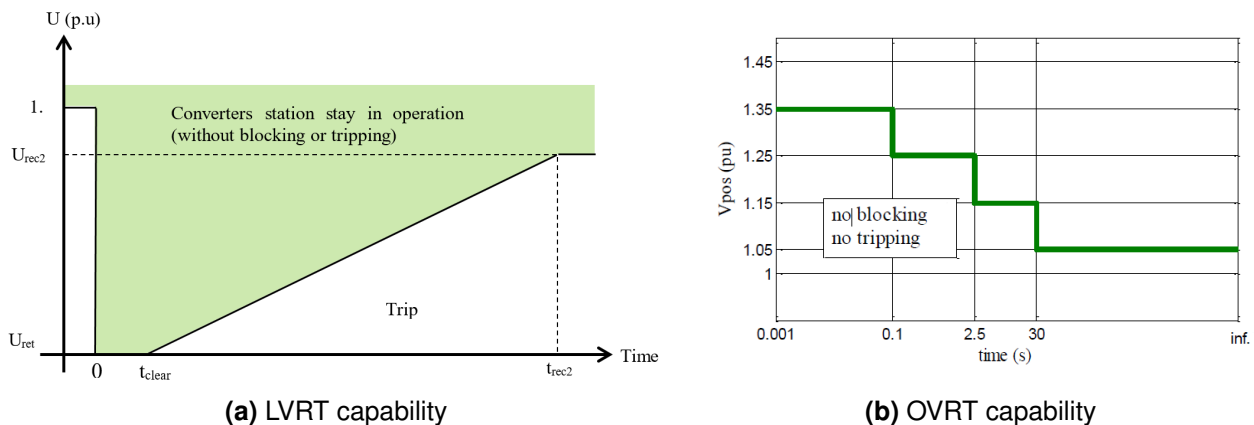


Figure 3.3: Low and Over Voltage Ride-Through capability requirements

15. **Fast active power recovery.** The system must exhibit a rise time to 90% of the reference active power in 150 ms, and a settling time (95% of the response) of 200 ms. The latter requirement might be slightly relaxed (up to 500 ms for stabilisation) when providing inertial response.

Finally, a standard grid following control must also be available as a backup, but it can only be activated by HMI command at the starting of the installation. The system must be designed to continuously operate in grid forming independently of the network conditions.

3.2.2. High level control specifications

16. **Multiservices.** It must be possible to manually define set points and ramps from the HMI or remotely from an external controller in order to include multi-service optimisation [102]. In this case, an active power reference signal, P_{set} , is computed by an external controller and can be sent at least every second through modbus protocol.
17. **Frequency regulation local controller.** In addition to power reference tracking and synchronisation services, the HESS shall be able to provide different balancing services in accordance with Fig. 3.4. The user must be able to enable / disable any combination of those services.

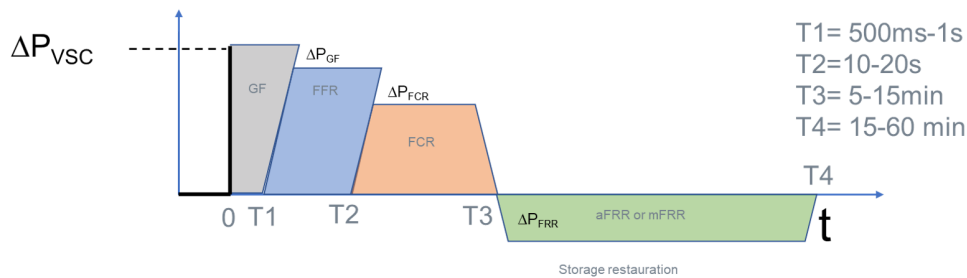


Figure 3.4: Active power related services - time scales

18. **DC side power sharing.** Following a grid event or a set point change the UC responds to the high frequency event, the contribution of each storage device should be settable through a power sharing criteria. In short, the expected power profile of the equipment is illustrated in Fig. 3.5. Synchronisation services must exhibit the same behaviour independently of the DC side energy source, whether the HESS is available, or only the UC or the BESS are connected.

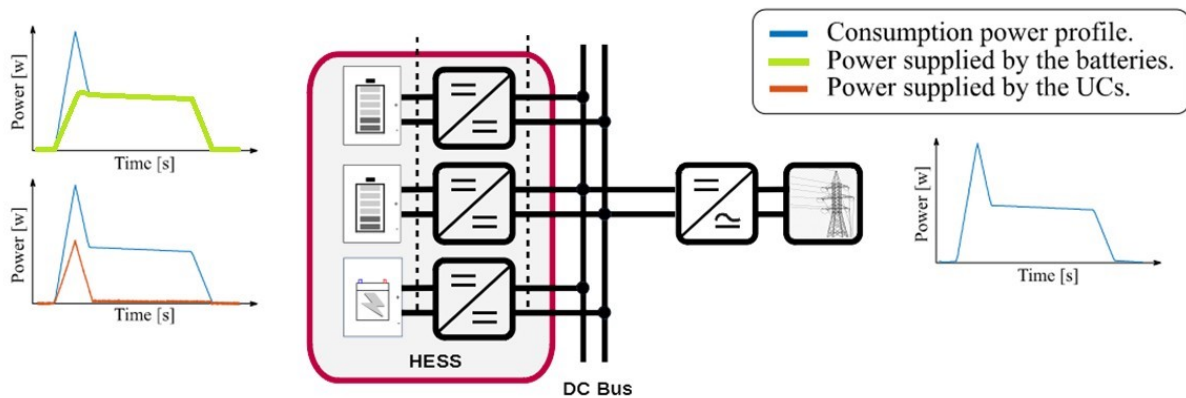


Figure 3.5: Power sharing functional requirements

19. **State of Charge (SoC) controller.**

- The BESS SoC must be automatically maintained within acceptable limits defined in Fig. 3.6a from [100] at all times through an inbuilt hysteresis control that brings back the SoC to a predefined value with a predefined active power ramp when a limit is reached.
- For each storage device it must be possible to enable an inbuilt continuous SoC control that regulates their values to predefined set points with settable dynamics.
- The UC must charge from the BESS when it is available without disturbing the power injected by the grid forming converter to the AC grid. The SoC control of BESS will act in the AC/DC converter power as shown in Fig. 3.6b.

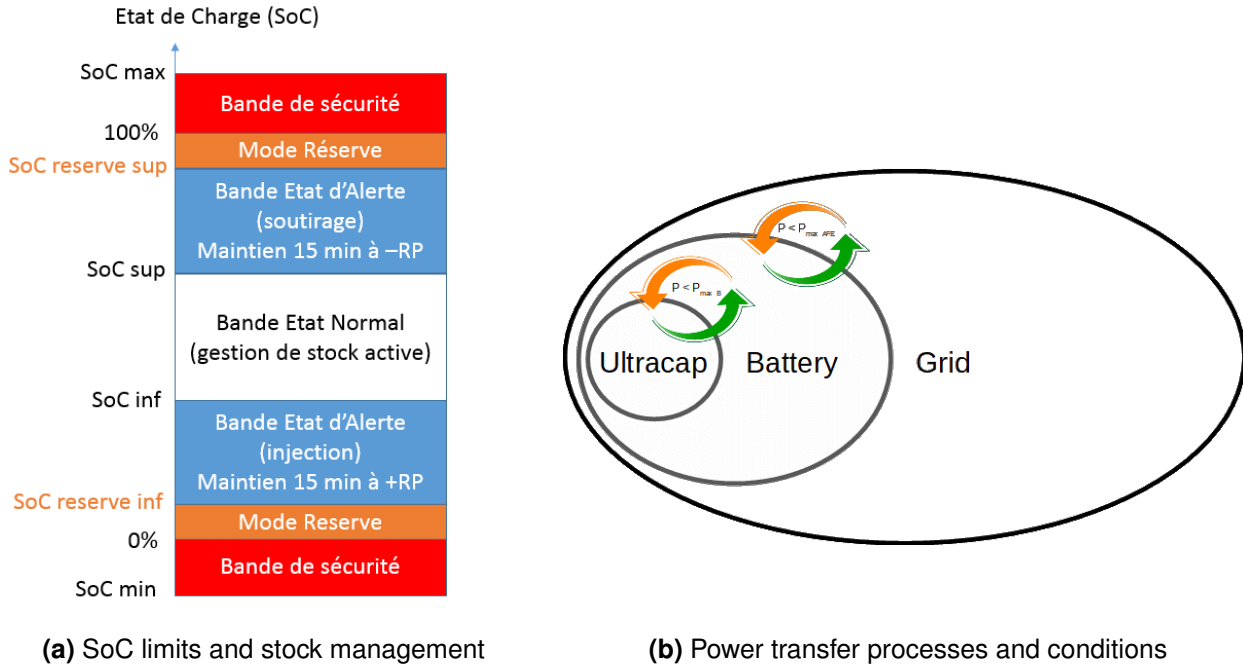


Figure 3.6: State of charge control functional requirements

20. **Synchronisation service prioritisation.** Operational SoC limits of each storage device must be defined to enable the absorption or injection of the maximum converter current while keeping a small energy buffer to continuously provide synchronisation services. Hence, a settable energy budget (SoC_{min} and SoC_{max}) is reserved for this purpose. When one of these thresholds is reached, all other services that push the SoC beyond this limit must be blocked by enforcing transient grid forming operation.
21. **Degraded modes.** The demo must still operate even though part of the storage capacity is unavailable. Moreover, it should be possible to isolate the contribution of one DC side device by blocking or disconnecting the two others DC/DC converters.

3.3. Control design

This section presents the control design proposed in this project to comply with the functional specification listed in the previous section.

3.3.1. Grid forming control

Regarding the grid forming control, here we consider the pll-free filtered droop proposed in the MIGRATE project [31]. The current limitation is based on a Threshold Virtual Impedance (TVI) and the droop gain is reduced during its activation [43] (see equation 2.1). This section shares the experience gained during the control design and implementation phases. Some parts of the results presented have been already published in [99], authored within the context of the OSMOSE project WP3 activities and more details are given in Appendix C. So in short:

- The outer active power control consists in a filtered droop with two settable parameters: T_f (equivalent to $1/\omega_c$ in [31]) and m_p . It can be shown that under certain hypothesis, the equivalent electrical inertia is defined as $H_e = \frac{T_f}{2m_p}$ and P is the PS injected power.

- The droop gain m_p adapts to the voltage as follows [43] where ω is the converter frequency:

$$\begin{aligned}\dot{\omega} &= \frac{1}{T_f}(\omega_{set} + m_{p,var}(P_{ref} - P) - \omega) \\ m_{p,var} &= m_p \left(\sqrt{(1 - \Delta e_{gd,TVI})^2 + \Delta e_{gq,TVI}^2} \right)\end{aligned}\quad (3.1)$$

- The outer voltage control consists in a reactive power droop with settable parameter n_q , where E_{ref} is the converter output voltage reference, Q is the absorbed PS reactive power, E_{set} and Q_{set} are user defined set points.

$$E_{ref} = E_{set} + n_q(Q - Q_{set}) \quad (3.2)$$

- A primary frequency controller with a settable dynamic T_{FR} and droop (K_{FR}) is implemented on top of the grid forming control, such that P_{ref} is the converter active power reference, f_m is the measured system frequency and P_{set} is a user defined set points:

$$P_{ref} = P_{set} - K_{FR}(f_m - f_0) \quad (3.3)$$

- The frequency reference (ω_{set}) can be fixed, and in that case K_{FR} is zero because the grid forming control (filtered droop control) is automatically providing PFR. But the system can be set to transient grid forming mode through an upper loop that slowly adapts the frequency set point to the droop output in order to ensure active power reference tracking in steady state and no interference with any multi service optimisation strategy. The dynamic is set with the T_{GF} time constant. If it is very low (≈ 100 ms [36]) the system is only providing inertial response.

$$\dot{\omega}_{set} = \frac{1}{T_{GF}}(\omega - \omega_{set}) \quad (3.4)$$

- TVI current limitation strategy reduces the converter voltage reference proportionally to the current when the threshold (I^{th}) set to 1.2 p.u., is reached as indicated in equation (3.5). There is not any switch to current control.

$$\begin{aligned}\Delta e_{gd,TVI} &= \begin{cases} Kp_{TVI} \left(\sqrt{i_{sd}^2 + i_{sq}^2} - I^{th} \right) (i_{sd} - D_{XR}i_{sq}) & \text{if } I_s \geq I^{th} \\ 0 & \text{otherwise} \end{cases} \\ \Delta e_{gq,TVI} &= \begin{cases} Kp_{TVI} \left(\sqrt{i_{sd}^2 + i_{sq}^2} - I^{th} \right) (i_{sq} + D_{XR}i_{sd}) & \text{if } I_s \geq I^{th} \\ 0 & \text{otherwise} \end{cases}\end{aligned}\quad (3.5)$$

- A sequence separation is performed but the use of decomposed signal is limited as delays associated to this treatment led to performance loss, especially for transient events. Hence, the implementation of a full NS control loop was excluded at the final stage of control design. As a consequence, the share between PS and NS current was not settable in the tested version of the control (FAT, see Chapter 4). An updated version of this control is published in open access in [96], but is only validated in simulation. Moreover, special attention was given to the computation of the current peak (I_s) for to TVI activation criteria to prevent intermittent switching when injecting harmonic currents.
- Inner current and voltage control loops as well as damping resistors are implemented.

3.3.2. Grid forming control implementation in of the shelf-equipment

With respect to implementation challenges, the subsystems of the selected grid forming strategies can be divided into three different groups:

1. The first group includes control modules that had already been implemented in other control strategies or at least very similar forms. This is the case of: the droop control (including adaptive droop during faults), the damping resistor, the TVI and typical abc to DQ transformation structures (Park and Clarke). They are well known and did not represent major challenges. For brevity, their detailed description is provided in Appendix C. All the structures included in this group were implemented in the of-the-shelf VSC without major issues. Furthermore, these control subsystems have shown a satisfactory performance during FATs as shown in Chapter 4.
2. The second group describes the new functionalities that needed to be developed within the framework of this project. Indeed, some gaps were found during the implementation and validation process and those gaps had been filled with new control structures. This group includes additional subsystems for the TVI or the soft connection.
3. Finally, we detail the modification required on standard control layer to ensure proper integration of the grid forming control strategy.

3.3.2.1. New control structures

Soft connection. In order to avoid hard transients and to ensure a smooth grid connection, the PCS is synchronised with the grid before the closure of the main breaker. The fundamental phase-angle at the POI is tracked on-line in order to estimate direct and quadrature axes. To do so, a PLL is implemented. The output voltage of the converter is increased with a low derivative (low enough not to excite the grid connection filter resonance) and once the output voltage of the PCS and the grid are synchronised and with almost identical voltage amplitude, the main breaker is closed. After the breaker closes, the PLL is deactivated and the active and reactive power set points evolve according to the droop characteristics. Thus, immediately after the synchronisation, the PCS will start controlling frequency and voltage. For the particular case when the grid magnitudes are identical to the set points, the PCS will not inject any current to the grid. Figure 3.7 shows simulation results of the synchronisation process obtained in Matlab-Simulink.

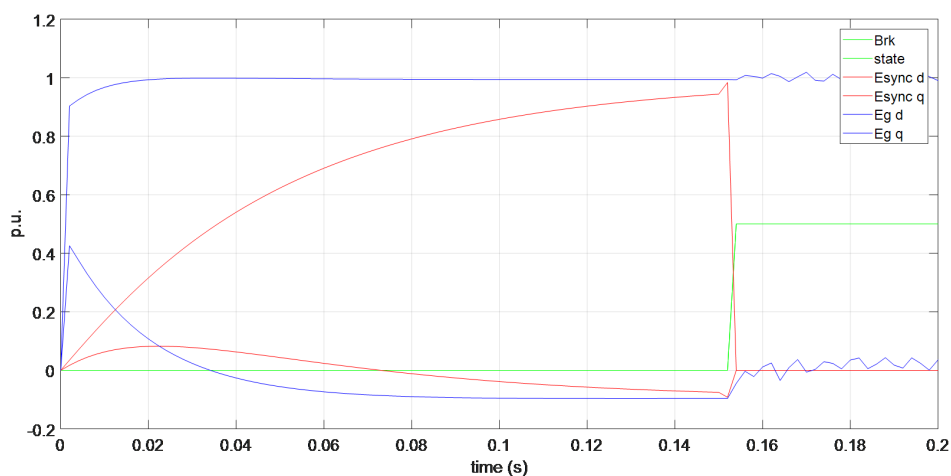


Figure 3.7: Synchronisation process results obtained in Matlab-Simulink

TVI under unbalanced faults. The injected current during unbalanced condition was initially not controlled and depends on the line impedance. If no countermeasures are taken, the unbalance leads to a 100Hz oscillation in the current that exceeds the maximum operation current, the virtual impedance actuates intermittently, behaving as a non-linear load and injects non-desired harmonics to the grid. To avoid this, a control algorithm was proposed and has been published in [96].

3.3.2.2. Adapted control structures

Set points hard limits. To avoid control loops to drive currents and voltages beyond hardware limits, the first protection action is the set points saturation or limitation. The VSC has two main limitations in continuous operation:

- Thermal limitation, driven by the current.
- Maximum output voltage: depending on DC bus voltage and functional parameters that limit the capacity of the converter, for example, modulation (3rd harmonic injection) or semiconductors dead time.

Based on those limits (output current and voltage) and the AC voltage at the POI (V_{POI}), the maximum active and reactive power that the converter can inject to the grid can be estimated [103]. The maximum output voltage depends on the DC bus voltage and the modulation technique characteristics. So, the maximum allowable active and reactive power of the converter can be estimated as follows:

$$PQ_{max} = f(IC_{conv_{max}}, K, Z_{filter}, V_{DC}, V_{POI}) \quad (3.6)$$

where $IC_{conv_{max}}$ is the current limit (constant), K is modulation technique gain (constant), Z_{filter} are the output power filter values (constant), V_{DC} is DC bus voltage. For an arbitrary grid voltage, the maximum apparent power of the converter considering only the current limit is:

$$S_{max}^2 = P^2 + Q^2 = (V_{POI}IC_{conv_{max}})^2 \quad (3.7)$$

As mentioned before, the second limit is the converter AC voltage. So, considering the output filter only as a reactance for the sake of simplicity $Z_{filter} \approx X_{filter}$, the expression of the voltage limit is:

$$P^2 + \left(Q + \frac{V_{POI}^2}{X_{filter}}\right)^2 = \left(\frac{V_{POI}V_{Conv}}{X_{filter}}\right)^2 \quad (3.8)$$

$$V_{Conv} = \sqrt{\left(P^2 + \left(Q + \frac{V_{POI}^2}{X_{filter}}\right)^2\right)} - \frac{V_{POI}}{X_{filter}} \quad (3.9)$$

$$V_{Conv_{max}} = V_{DC}K \quad (3.10)$$

The maximum converter active and reactive power values are given by expressions (3.7) and (3.9)-(3.10). Those PQ limits are absolute, converter hardware limits. A grid following VSC protects itself from unreachable set points, by limiting the P and Q set point values. But, this limitation has a degree of freedom, those limits do not determine the operation point. If the apparent power set point is bigger than the maximum apparent power allowed by the hardware, the active power (P), the reactive power (Q) or both can be reduced depending on a user defined priority. By default for generation units P priority is used for normal operation and Q priority during LVRT. This means that if the desired apparent power (S) is unreachable, first active power is dispatched and if there is still room available, the reactive power set point is limited to reach the maximum.

A function to limit external set points according to those default priorities and converter conditions is a common practice in grid following. As in grid following a regulator drives the error between the set point and the measured signal to zero, it is thus possible to assume: $P_{out} = S_p P$ and $Q_{out} = S_p Q$. However, in grid forming, but also in grid supporting with droop controls, the PQ set point does not determine the real PQ operation point. In droop control, the droop line is defined like point-slope form as shown in Fig. 3.8 and PQ set points are just a part on this point-slope definition. The other half of the “point” definition are the voltage and angular pulsation set points: E_{set} and ω_{set} . Thus, this set point limit protection layer was modified when implementing the grid forming control and extended also to E_{set} and ω_{set} set points.

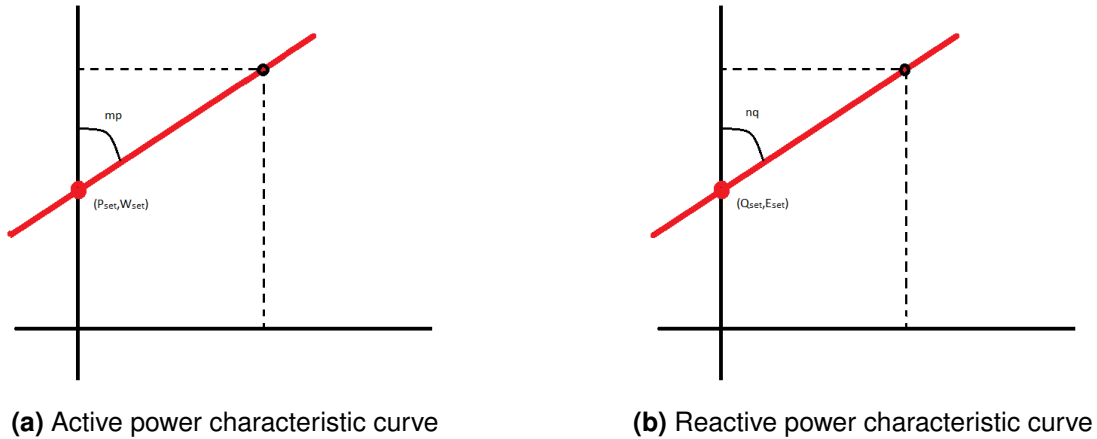


Figure 3.8: Droop control implemented at the grid forming control

Furthermore, even when the set points are constant (P_{set} , ω_{set}) and (Q_{set} , E_{set}), if an event in the power system changes the voltage or the frequency. The active and reactive power injected by the equipment is modified. Thus, the PQ set point limitation problem, has now much more variables.

$$PQ_{max} = f(IC_{convmax}, K, Z_{filter}, V_{DC}, V_{POI}) \quad (3.11)$$

$$PQ_{out} = f(Z_{filter}, V_{POI}, n_q, m_p, X_{grid}, R_{grid}, P_{set}, Q_{set}, W_{set}, E_{set}, f_{grid}) \quad (3.12)$$

where n_q and m_p are droop gains, X_{grid} and R_{grid} are the equivalent grid reactance and resistance seen from the equipment, P_{set} and Q_{set} are active and reactive power set points, and f_{grid} is the grid frequency. Looking to equation (3.12), the PQ limitation has several cross related terms. However, another way to limit unreachable set points can be implemented. In grid supporting applications reverse droop is usually applied and in grid forming applications droop control (see Fig. 3.9). This difference is caused by the characteristics of the inner control loops: in grid forming, inner PI controllers are implemented into voltage and current loops to eliminate steady state errors. While for the inner control loops in grid following mode, the objective is to obtain a good output power regulation [104].

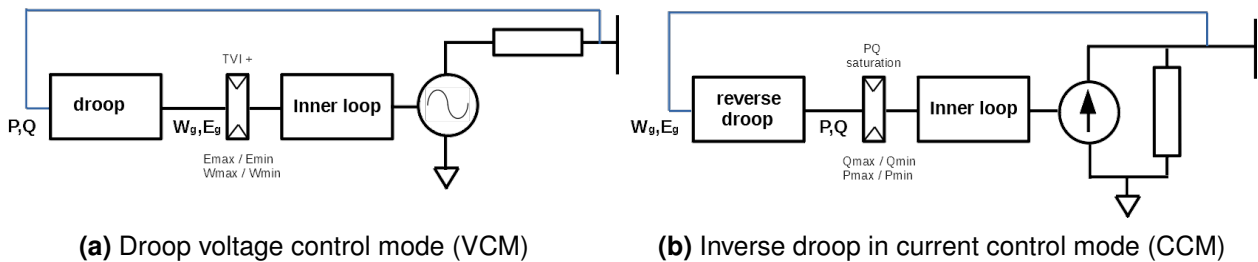


Figure 3.9: Simplified system droop configurations

If the active and reactive power are limited after the droop control, in grid following and in grid supporting applications the way to proceed is very similar since the inner control loops are still the same. In grid forming with droop control, the limitation problem is translated from active and reactive power to the voltage and frequency (see Fig. 3.9a). For the voltage and current limitation, in MIGRATE control a TVI is proposed. However, the TVI is meant to protect the system during transients, not in steady state, as long periods of TVI activation can lead to angle instability. In [105] is also pointed out the desynchronisation as a drawback for current limitation strategies, which is illustrated in the following simulation example, by setting the active power droop characteristic m_p as 0.01 ($P_{set} = 0$ and $\omega_{set} = 1$) and imposing a frequency set point step ($\Delta\omega$) of 0.013. Figure 3.10 shows that the angle instability is reached since the set points are not properly limited and the frequency step is too large extending the frequency gap in time.

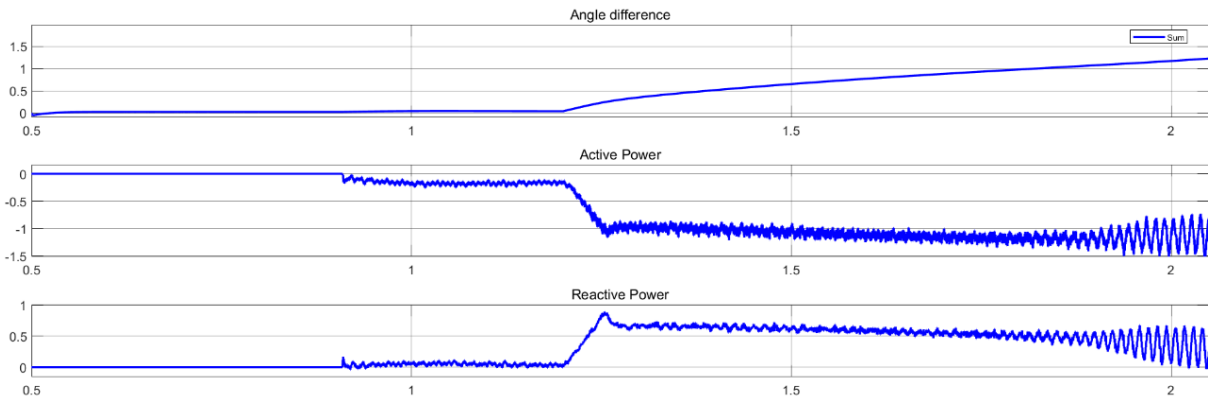


Figure 3.10: Simulation results for a frequency set point variation ($\Delta\omega$) of 0.013 with a $m_p = 0.01$.

The synchronisation and initial conditions are the same, $\omega_i = \omega_g = 0.9985$, but, when the frequency set point changes, the active power starts flowing to the grid. When the maximum current of the converter is reached, the TVI is activated limiting the output active and reactive power. At this point, the real frequency of the grid and the internal frequency of the equipment are different ($\omega_g < \omega_i$). As pointed out in [105], desynchronisation results in a power oscillation. Substituting measured values in equation: $0.01(0-1) = (\omega_i - 1.013)$, such that $\omega_i = -0.01 + 1.013 = 1.003$ and $\omega_g = 0.9985$.

In order to compare those results with a correct performance, results for the same system with a frequency set point step ($\Delta\omega$) of 0.005 are also shown in Fig. 3.11. In this second case, the converter first synchronises with the grid. Then, as the grid frequency is slightly different than the set point, a new equilibrium point is reached.

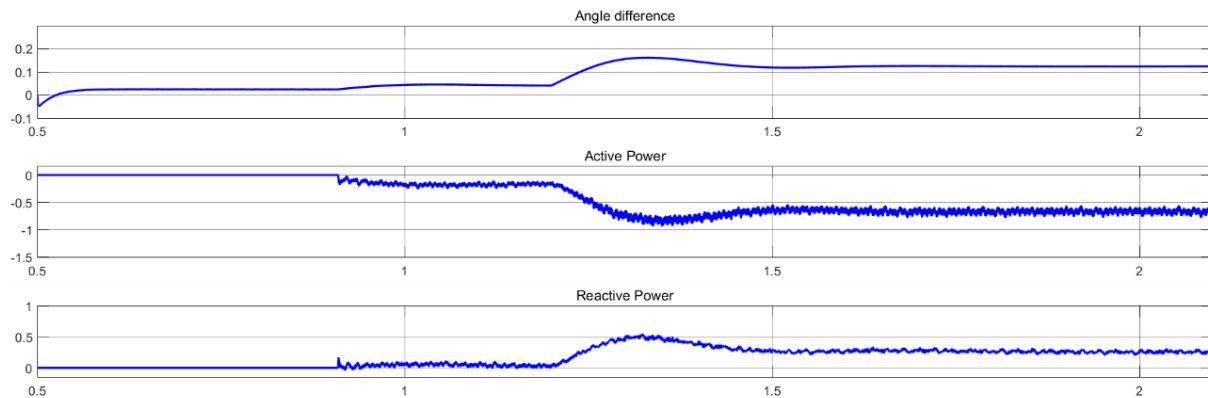


Figure 3.11: Simulation results for a frequency set point variation ($\Delta\omega$) of 0.005 with a $m_p = 0.01$.

Now the equipment injects 0.15 pu active power according to $m_p(P_{set} - P) = (\omega_i - \omega_{set}) = 0.01$ ($0-0.15$)= (ω_i-1) , so $\omega_i = \omega_g = 0.9985$, where ω_i is the equipment internal frequency, ω_g is the grid frequency measured independently and P is the measured active power. At $t=1.2s$ a frequency set point step $\Delta\omega$ of 0.005 is imposed and the grid forming converter reaches a new stable point. Substituting measured values as follows 0.01 ($0-0.65$)= $(\omega_i-1.005)$, and $\omega_i = \omega_g = 0.9985$.

The active power set point should be at least limited to meet the following expression:

$$\Delta Sp\omega_{max} = m_p * P_{nom} \quad (3.13)$$

Saturation and limitation after the droop (or reverse droop) helps to improve the grid forming control stability. However, other sources of instabilities might need further investigation and require more sophisticated limitation strategies. For example, if the converter is not prepared to inject to the grid a certain amount of reactive power, related to the intended amount of active power injection, the Q reference limitation can lead to voltage collapse in weak grids. Since the RTE-Ingeream demonstrator is to be connected in a strong network, the implemented set point limitation suffices to avoid transient instabilities and perturbations caused by unreachable set points. Real-time optimisation approached can also be used as proposed in EPFL demonstrator (see Chapter 6).

Semiconductors hard blocking threshold. One of the modified layers is related to the semiconductors hard blocking for protection. The TVI activation and the current limiting procedure is very different from grid following. In grid following as the control regulates directly the current, the hard blocking of the semiconductors is close to its nominal values. For grid forming control, the hard blocking activation threshold was increased significantly, around 45%. The hybrid current limitation presented in MIGRATE [31] has a saturation point at 1.4 pu. This overload capability should be extended at least for a 30ms (a parameter called TD). Furthermore, as the TVI has been modified in order to handle asymmetric faults and this modification has an impact in the system dynamic. The considered overload current period was estimated in 60-90ms, due to the fact that some delays have to be taken into account. Prior to allow this change, a thermal analysis of the operation points have been performed. In this case, the hardware allowed this overcurrent during 60-90ms.

Thus, in order to avoid further perturbations during faults, the hard blocking limit was re-adjusted specifically to this application. However, if this would not be the case, this current peaks should be taken into account at the design stage. Depending on the cooling technology of the converter, the overcurrent capability is different. For example, water cooled converters have more power density but less thermal inertia than air cooled converters. The capability of a 50-100% overcurrent in a water cooled converter is very limited. To meet certain overcurrent / overload requirements, high power converters oriented to the grid are usually air cooled [106].

If this maximum current specification is taken into account in the converter design stage, a converter hardware oriented to overload capacity / higher current peaks (i.e 1.5-2.5pu) during several seconds (1-3s) can be achieved without a significant oversizing for the converter.

For example, in [107] the datasheet of a STATCOM with a 250% overload capability during 3 sec is presented. However, current peaks of 1.4pu during 60-90ms, are in line with the converters general behaviour. In [108] the fault behaviour of converters in a general way is described. It divides the fault behaviour in 3 different stages: Initial current spike, regulation and current limited period.

- About the initial brief current spike, it says that it typically lasts only a few hundred microseconds or less. It is caused mainly by converter output filter capacitor, and therefore does not impact the converter.
- The bigger response diversity is seen in the second period: while the converter controls are trying to get back into regulation. The length of this period is often about 50 ms but ranges

from a few milliseconds to as much as 200 ms. It depends on each converter particular control and can be very different from one converter to another. The length of this period depends on several factors, such as the speed of the current regulation loop.

- In the third period, current limited period, the converter output current value reaches a constant maximum value, often a steady state current limit of 1.2 pu.

As a note, in [108] is pointed out that future revisions of IEEE 1547 standard could reduce the uncertainties in converter response during the regulation period (the second period).

3.4. High-level control design

This section presents the high level control strategies developed in collaboration between Ingeteam R&D Europe and RTE in order to comply with the specifications listed in section 3.2.2. They include the local frequency controller and the DC side control as shown in Fig. 3.12. This latter is structured in 3 layers: the lower voltage/current controllers, the power allocation level and the SoC control. The last two modules are packed in the energy management system (EMS). The first layer performs SoC control and monitoring, while the second determines power sharing within the HESS.

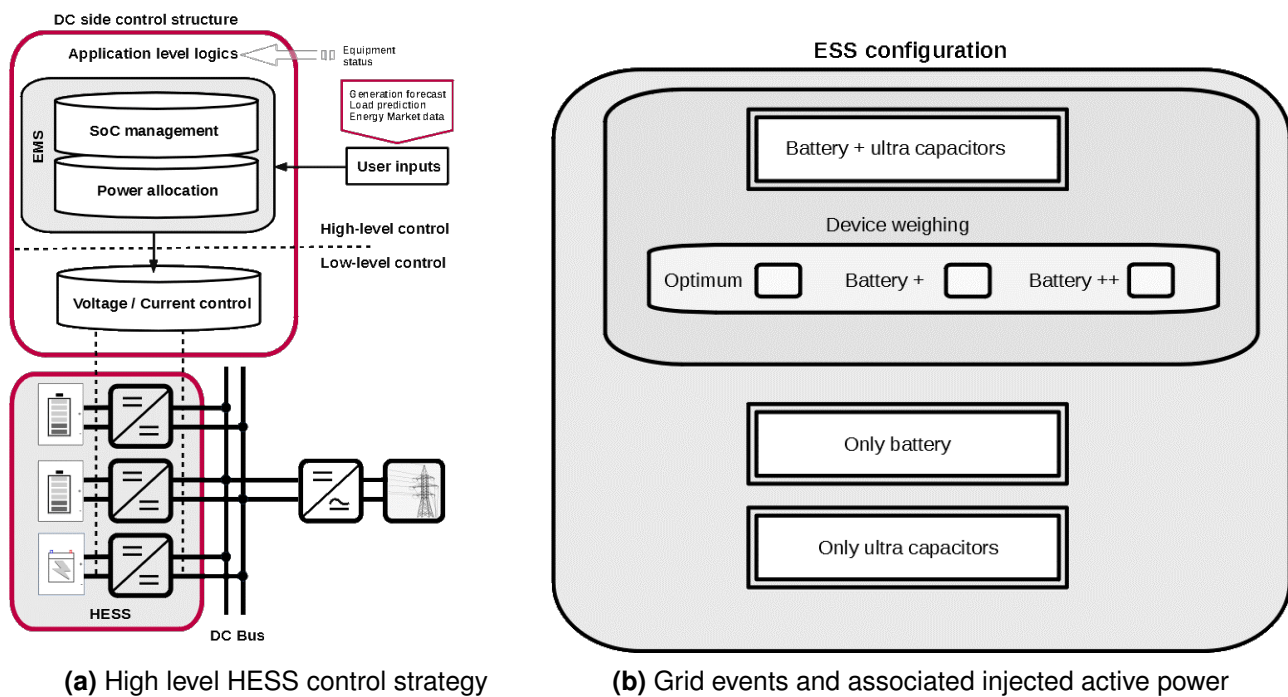


Figure 3.12: High level control structure

3.4.1. Voltage and current controllers

The first step is to control the input current of the DC/DC converters with an inner control loop (as done in current mode control converters). For this, the input current of each converter and the control variable, the duty cycle for a PWM converter, have to be related.

3.4.2. Power allocation controllers

One of the main interest of the grid forming control is to naturally provide electrical inertia to the grid, so, the converter provides the energy required in order to support the grid frequency. If the power required has a fast derivative, UC must react and inject power to smooth inrush current required to the BESS. For this purpose a PI-P controller is used, which consists in having a pure proportional controller for the UC, and a PI controller on the BESS that brings the DC voltage to its set point ensuring that the contribution of the UC goes to zero in steady state.

It must be possible to set different power sharing rations in operation when BESS and UC are working together. This can be done changing the gains of the PI-P controllers. In this project, three different set of predefined parameters for weighing the power allocation were provided as shown in Fig. 3.12b. They are identified as optimum, battery + and battery ++ which lead to an increase in the BESS participation to the transient. Previous works showed the stable association of the grid forming mode with different DC side power sharing and energy management strategies [97] and a preliminary performance assessment on EMTP [98] anticipates proper behaviour with the connection grid.

Degraded modes. In addition, it is possible to operate the system with only one storage technology or any combination of the three sources. In case of operating with only UC, all energy intensive services (P_{set}) including frequency regulation are blocked. Additional details are available in section C.3.

3.4.3. State of Charge controllers

The SoC relates the available capacity at a given time to the maximum available capacity. It is usually given as a percentile. The UC SoC is constantly regulated from the battery with a settable dynamic (in this project, $T_{socUC} \approx 1$ minute). For the BESS two superimposed SoC control strategies were implemented in the programmable logic controller (PLC):

1. The first strategy consists in a hysteresis control that automatically restores the BESS SoC to a predefined set point if extreme values (operational limits) are reached and if the network is at normal state to comply with requirements discussed in section 3.2.2. The operational limits (SoC reserve sup/inf in Fig. 3.13) must allow for nominal current injection and transient grid forming function, hence they take into account the inbuilt safety band to ensure nominal current (red area) and the reserve to provide synchronisation services (orange). If they are reached, all services are blocked and the demo switches to transient grid forming mode. In this project, hysteresis control activation limits were set to 10% and 90%, while Δ_{Hyst_Ctrl} defines the target SoC value that leads to the deactivation of the control. A ramp limit is set ($Ramp_{hyst}$).
2. A second strategy consists in a continuous control that, as for the UC, regulates the BESS SoC to a predefined value (50 % by default) with a settable dynamic ($T_{socBat} \geq 1$ hour). As shown in Fig. 3.13 if the continuous SoC regulation is enabled, it will remain active only if the SoC remains within certain bounds, the Continuous SoC regulation range that is set in this project between 20 % and 80%. The BESS continuous SoC control can be disable:
 - by an external signal from the HMI,
 - when the external controller (or the user through HMI) send active power orders,
 - when predefined limits (SoC sup/inf in Fig. 3.13) are reached. This limits must be tighter than the operational ones and defined the zone of active stock management. If they are reached, the demo switches to transient grid forming but can keep the frequency controller.

In conclusion, it is possible to manually disable the BESS continuous SoC control at any time, while the first strategy must remain always active.

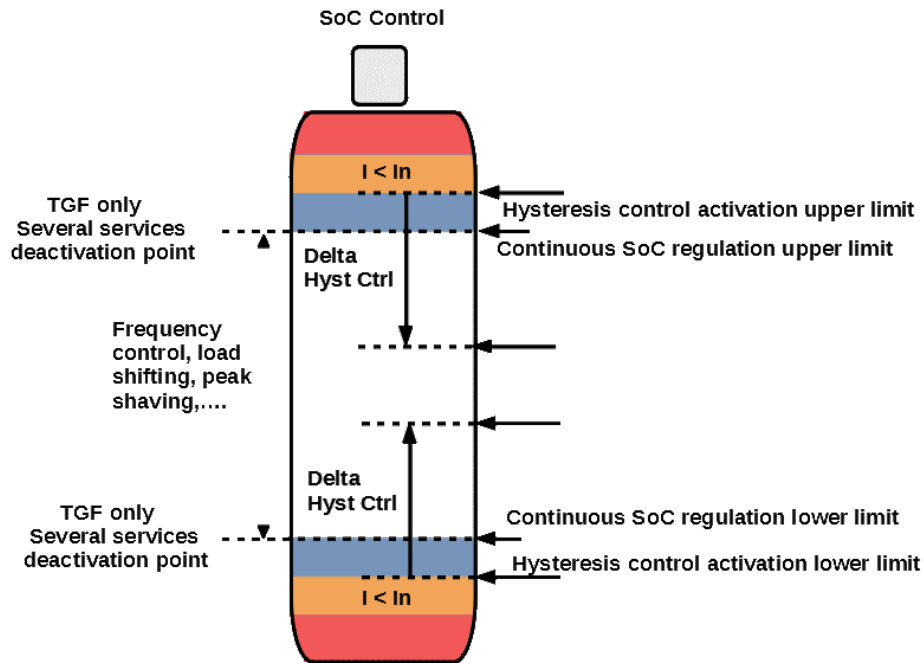


Figure 3.13: SoC controls limits

In addition, the continuous SoC control must be automatically deactivated if a SoC min or max limit is reached or when a signal indicates that the external control of active power is enable, as that means that the user is willing to use stored energy and SoC should evolve according to the grid needs and control parameters. Between the Hysteresis control activation and Continuous SoC regulation limits there is a band (blue area) where none of the SoC control strategies is expected to act and only TGFM and frequency regulation services are preserved. The global control strategy is depicted in Fig. 3.14a where 3 layers can be identified: the logics that enable/disable continuous SoC regulation, the continuous SoC control and the hysteresis one.

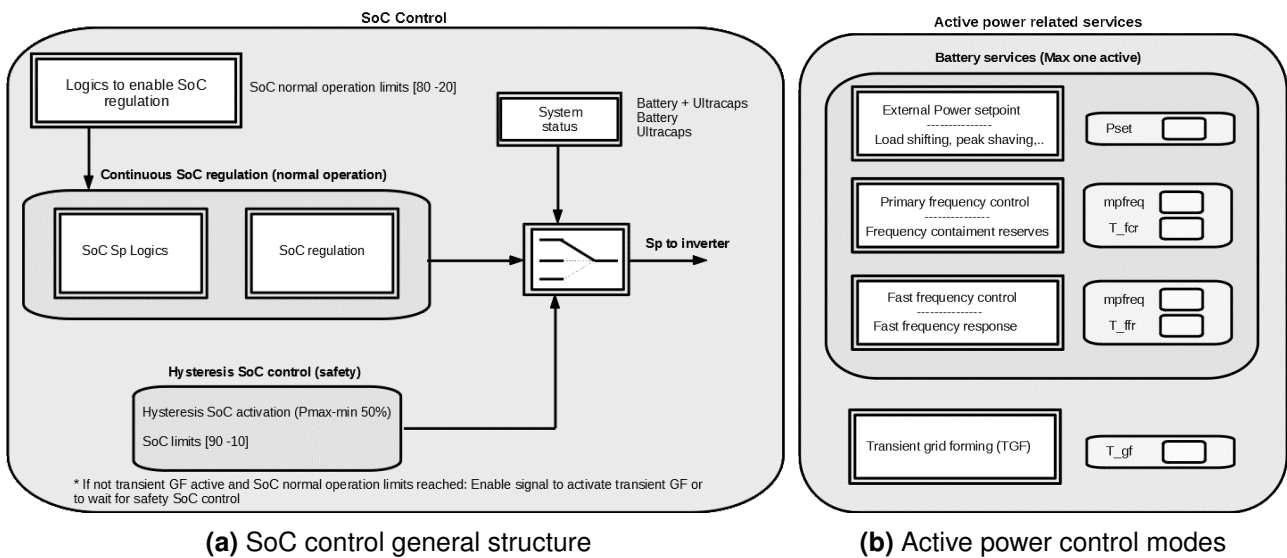


Figure 3.14: High level HESS control strategy

3.4.4. Reference tracking and local frequency controller

Figure 3.14b shows the different control modes available in the demonstrator:

1. A power set point input given by an external control for typical energy management ESS to participate in balancing and flexibility services (load shifting, peak shaving. . .).
2. A local Frequency Controller with settable static droop (R) and dynamics (T_{fc}). Setting the time constant to $T2$ shown in Fig. 3.4 allows us to provide Frequency Containment Reserves (FCR), while using $T_{fc} = T1$ would lead to a faster deployment with equal steady state which is compatible with the FFR services. It is possible to disable this controller through HMI settings. Its Matlab-Simulink model implementation is shown in Fig. 3.15.

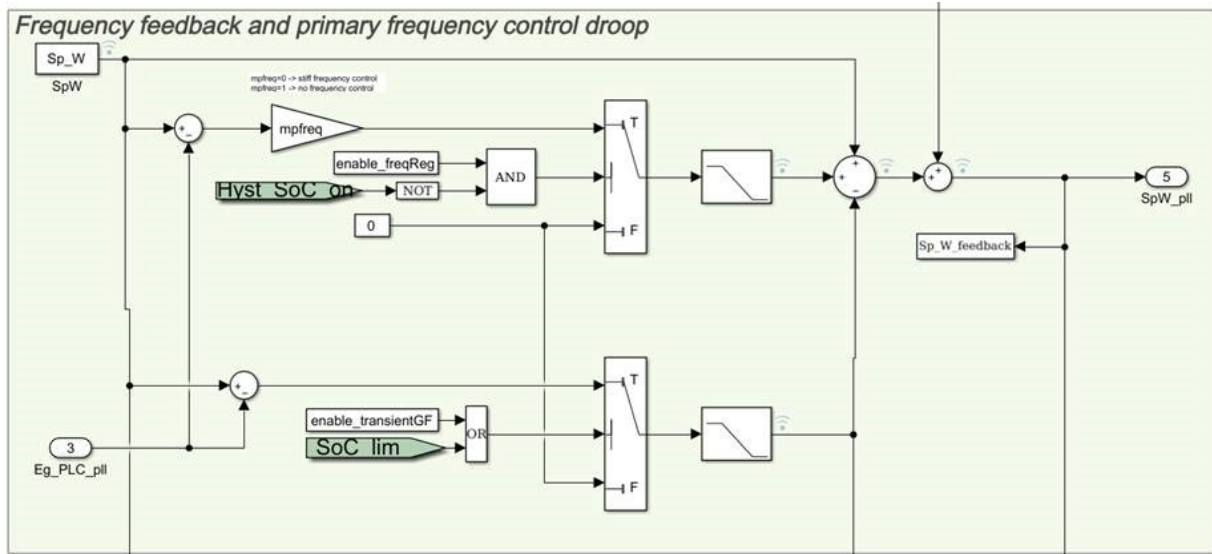


Figure 3.15: Local frequency controller (Matlab-Simulink model)

3. A grid forming function that is energetically neutral within a settable dynamic (T_{gf}), called transient GFM (TGFM), is also available. Using a filtered frequency feedback allows transient grid forming operation by making the frequency set point variable and dependant on grid frequency, which at the same time brings the injected active power to its reference value in steady state. Therefore the time constant of this filter (T_{gf}) and the logic variable must allow to enable / disable of this function (`enable_transientGF`) are settable. So, when $T_{gf} = T1$ and the frequency controller is disable the converter provides only TGFM service (depicted in grey in Fig. 3.4) which requires a small energy buffer. If $T_{gf} = T2$ the converter also provides FFR or what is called in the literature “synthetic inertia” services (grey + blue are in Fig. 3.4). Finally, FFR can also be seen as the combination of the FFR provided by a slow TGFM with classical FCR. The green area is an indication of the expected dynamic of the BESS SoC regulation ($T3=15$ min).

3.5. Performance validation

Prior to the FAT tests presented in Chapter 4, a simulation scenario was developed including both the real equipment and the virtual grid test bench. Simulations results of the performance assessment conducted at that time (beginning of 2020) are presented in Appendix D. They confirmed the proper behaviour of the equipment, allowing for the activation of the services at the specified cases and conditions. Based on these preliminary results, the test procedure and compliance criteria were agreed between RTE and Ingeteam. The proposed test matrix is provided in Appendix E (section E.4).

Synchronising power for different operating points. Figure 3.16 shows the synchronising power injected for 5° phase jump for different load conditions. At high initial power the grid disturbance lead to current saturation. The TVI successfully protect the converter but the resynchronisation takes longer. Control design improvements are expected to emerge that enhanced this type of behaviour.

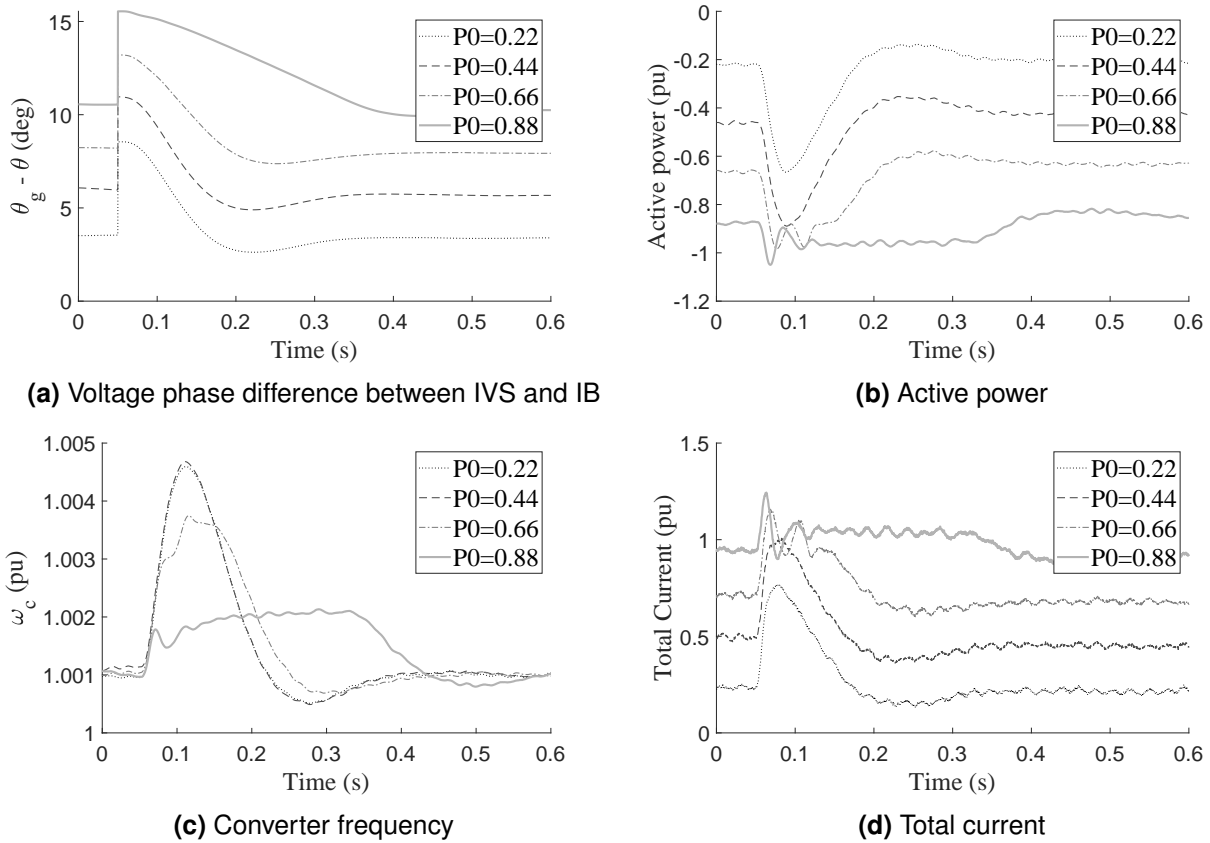
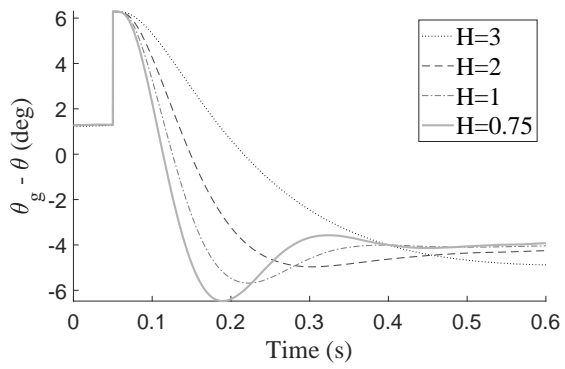
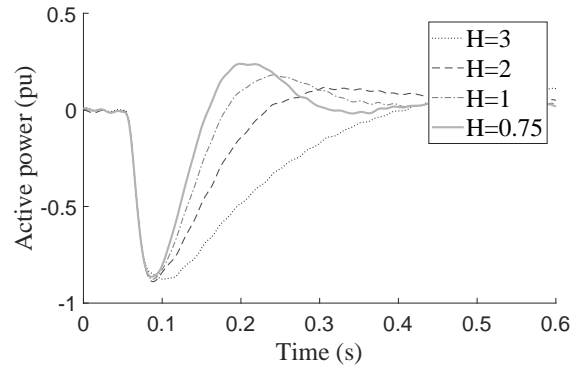


Figure 3.16: VSC response to a 5° phase jump - different operating points

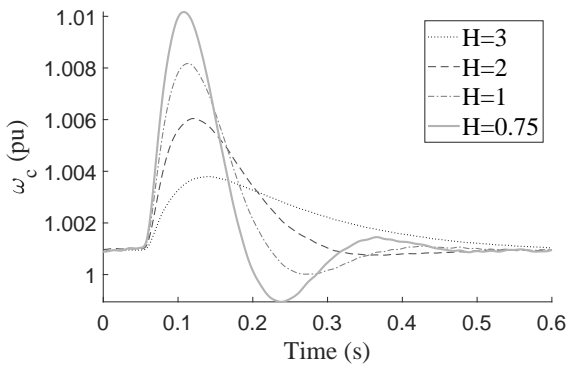
Synchronising power for different inertia settings. Figure 3.17 shows the synchronising power injected for 10° phase jump for different values of inertia obtained for $T_f = 30$ ms and changing only the droop gain (m_p) from 0.005:0.005:0.02. As explained in Chapter 2, the initial power peak depends only on the connection impedance so it is the same in all cases, while, the duration of the power injection, the frequency derivative and excursion can be adapt through control settings (related to the inertial response) depending on the available energy.



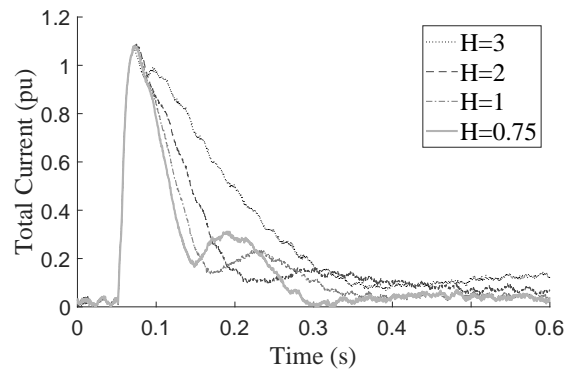
(a) Voltage phase difference between IVS and IB



(b) Active power



(c) Converter frequency



(d) Total current

Figure 3.17: VSC response to a 10° phase jump - different inertia settings

4. Testing grid forming capability: RTE-Ingteam demonstrator

After verifying in simulation the proper behaviour of the implemented grid forming control using a Matlab model of the system and the Ingteam test bench, factory acceptance tests (FAT) were then performed to validate the RTE-Ingteam demonstrator in more realistic conditions using a power-hardware-in-the-loop (PHIL) setup. In this Chapter we first describe the experimental platform in section 4.1 before discussing the performance obtained for the synchronisation service in section 4.2. Section 4.3 shows robustness tests and section 4.4 comments on reference tracking. Finally, conclusions on compliance with the specifications provided in Chapter 3 are presented in section 4.5.

4.1. Test bench description

The tests were performed in the virtual grid test bench located in Ingteam power laboratory facilities. The main scheme of the test bench is shown in Fig. 4.1. The AC/DC grid forming converter is connected to a grid emulator that represents the network through a controlled voltage source behind a virtual reactance. Transformer and grid inductance are considered and represented by the grid emulator output power filter and connection inductance. Regarding transformer's ΔY connection, it is taken into account at the grid emulator converter as it avoids zero sequence voltages.

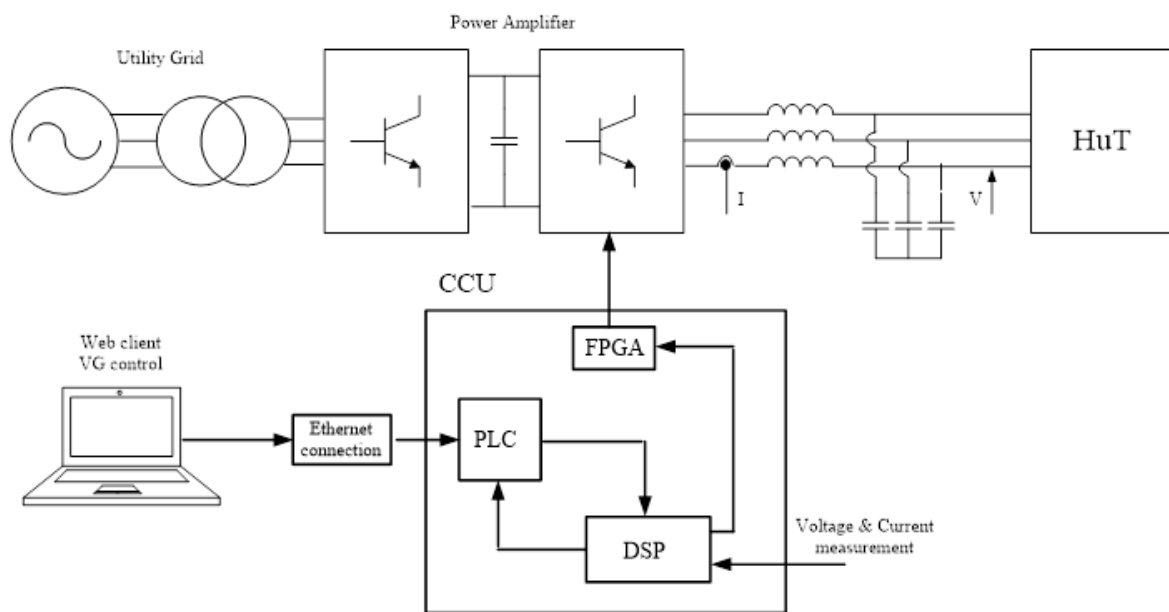


Figure 4.1: Main scheme of the Ingteam test bench to validate OSMOSE demonstrator

Impedance compatibility. The virtual grid test bench has an LC output power filter which has a resonant frequency. At the real settlement of the equipment, it is not expected to have such a resonance. So the spectra of the test bench is analysed in order to make sure a correct development of the tests by assessing the difference between connecting to the output filter of the grid emulator and a pure inductance to verify that its small capacitance does not represent an issue.

Figure 4.2 shows that the additional resonance added by the virtual grid LC filter is correctly damped considering the system impedances and a range of inductive connection impedances from $50\mu\text{H}$ to $800\mu\text{H}$, so it is not expected to significantly affect the system behaviour.

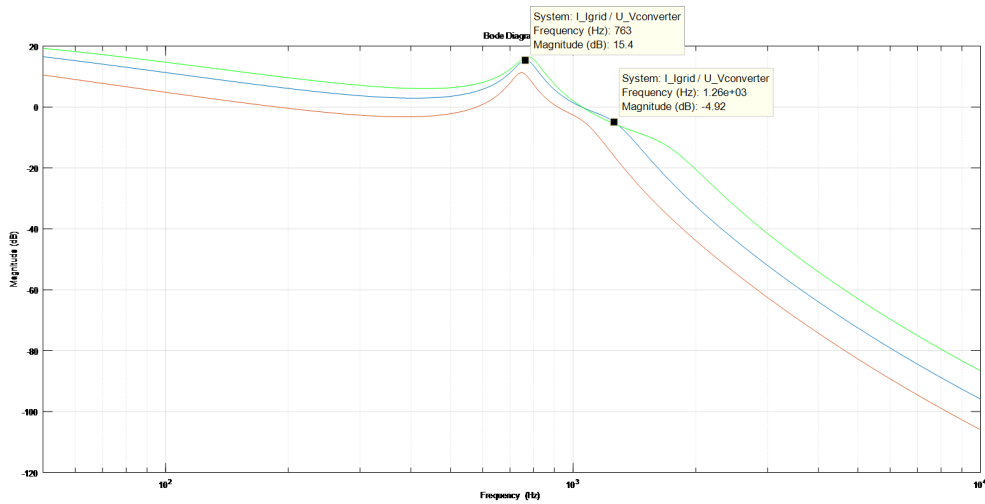


Figure 4.2: Test bench impedance spectre for inductive connection impedance from 50uH to 800uH.

4.1.1. Power elements

The scope of these FATs included the converter with its output filter, as well as the DC side converters and filters. Regarding the DC side, Ingeteam power lab cannot host 2 x 20 feet containers, only the PCS and some energy storage racks were moved to the power lab. Each DC/DC converter is connected to one rack of battery or supercapacitors as illustrated in Fig. 4.3.

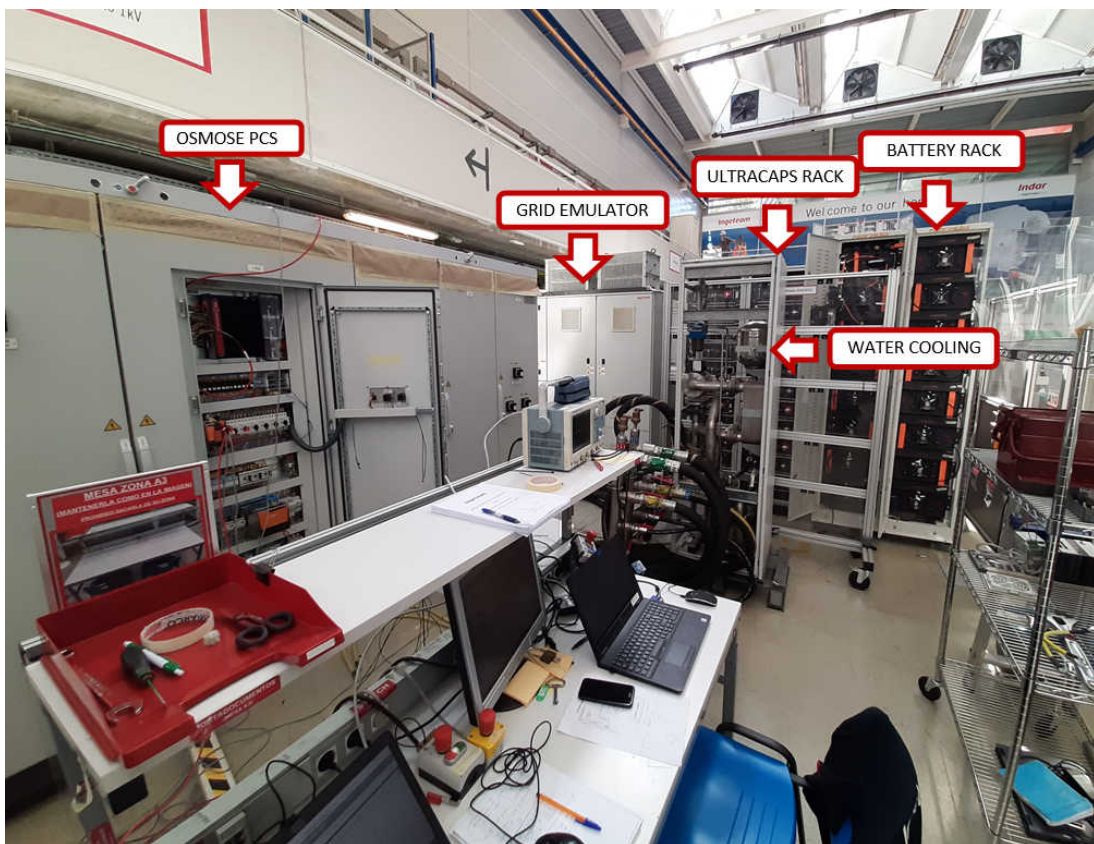


Figure 4.3: Experimental environment

More specifically the DC/DC converter 1 is connected to one of the four battery rack, which represent 25% of the nominal capacity (125 kWh). DC/DC converters 2 and 3 are connected to one rack of supercapacitors each one for a capacity of 333 KW (33% of the nominal capacity).

4.1.2. Grid emulator capabilities

The rated capacity of the grid emulator is a 777 kVA which, together with the DC side constraints, limit the maximal power involved in the testing procedure. In addition, its output current is limited to 650A. Exceeding this value, even transiently during a fault test, leads to the grid emulator disconnection. More details about the test bench capabilities, sizing and parameters can be found in Appendix E. Mainly limited by the grid emulator current capabilities, we performed reduced-scale HIL tests. Although the equipment hardware limits are not reached in reduced power tests, the control and stability can still be assessed.

4.1.3. List of tests

Grid forming control acceptance tests covered (see E, section E.4):

- Synchronization.
- Reference tracking following set point variations ($\pm\Delta SpV$, $\pm\Delta Spf$, $\pm\Delta SpP$ and $\pm\Delta SpQ$).
- Grid disturbances ($\pm\Delta V$, $\pm\Delta f$, faults and phase jumps, permanent unbalance and harmonic).
- DC side power sharing.
- Degradate modes.
- Overvoltage Ride Through (OVRT) capability¹.

4.2. Experimental results on synchronisation services

4.2.1. Synchronisation & islanding

The proposed synchronisation test starts by energising the converter from the DC side. While the breaker remains open, the control algorithm imposes the reference to be equal to the grid voltage (here 1.05 pu). Immediately after the breaker closing, the user defined reference is imposed (here 1 pu) generating a reactive power exchange. Figure 4.4 shows a well damped active power transient that leads to proper synchronisation in less than 300 ms. Figure 4.5 illustrates the grid forming converter voltage source behaviour after breaker opening when injecting maximal reactive power.

4.2.2. Synchronising power for a grid phase jump

Figure 4.6 shows that the DUT provides the expected synchronising power when submitted to a system phase jump. Due to low connection impedance, the response to a 5° phase jump yielded almost 60% of nominal active power. Most of it is provided by the UC but the battery also participates with a slower derivative. The peak power does not depend on the control parameters but the decay rate slightly depends on the set inertia. The DC side controls successfully regulate the DC voltage to a narrow band during the event.

¹This test can be limited to the first 1.35 pu/100ms limit with a balanced 3-phases scenario. The voltage of this test shall be adapted to take into account an OVRT limit calculated at the 20kV point of coupling. During this test, the PCS shall not block nor trip. This test will be performed with the PCS operating in GF and in PV-mode. For both tests, the PCS shall provide its widest capability during OVRT conditions. Laboratory tests will be performed at a reduced voltage.

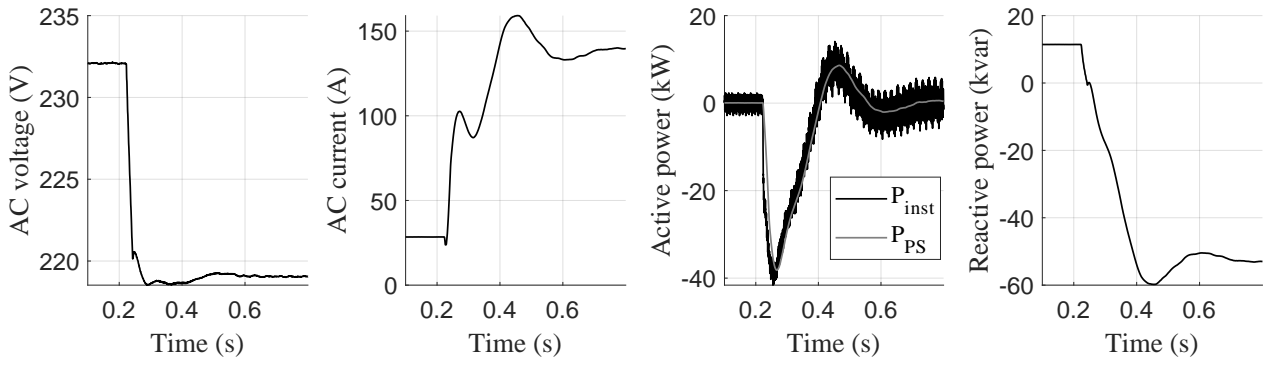


Figure 4.4: Grid connection ($V_g=1.05$ p.u. $E_{set} = 1$ p.u.)

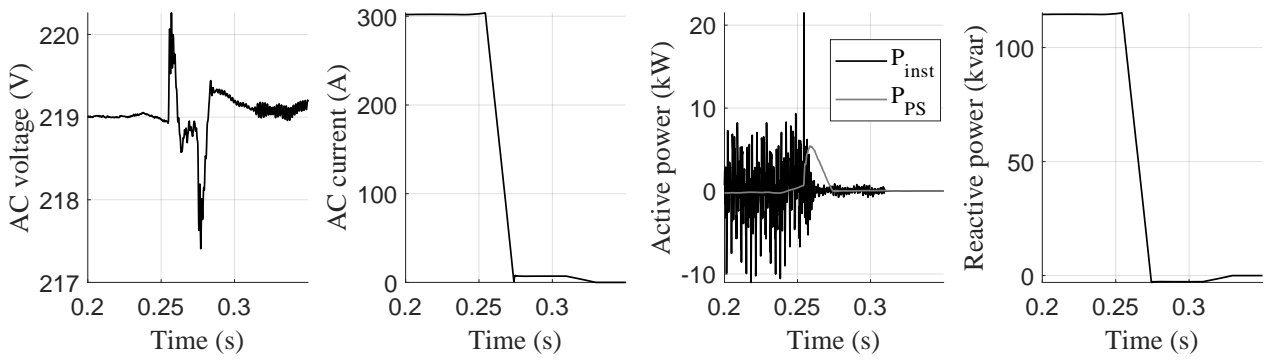


Figure 4.5: Islanding after breaker opening

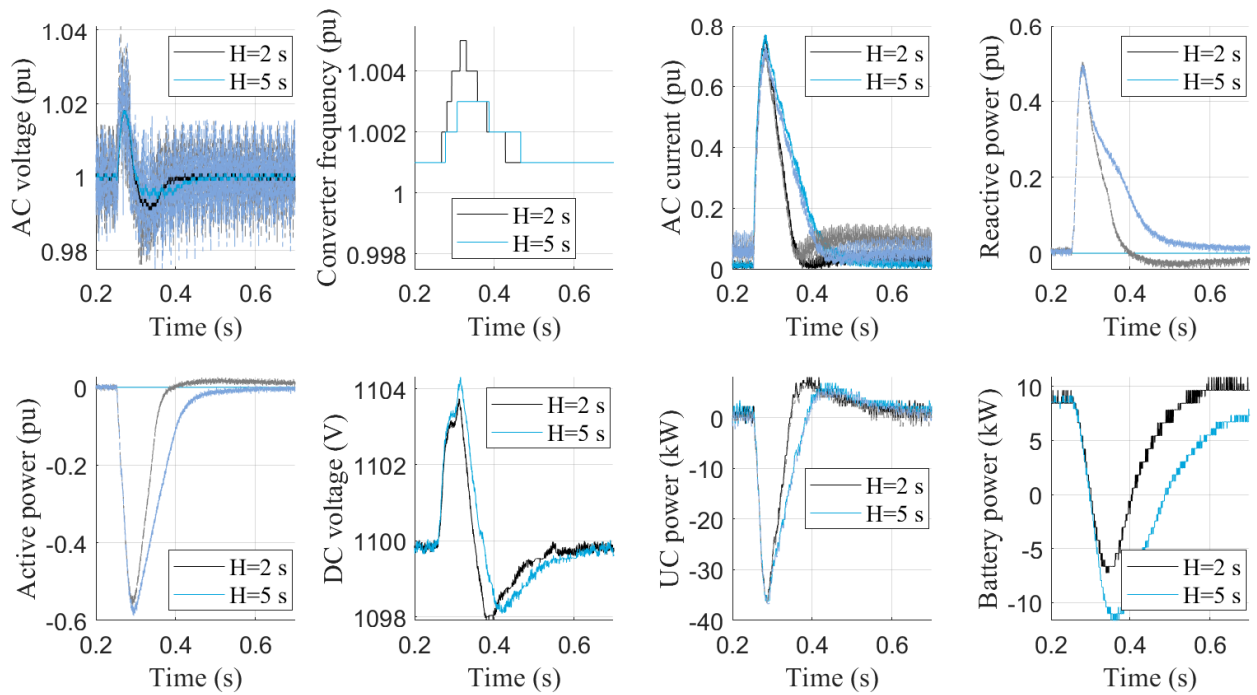


Figure 4.6: 5° phase jump

Degraded modes. Figure 4.7 shows that AC side response is independent of the DC side configuration considering:

- 3 DC-DC converters connected,
- the battery DC-DC converter disconnected (Only UC) and
- both DC/DC supercapacitors converters disconnected (Only Bat).

The control parameters of the DC/DC controller automatically switch to a degraded mode settings.

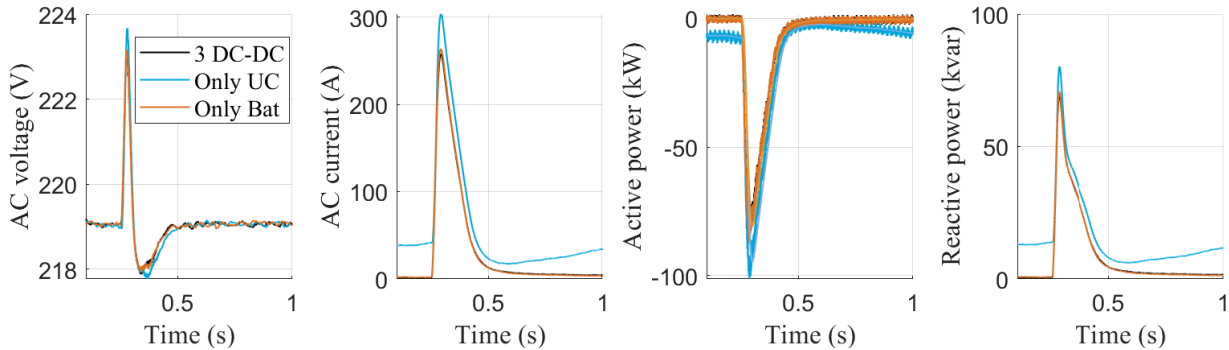


Figure 4.7: 5° phase jump ($H = 5$ s) - degraded modes

4.2.3. Inertial response and FFR for frequency step

The frequency controller is disabled so only the inertial response is observed. Following a 200 mHz step applied to the grid emulator frequency, the converter instantaneously provides active power. The fast transient is absorbed by the UC with low impact on the DC voltage, and their contribution is reduced as the battery takes over. Then, the battery will also reduce the active power with a settable dynamic proving that grid forming function is compatible and can be decoupled from other services. In the figure legend, $H1 = 2$ s and $H2 = 5$ s, while $T_{gf1} = 10$ s and $T_{gf2} = 2$ s. For $H = 5$ s the disturbance was limited to 150 mHz to avoid TVI activation. Battery power stabilises at 0 after 10 s.

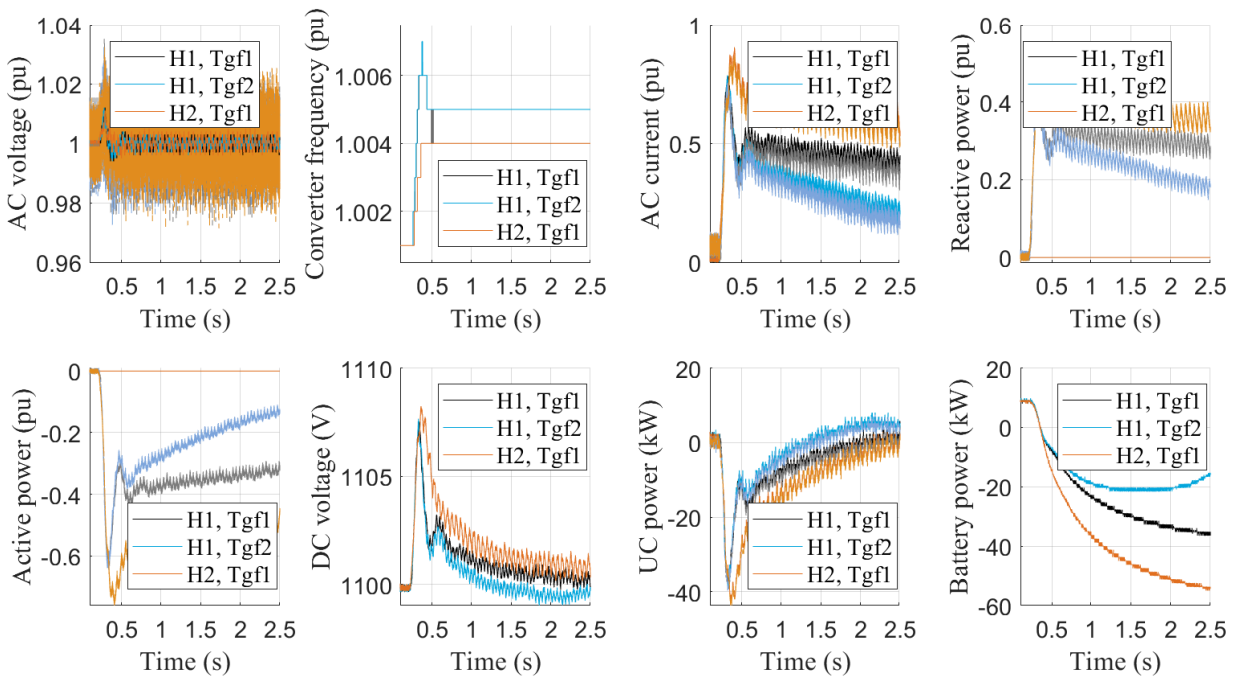


Figure 4.8: Inertial response: Grid frequency deviation

4.2.4. System strength for grid voltage step

Figure 4.9 confirms immediate reactive power injection and fast voltage control.

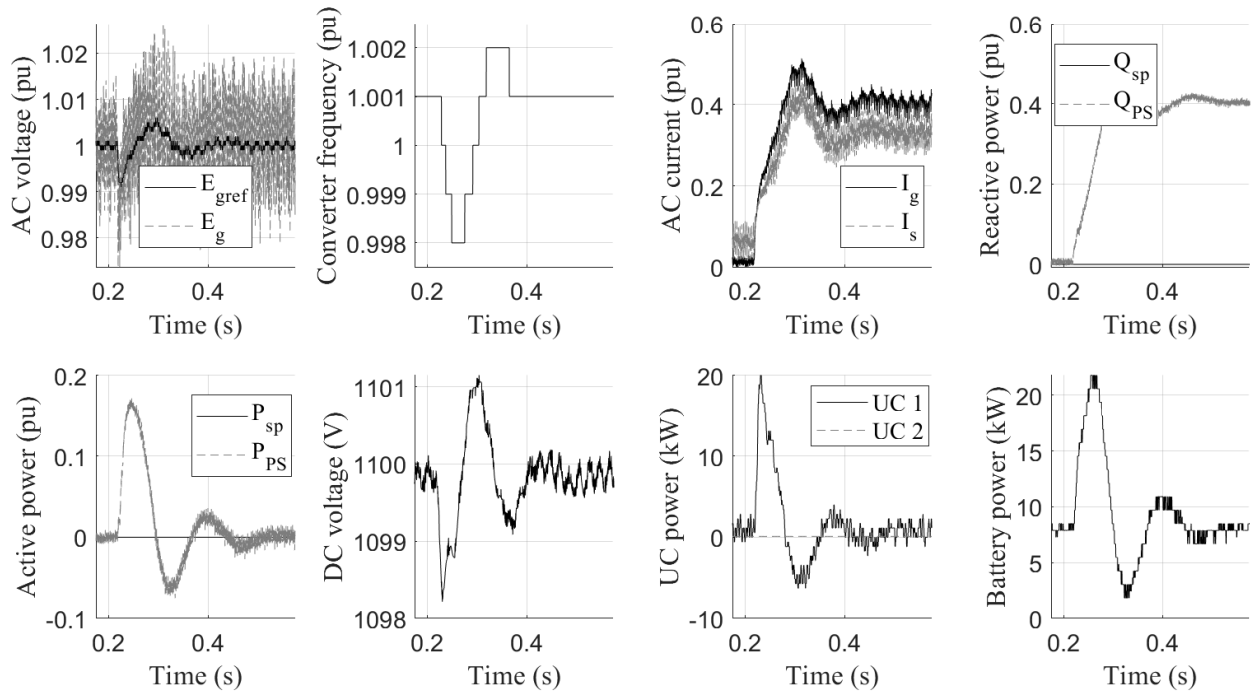


Figure 4.9: System strength: Grid voltage deviation

4.3. Grid forming converter robustness

4.3.1. Low voltage ride through capability

Symmetric voltage dips. Figure 4.10 shows three different tests:

- F1 = 100% for 250,
- F2 = 75% for 500 ms and
- F3 = 50% 700 ms

The residual voltage is due to the filter impedance. The low system resistance combined with a voltage source behaviour results in a high share of reactive current without any explicit control law defining a prioritisation strategy.

The TVI successfully limited the current to acceptable values in all cases. The recovery time after fault clearance depends on control parameters (inertia) and fault depth and duration. For a no load initial condition it is kept within 200 ms.

Asymmetric voltage dips. Figure 4.11 shows the DUT response to a type C voltage dip which represents a phase-to-phase fault or a single phase fault after a transformer connected in star-delta. The voltage unbalance is slightly reduced which lead to high unbalance in the current. The TVI is again effective in protecting the device while allowing negative sequence reactive current to flow.

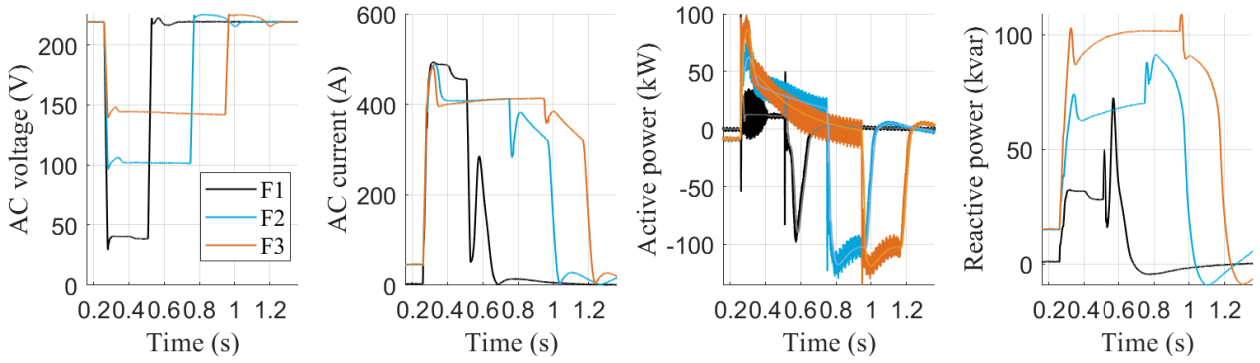
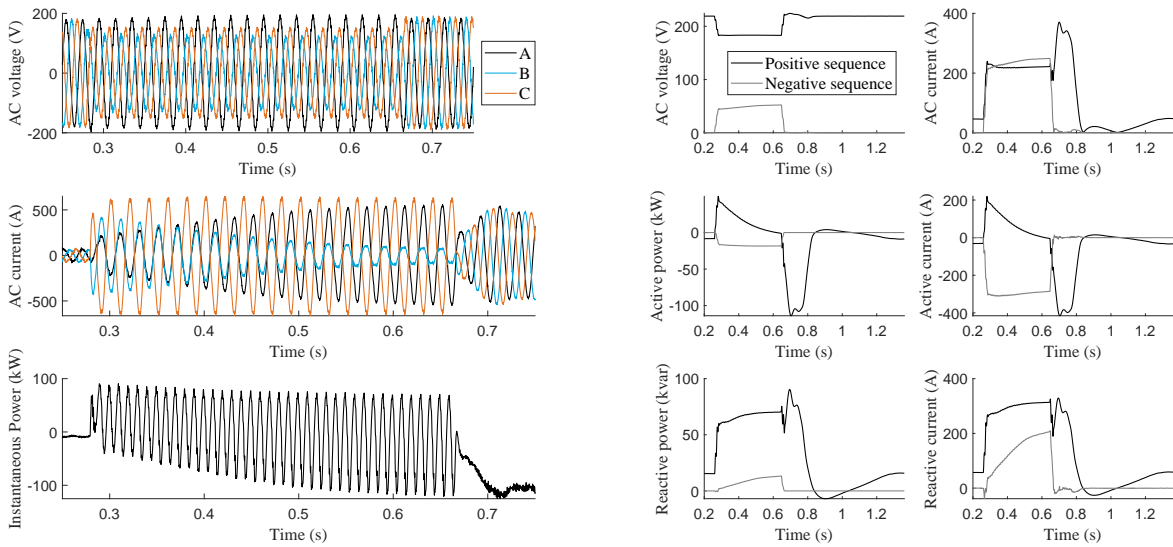


Figure 4.10: Symmetric fault ride through capability ($H = 2$ s)



(a) Wave form and instantaneous power

(b) PS and NS signals

Figure 4.11: 50% Type C fault for 400 ms

OVRT. Figure 4.12 shows that the system withstand 1.25 p.u. of grid voltage for at least 1 s and was tripped for 1.4 p.u.

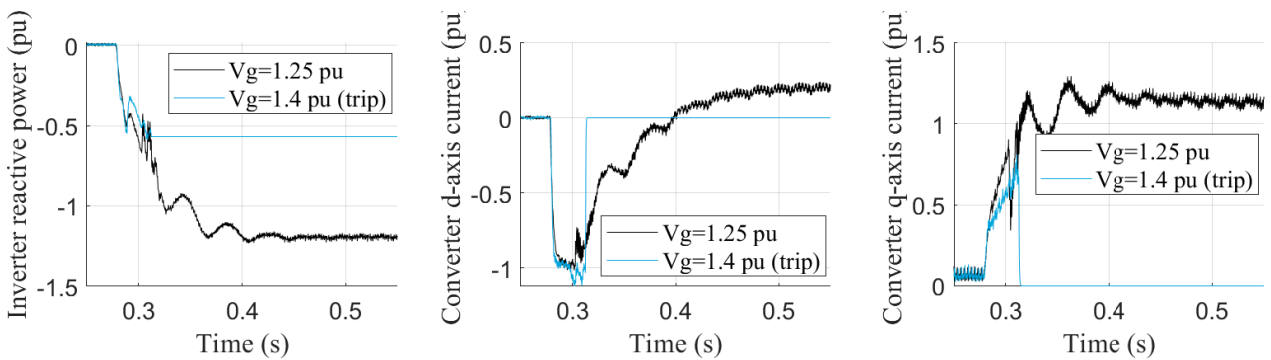


Figure 4.12: OVRT test

4.3.2. Grid voltage harmonic distortion

The virtual grid was set to produce 10% of the 5th harmonic voltage distortion (much more than what is expected in the grid). Figure 4.13a shows that the DUT absorbs large harmonic current and reduce the voltage distortion from 10% in the grid to 4% at its terminals associated to the filter's impedance.

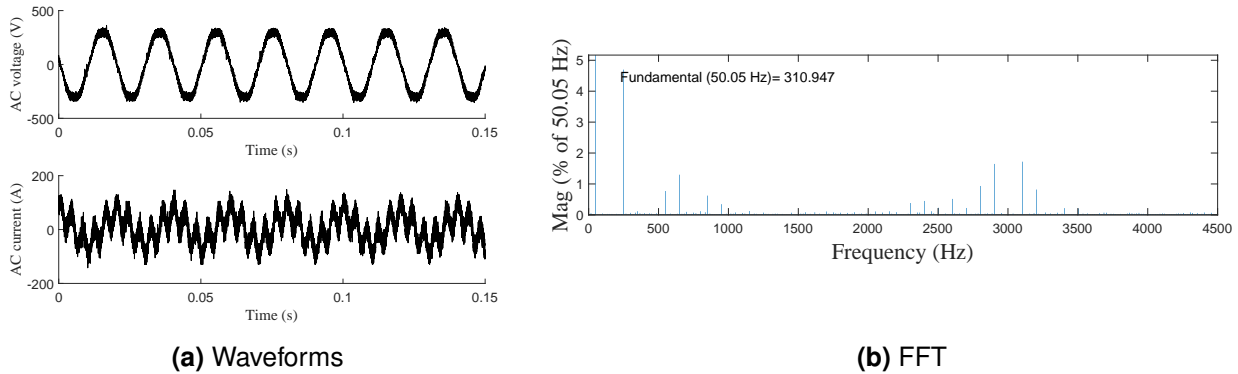


Figure 4.13: 10% of 5th harmonic distortion on the grid voltage

4.4. Experimental results on classic services

4.4.1. Active power reference tracking

Figures 4.14 and 4.15 shown that the active power does exhibit an overshoot and oscillatory behaviour, here well damped, for steps. It can be reduced through ramp limits.

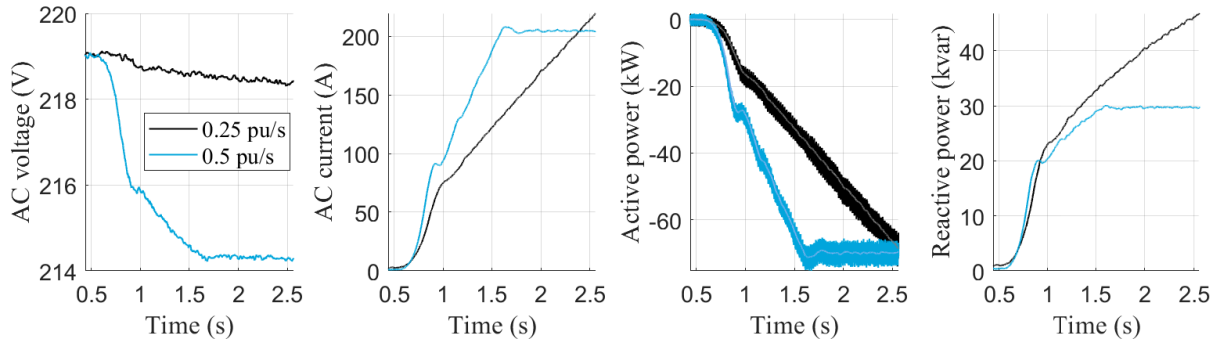


Figure 4.14: -70 kW active power ramp ($H = 2$ s, with different n_q)

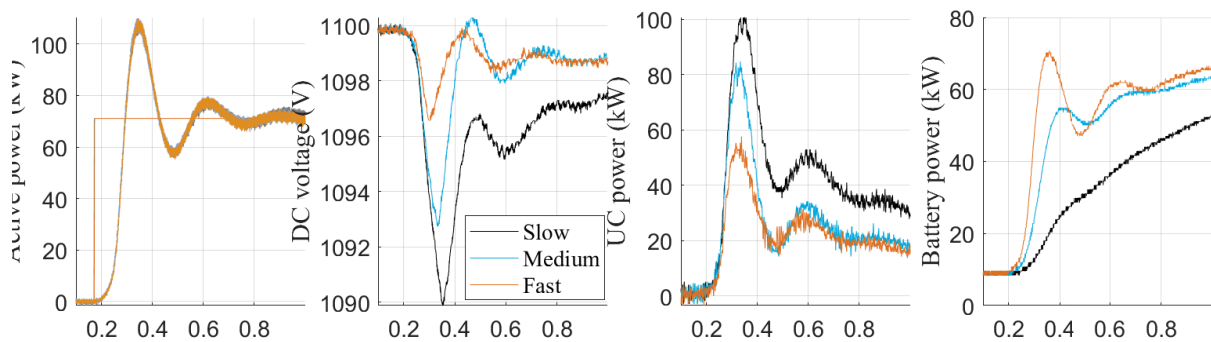


Figure 4.15: 70 kW active power step ($H = 2$ s)

Power sharing between storage devices. DC side converters parameters can be chosen to define different power sharing strategies. The default mode is the "slow" one which ensures that the power peak is provided by the supercapacitors while the battery ramps slowly after a power step for instance. As the battery control is accelerated, the DC voltage can be regulated to a tighter band. For any of the three settings, the DC voltage is regulated with 1% which illustrates the decoupling of the DC side dynamics from the network provided by the active parallel hybrid topology. As a consequence, the AC/DC converter gives the same response and control design hypotheses are validated.

4.4.2. Voltage and reactive power reference tracking

The voltage reference is tracked within 100 ms with good dynamics, independently of the reactive power droop (n_q). Figure 4.16 shows that the active power return to the set point after a 200 ms transient. In operation, ramp limits are applied to the set points as shown in Fig. 4.18 for a modification of the reactive power set point which lead to a smoother behaviour.

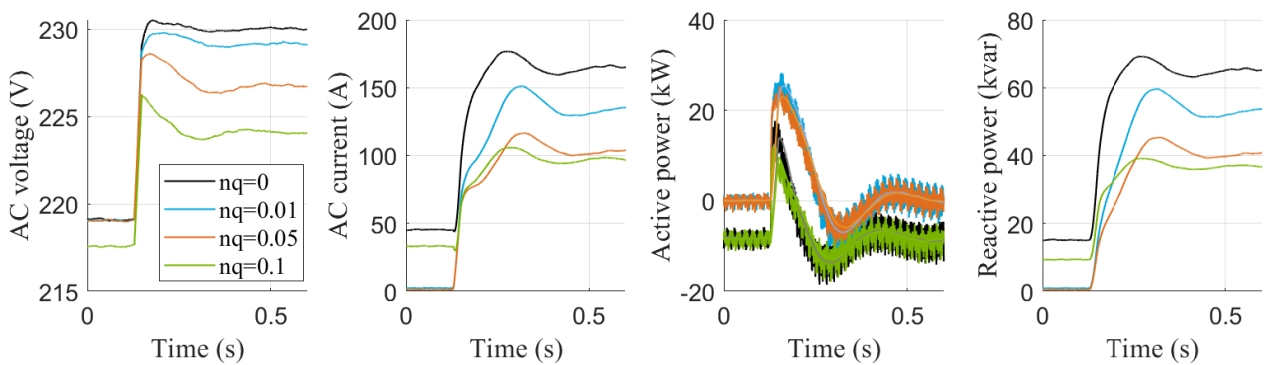


Figure 4.16: 5% Step on voltage set point ($H = 2$ s)

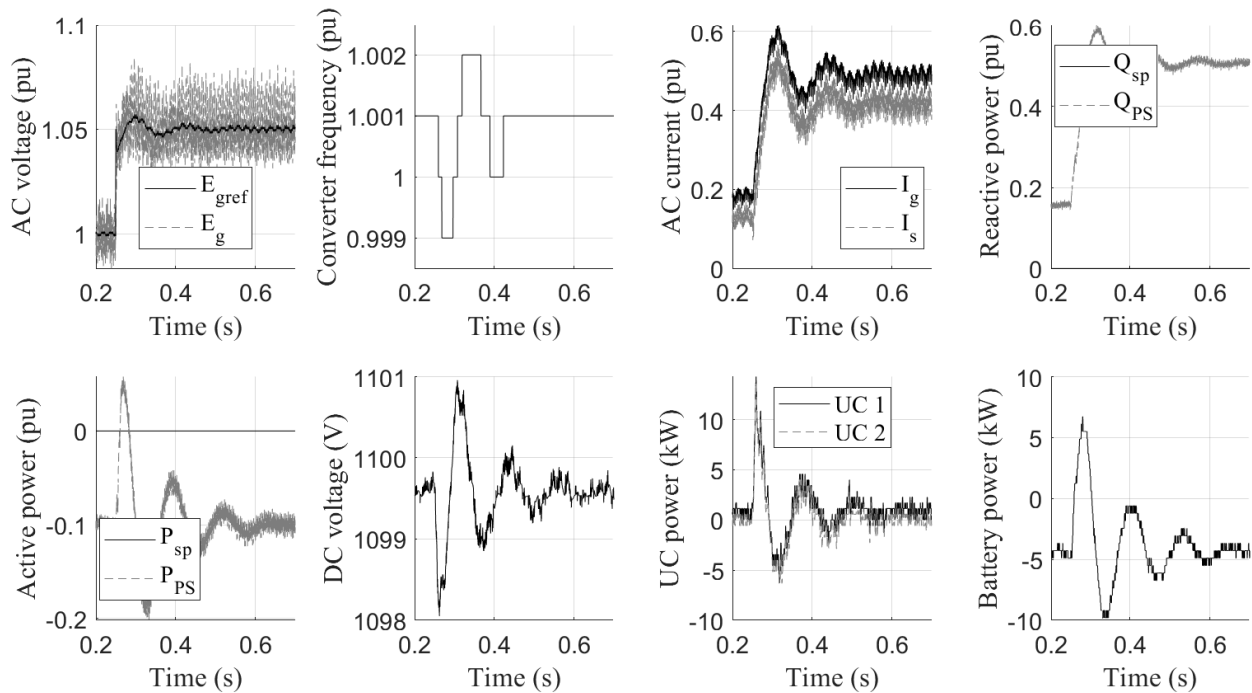


Figure 4.17: 5% Step on voltage set point ($H = 2$ s) - Impact on DC side

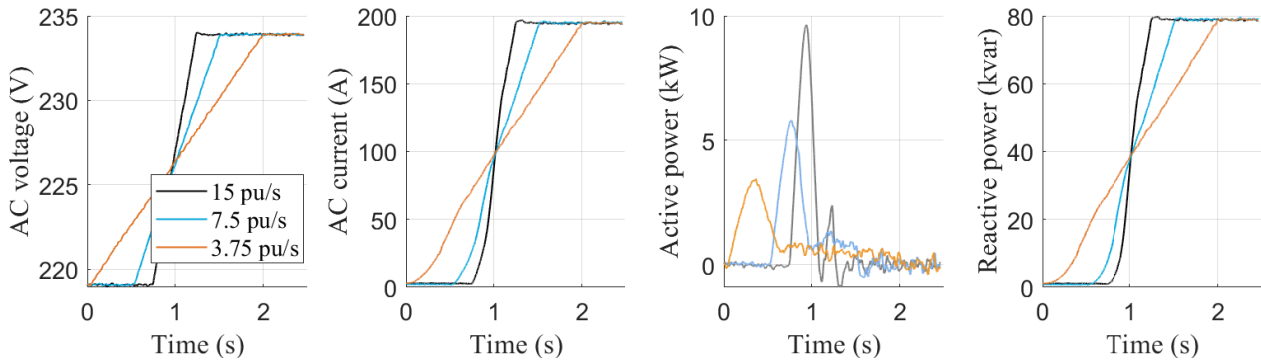


Figure 4.18: 80 kvar with different ramps for $n_q = 0.01$ ($H = 2$ s)

4.4.3. Active power droop with frequency set point

The frequency set point step lead to a steady state power change according to the droop gain. As shown in Fig. 4.19, the UC contribute to it the first second before the battery takes over. Attention must be payed to the intrinsic damping. Again, low impact is observed on the DC bus voltage.

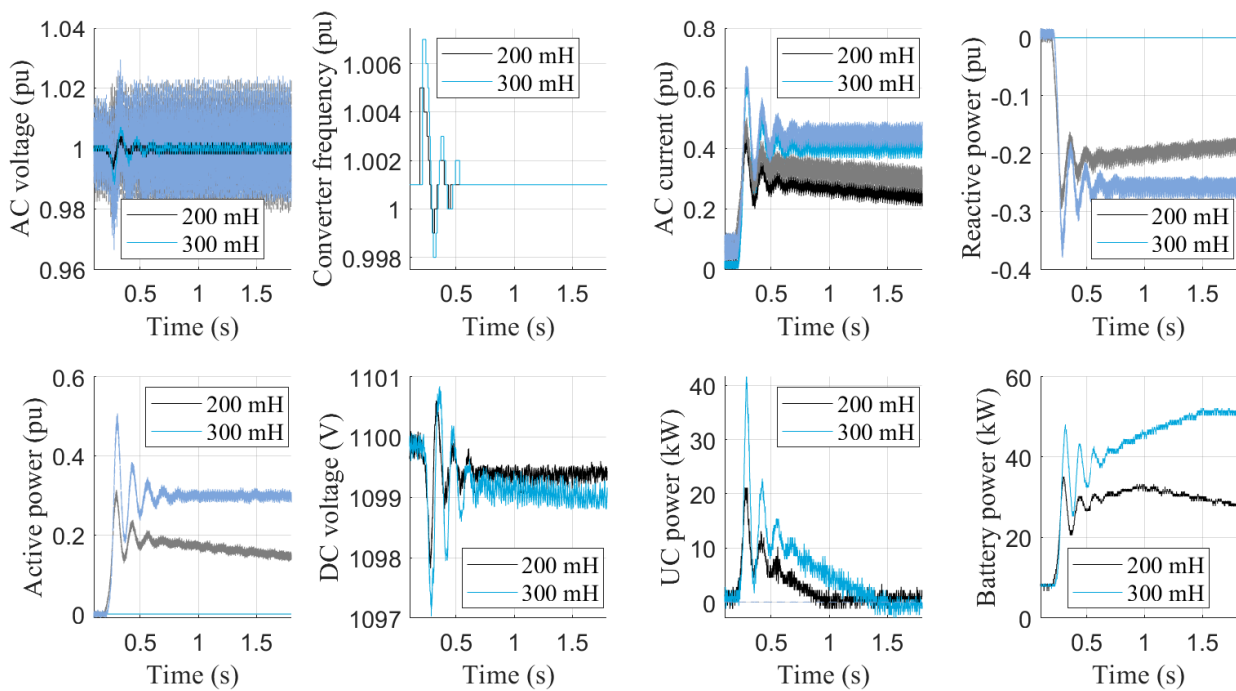


Figure 4.19: Step the frequency set point ($H = 2$ s) - Impact on DC side

4.5. Discussion

Specific FATs to validate the proper behaviour of the grid forming control of the RTE - Ingeteam demonstrator were successfully performed in July 2020 using a PHIL platform available at the Ingeteam Power Laboratory in Zamudio, Spain

4.5.1. Compliance criteria

Synchronising power and inertia active power, defined here and in accordance to [65] as the inherent capability to respond naturally, within less than 5 ms, to grid phase and frequency changes without any supplementary control, was verified. The contribution can be adapted through settable control parameters. However, the well known oscillatory behaviour of this type of grid forming controls was observed. The natural mode frequency and damping varies with the control parameters. A compensation term (P_s) can be computed by the external controller to improve damping [109] such that $P_{set} = P_{sp} + P_s$.

Immediate active power contribution following grid voltage amplitude changes was also confirmed. Moreover, LVRT capability and fast fault current injection proven to be compliant with MIGRATE recommendation and most requirements proposed in the UK grid code draft for grid forming plants [65], i.e. high reactive current is injected immediately (starts to rise in less than 5 ms) during voltage dips as a consequence of the voltage source behaviour, even when current limitation is reached (with TVI). However, some active current might still flow depending on the system impedance. Moreover, the phase, voltage magnitude and frequency are not fixed to their pre-fault value during low voltage events. Indeed the voltage magnitude is reduced by the TVI to achieve current limitation and the phase does tend to drift but quite slowly due to the reduction of the active power droop.

Finally, the installation also proven to be robust to unbalance (5% permanent unbalance tested) and distorted network conditions (10% of 5th harmonic and 7% of 7th harmonic).

4.5.2. Model validation

The model presented in Appendix B has been validated using FAT signals. The full validation report produced in the project is included in Appendix F. The main conclusions are:

- In grid forming applications, strong grid with very low nq and mp values are the most sensitive cases.
- The different types of power generating units (PGUs) have different limits. Grid forming converters, despite being converters, do not regulate their output current and also have inertia. As a consequence, measured results are much more dependent on the grid impedance. The activation and the nature of the TVI is one of the biggest causes of detected simulation-measurements deviations.
- For type 2 PGUs, active power errors have very low limits and that is understandable for grid following applications, but grid forming applications will face challenges to comply with such strong constraints associated to the model validation procedures since the re-synchronization entails a large active power component unlike for grid following applications.
- Big Kp values have shown the capability to damp the system better and to improve dynamic characteristics. Thus, the current loop Kp at real equipment is at its stability limits and the simulation model is unstable with the same value. It also causes errors, especially at fault recovery. It would be interesting to evaluate why the maximum Kp allowable at the real equipment is greater than the maximum Kp of the simulated equipment. The most probable cause is the filtering of the feedback signals.
- Finally, it is important to highlight that average errors are very low, but maximum errors have a significant peak values. The strong grid used for testing may have an impact. The lower the grid impedance, the bigger the voltage and current derivatives. With big derivatives a small delay stopping the current results in significant deviations. This is the case of the TVI activation.

4.5.3. Remaining challenges.

Further work should be carried out on robust negative sequence, damping and active filtering control design in grid forming mode.

4.5.4. BESS security: RTE-Ingeteam demonstrator commissioning incident.

The system has been delivered in August 2020 and the demonstrator was successfully connected to the RTE network in September 2020. However, a fire on December 1st, during the Site Acceptance Tests in RTE substation, led to the destruction of the storage container. There were no injuries and no other damage than the impacted container but the experimentation could not be continued during the project duration as it was not possible to redesign, purchase the component and obtain authorisation for a new installation within the year left of the project. More details about this incident together with some recommendations for similar projects are given Appendix G.

5. Performance assessment of synchronisation service on RTS

As broadly acknowledged in the power systems community, a large deployment of converter-interfaced generation determines lower grid inertia levels and calls for a review of frequency containment concepts and the identification of assets capable of maintaining the short-term power balance. In fact, some power systems are already facing this control challenge. In this context, converter-interfaced battery energy storage systems (BESSs) are advocated as a potential solution for grid frequency regulation (e.g., [110]) thanks to their fast ramping rates, high round-trip efficiency and commercial availability [111].

There are two main approaches to control converter-interfaced BESSs in terms of synchronisation mechanism: grid-following and grid-forming. In a grid-following converter, the current injected by the converter is controlled with a specific phase displacement from the grid voltage at the point of common coupling (PCC). As a consequence, the knowledge of the fundamental frequency phasor of the grid voltage is needed at any time for the correct calculation of the converter's reference current. In contrast, a grid-forming converter controls magnitude and angle of the voltage at its terminals. In this case, the knowledge of the fundamental frequency phasor of the grid voltage is not strictly necessary.

This Chapter presents the results of the performance assessment of Grid-forming vs Grid-following control for converter-interfaced BESS. In particular, the analysis proposes a comparison on the effects of the two different control strategies in a low-inertia power grid. A detailed model of the IEEE 39-bus has been implemented in a real-time (digital) simulator (RTS), and has been used for the validation of the 2 strategies by feeding the model with the same grid conditions, exploiting the flexible nature of a simulation environment.

The content included in this Chapter is taken from the scientific publications [112, 113], authored within the context of the Osmose project WP3 activities. Section 5.1 first provides a description of the test setup, then Section 5.2 defines relevant Key Performance Indicators (KPI) to enable a reliable and scalable assessment of the results, and finally Sections 5.3 and 5.4 present relevant results, which will be later on recalled in Chapter 6 when discussing the experimental results of the EPFL demonstrator.

5.1. EPFL IEEE-39 bus RTS test bench description and study cases

The proposed simulation framework is composed by two layers: real-time simulations and a scheduling stage. The former is used to evaluate the performance of the converter controllers by analysing the whole grid dynamic behaviour. The latter allows to size power reserve requirements and reproduce realistic operative scenarios for the real-time simulations. Fig. 5.1 illustrates the overall simulation process, where L and W denote measurements of power demand and wind generation, respectively. The process starts with dividing the measurements into two subsets, one for training the forecasting and model, and one to feed the real-time simulations.

Accordingly, the demand profile denoted by the sequence $L = \{l_1, l_2, \dots, l_n\}$ is separated as $L_1 = \{\tilde{l}_1, \tilde{l}_2, \dots, \tilde{l}_{n-24}\}$ and $L_2 = \{l_{n-23}, l_{n-22}, \dots, l_n\}$, and the wind generation profile denoted by the sequence $W = \{w_1, w_2, \dots, w_m\}$ is separated as $W_1 = \{\tilde{w}_1, \tilde{w}_2, \dots, \tilde{w}_{m-24}\}$ and $W_2 = \{w_{m-23}, w_{m-22}, \dots, w_m\}$.¹ L_2 and W_2 are directly applied to the RTS to be reproduced in the day-long simulations. At the day-head schedule layer, L_1 and W_1 are sent to the forecasting models to obtain the demand and wind

¹It should be noted that $l_i = \{l_{i,1}, l_{i,2}, \dots, l_{i,3600}\}$ is the 1-second resolution demand set for hour i and \tilde{l}_i is the average demand of hour i . w_i and \tilde{w}_i are likewise the 1-second resolution wind generation set and the average wind generation for hour i , respectively.

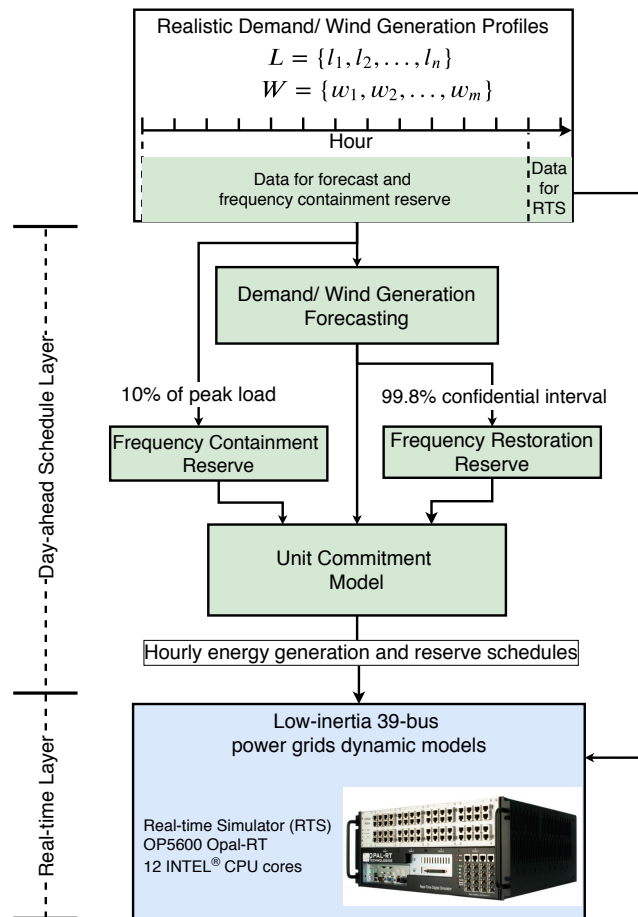


Figure 5.1: Simulation framework.

generation forecasting results, which are then used to compute the frequency restoration reserve. Additionally, L_1 is also used for computing the frequency containment reserve as is considered as 10% of peak load (i.e., ± 500 MW), covering the loss of half of the biggest generation unit. Then, a unit commitment model determines an optimal hourly generation and reserve schedule accounting for the demand and wind generation forecasting results, the frequency containment and restoration reserves, as well as the power network and operational constraints. Eventually, the RTS executes simulations of the dynamic models of the low-inertia 39-bus power grids which are implemented with the realistic demand and wind generation profiles (i.e., L_2 and W_2) and the energy generation and reserve schedules provided by the unit commitment model.

The low-inertia power system considered in this work is derived from the IEEE 39-bus benchmark system, where four of ten synchronous generators (one thermal power plant and three hydro power plants) are replaced with four wind farms. The detailed description of the model is given in the previous Deliverable D3.2. For clarity, its main features are summarized here. The configuration of the low-inertia 39-bus system is shown in Fig 5.2. Its inertia constant (referred to a 10 GW base and obtained by summing the inertia constant of all the conventional power plants) has decreased from 7.84 s of the original grid to 1.98 s.

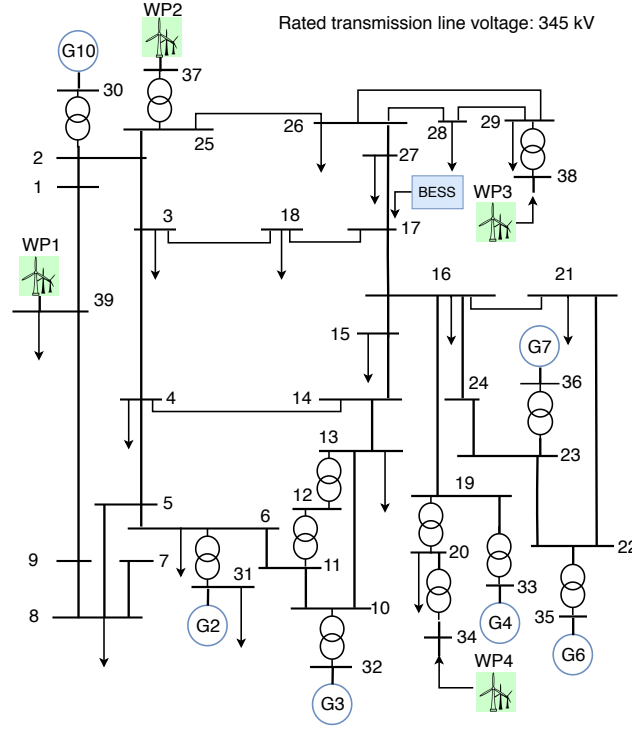


Figure 5.2: Diagram of 39-bus low-inertia power systems (The presence of the BESS at bus 17 is taken into account in grid).

5.2. Characterisation of the synchronisation service

In order to quantitatively evaluate the effectiveness of the implemented BESS controls in terms of grid regulation, it is indeed necessary to rely on KPI, as discussed in Deliverable D3.2, that can guarantee the quality of the analysis as well as the scalability of the obtained results. Another important aspect that has been considered was the possible dependency of the results on the size of the considered BESS and power systems. This has been taken into account by making absolute KPIs relative to the exchanged BESS power. The KPIs identified and utilized in this work are listed below:

- Integral Frequency Deviation (IFD):

$$\text{IFD} = \sum_i^L \sum_{k=1}^N |f_{k,i} - f_0| \quad (5.1)$$

where L is the number of phasor measurement unit (PMU) available in the grid and N is the total sampling number of frequency measurements for each PMU. In the description of the results included in section 5.3n, an analysis on the goodness of this KPI as a function of the number of the employed PMUs will be detailed.

- Relative Rate-of-Change-of-Frequency (rRoCoF):

$$\text{rRoCoF} = \frac{\Delta f_{pcc} / \Delta t}{\Delta P_{BESS}} \quad (5.2)$$

where Δf_{pcc} is the difference between one grid frequency sample and the next (once-differentiated value) at the bus where the BESS is connected to, ΔP_{BESS} is the once-differentiated BESS active power, and Δt is the sampling interval.

- Relative Phase Angle Difference Deviation (rPADD):

$$\text{rPADD} = \left| \frac{\Delta\sigma_k - \Delta\sigma_0}{\Delta P_{BESS}} \right| \quad (5.3)$$

where $\Delta\sigma_0 (= \sigma_{0,PMU1} - \sigma_{0,PMU2})$ is the phase-to-neutral phase angle difference between the measured phase angles at the two sides of the step-up transformer in case of 0kW delivered by the BESS, whereas $\Delta\sigma_k (= \sigma_{k,PMU1} - \sigma_{k,PMU2})$ is the phase angle difference when the BESS is exchanging power. ΔP_{BESS} is the once-differentiated BESS active power. Note that this KPI is computed only for the experimental demonstrator activities on the utility-scale BESS at EPFL, where two PMUs have been installed in specific locations, as it will be described in Chapter 6.

One has to note that on the one hand, the IFD is measured to quantify the grid frequency containment performance on the system level. On the other hand, the rRoCoF and the rPADD are utilized as mean of assessment of the local impact of the deployed grid-forming and grid-following control approaches. These 2 indexes are normalised by the delivered active power of the BESS, thus are used to compare the performance of grid-forming versus grid-following converters in two different battery scales (RTS and EPFL full-scale experimental setup) and different governor parameters.

5.3. Evaluation of the synchronisation service effectiveness

For the purpose of comparison, the grid-forming and grid-following interfaced BESS have been tested over 24-hour long simulations, where the same generation and reserve schedules obtained from the unit commitment model are reproduced. Table 5.1 lists the five cases tested over the 24-hour long simulations.

- *Case 1* is the base configuration with no BESS.
- *Case 2* and *Case 3* feature a BESS connected to the low-inertia power grid via a PLL-free grid-forming converter with the $p - f$ droop coefficients of 2% and 1%, corresponding to the $f - p$ control gains of 225 MW/Hz and 450 MW/Hz, respectively.
- *Case 4* and *Case 5* are the two cases where the BESS is connected to the low-inertia power grid through a grid-following converter. Grid supporting functions, such fast primary frequency regulation with $f - p$ control gains of 225 MW/Hz and 450 MW/Hz, respectively, and reactive current injection in response to voltage deviation are added on top of the grid following control ².

Table 5.1: Cases studied through day-long simulations

Case	BESS converter control	$f-p$ Droop
<i>Case 1</i>	No BESS	-
<i>Case 2</i>	Grid-forming	225 MW/Hz
<i>Case 3</i>	Grid-forming	450 MW/Hz
<i>Case 4</i>	Grid-following with supporting mode	225 MW/Hz
<i>Case 5</i>	Grid-following with supporting mode	450 MW/Hz

Figure 5.3a and 5.3b present the scheme of the adopted grid-forming control and grid-following control operating in grid-supporting mode, respectively.

Figure 5.4a shows the system frequency for the 5 cases. The zoomed region shows that the grid frequency dynamics at the beginning of the 15-th hour exhibits a considerable frequency deviation.

²It is worth noting that the dead zone of the $p - f$ regulator described in Deliverable 3.2 has been removed and a $q - v$ regulator is added in order to make a fair comparison with the grid-forming control.

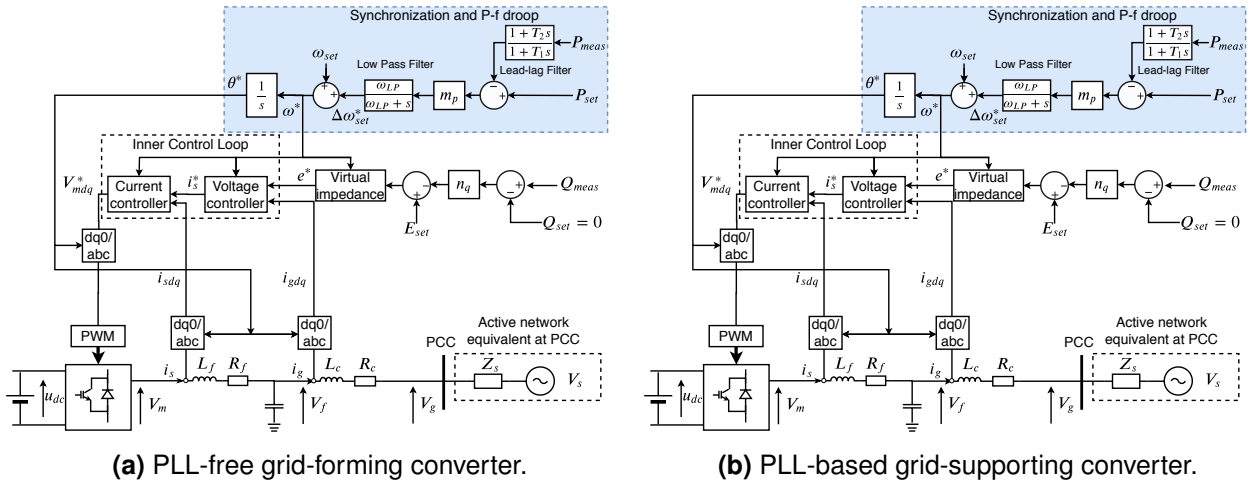


Figure 5.3: Power converter Controls.

The cases with a higher $f - p$ control gain attain more frequency containment because of the larger regulating power provided, as visible in the zoomed region of Figure 5.4b.

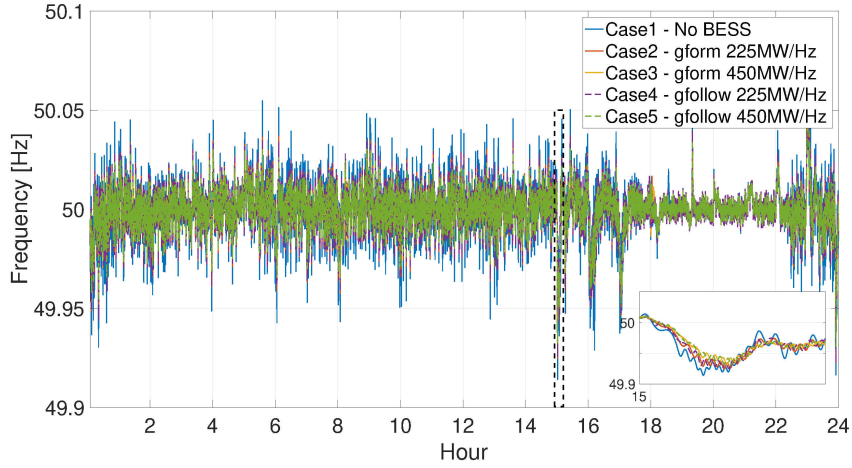
While Figure 5.4 provides a general view of the system frequency responses, the defined metrics allow a better scrutiny of the control performance and will be described next. The IFD and rRoCoF are computed with frequency measurements estimated by simulated PMUs embedding the e-IpDFT (enhanced Interpolate Discrete Fourier Transform) synchrophasor compliant with P-class [114]. The reporting rate of the adopted PMUs is 20 ms.

5.3.1. Integral Frequency Deviation

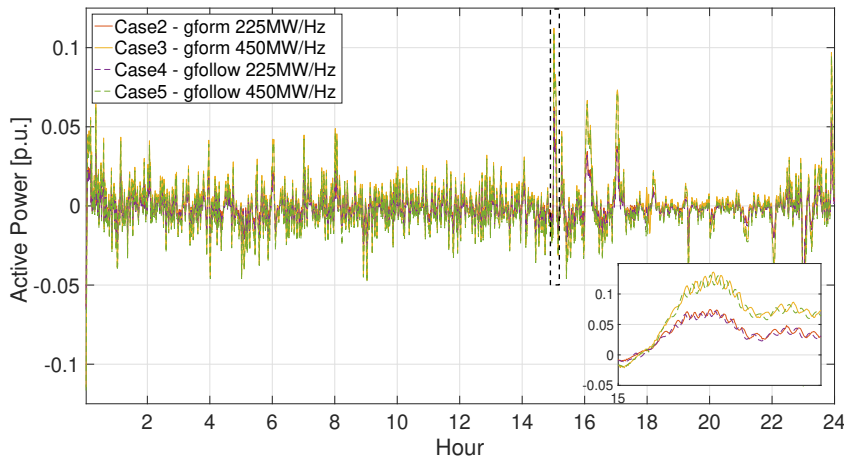
Table 5.2 shows that the case without BESS (i.e., *Case 1*) scores the highest IFD, which is considered as baseline (100%) for the other four cases. In order to show the sensitivity of IFD with respect to the number of deployed PMUs, the IFD values computed using measurements from different numbers of PMUs are provided in Table 5.2. It illustrates that, although the absolute values of IFD increase subsequent to the increase of the number of PMUs, the relative values with respect to the baseline are consistent³. Specifically, in *Case 2* and *Case 3*, IFD decreases by 11.0% and 20.3%, respectively, compared to *Case 1*. In *Case 4* and *Case 5*, IFD decreases by 10.0% and 18.8%, respectively.

On one hand, it quantitatively shows that the large-scale BESS are capable of significantly improving the system frequency containment, and the level of improvement is proportionally related to the level of $f - p$ gain. On the other hand, comparing *Case 2* vs *Case 4* and *Case 3* vs *Case 5*, the results exhibit that the grid-forming control strategy outperforms the grid-following one achieving better frequency containment. Finally, the advantage of the grid-forming control is more significant with higher level of $f - p$ gain.

³It is worth to note that, when the number of PMUs are small (i.e., 6 and 3 PMUs) compare to the size of the grid, the PMUs should be evenly distributed in order to capture frequency dynamics of the whole system.



(a) System frequency.



(b) BESS active power.

Figure 5.4: System frequency and BESS active power.

5.3.2. Relative Rate of Change of Frequency

The metric rRoCoF is computed over a time window of 60 ms. Namely, Δt in (5.2) is equal to 60 ms and:

$$\Delta f_{PCC}(n) = f_{pcc}(n+3) - f_{pcc}(n) \quad (5.4)$$

$$\Delta P_{PCC}(n) = P_{BESS}(n+3) - P_{BESS}(n) \quad (5.5)$$

where $n = 1, 2, \dots, N-3$ and N is the total sampling number of frequency measurements. Figure 5.5 shows a 15-minute window (i.e., from 15:00 to 15:15) time series of the computed rRoCoF.

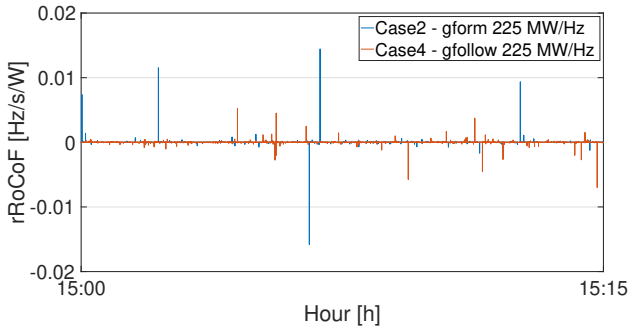
Figure 5.6 illustrates the Cumulative Density Functions (CDFs) of rRoCoF for the larger and smaller $f-p$ gains for both grid-forming and grid-following converter. For the smaller gain in Fig. 5.6a, the grid-forming converter performs better than the grid-following converter as it achieves lower RoCoF per Watt of regulating power. The standard deviation of rRoCoF for Case 2 and 4 are $\sigma_{case2}^{rRoCoF} = 0.0016$ and $\sigma_{case4}^{rRoCoF} = 0.0065$, respectively.

Figure 5.6b shows that also for the larger gain, the grid-forming converter performs better than the grid-following as it achieves smaller frequency rates. In this case, the corresponding standard devia-

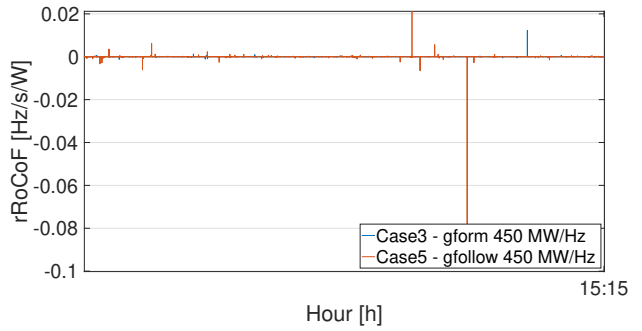
Table 5.2: Integrated Frequency Deviation for the 5 cases

	IFD [Hz]				
	19 PMUs	15 PMUs	10 PMUs	6 PMUs	3 PMUs
Case1	7.5476	5.9585	3.5751	2.3835	1.1918
Case2	6.7181	5.2952	3.1814	2.1240	1.0620
Case3	6.0147	4.7404	2.8483	1.9019	0.9508
Case4	6.7976	5.3572	3.2119	2.1419	1.0707
Case5	6.1376	4.8309	2.9009	1.9369	0.9679
	$\times 10^5$				

	IFD reduction compare to <i>Case 1</i> – Δ IFD [%]				
	19 PMUs	15 PMUs	10 PMUs	6 PMUs	3 PMUs
Case2	11.0%	11.1%	11.0%	10.9%	10.9%
Case3	20.3%	20.4%	20.3%	20.2%	20.2%
Case4	9.9%	10.0%	10.2%	10.1%	10.2%
Case5	18.7%	18.9%	18.9%	18.7%	18.8%



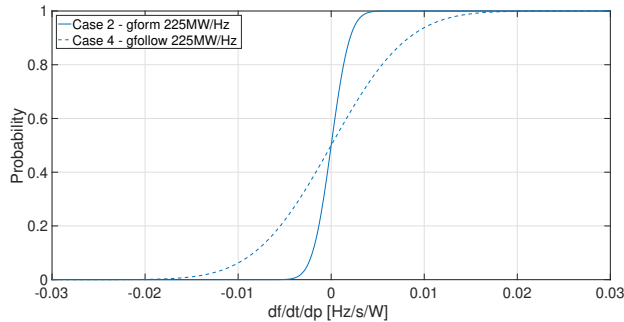
(a) Case 2 and Case 4.



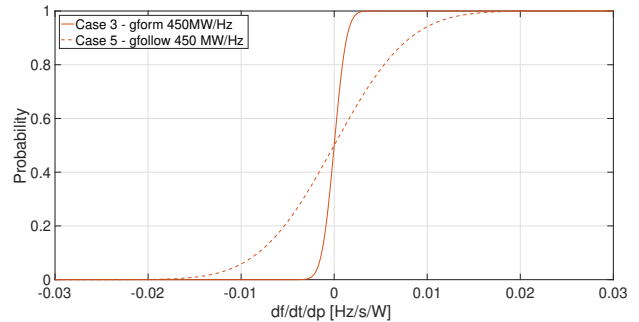
(b) Case 3 and Case 5.

Figure 5.5: Computed rRoCoF time series.

tions of rRoCoF are $\delta_{case3}^{rRoCoF} = 0.0013$ and $\delta_{case5}^{rRoCoF} = 0.0064$ for Case 3 and 5, respectively.



(a) Case 2 and Case 4.



(b) Case 3 and Case 5.

Figure 5.6: Cumulative density function (CDF) of rRoCoF.

To conclude, the suitably defined KPIs allowed the assessment of the performance of grid-forming

control with respect to to grid-following control operating in grid-supporting mode. The proposed criteria can be conveniently computed as they do not require the knowledge of implemented control structure, and instead are based on external frequency measurements estimated by PMUs (the precision of P-class PMUs is sufficient) installed in power grids.

5.4. Evaluation of the synchronisation service robustness

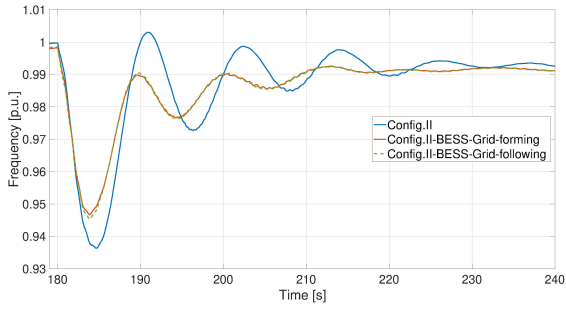
The robustness of the grid-following and grid-forming units is studied with the following contingencies:

- *Case 1*: tripping of G6 (800 MW generation loss).
- *Case 2*: tripping of G4 (545 MW generation loss).

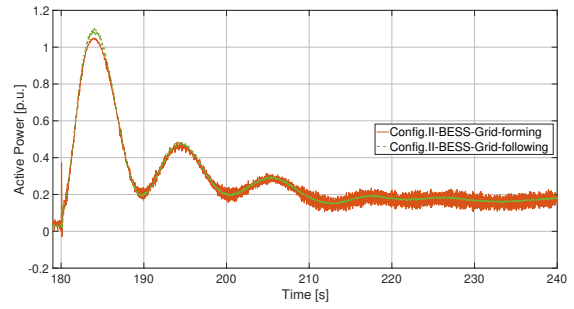
Fig. 5.7a shows the post-contingency frequency performance of low-inertia 39-bus power grid (denoted as Config. II) without BESS, the low-inertia 39-bus power grid with grid-forming based BESS and the low-inertia 39-bus power grid with grid-following based BESS. It shows that the VSC-based BESS achieves to increasing frequency Nadir from 0.9366 p.u. to 0.9480 p.u. and a better damping of the frequency oscillations by decreasing the overall transient interval from 80 s to 40 s. Fig. 5.7b and Fig. 5.7c show the active and reactive power for the installed converter unit. The grid-following and the grid-forming controllers use the same frequency droop coefficient, thus both controllers inject active power into the power system following the same droop characteristic. The considered grid-following control injects reactive power as the result of external voltage regulation, whereas the reactive power injected by the considered grid-forming control is due to the implicit coupling between active power and reactive power. As shown by Fig. 5.7c, during the transient the reactive power injected by the grid-following converter rises up to 0.31 p.u., while the reactive power injected by the grid-forming converter only goes up to 0.34 p.u. Fig. 5.7d presents the amplitudes of the grid voltage at the PCC of the installed converter unit (i.e., bus 17). It denotes that, after the contingency there is a voltage sag within 100 ms and the grid-following unit experiences a higher voltage drop (i.e., decrease 6% and nominal voltage) than the grid-forming units (i.e., decrease of 4.5% of nominal voltage).

To represent a less extreme contingency, in *Case 2* we trip G4 to cause less generation loss. Fig. 5.8 shows the simulation results of reproducing the same contingency for Config. II and Config. II with converter-interfaced BESS. Fig. 5.8a presents the frequency responses for Config. II and Config. II-BESS. It illustrates that the converter unit increases the frequency Nadir from 0.9589 for Config. II to 0.9665 for Config. II-BESS and ameliorates the frequency oscillations by decreasing the transient duration from 75 s to 35 s. Fig. 5.8b and Fig. 5.8c show the active and reactive power injected by the converter unit. For both the grid-following and grid-forming control, the injected active power tracks frequency deviations accordingly with their droop coefficients. During the transient, the reactive power injected by the grid-following converter rises up to 0.30 p.u., while the reactive power injected by the grid-forming converter only goes up to 0.32 p.u. Fig. 5.8d shows the amplitude of the grid voltage at the PCC of the converter units. It demonstrates the benefit of the grid-forming converter as voltage source in preventing the PCC voltage from large variation. In contrast, the grid-following converter experiences a voltage sag (-5.5% of nominal voltage) within 100 ms after the contingency and a generally higher voltage variation during the transient.

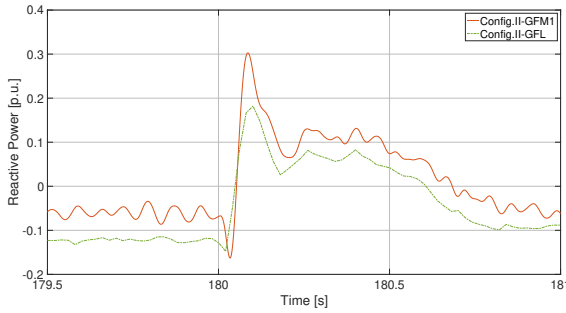
To conclude, the full-replica dynamic model of the low-inertia 39-bus power grid has been used to assess the performance of grid-forming and grid-following converter-interfaced BESS in enhancing frequency containment regulation. By means of suitably-defined frequency metrics, the day-long real-time simulation results show that the grid-forming control strategy outperforms the grid-following one achieving better IFD and lower relative RoCoF. In the following, the experimental assessment and validation activities relying on the setup of the EPFL campus MV grid hosting the utility-scale 720kVA/500kWh BESS will be presented in Chapter 6.



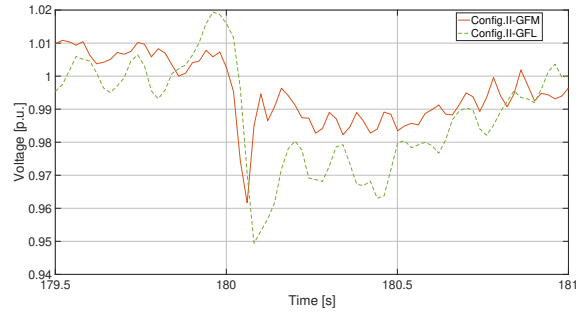
(a) Frequency.



(b) Active power.

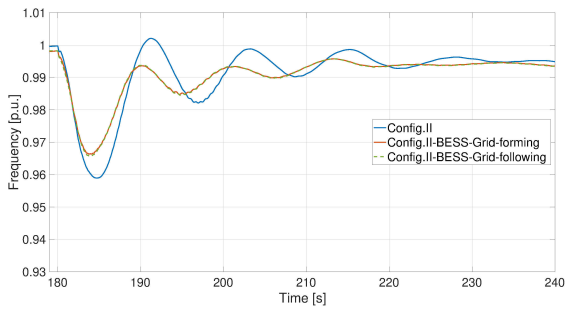


(c) Reactive power.

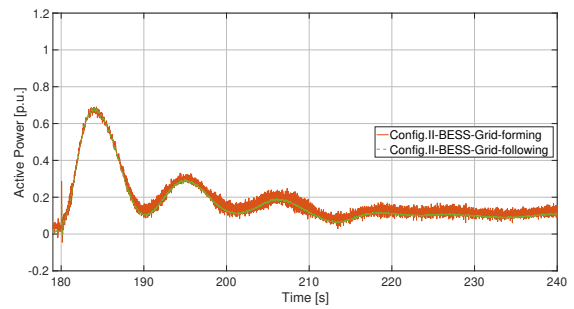


(d) Grid voltage at PCC.

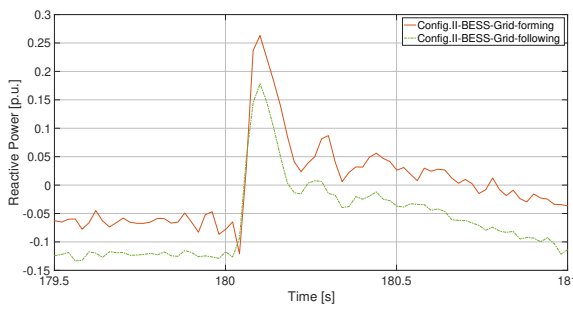
Figure 5.7: Frequency, power injections and grid voltage at bus 17 in Config. II-BESS for *Case 1*.



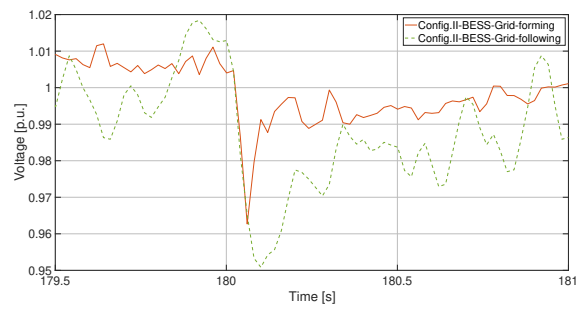
(a) Frequency.



(b) Active power.



(c) Reactive power.



(d) Grid voltage at PCC.

Figure 5.8: Frequency, power injections and grid voltage at bus 17 in Config. II-BESS for *Case 2*.

6. Providing a synchronisation service with ESS: EPFL demonstrator

6.1. Upgrading the control of EPFL BESS

As extensively demonstrated in the literature, one of the power system services provided by BESSs is primary frequency control (PFC), which is increasingly needed from transmission system operators (TSOs) given the progressive displacement of conventional generation plants in favor of stochastic renewable-based generation units. PFC is typically performed by a frequency droop controller that determines the variation of the active power (ΔP) exchanged with the AC grid for a given frequency deviation from a reference value. Since power converters are normally able to operate on the 4 quadrants of their PQ capability curve, they are also capable of exchanging reactive power concurrently with the active power. Within this context, the proposed control approach considers the additional simultaneous exchange of reactive power, which is seen as a viable mean for local voltage regulation at distribution grid level. Similarly to the case of PFC, local voltage deviations from the nominal value can be used as input for determining the necessary variation on reactive power (ΔQ).

In the scientific contributions [110] and [115] authored within the framework of the Osmose project, a BESS control framework is proposed, which includes the joint PFC-voltage control actions. The details of the proposed control framework are thoroughly described in Deliverable D3.4 [95], whereas here we recall some of its features, which should be considered when implementing grid services with BESS power converters. This is achieved within the real physical constraint of having a non-unique PQ region of feasibility of the BESS power converter: this region is in fact a function of the battery DC-link and AC grid statuses. This aspect goes beyond the typical assumptions present in the existing scientific literature where it is assumed that the PQ capability curve of the BESS converter is static and does not depend on battery state-of-charge (SoC) and AC grid voltage conditions. In fact, commonly in the current literature the converter capability is considered to be constantly expressed as $(P_t^{AC})^2 + (Q_t^{AC})^2 \leq (S^{AC})^2$, where P_t^{AC} , Q_t^{AC} , and S^{AC} are the converter output active, reactive and maximum apparent power of the grid converter, respectively. This assumption, however, does not hold in practice. The realistic feasible operation region identified by the PQ converter capability curves h in Fig. 6.1 can be considered as:

$$h(P_t^{AC}, Q_t^{AC}, v_t^{DC}, v_t^{AC}, SOC_t) \leq 0 \quad (6.1)$$

being v_t^{DC} the voltage of the BESS DC bus and v_t^{AC} the module of the direct sequence component of the phase-to-phase voltages at the AC side.

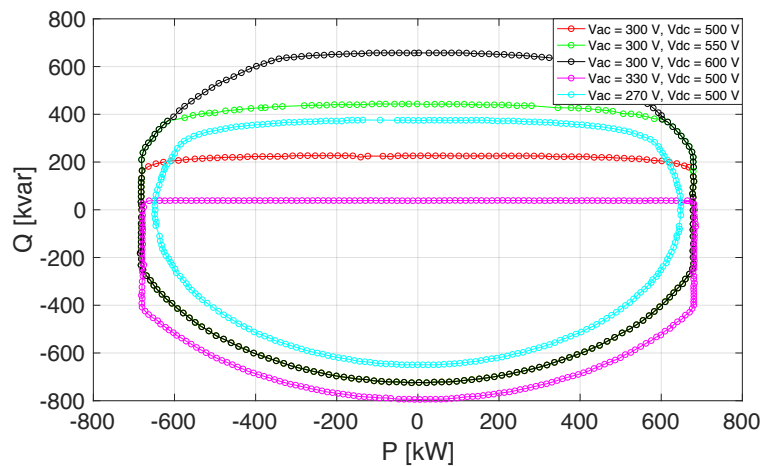


Figure 6.1: BESS converter PQ capability curves as function of v_t^{AC} and v_t^{DC} .

Notably, the capability curves h are specific for the employed hardware, but similar dependencies are expected in all kinds of utility-scale BESS converters. As shown in Fig. 6.1, the region of feasible operating points of the power converter depends on the grid AC voltage and on the DC battery voltage in a non-linear way. In fact, for increasing battery DC voltages only the maximum positive Q value is increasing. The curve is shifted down vertically for AC voltages higher than the nominal value, meaning that both the maximum positive Q is decreased, whereas the maximum negative Q is increased. A different pattern is present for AC voltages lower than the nominal value: the limit values are shrank both for the active and the reactive part of the apparent power set-point in both negative and positive signs. The capability curves of the employed power converter are fitted using datasheet information from the manufacturer and, then, scaled proportionally to the available BESS capacity. The fitted capability curves consist of a series of linear and quadratic functions [110].

In the framework presented in [110] and [115] the BESS converter was operated in grid-following mode, meaning that the joint PFC-voltage control actions were achieved by setting PQ set-points on the BESS, following a computation in an external outer loop. In particular, the converter was controlled to provide PFC and local voltage regulation adjusting the active and reactive power set-points, respectively. The initial power set-points are achieved via droop logics:

$$P_{0,t}^{AC} = \alpha_0 \Delta f_t; Q_{0,t}^{AC} = \beta_0 \Delta v_t^{AC}, \quad (6.2)$$

where $t \in T$ is the discrete index of time, $P_{0,t}^{AC}, Q_{0,t}^{AC}$ are the initial active and reactive power set-points that the BESS will set for given grid frequency and AC voltage magnitude deviations from their nominal values $(\Delta f_t, \Delta v_t^{AC})$, according to the initial droop coefficients α_0, β_0 .

These active and reactive power set-points will be adjusted when considering the converter capability curves, solving an optimization problem that needs to satisfy, among others, the constraint (6.1) as for the converter feasible points of operation. When providing ancillary services to grid operators one wants to exploit as much as possible the available controllable asset, meaning that it is of interest for the BESS operator to maximize as much as possible the potential revenues coming from the provision of the grid services. To maximize the frequency and voltage regulation performance, the initial droop coefficients α_0, β_0 can be set as:

$$\alpha_0 = \frac{P^{max}}{\Delta^{max} f_t}; \beta_0 = \frac{Q^{max}}{\Delta^{max} v_t^{AC}}, \quad (6.3)$$

where P^{max} and Q^{max} are the maximum active and reactive power that the BESS can exchange, as specified by the BESS technical specifications. For the determination of the maximum frequency and voltage deviation $\Delta^{max} f_t, \Delta^{max} v_t^{AC}$, historical measurements have been used as shown in Fig. 6.2.

In particular, historical measurements acquired by the synchrophasor network on the EPFL MV network are used for this purpose, whose P-class phasor measurement units (PMUs) allowed the acquisition of data with a timestamp of 20 ms. The values of $\Delta^{max} f$ and $\Delta^{max} v^{AC}$ have been obtained by approximating their distribution with normal distribution functions and by considering a relevant multiplication factor for the standard deviations σ .

On the one hand, the maximum deviations of $\pm 3.3\sigma_f$ was considered for the system frequency measurements, meaning that the thresholds $\mu_f \pm 3.3\sigma_f$ are statistically exceeded only 0.1% of the times, being μ_f the average value of the frequency dataset, equal to 50.000 Hz. This rather strict assumption is motivated by the requirement from the Swiss TSO grid code on the quality of the supply of primary frequency control power, which sets a maximum tolerable time of 0.1% of the tender period for which the regulating power cannot be delivered without running into penalties. Indeed, the undelivered service will not happen simultaneously on all the BESSs controlled with the proposed framework, since as discussed above and shown by Fig. 6.1, the delivered power is a function of the local grid state, namely v_t^{AC} .

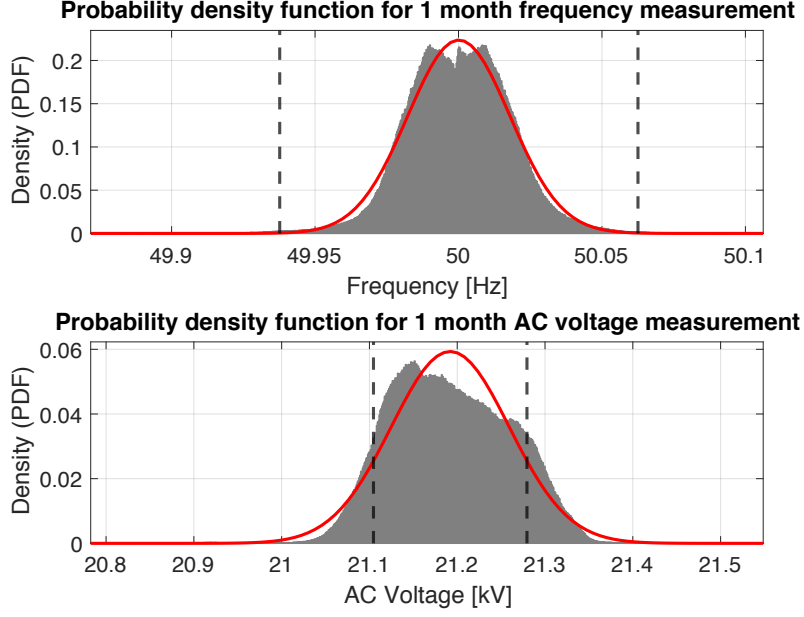


Figure 6.2: 1 month historical data of frequency and phase-to-phase voltage at the BESS PCC at 21 kV, acquired via PMUs installed at the EPFL MV network. The dashed lines represent the limits of $\mu_{fp} \pm 3.3\sigma_f$ and $\mu_V \pm 1\sigma_V$ for frequency and voltage measurements, respectively.

On the other hand, since less strict requirements regulate the quality of the supply of local voltage control, smaller maximum deviations can be considered: the calculated thresholds for the activation of the maximum reactive power capacity are $\mu_V \pm 1\sigma_V$, where μ_V is the average value of the AC phase-to-phase voltage dataset, equal to 21.192 kV. Since the obtained μ_V differs from the nominal value of 21 kV, it was decided to consider μ_V as reference for the calculation of $\Delta^{max} v^{AC}$ in (6.2). Given the considered historical dataset, $\Delta^{max} f = \pm 3.3\sigma_f = \pm 58.8$ mHz and $\Delta^{max} v^{AC} = \pm 1\sigma_V = \pm 0.0672$ kV. The calculated $\Delta^{max} f$ and $\Delta^{max} v^{AC}$ enable the computation of the initial droops α_0 and β_0 , which resulted in 11.575 MW/Hz and 10.78 kvar/V, respectively.

It is clear that the initial values of the employed droops can be calculated in different ways as well, such as by including in the problem an additional level of control objectives, as for example the day-ahead computation of the droop values for the next day, following MV grid dispatch-based strategies. In fact, an alternative way of computing the initial droop values is proposed within the multi-service control framework included in the Deliverable D3.4 [95]. Analogously, one service can be prioritised over the other, when the set-point that has to be implemented falls outside of the capability curve of the converter. In particular, the optimal active and reactive power set-points are given by solving an optimization problem with the following objective:

$$\text{Minimize } \lambda_P (P_t^{AC} - P_{0,t}^{AC})^2 + \lambda_Q (Q_t^{AC} - Q_{0,t}^{AC})^2 \quad (6.4)$$

Where λ_P and λ_Q are weight coefficients used by the modeler to prioritize the provision of active or reactive power, i.e., to prioritize one grid service over the other. In the case of equal priority for frequency and voltage control, the weight of 1 is assigned to both coefficients, meaning that the optimal power set-points P_t^{AC}, Q_t^{AC} are the closest to the initial power set-points $P_{0,t}^{AC}, Q_{0,t}^{AC}$ inside the feasible operational region of the BESS defined by (6.1). After finding the optimal power set-points P_t^{*AC}, Q_t^{*AC} , the optimal droop parameters α_t^*, β_t^* are defined as:

$$\alpha_t^* = \frac{P^{*AC}}{\Delta f_t}; \beta_t^* = \frac{Q^{*AC}}{\Delta v_t^{AC}} \quad (6.5)$$

In the experimental validation, a time granularity of 1 second has been used for data acquisition and optimal set-point computation, meaning that at each second a new operating point within the corresponding feasible PQ region is sent to the BESS converter controller. The choice of 1-second response is considered as a realistic assumption in BESS applications as indicated, for instance, by the newly-released grid code by the Danish TSO Energinet.dk [116]. However, the Authors are aware that in low-inertia power systems rapid (i.e., sub-second) frequency variations are more likely to be experienced [117], meaning that even faster response from control providers may be needed. In this regard, in case a grid disturbance occurs between two iterations of the optimisation problem (i.e. in the sub-second time window), the safety of the system is ensured because:

- In grid-following mode the converter's inputs are power set-points, which are computed by the optimization problem itself. Therefore, changes in the frequency between two iterations of the optimization problem won't affect the delivered power. Simply, in the next iteration, the new frequency value will be fed to the optimization problem.
- In grid-forming mode, the converter output is limited by the P-f and Q-V droops that can be embedded when operating as voltage source converter (see Fig. 6.3 for more information).

For more details on the problem formulation, especially concerning the additional constraints of the problem and their relaxation, the reader is invited to refer to [110] and to Deliverable D3.4 [95].

It is important to remark that the considerations done so far with regards to the BESS converter capability curves and the maximization of the droop constants are valid also when the converter is operating both in grid-following mode and in grid-forming mode. In fact, it is now of interest to present the capabilities of the converter in terms of grid-forming mode operation. Fig. 6.3 shows the P-f and Q-V droops that can be embedded in the converter when operating as a voltage source converter in grid-forming mode. It can be noticed that the configuration parameters that can be set for the grid-forming operation are (F_{ref} , F_{lim} and P_{lim}) and (V_{ref} , V_{lim} and Q_{lim}) for the frequency and voltage grid-forming control, respectively.

Due to the internal limitations of the BESS converter, the above-mentioned configuration parameters can be set within given boundaries. In particular, the maximum values of F_{lim} and P_{lim} that can be set are 0.5 Hz and 720 kW, and for V_{lim} and Q_{lim} the limits are 10% and 720 kvar. This means that the maximum PFC droop that can be implemented in the converter system running as a voltage source is 1.44 MW/Hz, which is way lower than the maximum ideal droop calculated with the above-presented analysis on the historical data to maximise the service provision, which was then possible to implement only when utilising the droop in an outer control layer, hence in grid-following mode. This aspect highlights the importance of a deep knowledge of the employed hardware when implementing control strategies for grid regulation.

In the next Subsection, the experimental test activities at the EPFL demonstrator are presented. The BESS is controlled both in grid-forming and in grid-following mode, and the identified limitations in terms of the BESS converter capabilities are indeed included in the experimental validation campaign.

6.2. EPFL demo: experimental results on grid connected demonstrator

The main objective of the EPFL demonstrator is the full-scale experimental validation of a grid-connected grid-forming BESS control for which it is possible to assess the impact on the local grid frequency. Indeed, for a comprehensive interpretation of the outcome of the grid-forming performance assessment analysis, a comparison is proposed with the standard grid-following approach for BESS operation. The available commercial utility-scale 720 kVA/560 kWh BESS, has the capability of operating in grid-forming mode while being grid connected. As presented in the previous subsection, the configuration parameters that can be set for the grid-forming operation are (F_{ref} , F_{lim} and P_{lim}) and (V_{ref} , V_{lim} and Q_{lim}) for the frequency and voltage grid-forming control, respectively.

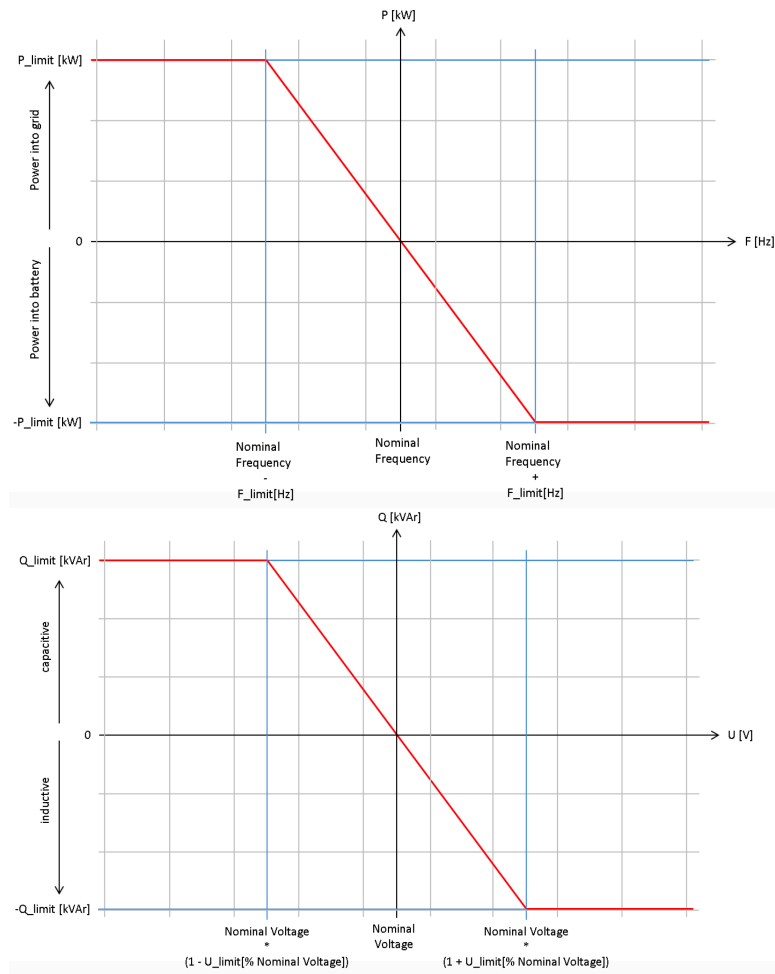


Figure 6.3: Converter P-f and Q-V droops

For the sake of the experimental performance assessment of the grid-connected grid-forming BESS control operation, a comparison is proposed with the standard grid-following approach. In this case, the active power set-point is computed by means of an outer loop, as a function of the measured grid frequency deviation from 50 Hz, while implementing the same droop of 1.44 MW/Hz.

Then, in order to achieve conditions that enable the assessment of the impact on the local grid frequency of the grid-forming BESS control, it is necessary to have a measurement infrastructure capable of providing reliable and accurate measurements when the BESS is in operation. Specifically, this is required for the computation of the KPIs defined in Section 5, such as the rRoCoF and rPADD. For this purpose, the PMU-based distributed sensing infrastructure deployed in the EPFL campus was utilized. As shown in Fig. 6.4, 2 PMUs (PMU0 and PMU1) at the different voltage levels of 50 kV and 21 kV were utilized to compute the difference in the voltage phase angles at the two sides of the impedance in-between (line + 50kV/21kV transformer) when a given power was provided by the BESS. A first set of experimental tests showed that when operating the BESS with the maximum possible droop of 1.44 MW/Hz, the BESS active power was not large enough to guarantee meaningful displacements of the phasors at the two measurements points, given the PMU capabilities in terms of accuracy and precision described in Section 5. For this reason, it was decided to consider a larger impedance between the two measurement points, which could provide larger displacements of the phasors for the same amount of BESS active power. In particular, a new PMU (PMU2) was installed at the 300 V LV side of the BESS step-up transformer.

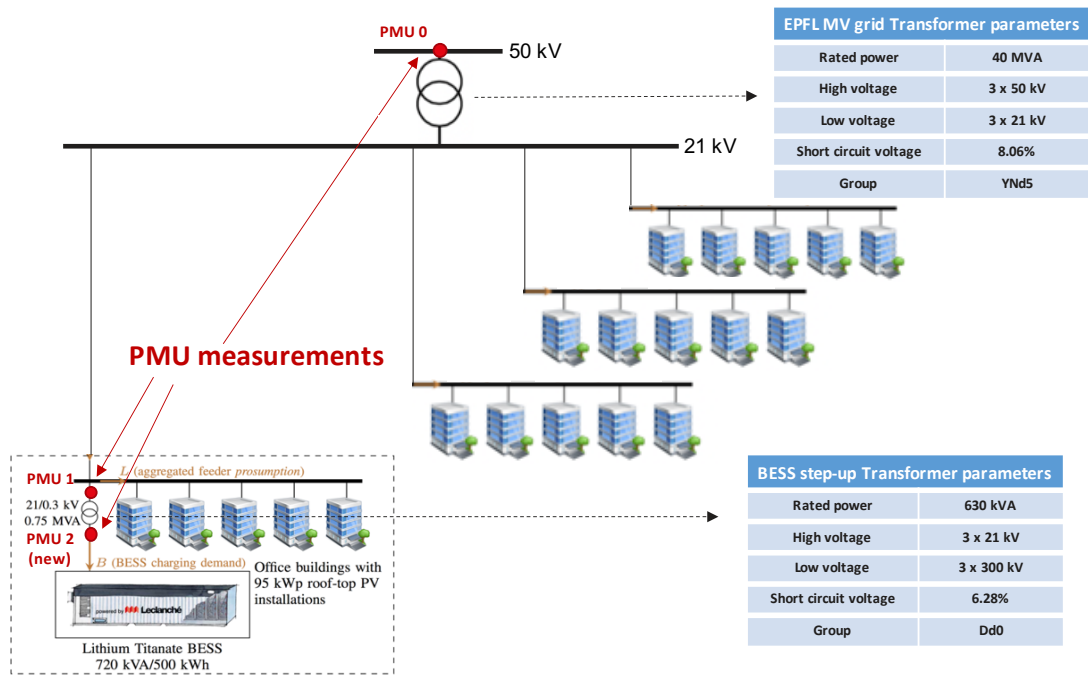


Figure 6.4: Experimental setup of the EPFL campus MV grid hosting the utility-scale 720kVA/500 kWh BESS.

This enabled the comparison of the 2 measurements with a higher impedance in-between, given the high value of the impedance of the BESS step-up transformer, as detailed in Fig. 6.4. A picture of the new PMU installed in the BESS container is shown in Fig. 6.5.



Figure 6.5: Ad-hoc installation of the adopted PMU inside the BESS container.

The proposed study considers real operation conditions that are determined by the uncontrollable variation of the power system frequency of the Continental Europe Synchronous Region, which indeed the MV grid of the EPFL campus is connected to. For this reason, it was decided to focus the analysis on periods around the transition of the hour, which typically present fast frequency ramps due to mechanisms related to electricity markets. Such frequency ramps have been utilized to provide corresponding BESS active power exchanges, following the 1.44 MW/Hz droop implemented both in the case of grid-connected grid-forming and in the case of grid-following control.

Furthermore, one has to note that the proposed tests have been carried out during evening hours, i.e., when the base consumption of the local MV grid was mostly constant. This enabled a better identification of the impact of the BESS provided power in the local phase angle displacements.

Figure 6.6 shows the results of the experimental assessment of the BESS response when operated in grid-following mode with a 1.44 MW/Hz f-P droop. On the left side, the frequency measured by the PMUs and the BESS active power response are provided. At the hour transition (19:00) the frequency ramp can be noticed in line with the previous consideration, which is in fact reflected by the active power ramp provided by the BESS. On the right side, the computation of $\Delta\sigma_k (= \sigma_{k,PMU1} - \sigma_{k,PMU2})$ is shown, according to the definition included in Section 2. One can note that $\Delta\sigma_k$ is stable before 18:50, i.e., before the BESS starts being controlled. This is the period when $\Delta\sigma_0 (= \sigma_{0,PMU1} - \sigma_{0,PMU2})$ is computed to provide values of the rPADD, as it will be seen in the following.

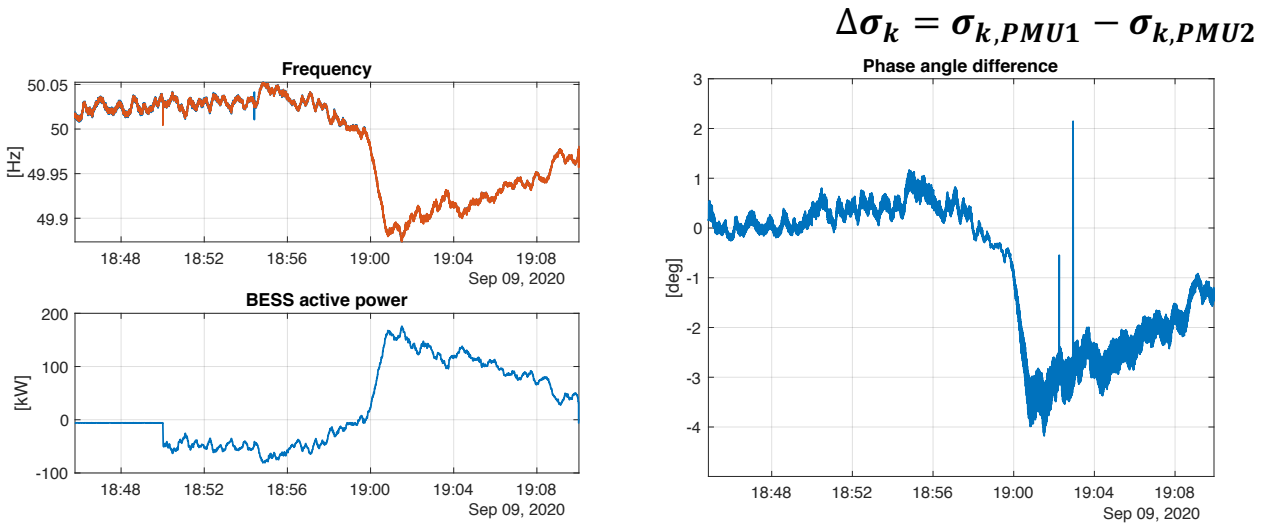


Figure 6.6: Experimental test results using the EPFL BESS converter in grid-following mode with 1.44 MW/Hz droop.

Similarly, Fig. 6.7 shows the results of the experimental assessment of the BESS response when operated in grid-forming mode with the maximum f-P droop (1.44 MW/Hz) allowed by the available converter technology. Again, on the left side, the frequency measured by the PMUs and the BESS active power response are provided, and the frequency ramp at the hour transition (21:00) reflected by the BESS power ramp are noticeable. Before the activation of the BESS control at 20:50, the stable condition of the phase angle difference was computed $\Delta\sigma_0 (= \sigma_{0,PMU1} - \sigma_{0,PMU2})$, while afterwards the phase angle difference $\Delta\sigma_k (= \sigma_{k,PMU1} - \sigma_{k,PMU2})$ started varying, impacted by the BESS power contribution.

It is now of interest the quantitative assessment of the comparison of the two cases with respect to the impact on the local grid frequency. To do this, the two relative KPIs presented in Section 5 are now computed and discussed, namely the Relative Rate-of-Change-of-Frequency (rRoCoF) and the Relative Phase Angle Difference Deviation (rPADD).

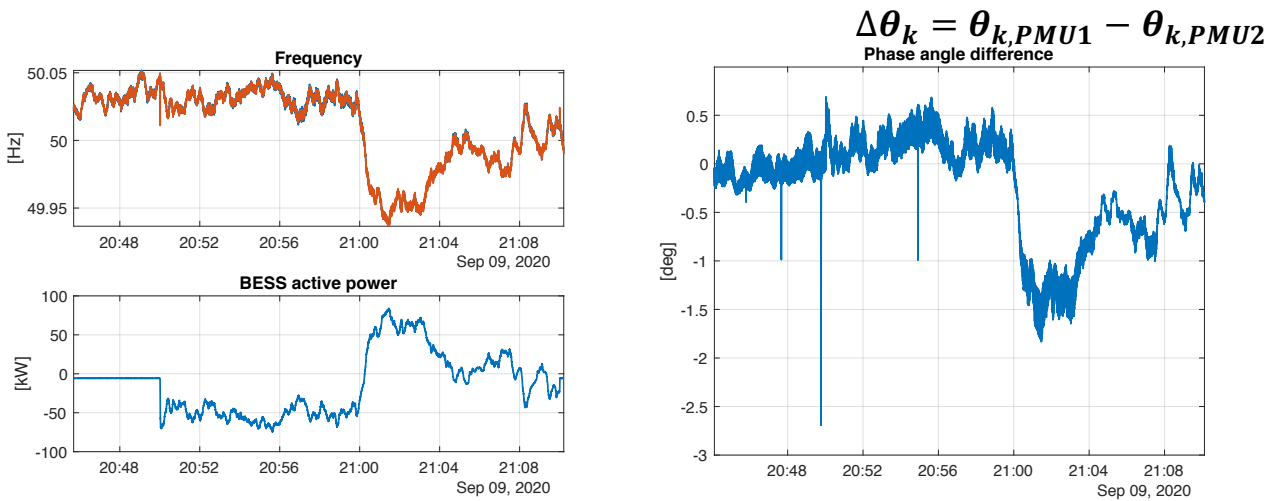


Figure 6.7: Experimental test results using the EPFL BESS converter in grid-forming mode with 1.44 MW/Hz droop.

As discussed in Section 5, the rRoCoF has been computed over a time window of 60 ms. For the sake of clarity and simplicity of the interpretation, results of the rRoCoF the rPADD computation are reported in terms of cumulative distribution functions (CDF).

Figure 6.8 shows the CDF probability of the rRoCoF of having a given value expressed in [Hz/s/kW]. It is clear that the more vertical trend of the red line representing the grid-forming case implies higher probabilities of having smaller values of rRoCoF. This means that for a higher number of stamps (instances) for which the rRoCoF has been computed, it is more likely to have smaller values when controlling the BESS in grid-forming mode, rather than in grid-following mode. This demonstrates that the implemented grid-connected grid-forming BESS control can guarantee larger containment of the rate of fast changes of the frequency, compared to the more traditional grid-following strategy. These results are in line with what was found previously in occasion of the simulation activities on the IEEE 39-bus emulated grid.

Figure 6.9 shows the CDF probability of the rPADD of having a given value expressed in [deg/kW]. It is clear that larger values of the index mean larger impact on the local phase angle displacement of the voltages measured at the two different voltage levels. It can be noticed that in this case larger values are found for the grid-forming case, demonstrating that the implemented grid-connected grid-forming BESS control can guarantee larger impact on the local phase angle difference, compared to the more traditional grid-following strategy. These results are in line with what was found previously in occasion of the simulation activities on the IEEE 39-bus emulated grid.

To conclude, the experimental tests confirmed the outcome of the analysis carried out by means of simulation activities on the low-inertia configuration of the IEEE 39-bus emulated grid, validating the positive effects of the grid-forming strategy in the control of the local frequency. The experimental assessment was possible thanks to the upgrade of the PMU-base sending infrastructure, by adding a PMU inside the BESS container at the 300 V side of the step-up transformer, enabling the assessment of impacts on the local frequency with the BESS control running with maximum possible f-P 1.44 MW/Hz droop. The evolution of the two relative KPIs (rROCOF and rPADD) confirmed the positive impacts provided by the implemented grid-forming strategy, being the rROCOF more contained when operating in grid-forming mode rather than in grid-following mode, and at the same time larger impacts in the local phase angle were also caused.

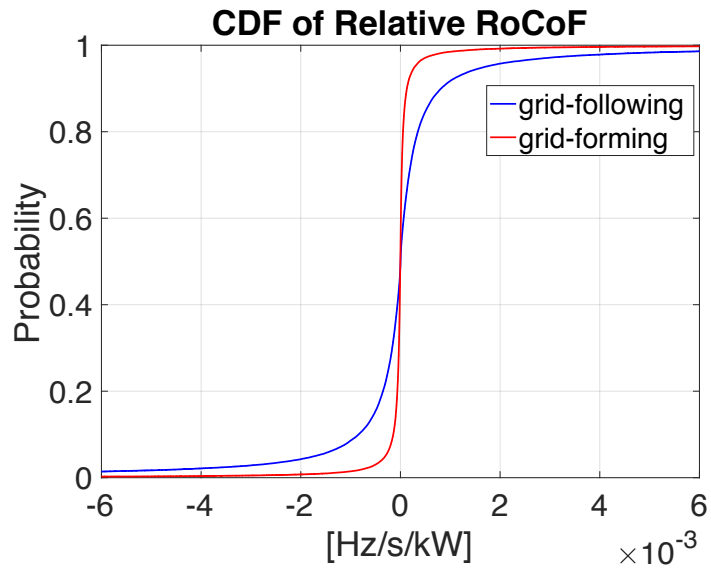


Figure 6.8: Cumulative distribution function of the rRoCoF [Hz/s/kW] for the two experimental tests.

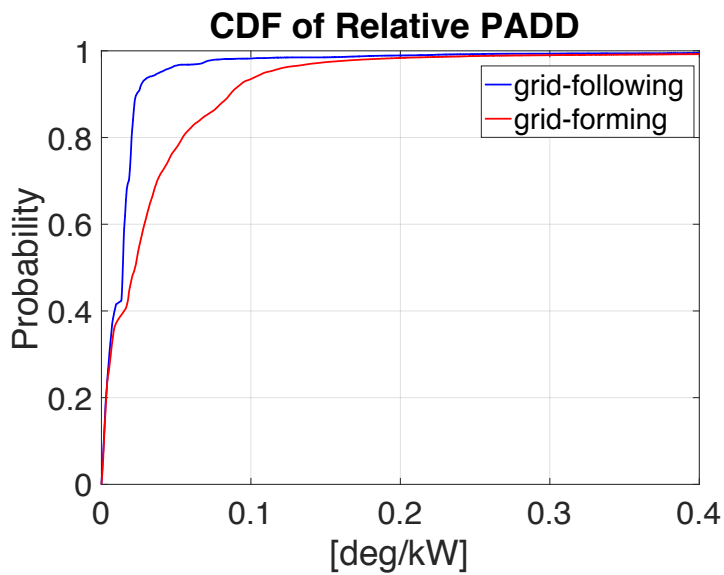


Figure 6.9: Cumulative distribution function of the rPADD [deg/kW] for the two experimental tests.

7. Conclusion

After 4 years the WP3 of the OSMOSE H2020 project has illustrated that turning an off-the-shelf storage device into grid forming unit is possible and has provided the details on all the controls upgrades that are necessary. It has also developed indicators that would allow system operators to understand the behaviour of a unit using only output measurement. Eventually, it has proposed a definition of grid forming capability that is suited to grid code requirements in a differentiated manner with respect to the services that it provides: the synchronisation services, and independently of the control design. This approach is similar to the one that has been effectively used for frequency and voltage regulation services in the past.

An initial part pays specific attention to the synchronisation mechanisms of the different converters to fully explain the needs of the transmission system regarding the generating units to ensure system stability. Combining a state-of-the-art of new requirements for inverters throughout the world and the knowledge gained in this project, the grid forming capability and synchronisation services are defined, fitting together with already existing grid code requirements, and adapting a few of them. Having split the services will allow the units to participate in what is technically possible for each type of unit making the best use of the already existing capability.

The Ingeteam-RTE demo has then been extensively described, both from the hardware point of view and the control point of view, to illustrate what have been the changes compared to more traditional grid following solutions. It also focuses on the specific control upgrades that were necessary to implement a typical filtered droop control from the previous MIGRATE project on a full-scale grid forming converter connected to the grid. This includes but is not limited to soft connection, current limitation for unbalanced situations (presently an adaption of the TVI), as well as specific energy management of both battery and ultracapacitor.

The tests that have been carried out during the FAT are highly detailed here. Both classical services (voltage step, active power ramp...) and grid forming related services (phase jumps, frequency step...) have been tested. It helps demonstrate the positive impact that grid forming converters can bring to the grid. Moreover, the specific hybrid architecture of the Ingeteam demonstration has also been tested, showing that the UCs are efficient at dealing with fast transients, releasing the burden put on the battery.

In addition, EPFL developed a Real-Time Simulation test case, that allows for complementary testing. A modified version of the IEEE 39-bus to achieve low inertia has been implemented and released open-source. Novel metrics to quantitatively assess the local impact of BESSs providing frequency regulation to the bulk power grid have been proposed. Experimental tests confirmed the outcome of the analysis carried out by means of simulation activities on the low-inertia configuration of the IEEE 39-bus emulated grid presented in [112], validating the positive effects of the grid forming strategy in the control of the local frequency. The upgrade of the PMU-based sensing infrastructure, enabled the assessment of impacts on the local frequency with the BESS control running with maximum possible frequency droop. The proposed metrics (rROCOF and rPADD) can potentially be of use for the quantification of frequency reserve provision to distribution systems. Moreover, both metrics confirmed the superior performance of the grid forming strategy, characterised by a more contained rROCOF and a larger impact in the local phase angle than the grid following mode.

8. Bibliography

- [1] P. Kundur, *Power System Stability And Control*, ser. EPRI power system engineering series. McGraw-Hill, 1994.
- [2] P. Kundur, J. Paserba, V. Ajjarapu, G. Andersson, A. Bose, C. Canizares, N. Hatzargyriou, D. Hill, A. Stankovic, C. Taylor, T. Van Cutsem, and V. Vittal, "Definition and classification of power system stability ieeecigre joint task force on stability terms and definitions," *IEEE Transactions on Power Systems*, vol. 19, no. 3, pp. 1387–1401, 2004.
- [3] S. Golestan, J. M. Guerrero, and J. C. Vasquez, "Three-phase plls: A review of recent advances," *IEEE Transactions on Power Electronics*, vol. 32, no. 3, pp. 1894–1907, 2017.
- [4] C. Zhang, X. Cai, Z. Li, A. Rygg, and M. Molinas, "Properties and physical interpretation of the dynamic interactions between voltage source converters and grid:electrical oscillation and its stability control," *IET Power Electronics*, vol. 10, 02 2017.
- [5] R. Rosso, M. Andresen, S. Engelken, and M. Liserre, "Analysis of the interaction among power converters through their synchronization mechanism," *IEEE Transactions on Power Electronics*, vol. 34, no. 12, pp. 12 321–12 332, 2019.
- [6] L. Huang, H. Xin, Z. Li, P. Ju, H. Yuan, Z. Lan, and Z. Wang, "Grid-synchronization stability analysis and loop shaping for pll-based power converters with different reactive power control," *IEEE Transactions on Smart Grid*, vol. 11, no. 1, pp. 501–516, 2020.
- [7] N. Hatzargyriou, J. V. Milanovic, C. Rahmann, V. Ajjarapu, C. Canizares, I. Erlich, D. Hill, I. Hiskens, I. Kamwa, B. Pal, P. Pourbeik, J. J. Sanchez-Gasca, A. M. Stankovic, T. Van Cutsem, V. Vittal, and C. Vournas, "Definition and classification of power system stability revisited extended," *IEEE Transactions on Power Systems*, pp. 1–1, 2020.
- [8] T. Prevost, Y. Vernay, C. Cardozo, G. Denis, Y. Zuo, A. Zecchino, Z. Yuan, R. Cherkaoui, M. Paolone, M. Zubiaga, and J. J. Valera, "Overall specifications of the demonstrations," OS-MOSE H2020 project, Deliverable 3.2, Jun. 2019.
- [9] C. Pisani, G. Bruno, H. Saad, P. Rault, and B. Clerc, "Functional validation of a real vsc hvdc control system in black start operation," 05 2019, pp. 1–6.
- [10] A. Roscoe, P. Brogan, D. Elliott, T. Knuettel, I. Gutierrez, P. Crolla, R. D. Silva., and J.-C. P. Champion, "Practical experience of providing enhanced grid forming services from an onshore wind park," in *19th Wind Integration Workshop*, 2020.
- [11] COMMISSION REGULATION (EU), "2016/631 of 14 april 2016 establishing a network code on requirements for grid connection of generators," https://www.entsoe.eu/network_codes/rfg/, 2016.
- [12] COMMISSION REGULATION (EU), "2016/1447 of 26 august 2016 establishing a network code on requirements for grid connection of high voltage direct current systems and direct current-connected power park modules," https://www.entsoe.eu/network_codes/hvdc/, 2016.
- [13] A. Tayyebi, F. Dorfler, F. Kupzog, Z. Miletic, and W. Hribernik, "Grid-forming converters – inevitability, control strategies and challenges in future grids application," 2018.
- [14] K. De Brabandere, "Voltage and frequency droop control in low voltage grids by distributed generators with inverter front-end (spannings- en frequentieregeling in laagspanningsnetten door gedistribueerde opwekkers met vermogenelektronische netkoppeling)," 2006.
- [15] P. Rodríguez, A. Luna, R. S. Muñoz-Aguilar, I. Etxeberria-Otadui, R. Teodorescu, and F. Blaabjerg, "A stationary reference frame grid synchronization system for three-phase grid-connected power converters under adverse grid conditions," *IEEE Transactions on Power Electronics*, vol. 27, no. 1, pp. 99–112, 2012.

-
- [16] M. Karimi Ghartemani, S. A. Khajehoddin, P. K. Jain, and A. Bakhshai, "Problems of startup and phase jumps in pll systems," *IEEE Transactions on Power Electronics*, vol. 27, no. 4, pp. 1830–1838, 2012.
- [17] S. Golestan, J. M. Guerrero, J. C. Vasquez, A. M. Abusorrah, and Y. Al-Turki, "A study on three-phase flls," *IEEE Transactions on Power Electronics*, vol. 34, no. 1, pp. 213–224, 2019.
- [18] P. Rodríguez, A. Luna, I. Candela, R. Mujal, R. Teodorescu, and F. Blaabjerg, "Multiresonant frequency-locked loop for grid synchronization of power converters under distorted grid conditions," *IEEE Transactions on Industrial Electronics*, vol. 58, no. 1, pp. 127–138, 2011.
- [19] J. Rocabert, A. Luna, F. Blaabjerg, and P. Rodríguez, "Control of power converters in ac microgrids," *IEEE Transactions on Power Electronics*, vol. 27, no. 11, pp. 4734–4749, 2012.
- [20] X. Wang, M. G. Taul, H. Wu, Y. Liao, F. Blaabjerg, and L. Harnefors, "Grid-synchronization stability of converter-based resources—an overview," *IEEE Open Journal of Industry Applications*, vol. 1, pp. 115–134, 2020.
- [21] National Grid, "Performance of phase-locked loop based converters," Aug. 2017.
- [22] T. Prevost and G. Denis, "Deliverable 3.6: Requirement guidelines for operating a grid with 100% power electronic devices." <https://www.h2020-migrate.eu/downloads.html>, MIGRATE H2020 project, Deliverable 3.6, Dec. 2019.
- [23] L. Zhang, L. Harnefors, and H.-P. Nee, "Power-synchronization control of grid-connected voltage-source converters," *IEEE Transactions on Power Systems*, vol. 25, no. 2, pp. 809–820, 2010.
- [24] K. De Brabandere, B. Bolsens, J. Van den Keybus, A. Woyte, J. Driesen, and R. Belmans, "A voltage and frequency droop control method for parallel inverters," *Power Electronics, IEEE Transactions on*, vol. 22, pp. 1107 – 1115, 08 2007.
- [25] G. Seo, M. Colombino, I. Subotic, B. Johnson, D. Groß, and F. Dörfler, "Dispatchable virtual oscillator control for decentralized inverter-dominated power systems: Analysis and experiments," in *2019 IEEE Applied Power Electronics Conference and Exposition (APEC)*, 2019, pp. 561–566.
- [26] A. P. Asensio, S. A. Gomez, J. L. Rodriguez-Amenedo, and M. A. Cardiel-Alvarez, "Reactive power synchronization method for voltage-sourced converters," *IEEE Transactions on Sustainable Energy*, vol. 10, no. 3, pp. 1430–1438, 2019.
- [27] Q.-C. Zhong and G. Weiss, "Synchronverters: Inverters that mimic synchronous generators," *IEEE Transactions on Industrial Electronics*, vol. 58, no. 4, pp. 1259–1267, 2011.
- [28] S. D'Arco and J. A. Suul, "Virtual synchronous machines — classification of implementations and analysis of equivalence to droop controllers for microgrids," in *2013 IEEE Grenoble Conference*, 2013, pp. 1–7.
- [29] P. Unruh, M. Nuschke, P. Strauß, and F. Welck, "Overview on grid-forming inverter control methods," *Energies*, vol. 13, no. 10, 2020. [Online]. Available: <https://www.mdpi.com/1996-1073/13/10/2589>
- [30] D. B. Rathnayake, M. Akrami, C. Phurailatpam, S. P. Me, S. Hadavi, G. Jayasinghe, S. Zabihi, and B. Bahrani, "Grid forming inverter modeling, control, and applications," *IEEE Access*, vol. 9, pp. 114 781–114 807, 2021.
- [31] T. Qoria, Q. Cossart, C. Li, X. Guillaud, F. Colas, F. Gruson, and X. Kestelyn, "Local control and simulation tools for large transmission systems," MIGRATE H2020 project, Deliverable 3.2, Dec. 2018.

-
- [32] T. Qoria, T. Prevost, G. Denis, F. Gruson, F. Colas, and X. Guillaud, "Power converters classification and characterization in power transmission systems," in *2019 21st European Conference on Power Electronics and Applications (EPE '19 ECCE Europe)*, 2019, pp. P.1–P.9.
- [33] T. Qoria, E. Rokrok, A. Bruyere, B. François, and X. Guillaud, "A pll-free grid-forming control with decoupled functionalities for high-power transmission system applications," *IEEE Access*, vol. 8, pp. 197 363–197 378, 2020.
- [34] M. Mousavi, A. Mehrizi-Sani, D. Ramasubramanian, and E. Farantatos, "Performance evaluation of an angle droop—based power sharing algorithm for an inverter-dominated power system," in *2019 IEEE Power Energy Society General Meeting (PESGM)*, 2019, pp. 1–5.
- [35] M. Paolone, T. Gaunt, X. Guillaud, M. Liserre, S. Meliopoulos, A. Monti, T. Van Cutsem, V. Vittal, and C. Vournas, "Fundamentals of power systems modelling in the presence of converter-interfaced generation," *Electric Power Systems Research*, vol. 189, p. 106811, 2020. [Online]. Available: <https://www.sciencedirect.com/science/article/pii/S037877962030482X>
- [36] D. Lepour, M. Paolone, G. Denis, C. Cardozo, T. Prevost, and E. Guiu, "Performance assessment of synchronous condensers vs voltage source converters providing grid-forming functions," in *2021 IEEE Madrid PowerTech*, 2021, pp. 1–6.
- [37] H. GONG, "Impedance measurement and estimation of three-phase voltage-source converters," Ph.D. dissertation, Aalborg University, 2020.
- [38] D. Wilson, V. Terzija, J. Yu, A. Nechifor, and M. Eves, "Requirements for monitoring & forecasting pe-based kpis," MIGRATE H2020 project, Deliverable 2.1, Feb. 2018.
- [39] D. Groß and F. Dörfler, "Projected grid-forming control for current-limiting of power converters," in *2019 57th Annual Allerton Conference on Communication, Control, and Computing (Allerton)*, 2019, pp. 326–333.
- [40] M. G. Taul, X. Wang, P. Davari, and F. Blaabjerg, "Current limiting control with enhanced dynamics of grid-forming converters during fault conditions," *IEEE Journal of Emerging and Selected Topics in Power Electronics*, vol. 8, no. 2, pp. 1062–1073, 2020.
- [41] H. Saad, S. Denetière, and P. Rault, "Ac fault dynamic studies of islanded grid including hvdc links operating in vf-control," in *15th IET International Conference on AC and DC Power Transmission (ACDC 2019)*, 2019, pp. 1–8.
- [42] H. Saad, P. Rault, and S. Denetière, "Investigation on parallel operation of two mmc-hvdc links in grid forming connected to an existing network," in *2020 22nd European Conference on Power Electronics and Applications (EPE'20 ECCE Europe)*, 2020, pp. P.1–P.10.
- [43] T. Qoria, F. Gruson, F. Colas, G. Denis, T. Prevost, and X. Guillaud, "Critical clearing time determination and enhancement of grid-forming converters embedding virtual impedance as current limitation algorithm," *IEEE Journal of Emerging and Selected Topics in Power Electronics*, vol. 8, no. 2, pp. 1050–1061, 2020.
- [44] E. Rokrok, T. Qoria, A. Bruyere, B. Francois, and X. Guillaud, "Transient stability assessment and enhancement of grid-forming converters embedding current reference saturation as current limiting strategy," *IEEE Transactions on Power Systems*, pp. 1–1, 2021.
- [45] G. Lisciandrello, A. S. F. Silletti, G. Albimonti, L. Petrocchi, G. Coletta, D. Ronzio, E. Collino, M. Lazzaro, M. D. Ieso, G. Camorali, C. Noce, R. Klose, M. Radicioni, A. Guzzetti, S. Bedogni, R. Riva, R. Bazzani, M. D. Francesca, A. Pesce, D. Poli, A. Vaccaro, and A. Pepicello, "Final report on demo execution results," OSMOSE H2020 project, Deliverable 5.5, Feb. 2022.
- [46] L. Huang, H. Xin, W. Dong, and F. Dörfler, "Impacts of grid structure on pll-synchronization stability of converter-integrated power systems," 03 2019.
- [47] J. Gleadow, G. Love, H. Saad, T. Rauhala, C. Barker, A. Canelhas, M. Barnes, G. Denis, S. Bartlett, E. P. Arujo, X. Chen, S. Iftekharul, V. Pathirana, K. Schonleber, J. Rittinger, K. Kore-

-
- man, J. Paquin, and J. Sakamuri, "Ac fault response options for vsc hvdc converters," *CIGRE SCIENCE & ENGINEERING*, vol. 15, pp. 105–110, 2019.
- [48] C. Zhang, X. Wang, and F. Blaabjerg, "Analysis of phase-locked loop influence on the stability of single-phase grid-connected inverter," *2015 IEEE 6th International Symposium on Power Electronics for Distributed Generation Systems, PEDG 2015*, 2015.
- [49] H. Gong, X. Wang, and L. Harnefors, "Rethinking current controller design for pll-synchronized vscs in weak grids," *IEEE Transactions on Power Electronics*, vol. 37, no. 2, pp. 1369–1381, 2022.
- [50] J. Z. Zhou, H. Ding, S. Fan, Y. Zhang, and A. M. Gole, "Impact of short-circuit ratio and phase-locked-loop parameters on the small-signal behavior of a vsc-hvdc converter," *IEEE Transactions on Power Delivery*, vol. 29, no. 5, pp. 2287–2296, 2014.
- [51] J. Bialek, T. Bowen, T. Green, D. Lew, Y. Li, J. MacDowell, J. Matevosyan, N. Miller, M. O'Malley, and D. Ramasubramanian, "System needs and services for systems with high ibr penetration," Global PST Consortium, Tech. Rep., Oct. 2021.
- [52] S. DENNETIERE, P. RAULT, H. SAAD, Y. FILLION, K. SHARIFABADI, J. H. JOHANSSON, and N. KRAJISNIK, "Technical solutions to predict and mitigate inadvertent interaction of two parallel connected vsc-hvdc schemes feeding an islanded offshore oil and gas grid," in *CIGRE session 48*, 2020.
- [53] S. D'Arco, J. A. Suul, and O. B. Fosso, "Control system tuning and stability analysis of virtual synchronous machines," in *2013 IEEE Energy Conversion Congress and Exposition*, 2013, pp. 2664–2671.
- [54] T. Qoria, F. Gruson, F. Colas, X. Guillaud, M.-S. Debry, and T. Prevost, "Tuning of cascaded controllers for robust grid-forming voltage source converter," in *2018 Power Systems Computation Conference (PSCC)*, 2018, pp. 1–7.
- [55] T. Qoria, C. Li, K. Oue, F. Gruson, F. Colas, X. Guillaud, and T. Prévost, "Tuning of ac voltage-controlled vsc based linear quadratic regulation," in *2019 IEEE Milan PowerTech*, 2019, pp. 1–6.
- [56] H. Yu, M. A. Awal, H. Tu, I. Husain, and S. Lukic, "Comparative transient stability assessment of droop and dispatchable virtual oscillator controlled grid-connected inverters," *IEEE Transactions on Power Electronics*, vol. 36, no. 2, pp. 2119–2130, 2021.
- [57] RTE, "Documentation technique de reference," https://www.services-rte.com/files/live/sites/services-rte/files/documentsLibrary/01-12-2021_COMPLET_4421_fr, 2017.
- [58] Western Power, "Loss of mains protection," 2018. [Online]. Available: <https://www.westernpower.co.uk/downloads/4096>
- [59] "Nf en 50549-1: Requirements for generating plants to be connected in parallel with distribution networks - part 1 : connection to a lv distribution network - generating plants up to and including type b," <https://www.boutique.afnor.org/fr-fr/norme/nf-en-505491/exigences-relatives-aux-centrales-electriques-destinees-a-etre-raccordees-e/fa187555/260493AreasStoreProductsSummaryView>, Apr. 2019.
- [60] RTE, "Exigences de conception et de fonctionnement pour le raccordement au rpt d'une unite de production," 2020. [Online]. Available: <https://services-rte.net/files/live//sites/services-rte/files/documentsLibrary/Article%205.1.1%20-%20Exigences%20de%20conception%20et%20de%20fonctionnement%20pour%20le%20raccordement%20au%20RPT%20d%E2%80%99une%20unit%C3%A9%20de%20production.fr>
- [61] RTE, "Documentation technique de référence chapitre 8 – trames types article 8.24 – cahier des charges des capacités constructives pour un système hvdcn," 2020. [Online]. Available: <https://services-rte.net/files/live//sites/services-rte/files/documentsLibrary/Article%208>.

24%20-%20Cahier%20des%20charges%20des%20capacit%C3%A9s%20constructives%20pour%20un%20syst%C3%A8me%20HVDC_fr

- [62] RTE, “Cahier des charges des capacités constructives conditions générales parc non synchrone de générateurs y compris en mer,” 2020. [Online]. Available: https://services-rte.net/files/live//sites/services-rte/files/documentsLibrary/Article%208.3.1%20-%20Trame%20type%20de%20Cahier%20des%20charges%20des%20capacit%C3%A9s%20constructives%20-%20parcs%20non%20synchrone_fr
- [63] RTE, “Documentation technique de reference. chapitre 8 – trames types article 8.3.3 – trame de procedure de controle de conformite pour le raccordement d’une installation de production ou de stockage,” <https://www.enerplan.asso.fr/dl-fichier-actualite?media=40252>, 2020.
- [64] Entso-e, “High penetration of power electronic interfaced power sources and the potential contribution of grid forming converters. technical report,” <https://euagenda.eu/upload/publications/untitled-292051-ea.pdf>, 2020, accessed: 12.04.2021.
- [65] National Grid, “Draft grid code – grid forming converter specification,” <https://www.nationalgrideso.com/document/159296/download>, 2020.
- [66] Guideline, VDE FNN, “VDE FNN Guideline : Grid forming behaviour of HVDC systems and DC-connected PPMs,” 2020.
- [67] AEMO, “Application of advanced grid scale inverter s in the nem. white paper,” Aug. 2021.
- [68] S. Cherevatskiy, S. Zabihi, R. Korte, and H. Klingenberg, “A 30mw grid forming bess boosting reliability in south australia and providing market services on the national electricity market,” in *18th Wind Integration Workshop*, 2019.
- [69] A. Roscoe, P. Brogan, D. Elliott, T. Knueppel, I. Gutierrez, J.-C. P. Campion, and R. D. Silva., “Practical experience of operating a grid forming wind park and its response to system events,” in *18th Wind Integration Workshop*, 2019.
- [70] IEEE, “Ieee draft standard for interconnection and interoperability of inverter-based resources (ibr) interconnecting with associated transmission electric power systems,” *IEEE P2800/D6.0*, March 2021, pp. 1–170, 2021.
- [71] S. C. Chevalier, “Inference, estimation, and prediction for stable operation of modern electric power systems,” Ph.D. dissertation, MASSACHUSETTS INSTITUTE OF TECHNOLOGY, 2021.
- [72] B. Philippe, *Régimes transitoires des machines tournantes électriques / Philippe Barret ; préface de Maurice Magnien*, 2nd ed., ser. Collection de la Direction des études et recherches d’Electricité de France. ESE. Paris: Eyrolles, 1987.
- [73] COMMISSION REGULATION (EU), “Directive (eu) 2019/944 of the european parliament and of the council of 5 june 2019 on common rules for the internal market for electricity and amending directive 2012/27/eu,” <https://eur-lex.europa.eu/legal-content/EN/TXT/PDF/?uri=CELEX:32019L0944&from=FR>, 2016.
- [74] RTE, “Description of system needs and test cases,” MIGRATE H2020 project, Deliverable 3.1, Dec. 2016.
- [75] CIGRE JWG C2/C4.41, “Impact of high penetration of inverter-based generation on system inertia of networks,” <https://e-cigre.org/publication/851-impact-of-high-penetration-of-inverter-based-generation-on-system-inertia-of-networks>, 2021.
- [76] EirGrid and SONI, “Shaping our electricity future,” <https://www.eirgridgroup.com/site-files/library/EirGrid/Full-Technical-Report-on-Shaping-Our-Electricity-Future.pdf>, Feb. 2021, accessed: 2021-12-05.

-
- [77] R. Eriksson, N. Modig, and K. Elkington, "Synthetic inertia versus fast frequency response: a definition," *IET Renewable Power Generation*, vol. 12, no. 5, pp. 507–514, 2018. [Online]. Available: <https://ietresearch.onlinelibrary.wiley.com/doi/abs/10.1049/iet-rpg.2017.0370>
- [78] TransEnergie, "Exigences techniques de raccordement decentralises au reseau de transport d'hydro-quebec," https://www.hydroquebec.com/data/transenergie/raccordement-reseau/2_Exigences_raccordement_centrales_D-2018-145_2018-11-15.pdf, 2019.
- [79] AEMO, "Fast frequency response in the nem," Aug. 2017.
- [80] National Grid, "National grid eso - frequency response services," <https://www.nationalgrideso.com/industry-information/balancing-services/frequency-response-services>, accessed: 2021-12-05.
- [81] Enedis, "Description et étude des protections de découplage pour le raccordement des installations de production raccordées au réseau public de distribution," https://www.enedis.fr/sites/default/files/Enedis-NOI-RES_13E.pdf, 2020.
- [82] D. Wilson, J. Warichet, M. Eves, and N. Al-Ashwal, "Lessons learned from monitoring & forecasting kpis on impact of pe penetration," MIGRATE H2020 project, Deliverable 2.3, Feb. 2018.
- [83] National Grid ESO, "Performance monitoring csv file format," <https://www.nationalgrideso.com/document/176746/download>, 2021.
- [84] EirGrid SONI, "Ds3 system services protocol – regulated arrangements. ds3 system services implementation project," <https://www.eirgridgroup.com/site-files/library/EirGrid/DS3-SS-Protocol-v3.0.pdf>, 2020.
- [85] EirGrid SONI, "Ds3 performance measurement device standards for fast acting services," <http://www.eirgridgroup.com/site-files/library/EirGrid/DS3-Performance-Measurement-Device-Standards-for-Fast-Acting-Services.pdf>, 2017.
- [86] EirGrid PLC, "Ds3 system services agreement," https://www.eirgridgroup.com/site-files/library/EirGrid/Ire-DS3-System-Services-Regulated-Arrangements_final.pdf, 2018.
- [87] EirGrid and SONI, "Ds3 system services portfolio capability analysis," <https://www.eirgridgroup.com/site-files/library/EirGrid/DS3-System-Services-Portfolio-Capability-Analysis.pdf>, Nov. 2014, accessed: 2021-12-05.
- [88] Government of South Australia, "Generator development approval procedure," https://www.sa.gov.au/_data/assets/pdf_file/0003/311448/OTR-Generator-Development-Approval-Procedure-Version-1.2.pdf, Jul. 2017, accessed: 2021-12-05.
- [89] AEMO, "2020 system strength and inertia report," Mar. 2020.
- [90] National Grid, "National grid eso - noa stability pathfinder – phase 1 updates," <https://www.nationalgrideso.com/future-energy/projects/pathfinders/stability/Phase-1>, accessed: 2021-12-05.
- [91] AEMO, "System strength in the nem explained," <https://aemo.com.au/-/media/files/electricity/nem/system-strength-explained.pdf>, Mar. 2020.
- [92] Entso-e, "Grid-forming capabilities: Towards system level integration," <https://www.entsoe.eu/news/2021/04/01/grid-forming-capabilities-ensuring-system-stability-with-a-high-share-of-renewables/>, 2021, accessed: 12.04.2021.
- [93] CIGRE Working Group B4.62, "Connection of wind farms to weak ac networks," 2016.
- [94] RTE, "Le schéma décennal de développement du réseau," <https://www.rte-france.com/analyses-tendances-et-prospectives/le-schema-decennal-de-developpement-du-reseau>, 2019.

-
- [95] Y. Zuo, F. Gerini, A. Zecchino, R. Cherkaoui, and M. Paolone, "Quantification of multi-service synergy and impact on sizing," OSMOSE H2020 project, Deliverable 3.4, Feb. 2022.
- [96] M. Zubiaga, C. Cardozo, T. Prevost, A. Sanchez-Ruiz, E. Olea, P. Izurza, S. H. Khan, and J. Arza, "Enhanced tvi for grid forming vsc under unbalanced faults," *Energies*, vol. 14, no. 19, 2021. [Online]. Available: <https://www.mdpi.com/1996-1073/14/19/6168>
- [97] C. Cardozo, G. Denis, T. Prevost, M. Zubiaga, J. J. Valera, and Y. Vernay, "Upgrade of a grid-connected storage solution with grid-forming function," in *9th Solar & storage integration workshop*, 2019.
- [98] C. Cardozo, Y. Vernay, G. Denis, T. Prevost, M. Zubiaga, and J. J. Valera, "Osrose: Grid-forming performance assessment within multiservice storage system connected to the transmission grid," in *CIGRE session 48*, 2020.
- [99] C. Cardozo, G. Denis, T. Prevost, M. Zubiaga, A. Sanchez-Ruiz, J. J. Valera, and Y. Vernay, "Osrose wp3: Factory acceptance test of the grid forming demonstrator," in *10th Solar & storage integration workshop*, 2020.
- [100] RTE, "Cahier des charges des capacités constructives. conditions générales. unité de stockage non synchrone," https://www.services-rte.com/files/live//sites/services-rte/files/documentsLibrary/Article.8.3.4.-_Cahier_des_charges_des_capacit%C3%A9s_constructives_stockage_6409_fr, Aug. 2021, accessed: 2021-12-05.
- [101] Entso-e, "Entso-e storage expert group *PHASE I FINAL REPORT*," https://www.entsoe.eu/network_codes/cnc/expert-groups, 2020, accessed: 12.04.2021.
- [102] E. Namor, F. Sossan, R. Cherkaoui, and M. Paolone, "Multi-service control algorithm for converters," OSMOSE H2020 project, Deliverable 3.2, Dec. 2018.
- [103] M. Zubiaga, A. Sanchez-Ruiz, E. Olea, E. Unamuno, A. Bilbao, and J. Arza, "Power capability boundaries for an inverter providing multiple grid support services," *Energies*, vol. 13, no. 17, 2020. [Online]. Available: <https://www.mdpi.com/1996-1073/13/17/4314>
- [104] D. Wu, F. Tang, J. C. Vasquez, and J. M. Guerrero, "Control and analysis of droop and reverse droop controllers for distributed generations," in *2014 IEEE 11th International Multi-Conference on Systems, Signals Devices (SSD14)*, 2014, pp. 1–5.
- [105] P. Ernst, R. Singer, S. Rogalla, R. Denninger, and K. Jalili, "Testing characteristics of grid forming converters part iv: Overload behavior and response to grid faults," in *19th Wind Integration Workshop*, 2020.
- [106] INGEGRID, "Reactive power compensators," <https://www.ingeteam.com/Download/3709/attachment/pc16iptt01-statcom-catalogue-.pdf.aspx>, 2021, accessed: 23.03.2021.
- [107] INGETEAM, "Ingrid mv700 (statcom datasheet) code: Mv7d4-26-001aa-460+sf+z," 2018.
- [108] Industry Technical Support Leadership Committee (ITSLC), "Impact of iee 1547 standard on smart inverters and the applications in power systems," 28 Aug 2020.
- [109] S. Cherevatskiy, S. Sproul, S. Zabihi, R. Korte, H. Klingenberg, B. Buchholz, and A. Oudalov, "Grid forming energy storage system addresses challenges of grids with high penetration of renewables (a case study)," in *CIGRE session 48*, 2020.
- [110] A. Zecchino, Z. Yuan, F. Sossan, R. Cherkaoui, and M. Paolone, "Optimal provision of concurrent primary frequency and local voltage control from a bess considering variable capability curves: Modelling and experimental assessment," *Electric Power Systems Research*, vol. 190, p. 106643, 2021.
- [111] B. Dunn, H. Kamath, and J.-M. Tarascon, "Electrical energy storage for the grid: A battery of choices," *Science*, vol. 334, no. 6058, pp. 928–935, 2011.

-
- [112] Y. Zuo, Z. Yuan, F. Sossan, A. Zecchino, R. Cherkaoui, and M. Paolone, "Performance assessment of grid-forming vs grid-following converter-interfaced bess on frequency regulation in low-inertia power grids," under review.
- [113] Y. Zuo, M. Paolone, and F. Sossan, "Effect of voltage source converters with electrochemical storage systems on dynamics of reduced-inertia bulk power grids," *Electric Power Systems Research*, vol. 189, p. 106766, 2020.
- [114] P. Romano, M. Pignati, and M. Paolone, "Integration of an IEEE Std. C37.118 compliant PMU into a real-time simulator," in *2015 IEEE Eindhoven PowerTech*, June 2015, pp. 1–6.
- [115] Z. Yuan, A. Zecchino, R. Cherkaoui, and M. Paolone, "Real-time control of battery energy storage systems to provide ancillary services considering dynamic capability of dc-ac converters," under review.
- [116] "Danish technical standard - technical regulation 3.3.1 for electrical energy storage facilities," 2019. [Online]. Available: <https://en.energinet.dk/Electricity/Rules-and-Regulations/Regulations-for-grid-connection>
- [117] AEMC, "Review of the system black event in south australia on 28 september 2016," Technical Report - 2019. [Online]. Available: https://www.aemc.gov.au/sites/default/files/documents/aemc_-_sa_black_system_review_-_final_report.pdf
- [118] RTE, "Règles services système fréquence," https://www.services-rte.com/files/live/sites/services-rte/files/documentsLibrary/2021-09-01_REGLES_SERVICES_SYSTEME_FREQUENCE_2077_fr.7z, 2021.
- [119] RTE, "Règles services système tension," https://www.services-rte.com/files/live/sites/services-rte/files/pdf/Systeme%20tension/20170401_article_8-10_v4.pdf, 2017.
- [120] G. Denis, T. Prevost, P. Panciatici, X. Kestelyn, F. Colas, and X. Guillaud, "Improving robustness against grid stiffness, with internal control of an ac voltage-controlled vsc." in *2016 IEEE Power and Energy Society General Meeting (PESGM)*, 2016, pp. 1–5.
- [121] IEEE Std 115-2009 (Revision of IEEE Std 115-1995), "IEEE guide for test procedures for synchronous machines part i—acceptance and performance testing part ii—test procedures and parameter determination for dynamic analysis - redline," May 2010.
- [122] FGW, "Technical guidelines for power generating units. part 4 demands on modeling and validating simulation models of the electrical characteristics of power generation units and systems," Sep. 2009.
- [123] DlgSILENT, "Digsilent gridcode 2.3: Model validation according to fgw tr4 revision 8," <http://www.digsilentiberica.es/noticia/24/DlgSILENT-GridCode-23-Model-validation-according-to-FGW-TR4-Revision-8/>, 2016.
- [124] F. Sossan, E. Namor, R. Cherkaoui, and M. Paolone, "Achieving the dispatchability of distribution feeders through prosumers data driven forecasting and model predictive control of electrochemical storage," *IEEE Transaction on Sustainable Energy*, vol. 7, no. 4, pp. 1762–1777, Oct 2016.
- [125] E. Namor, F. Sossan, E. Scolari, R. Cherkaoui, and M. Paolone, "Experimental assessment of the prediction performance of dynamic equivalent circuit models of grid-connected battery energy storage systems," in *IEEE ISGT*, 2018.

A. Traditional ancillary services

A.1. Frequency regulation.

Technical capabilities in CNC. A frequency sensitive mode (FSM) in the normal operational range (± 200 mHz in RGCE) is requested for type C and D units (art. 15-2.d. in RfG [11]): they have to be able to adapt their active power according to the system frequency based on a settable droop. Beyond the normal operational range, limited FSM (LFSM) is requested in the same condition from type B (so including type C and D) in underfrequency (LFSM-U, art. 15-2.c. in RfG) but from type A units in overfrequency (LFSM-O) situations (art. 13-2. in RfG).

In addition, type C and D units have also to be able to take into account additional information to help in frequency restoration (cf. art. 15.2.e of RfG). It must be noted that to prove FSM capability during the connection procedure, the unit shall be able to constitute an active power reserve, but at this stage and at present time, nothing is requested in operation. Even if the provision of the capability is mandatory as a grid connection requirement for the specified units, the service provision (Frequency Containment Reserve, FCR) remains voluntary as it implies capacity reservation (opportunity cost).

Other system operators started earlier requiring technical capabilities for frequency regulations to PPM. For instance ERCOT that requires all wind resources with interconnection agreements after 2008 to provide FCR with at most 5% droop and 17 mHz deadband. Capacity reservation is not required. This means that only wind power plants that are curtailed (e.g. due to transmission constraints) are expected to provide FCR at underfrequency [93].

Service rules. French rules are described in [118] (technical part in section 14.2) and declined in chapter 4.1 of the DTR [57] in which all requirements for connection of production units are detailed. There are two kinds of automatic frequency regulation: FCR which corresponds to FSM capability, and automatic Frequency Restoration Reserve (aFRR), which depends on an external signal. In order to participate as a service provider, the unit must now perform capacity reservation. In terms of dynamic performance, FCR must be released in less than 30 seconds and aFRR is currently requested to be deployed with a time constant below 60 seconds [118] (section 15.2.3).

Service provision. FCR is market based, it is bought through a daily cross-border call for tenders. Any certified stakeholder (producer or consumer) can participate, but LFSM-O deployment is mandatory. From 2022, a similar approach should be adopted for the aFRR with the activation of a new European exchange platform allowing for a cross-border call for tenders.

Certification and performance control in France. In order to prove compliance with grid connection requirements, in France producers must provide the results of a series of tests (available in chapter 5 part 3.5 of [57], numbered from 13 to 18 for ancillary services). Once certified, they can participate to the service provision. Then, continuous monitoring is performed by RTE in order to detect any deviation, based on a tool that collects schedules of units, estimates its expected behaviour and compares it to the measurements (external signal level and active, today with a 10 s resolution). In France, BESS have been getting certified to participate to FCR as shown in Fig. A.1 and they represent more than 35% of the French FCR prescription at the moment of writing this document. The majority (around 70%) are connected to the distribution network. Technical specification regarding stock management and recharge rules mainly in terms of dynamic were created [100]. In practice, performance assessment shows that they response much faster than the minimal 30s requested. They are indeed suited for FFR services which do not exist yet in France.

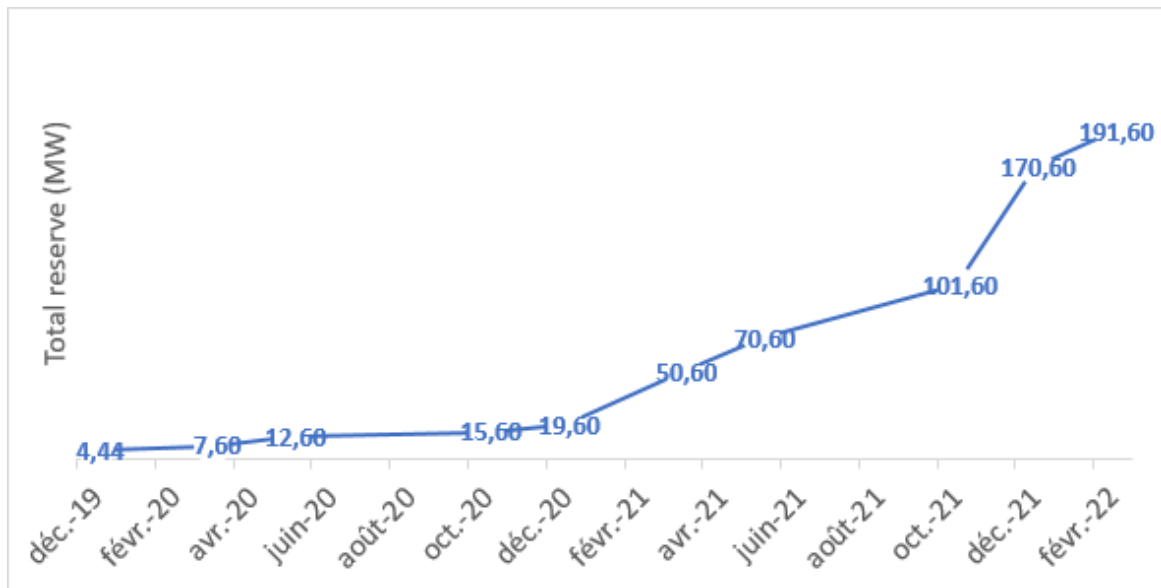


Figure A.1: Evolution of BESS certified in France to provided FCR since 2020

A.2. Voltage regulation

Technical capabilities in CNC. Reactive power capabilities and control modes are described in article 21.3 of [11] for PPM (resp. art. 18 for synchronous units) and apply for type C and D units. Capabilities of HVDC links are detailed in article 20 of [12] and control modes in art. 22. This capability is specified through PQU diagrams (roughly +/- 30% of max active power must be reached in reactive power). In France, the technical capability to participate to the primary voltage regulation is a grid connection requirement for generators of type B, C, D and Offshore PPM, while only type D and Offshore PPM generators are requested to be able to participate to the secondary voltage control (SVC).

Service rules. French rules are described in [119] (technical part in section 4.5.2) and declined in chapter 4.2 of the DTR [57]. For generators units, the primary voltage controller settling time (at 5% of the reference value) must be below 10 seconds. For HVDC system voltage regulation this value is reduced to 2 s [61]. As proposed in Chapter 2 a fast voltage support service could be more suited to IBR in the future, which could include extra capacity using the remaining current headroom when the unit operates a low active power and other technical constraints (voltage limits at converter side or compliance with LVRT and OVRT profiles) allow for it (analogously to truncated PQU diagrams of synchronous generators, beyond nominal reactive power at different active power levels).

Service provision. Participation to the primary and secondary voltage control is mandatory for all transmission connected generating unit with a rated power above 50MW.

Certification and performance control in France. As done it for the frequency related ancillary services, RTE monitors the performance of the voltage regulation from the external signal level, voltage, active and reactive power. Special attention is given to the effective availability of the reactive power capabilities, the static droop for the units in primary voltage control and the SVC response. The dynamic of the primary voltage control is only verified during the grid connection testing procedure as it can not be continuously assessed with the current 10 s measurement resolution.

B. RTE-Ingteam Demo: models

B.1. Test system and power elements model description

The simulation model has been implemented in the Matlab-simulink platform. All the power elements are represented in the simulation scenario including the output power filter, the connection breaker (commanded for soft connection), the power transformer (Δ -Y connection) and the grid impedance (SCR and X/R ratio) as illustrated in Fig. B.1.

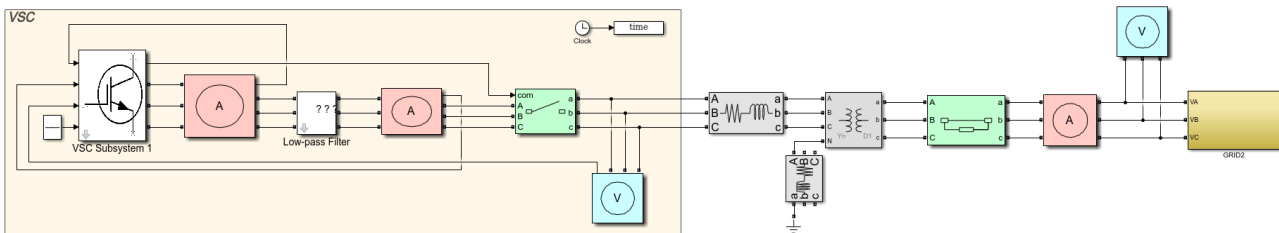


Figure B.1: Matlab-simulink test system model

B.1.1. AC/DC converter model

The AC/DC converter is represented by a standard model available in the Simulink library. This component allows the simulation of power semiconductors and it can be commanded by firing signals as shown in Fig. B.2.

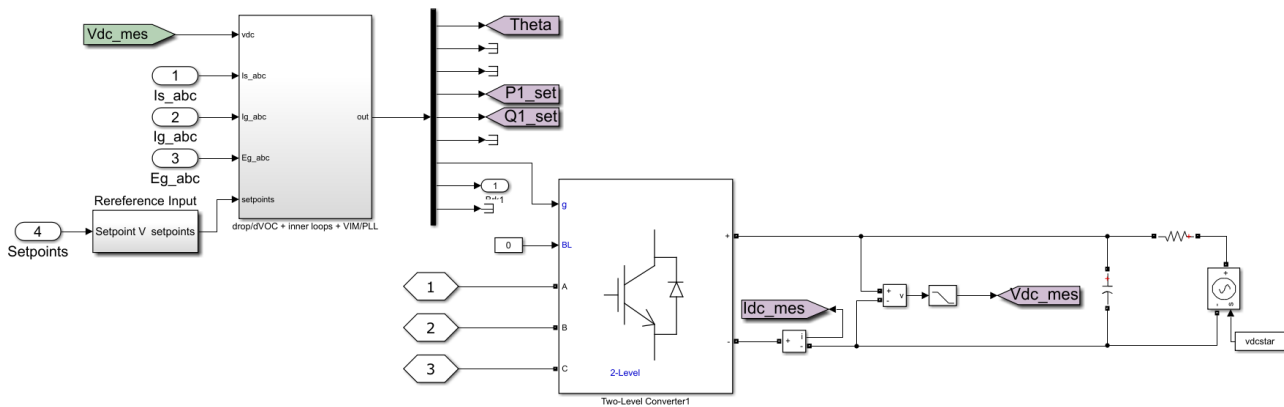


Figure B.2: Matlab-simulink converter model with simplified DC side

B.1.2. DC side model

For the DC side, we considered two different models: a complete one to assess the power sharing dynamics between storage devices, and a simplified one that limits the computational burden of the simulations when focusing on the AC side dynamics.

- **Complete model:** the battery DC/DC converter and the two DC/DC converters associated to the ultracapacitors are represented with their own control and the SoC of the elements is commanded externally by the programmable logic controller (PLC) as depicted in Fig. B.3.

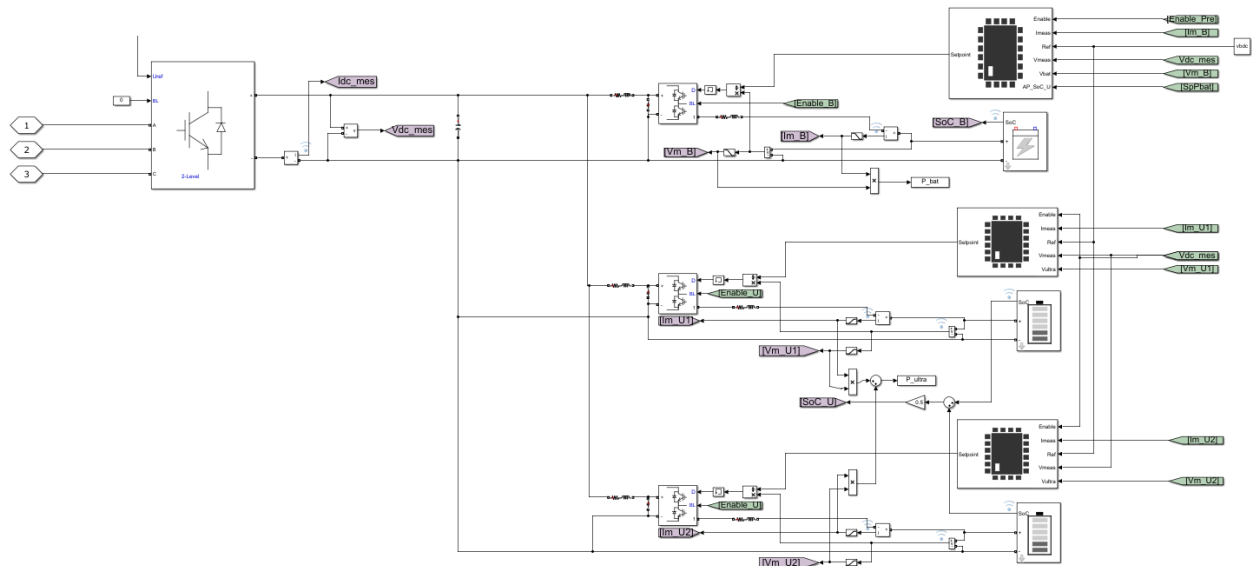


Figure B.3: Matlab-simulink complete DC side model

- **Simplified model:** since the three DC/DC converters are programmed to regulate the bus voltage close to its nominal value and the modulation index is corrected with the DC bus amplitude we can consider that the DC and AC dynamics are decoupled (if enough energy is available on the DC side and there is no malfunction). Under these hypotheses that were confirmed during the factory acceptance tests (FAT, see Chapter 4), the DC side can be reduced to a DC voltage source and a small resistor (to capture the voltage variation with the absorbed/injected current) as shown in Fig. B.2 when validating the AC side performances of the grid forming control.

B.2. AC/DC converter control models

B.2.1. Grid forming control model

The grid forming control described in Chapter 3 is implemented in programming Matlab language and C++. In order to get a closer representation of the real equipment, the converter model block is implemented in discrete time frame with a control execution time of $200 \mu\text{s}$, which is two times faster than the switching frequency. Voltage and current transductions along with the ADC (Analog to digital converter) are also modelled with an equivalent delay and respective digital filters (OVS block shown in Fig. B.4). Finally, a Matlab block executed each time step ($1 \mu\text{s}$) is programmed in order to calculate the semiconductor firing signals and hard blocking (FPGA block). This model is proprietary and will not be publicly released.

B.2.2. Transient grid forming control model

Transient grid forming control (or rather *pure* grid forming according to the definition proposed in this work, i.e. without participation to FCR) is in practice and in the Matlab-Simulink model implemented at high level control, in the PLC, together with the SoC control and regulation as illustrated in Fig. B.5. The control structure is executed each time step. Nevertheless, the large filtering constants (several hundred of milliseconds to seconds), make both dynamics (real and simulation) the same as confirmed during model validation (see Appendix F).

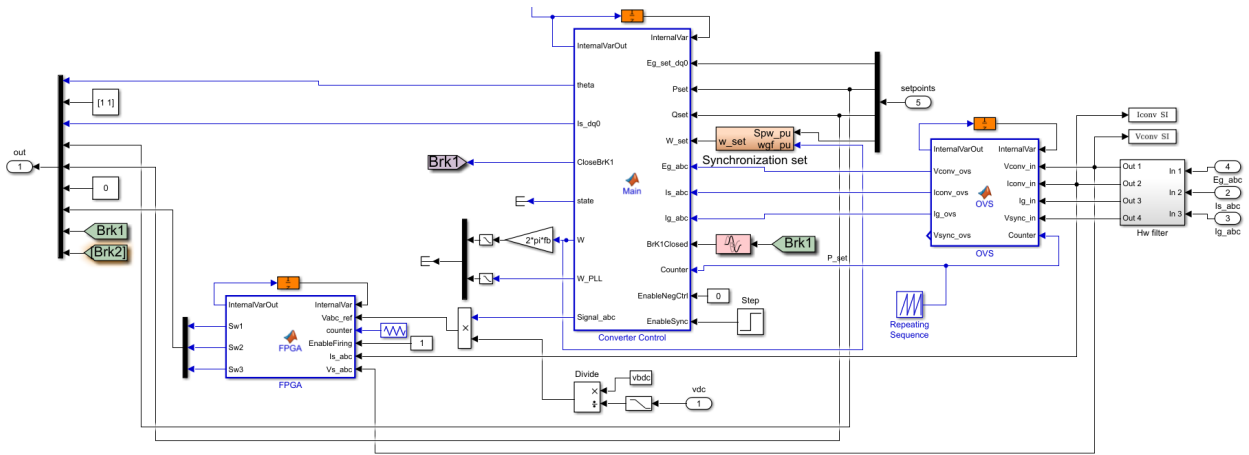


Figure B.4: Matlab-simulink grid forming control model

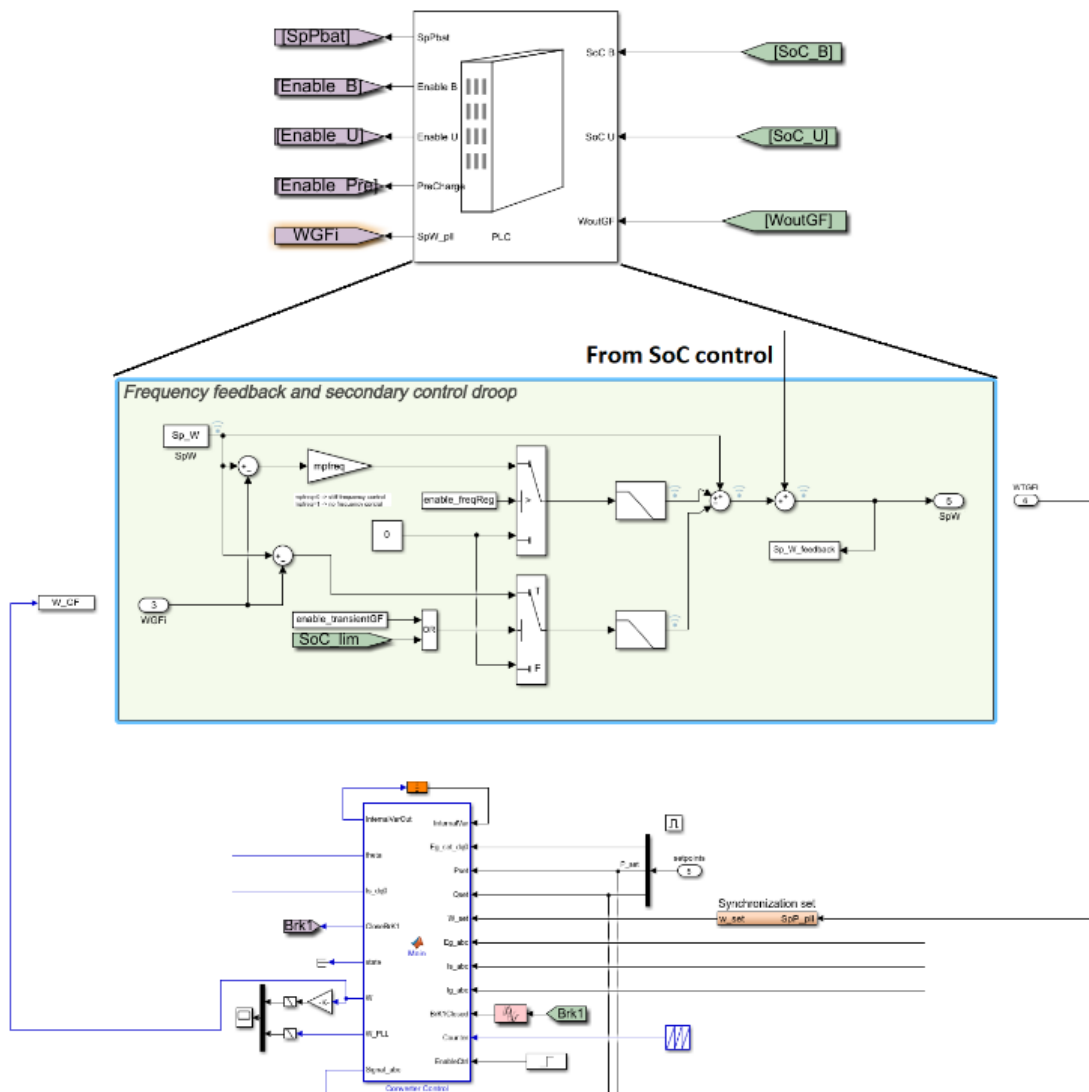


Figure B.5: Matlab-simulink transient grid forming control model

C. RTE-Ingteam Demo: further details on control design

C.1. Known control modules

Park and Clarke transforms. These transforms are very common and basic function blocks for any control implemented in the DQ synchronous reference frame (SRF). These structures get very low attention as they are quite simple. Nevertheless, the input angle used in this functions in grid forming control varies depending on the operation mode (soft connection / normal operation).

Droop control (including adaptive droop during faults). Droop controls (with or without dead-band) are widely used in grid supporting VSCs. So, many manufacturers have experience with similar control structures. The main difference can be found at the P/F droop. In grid forming applications the resultant frequency is integrated in order to estimate the internal angle. In any case, a droop control is a well-known structure. The adaptive droop during faults is another step of development for this control loop. It requires more complex control functions such as: a fault detection, a way to estimate a new droop value depending on the fault conditions and then applying the new droop gain accordingly. So it entails more work from code developers associated to the need of modifying the control algorithm in different parts, but it does not possess any particular challenge.

Damping resistor. Droop controllers in SRF have some poorly damped modes around the natural frequency, as shown in Section I.1.3.2 of [31]. Thus, a damping resistor is used to improve transient behaviour. The controller emulates a virtual resistor, a small change in the output AC voltage. In order to make this added resistor transparent for the droop control, a high-pass filter (HPF) is also added. The virtual resistor works only in transients and the static voltage error is zero. All the structures starting from the HPF filter to the virtual impedance are also used in other control techniques, not only in grid forming control. Thus, the implementation of this control subsystem was straightforward.

The threshold virtual impedance (TVI). This is the solution selected in this work for limiting the output current of the converter as described in section 2.2.2. Its structure is very similar to the virtual resistor. The main difference comes from its variable gain nature implemented through three well known steps:

- Overcurrent detection and virtual impedance activation,
- Virtual impedance calculation,
- Equivalent AC voltage droop estimation.

Once all the 3 steps are performed, the estimated AC voltage droop is applied to the output voltage following different strategies depending on the grid forming algorithm. Some grid forming controls have a virtual impedance per phase, others control only in the voltage module, while the majority of them implement the algorithm in DQ reference frame. The latter approach is selected in this work.

Inner control loops in DQ SRF. Two cascaded PIs in DQ SRF is a very common structure in converter control. This control structure was easy to adapt from grid following. The most challenging part is related to the tuning of the controller values. The tuning for grid following PI control loops is widely analysed and it is possible to obtain some working values by only doing few algebraic operations. Conventionally, controllers in cascaded structure are independently tuned by setting first the fastest loop, the inner current loop. The response time of the voltage loop is considered large compared to the current loop, 10 times higher. This way, the effect of the current loop can be simplified into a transfer function as shown below according to [54].

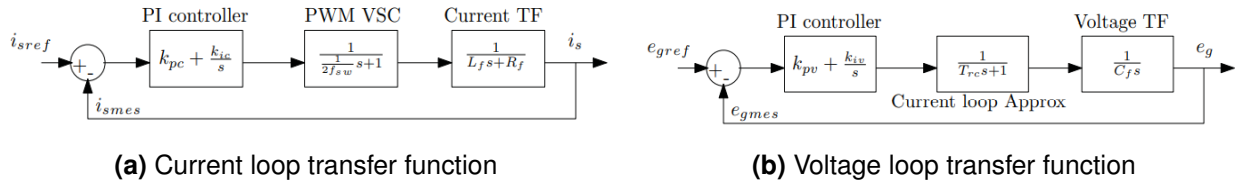


Figure C.1: Inner controls transfer function

For grid forming control, the tuning of these parameters is not that widely analysed. The droop control provides references to the inner voltage loop, likewise, the voltage loop provides current references to the inner current loop which is responsible for current control. In addition, a good decoupling is obtained between direct and quadrature components in this control as long as synchronisation is ensured: $\omega = \omega^*$, but synchronisation is here performed with the active power droop. The dependencies between control loops have been evaluated and some authors have concluded that the conventional controller design approach has its limits. According to [120] the conventional design approach has satisfying performances in standalone (island operation), but suffers from instability issues when is connected to a grid above a certain SCR.

The MIGRATE project proposed a more sophisticated way for the controller design, involving a state space representation in order to take into account the interaction between all the system modes and find a setting for the controller satisfying a stability criteria, damping and robustness [31]. The state-space equations in MIGRATE project were developed considering a continuous time frame and therefore discretisation is not taken into account. So, the application of the method to the OSMOSE WP3 demonstrator is not straightforward, and the parameters where tuned based on the conventional approach.

At this point it is important to highlight that it was impossible to verify the tuning method by overlapping theoretical step response with the real step response for the current loops. This way to verify can be used in grid following mode (current loop with the PLL), but in grid forming, current loops cannot be tested against a step without upper control loops as there is no PLL. This can only be achieved in standalone / island mode [54]. Thus, only the stability and dynamics of the whole system were measured. Some other solutions for the grid forming inner control loops can also be found in the literature [55], but all of them are theoretical analyses. The verification of the methods should be assessed and the limits of the method and dynamics evaluated in a real system.

Lead-lag filter or compensator A lead lag compensator adds a zero as well as a pole to the system at chosen frequencies. It is important to place the zero at the desired frequency in order to improve the system performance. A low pass filter is a more stable structure, as it only adds a pole. The tuning method used in the OSMOSE project was the classical approach, the whole system modelling was not performed. Thus, as the complete system pole map was not available, a low pass filter was chosen and the lead-lag compensator was disregarded at the expenses of lower damping for high inertia settings.

C.2. Grid forming control settings

The list of Grid Forming Control parameters is provided below. Preliminary values for the inner control loop and damping control are included. They will be validated during FAT. Once fixed, they will remain unchanged after commissioning as it is acknowledge that changing these values without verification and Ingeteam supervision may affect the performance of the equipment. Regarding Droop param-

ters (mp , nq and $Tfmp$), the table includes a range since RTE has requested the possibility to modify them through HMI in operation. Proper functioning within these ranges has to be validated. Regarding TVI, additional studies will be performed jointly between RTE R&D and Ingeteam R&D Europe to validate lower current threshold for TVI triggering. The goal is to force the current limiting mode even though grid conditions are not severe enough. The proper functioning of the system will be confirmed in FAT. The RTE-Ingeteam demo has been designed from Migrate control developments [31], adapted to Ingeteam power converters [8]. The listed of defined parameters in per-units are recalled in table 1. In this note will be described, the system parameters that can be adjusted by the future user through the HMI in an authorised variation range. By changing the parameters of the system, the goal pursued by the user is threefold:

- Evaluate the relationship between grid-forming character of the HESS and the main parameters of external loop (mp , nq , $Tfmp$)
- Change the allocation of services on DC side, from the ultra capacitors (UC) to the battery
- Push virtually the control in its limit by lowering the trigger threshold of limiting strategies.

Internal loops, dampers will not be adjusted because their tuning is related to the system and grid hardware, not to the functionality of the system.

Table C.1: Example of AC control parameters in per-unit

Parameter		Value	Description
Droop	mp	[0.001-0.02- 0.05]	Active power droop
	nq	[0 – 0.01 - 0.10]	Reactive power droop
	$Tfmp$	[0.001-0. 014-0.06]	Active power droop LPF time constant
Damping	$Rdamping$	0.11	Damping resistor value
	$Tfdamping$	0.006	Damping resistor time constant
TVI	Xr	0.8	Inductive component of the virtual impedance
	Kr	1.54	Gain of the virtual impedance
	$Imax$	1.35	Maximun current
	$Ithreshold$	1	VI threshold (positive and negative sequence)

C.3. High level control logic

C.3.1. SoC control logic

A logic variable allows to disable the continuous SoC control to leave only the hysteresis control. Then, the hysteresis can take over at any moment to restore SoC if threshold are reached. Finally, the continuous SoC control must be deactivated if the external set point is enable as summarised in Tab. C.2.

Hence, the condition for Continuous SoC control activation are:

- The external active power is disabled (Enable_SpExt=0, external set point) and,
- The SoC is within control range (within limits) and,
- The Continuous SoC control is enabled (Enable_ctrl=1, internal variable) and,
- The hysteresis control is not activated.

The expected functioning of those control in degraded modes is summarised in Tab. C.3:

Table C.2: SoC control logic

SoC controls	Activation	Deactivation	Priority	Action
Hysteresis SoC (safety)	operational SoC limits	SoC reach Delta_Hyst_Ctrl	High	Bring back SoC of device (U or B) around SoC_set
Continuous SoC (regulation)	manual	manual manual or SoC limits or enable ext_Pset	Low	Continuously maintain SoC_set on T_x time constant
ext_Pset (HMI or modbus)	manual	manual or SoC operational limits	Mid	SoC is not controlled to follow only Power demand variation

Table C.3: SoC control logic in degraded modes

SoC control mode	HESS	UC only	Battery only
Hysteresis SoC/ safety	available	not defined for UC	available
Continuous / SoC regulation	available	available for UC	available
ext_Pset (HMI or modbus)	available	not available	available

Matlab-simulink model of SoC control logic. These priority logic are implemented in Matlab-Simulink for control validation purposes as illustrated in Fig. C.2.

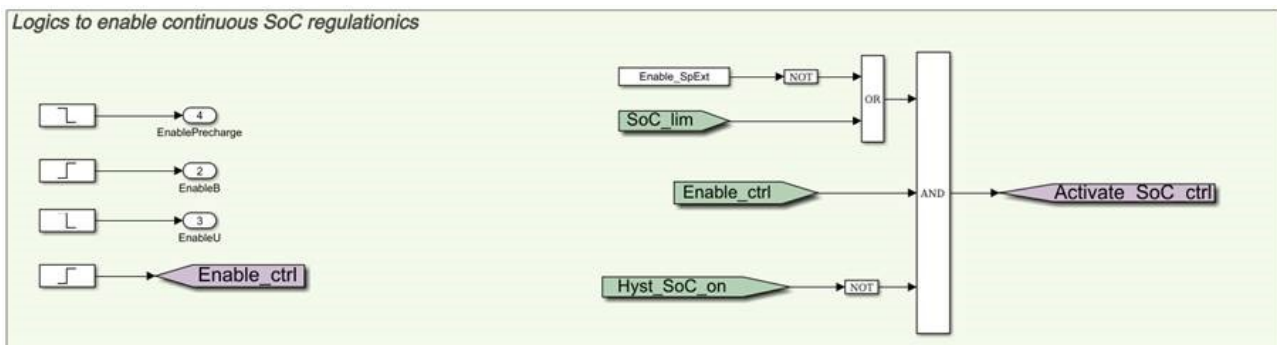


Figure C.2: SoC regulation enable signal logic implemented in Matlab-Simulink

C.3.2. SoC Set Point logic

When the continuous SoC control is activated, it will charge a reference value. It can be set:

- Externally through the HMI and this value has top priority.
- If the hysteresis control is activated, then, reference value defined in the hysteresis SoC control (Sp_hyst_SoC) is imposed with mid priority.
- Finally, the measured SoC value at the specific time when the external power set point is disabled will be maintained as low priority condition (see Fig. C.3).

C.3.3. Continuous SoC regulation

For the UC, the battery power reference is modified as shown in Fig. C.3 if it is available, allowing the UC to act as a buffer to power variations. The implemented SoC regulation is depicted in Fig. C.4.

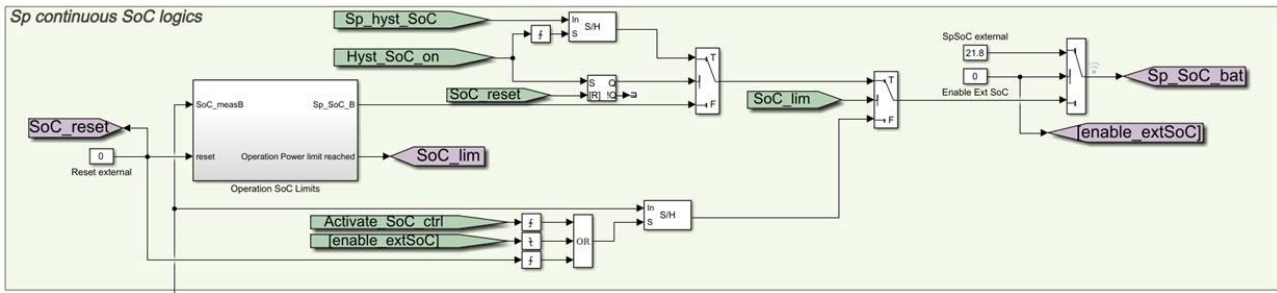


Figure C.3: SoC set point logic implemented in Matlab-Simulink

For the battery SoC regulation we consider two PIs: Normal operation and hysteresis control. The actuation of the first SoC regulation is limited to low power values, so this loop is a smooth or slow SoC control. Its operation limits are tighter than the hysteresis SoC control. If the first SoC regulation is enabled and works properly, the second should not be activated.

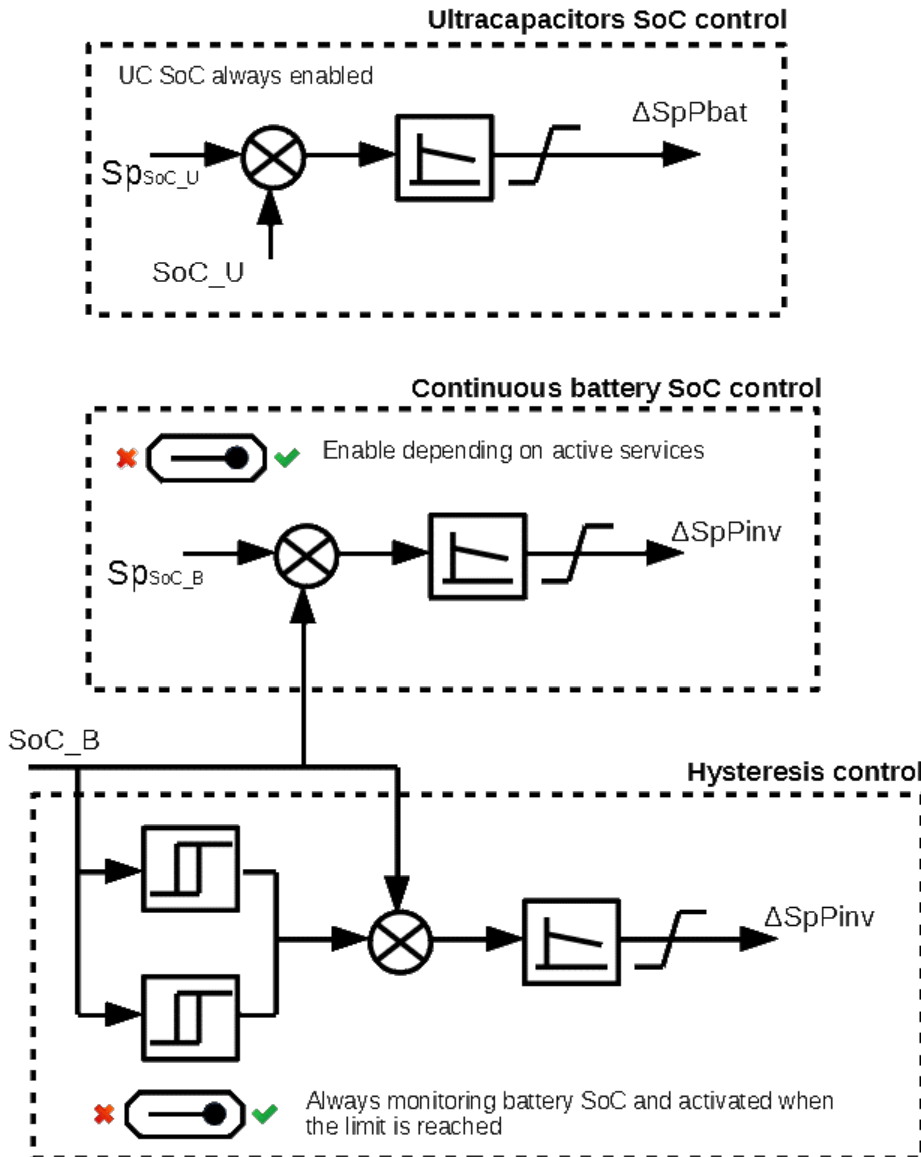


Figure C.4: SoC regulation

C.3.4. Hysteresis SoC control

The second loop can be considered as a safety mode where the maximum / minimum output power of the hysteresis SoC control is increased to 0.4-0.45 pu and instead of continuous SoC regulation, the SoC is increased or decreased to a safe zone. Once the safe SoC is reached the hysteresis control is disabled. This new safe SoC value is defined with delta SoC. If by any means the SoC reaches a limit (continuous or hysteresis SoC control limit), the user have to reset the control in order to re-activate the most active power consuming service (external set point).

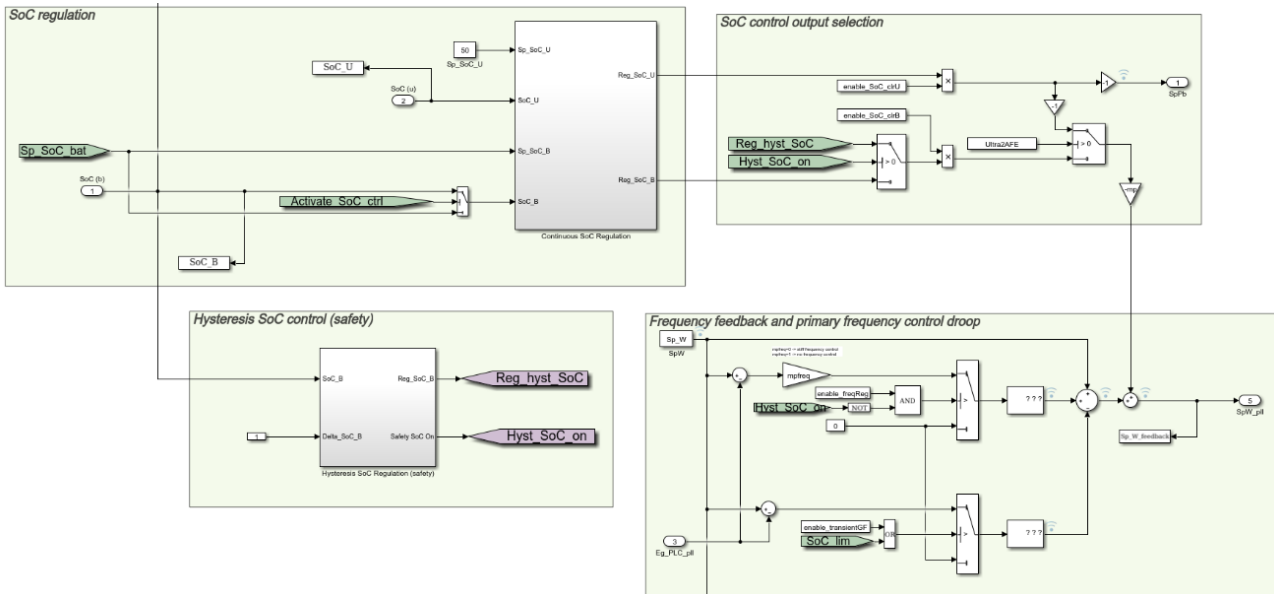


Figure C.5: Battery and UC SoC control implemented in Matlab-Simulink

C.3.5. Power limits and SoC control for UC

UC SoC control is always active (even with external set points). The control stops working only under 2 conditions: Malfunction of the UC and manually forced to disable. The latest is related to the SoC control logic selected output signals. Depending on the configuration and some enable signals, the correct output signal is directed to the AC side equipment. In UC only “Ultra2AFE=1”, so the UC will charge from the grid

This power transfer has to be performed taking into account the power limit of each device. Thus, the UCs cannot be charged from the battery if the battery is injecting or absorbing its rated power. The same goes to the battery, it cannot be charged from the converter if that action implies an unacceptable power exchange with the grid.

C.3.6. Control application logic

Table C.4 lists all the service combination and indicates their availability in degraded mode.

Matlab-simulink model of application level logic. The model include two block displaying the selected configuration as shown in Fig. C.7. Behind each configuration, some signals to enable / disable circuit parts are selected. *Pset* mode allows us to disable the battery continuous SoC control.

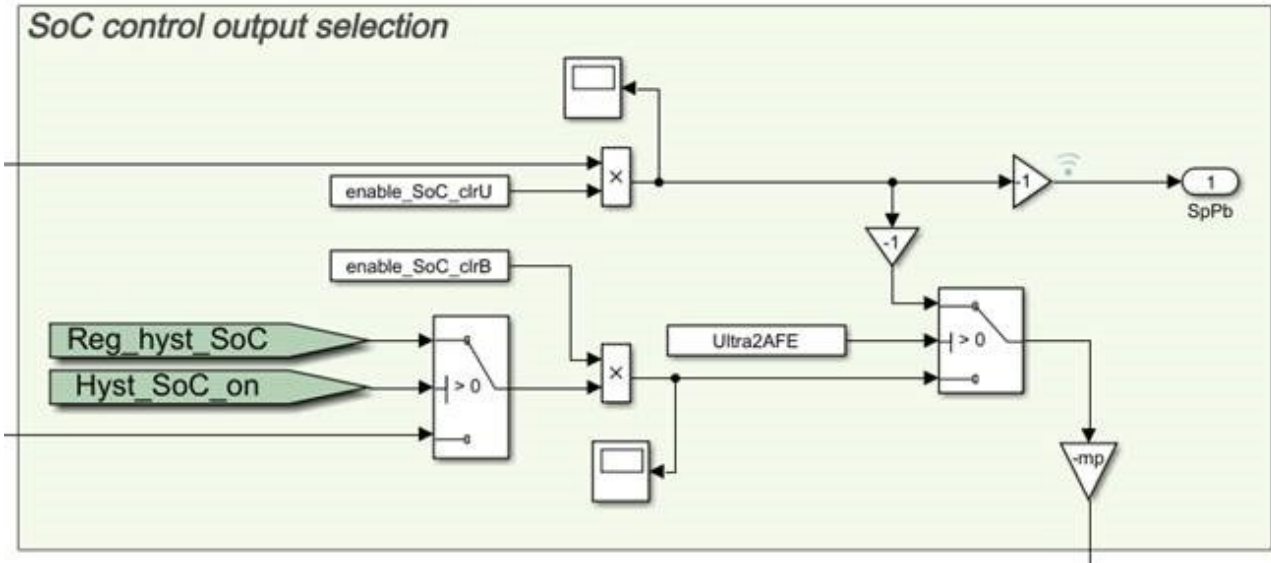


Figure C.6: SoC output selection logic

Table C.4: Service combination

Active power services	Activation	Deactivation	HMI param	Simulink parameter
Transient grid forming (TGF only)	default if UC here	when battery only if it cannot hold specified charging/discharging currents	T_{gf}, mp	$tf_Wpll_PLC_TGF = T1$
TGF plus FC	manual	manual or UC Only or SoC lim or ext.Pset (if modbus 200ms)	T_{fc}, R	$tf_Wpll_PLC_FCR = T3$ and $R = mp \cdot mp_{freq}$
GF (equivalent to TGF with FC but with the same droop and same Time constant)	manual	manual or UC Only or SoC lim or ext.Pset (if modbus 200ms)		$R = mp$
TGF plus ext.Pset (HMI or modbus)	manual	manual or SoC lim	T_{gf}	$tf_Wpll_PLC_TGF = T1$ (for TGF only)

Table C.5: Services availability on degrade modes

Active power services	HESS	UC only	Battery only
Transient grid forming (only)	available	available	available
TGF plus FC	available	not available	available
GF (equivalent to FC plus TGF but with the same droop and same Time constant)	available	not available	available
TGF plus ext.Pset (HMI or modbus)	available	not available	available

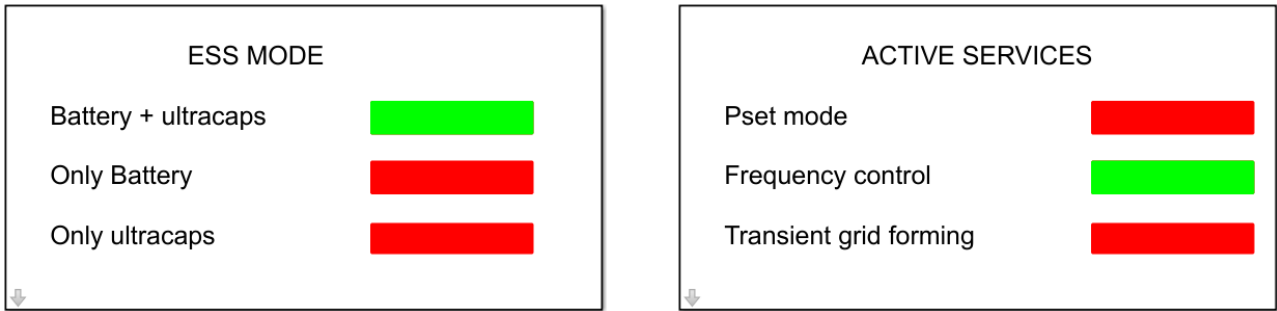


Figure C.7: User configuration display blocks implemented in Matlab-Simulink

```

% DC bus configuration
switch ESS_config
  case 1
    % battery + ultracap
    run Batt_plus_Ultra
    Ultra2AFE=0;
    enable_SoC_clrB=1;
    enable_SoC_clrU=1;
  case 2
    % battery
    run Batt_only
    Ultra2AFE=0;
    enable_SoC_clrB=1;
    enable_SoC_clrU=0;
  case 3
    % Ultracap
    run Ultra_only
    Ultra2AFE=1;
    enable_SoC_clrB=0;
    enable_SoC_clrU=1;
    %% TRF only allowed
    Enable_SpExt = 0;
    enable_transientGF=1;
    enable_freqReg=0;
  case 4 % only for testing, to get rid of battery management
    % battery + ultracap
    run Batt_plus_Ultra
    Ultra2AFE=0;
    enable_SoC_clrB=0;
    enable_SoC_clrU=0;
  otherwise
    disp('ERROR bad ESS config');
end

% Grid services
switch Active_services
  case 1
    %% Sp_pext enable + ffr
    Enable_SpExt=1;
    enable_transientGF=1; % ? ? ? ?
    enable_freqReg=0;
  case 2
    %% mpfreq enable + ffr
    Enable_SpExt = 1;
    enable_transientGF=0;
    enable_freqReg=1;
  case 3
    %% TGF enable
    Enable_SpExt = 0;
    enable_transientGF=1;
    enable_freqReg=0;
  case 4
    %% TGF enable + Freq reg with other droop
    Enable_SpExt = 0;
    enable_transientGF=1;
    enable_freqReg=1;
  case 5
    %% PLC SoC disabled
    Enable_SpExt = 1;
    enable_transientGF=0;
    enable_freqReg=0;
  otherwise
    disp('ERROR: Active power services allocator');
end

```

Figure C.8: Parameter initialisation cases to configure system. Grid services related case (left) and ESS configuration related case (right)

D. RTE-Ingeteam Demo: simulations for control validation

D.1. Synchronisation

Figure D.1 shows a smooth and stable current and voltage evolution following the synchronisation event thanks to the soft connection function.

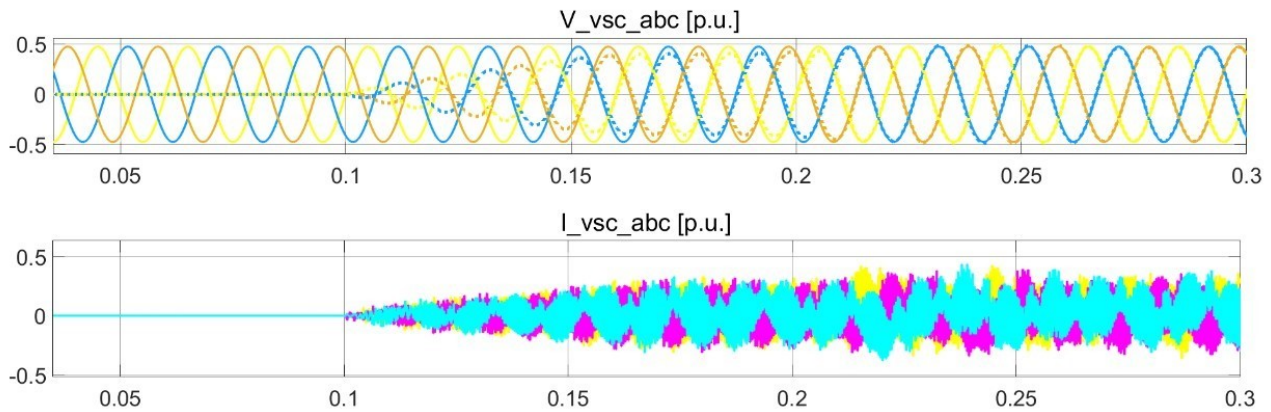


Figure D.1: Voltage and current during the synchronisation at converter terminals

D.2. Reference tracking

D.2.1. Voltage set point variation (ΔSpV)

Figure D.2 shows the active and reactive power following a voltage amplitude reference step. The current and voltage waveforms are shown in Fig. D.3. Tracking is achieved within less than 100 ms. An active power transient is generated in the process.

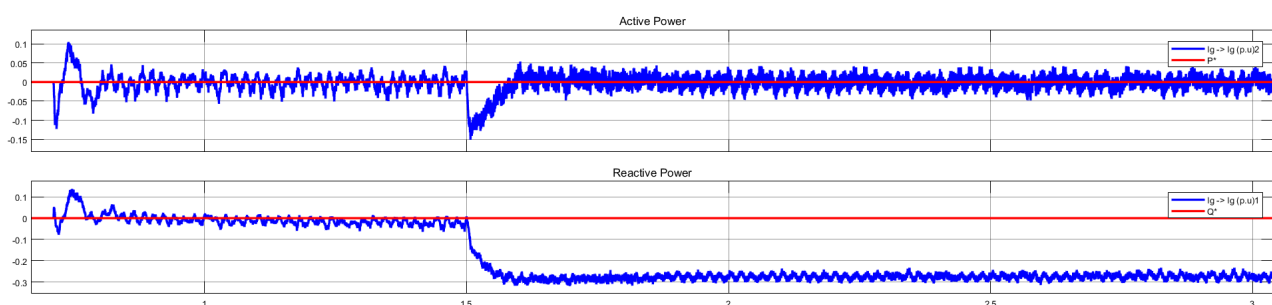


Figure D.2: Active and reactive power evolution for a voltage set point variation

D.2.2. Frequency set point variation (ΔSPf)

Figure D.4 shows the converter frequency following a set point ramp from 1 to 0.99 (50Hz to 49,5Hz) with a rate of change of the frequency (RoCoF) of 10 Hz /s (2 pu/s). The active and reactive power evolution are shown in Fig. D.5 considering a grid forming equipment droop of $mp=0.02$ p.u., while

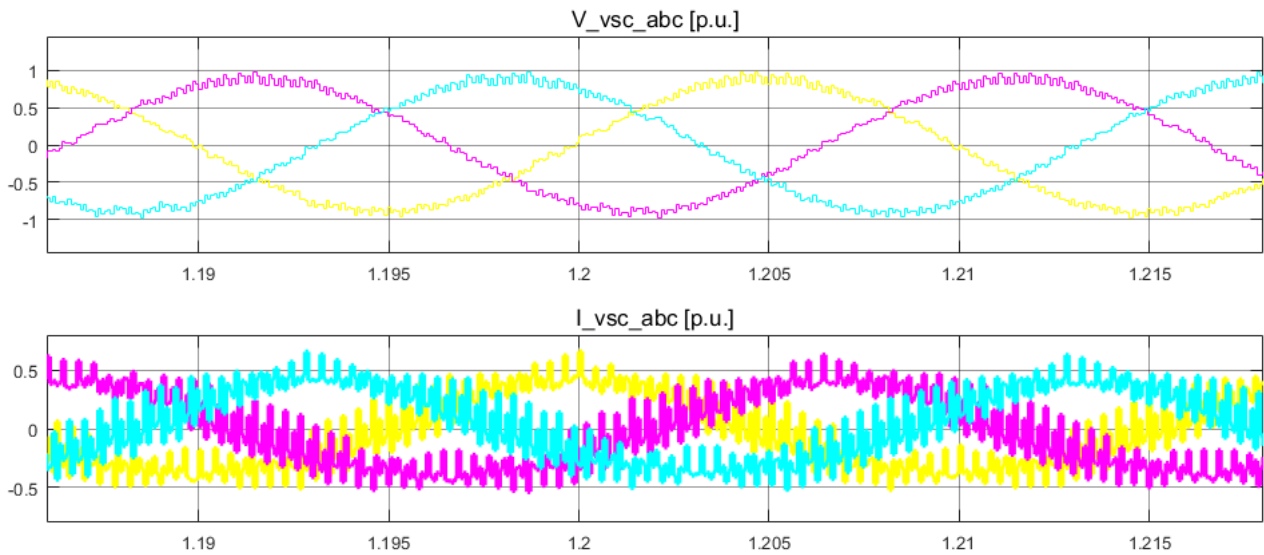


Figure D.3: Three phase voltage and current for a voltage set point variation

the virtual grid droop is $mpVG=0$. The reactive power doesn't come back to its nominal value as it needs to compensate for the losses in the filter from active power flow.

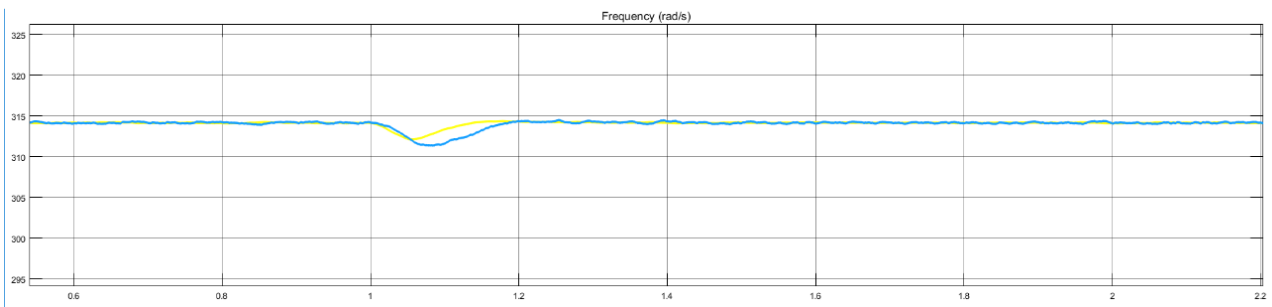


Figure D.4: Grid forming equipment measured frequency and internal frequency

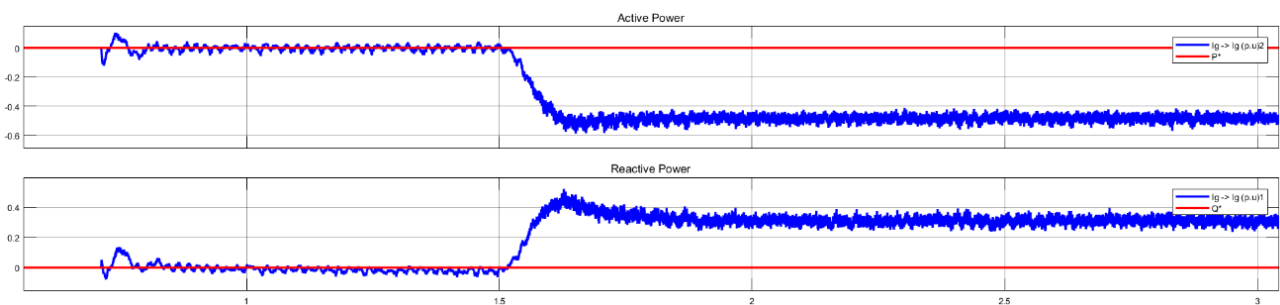


Figure D.5: Active and reactive power evolution for a frequency set point variation

D.3. Synchronisation services to grid disturbances

D.3.1. Phase Jump (30 degrees)

Injected synchronising power is shown in Fig. D.6 while voltage and current waveforms are displayed in Fig. D.7. Almost nominal power without current limitation is reached in the 30 degrees phase jump test for the benchmark connection impedance. Phase jump is done in both direction at $t=1.1\text{s}$ and $t=1.3\text{s}$

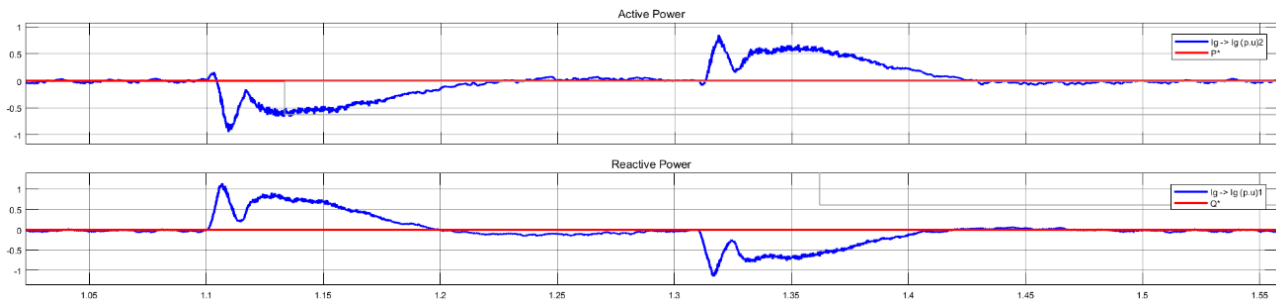


Figure D.6: Active and reactive power for a 30 degrees grid phase jump

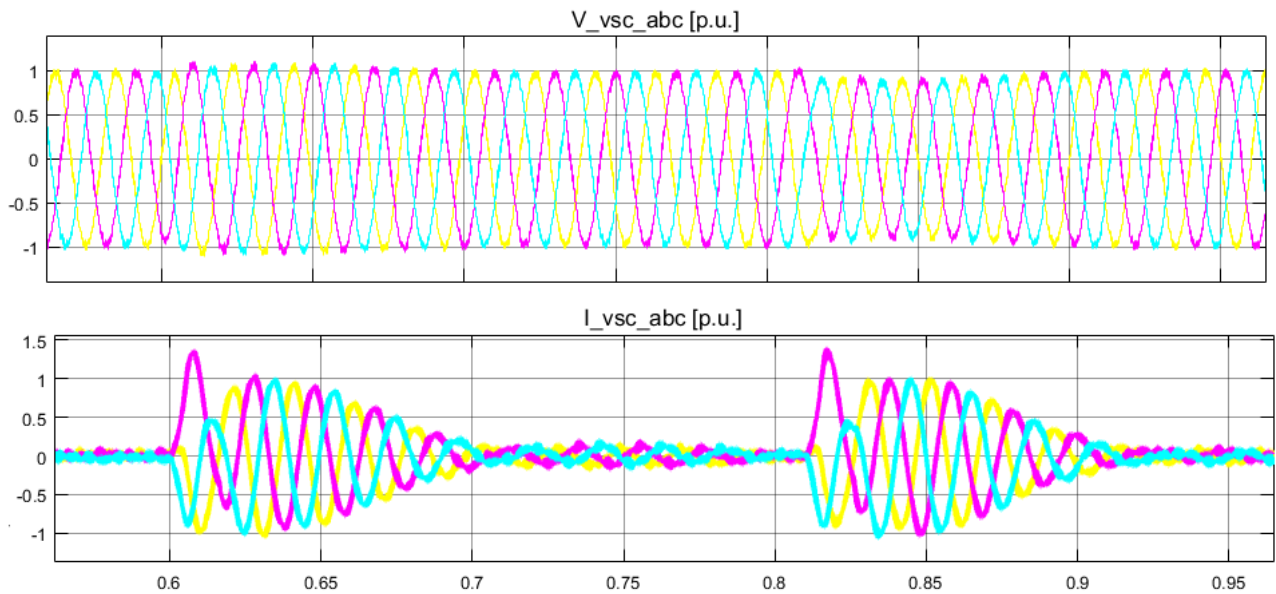


Figure D.7: Three phase voltage and current for a 30 degrees grid phase jump at converter terminals

D.3.2. Grid voltage variation (ΔV)

Figures D.8 and D.9 show the active and reactive power, as well as the current and voltage waveforms following a disturbance in the grid voltage amplitude. Immediate and well damped response is observed.

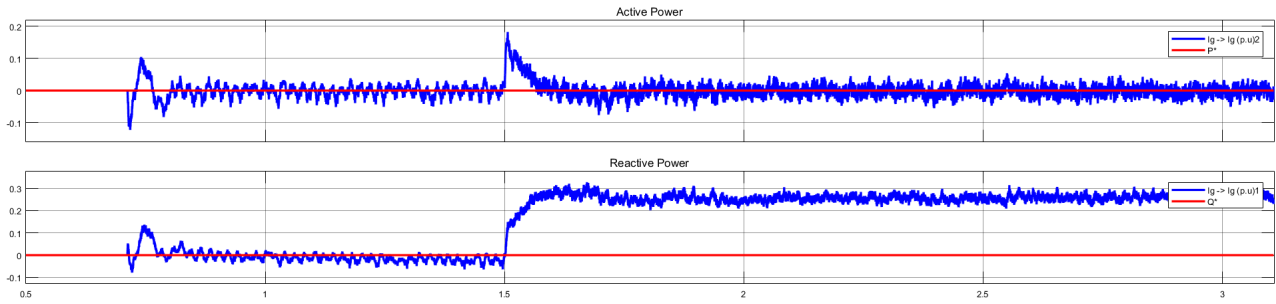


Figure D.8: Active and reactive power for a grid voltage variation

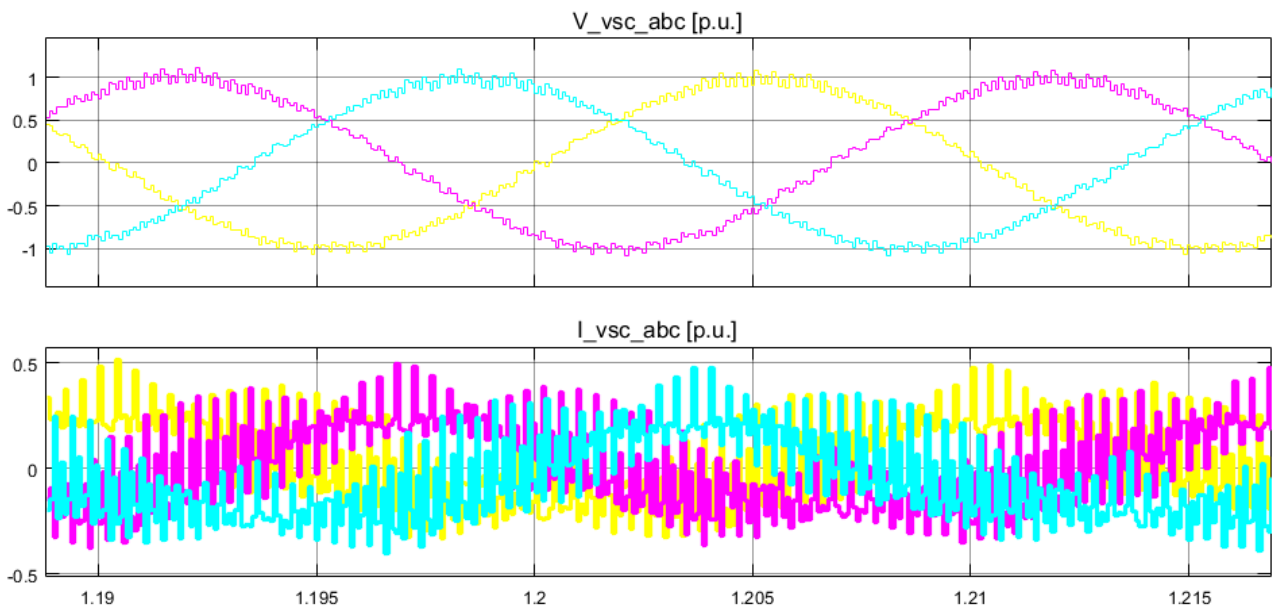


Figure D.9: Three phase voltage and current for a grid voltage variation

D.3.3. Grid frequency variation (Δf_g)

The evolution of the main variables following a grid frequency ramp of 2 Hz /s (0.04 pu/s) from 1 to 0.98 (50Hz to 49Hz) in 0.5 seconds are shown in Figs. D.10 and D.11.

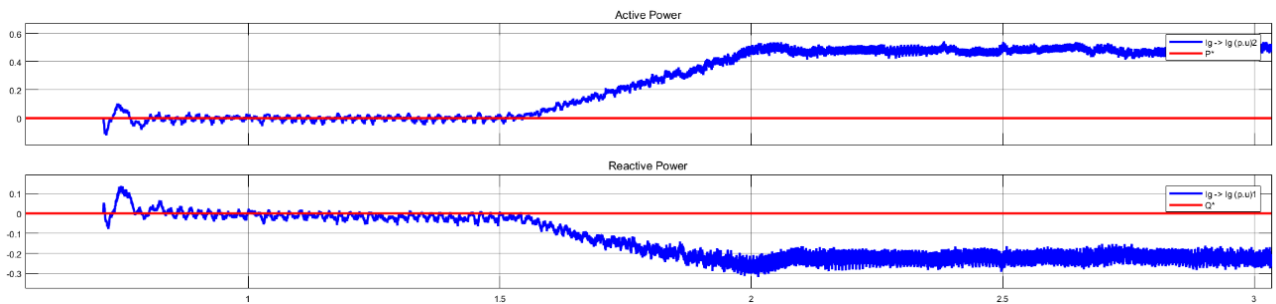


Figure D.10: Active and reactive power evolution for a grid frequency variation

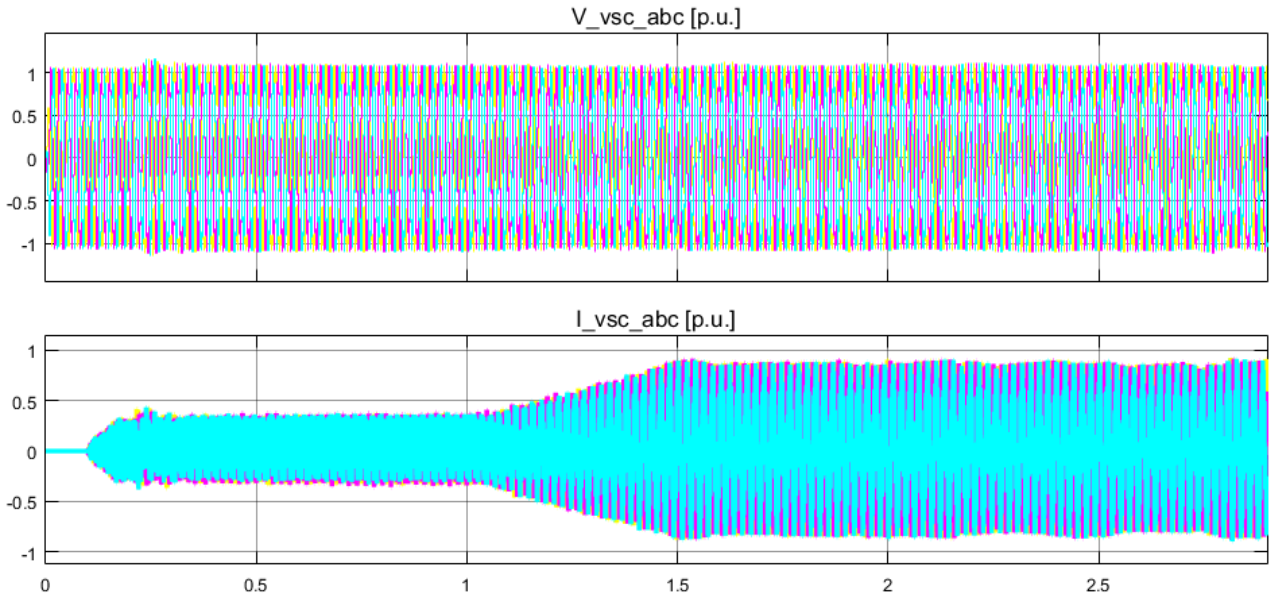


Figure D.11: Three phase voltage and current for a grid frequency variation

D.3.4. Faults

Three phase faults: TVI current limitation works properly for a fault depth of 90% (10% residual voltage) as shown in Figs. D.12 and D.13.

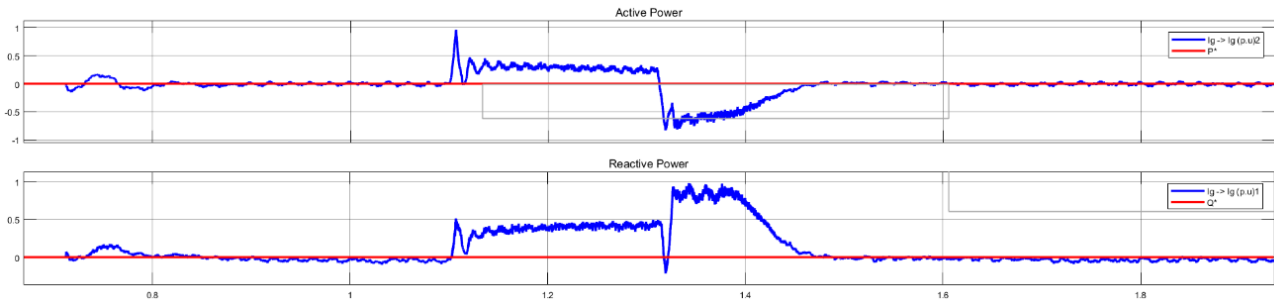


Figure D.12: Active and reactive power evolution for a 90% 3-phase fault at the virtual grid

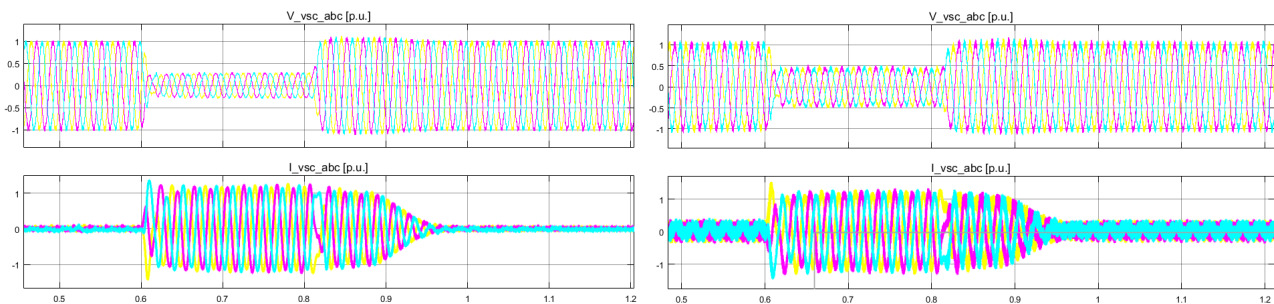


Figure D.13: Three phase voltage and current for a 90% 3-phase fault at grid and converter terminals

Asymmetrical faults: NS-TVI current limitation behaves properly for 70% type C (2 phases) fault ($V_{res}=30\%$) as shown in Figs. D.14 and D.15.

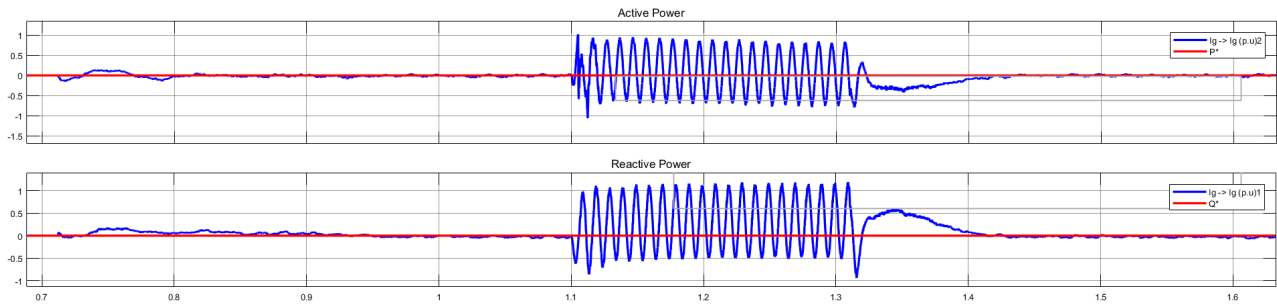


Figure D.14: Active and reactive power for a 70% type C fault

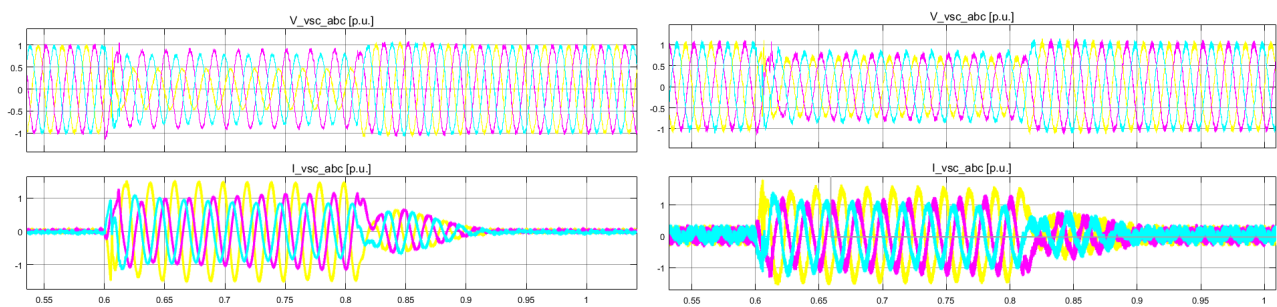


Figure D.15: Three phase voltage and current for a 70% type C fault at grid and converter terminals

D.4. Robustness to grid distortion

Permanent grid voltage unbalanced (10%): the system withstand high unbalance in the grid as shown in Fig. D.16.

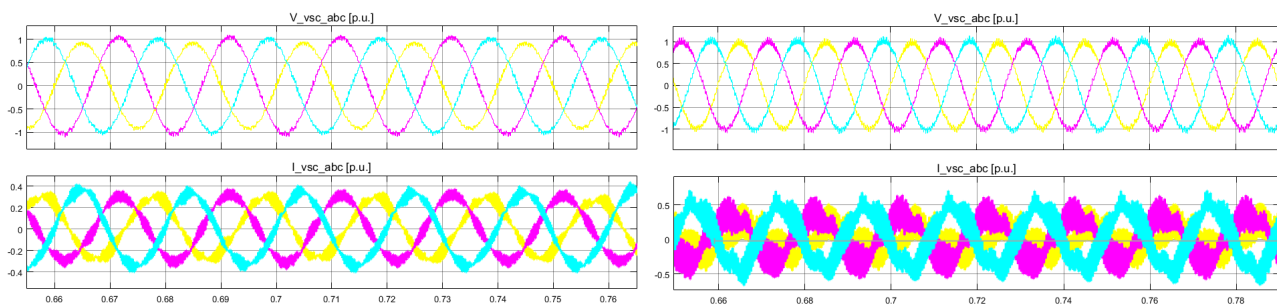


Figure D.16: Three phase voltage and current for a 10% voltage unbalance, VG and GF terminals

Harmonic Sensitivity Evaluation (5th,7th): the grid forming equipment is first connected to the virtual grid with a 5% 5th harmonic component and then connected to a 5% 7th harmonic component. The virtual grid continues generating only nominal frequency components (plus modulation) absorbing harmonic current. Active and reactive power, as well as voltage and current waveform when the grid have 5% of 5th or 7th harmonics are described in Fig. D.17, Fig. D.18, Fig. D.19 and Fig. D.20

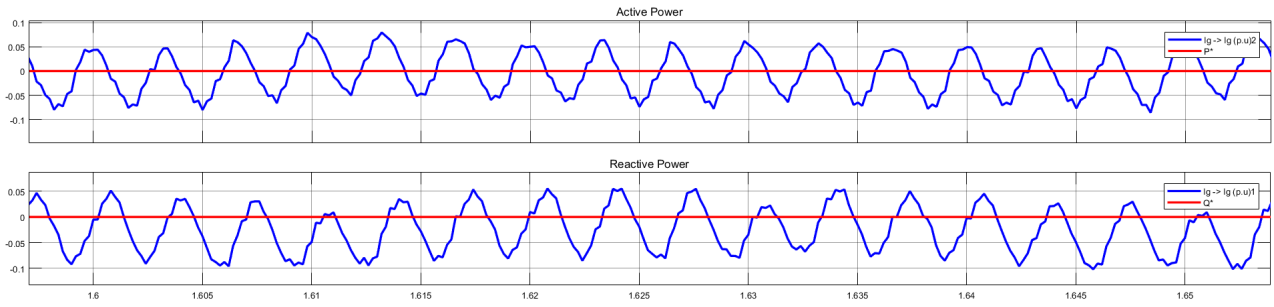


Figure D.17: Active and reactive power when connected to a grid with a 5% of 5th harmonic component

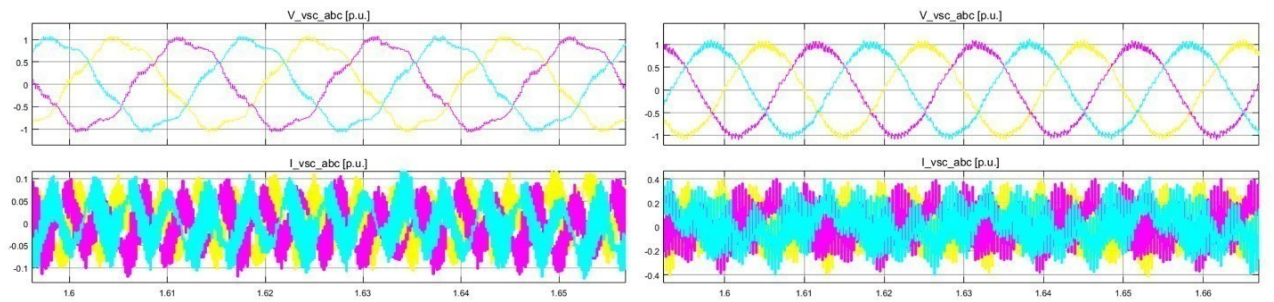


Figure D.18: Voltage and current at grid forming equipment and the virtual grid when connected to a grid with a 5% of 5h harmonic component

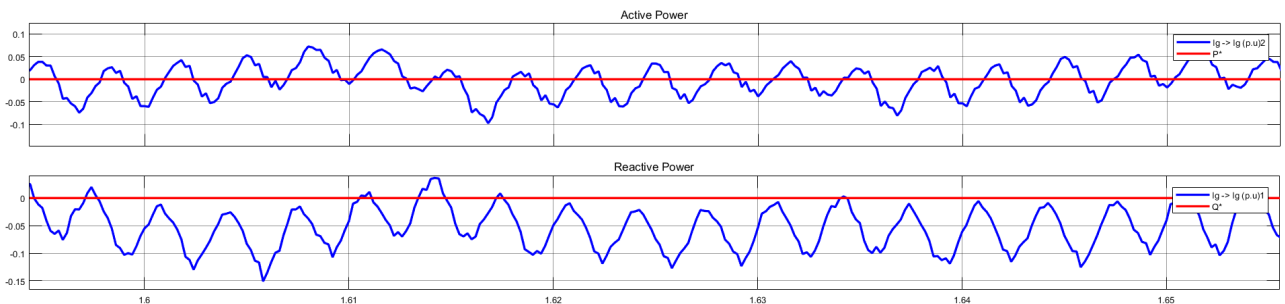


Figure D.19: Active and reactive power when connected to a grid with a 5% of 7th harmonic component

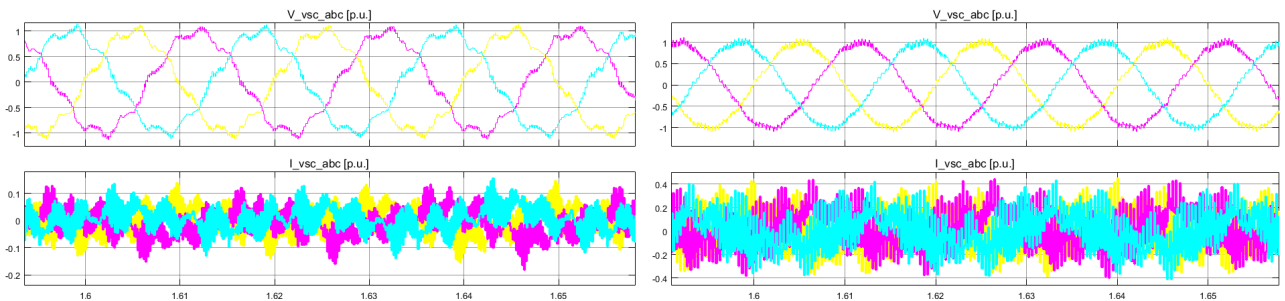


Figure D.20: Voltage and current at grid forming equipment and the virtual grid when connected to a grid with a 5% of 7h harmonic component

D.5. DC side control performance

D.5.1. Nominal conditions: battery with ultra capacitors (UC)

This section includes simulation results for the DC side control validation considering three different configurations of the DC bus:

- full hybrid energy storage system (HESS) with both the batteries and the UC in service,
- degraded modes: only battery and only UC.

For each case, different events with different active services have been simulated. No TVI activation is considered for the sake of simplicity when the SoC control is tested. In addition, the capacity of the battery has been reduced with a factor of 5 (five times smaller). Otherwise, the simulation times became prohibitive.

Long-period frequency downfall with transient grid forming. For transient grid forming control the continuous SoC regulation is activated. In this case, after few seconds, the grid forming equipment stops injecting active power and starts SoC control as shown in Figs. D.21 and D.22. The UC is charged from the battery and it does not inject any power in steady state (see Fig. D.23).

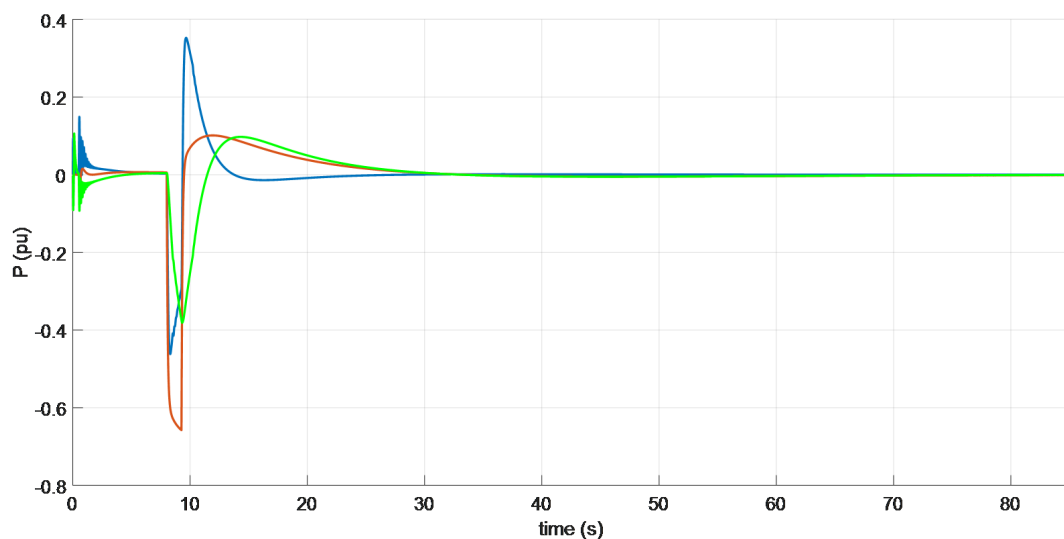


Figure D.21: Injected active power for transient grid forming by device with HESS configuration. UCs (blue), AC side converter (red) and battery (green)

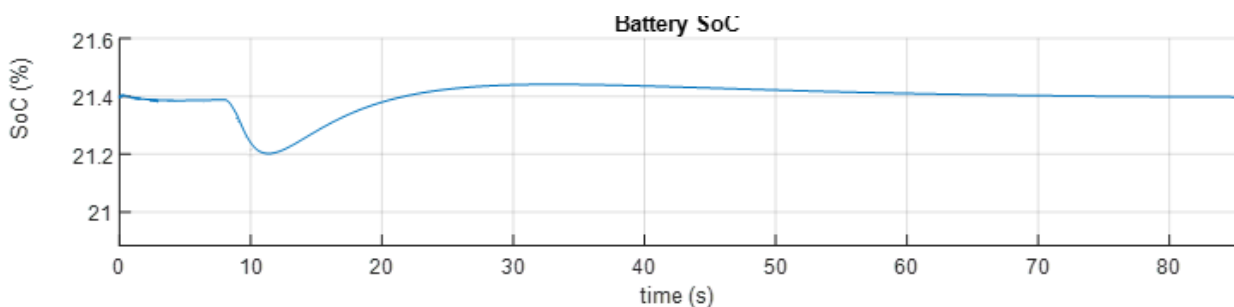


Figure D.22: Battery SoC evolution for transient grid forming in HESS configuration

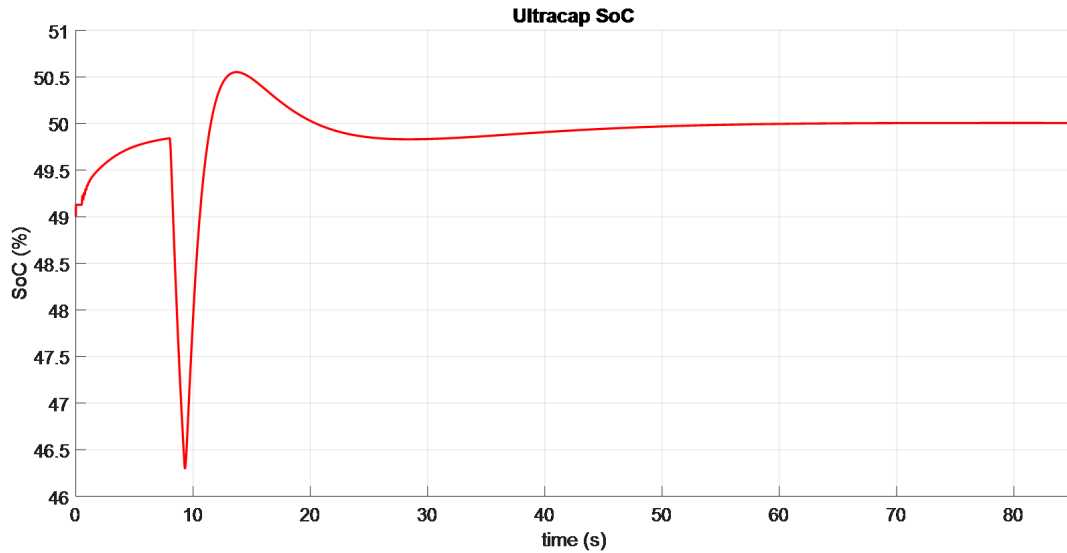


Figure D.23: UC SoC evolution for transient grid forming in HESS configuration

Active power external set point in normal operation. Figure D.24 shows the expected power sharing between the different devices and the response of the SoC control strategies when no limits are reached.

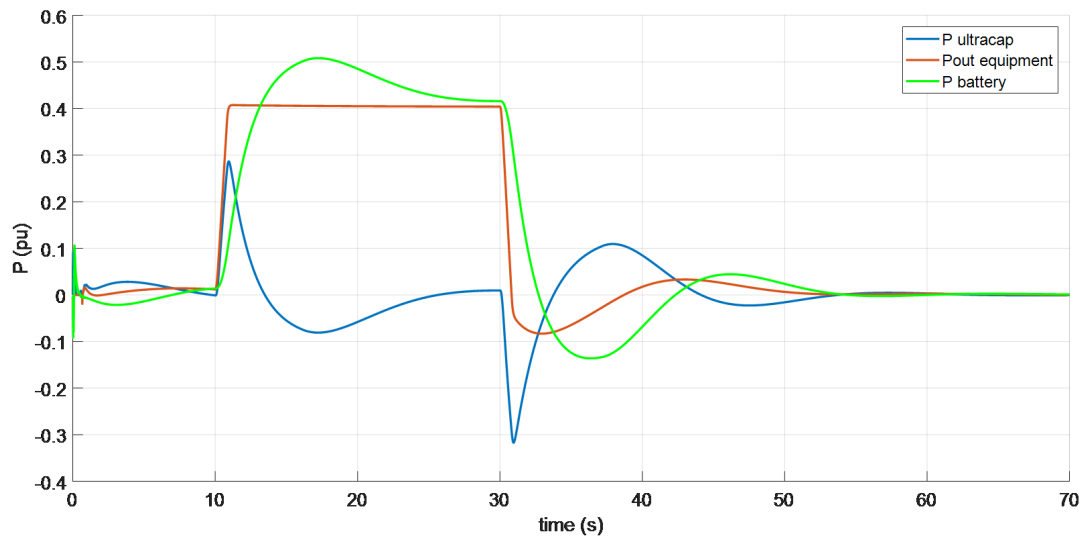
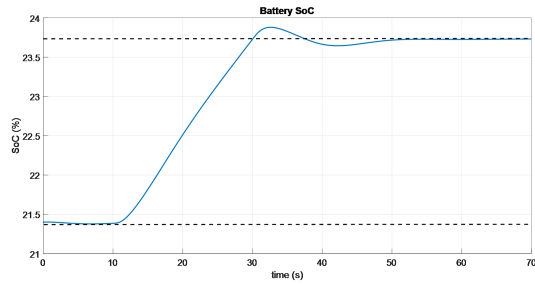


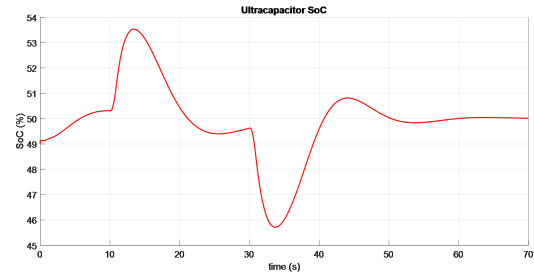
Figure D.24: Injected active power by device with HESS configuration for external set point. UCs (blue), AC side converter (red) and battery (green)

Energy capacity verification. Taking into account the evolution of the SoC and the measured output power, the amount of the energy delivered to the grid and the modelled battery capacity are confronted as follows:

- $C_{\text{battery}} = 0.5\text{Mw} \cdot 60 \text{ min} = 0.5 \cdot 3600 \text{ Mws}$
- $C_{\text{consumed}} = 0.4 \cdot 20 \text{ Mws}$
- $\text{Percentile} = 0.4 \cdot 20 / 1800 \cdot 0.2 = \mathbf{2.22\%}$ (0.2 reduced capacity to accelerate simulations)



(a) Battery



(b) UCs

Figure D.25: SoC evolution for external set point in HESS configuration

External active power set point when the SoC limit is reached (hysteresis control). First at 20% SoC operational limit is reached and the SoC regulation is activated, transient grid forming mode is activated and external active power set point is disabled. If due to a bad parameterisation or any other reason, the hysteresis SoC limit is reached, hysteresis SoC control is activated. This SoC control is not based on limiting the SoC, it takes the SoC to a safe zone. The delta SoC value should be around 20-30%. In order to force the SoC to reach hysteresis limit in the simulation, the set point slope have been reduced to 0.1 pu/s and lower hysteresis limit increased to 19.85%. Delta SoC is also reduced from 25% to 1% for the same reason.

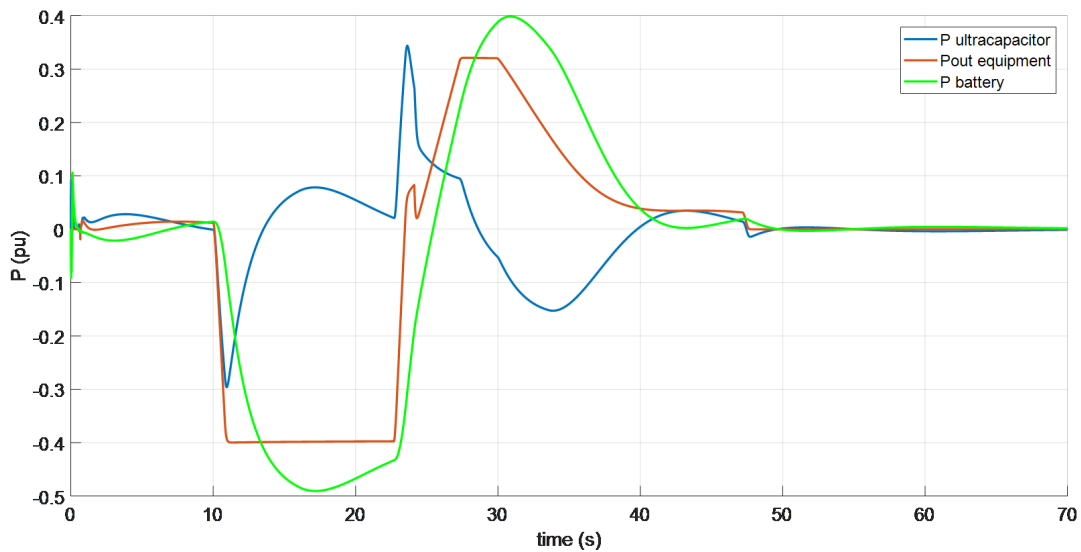
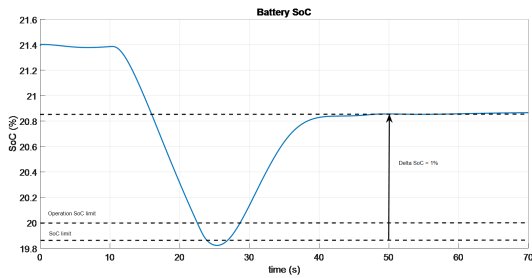


Figure D.26: Injected active power by device with HESS configuration for external set point. UCs (blue), AC side converter (red) and battery (green)

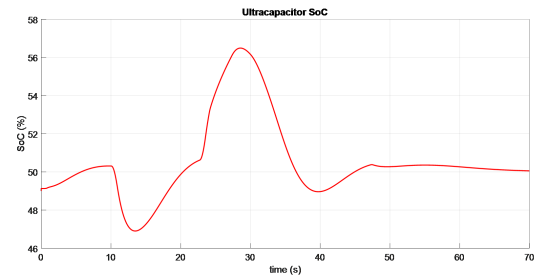
D.5.2. Degraded modes

D.5.2.1. Only battery

In the *only battery* degraded mode the maximal DC side power is limited to 0.5 MW.



(a) Battery



(b) UCs

Figure D.27: SoC evolution for for active power external set point - Only batteries

External active power set point when the Soc limit is reached (hysteresis control). Once the operational limit is reached, transient grid forming mode is activated and external active power set point disabled. In this case, a manual reset is required. Furthermore, as the SoC is in its limit value, it should be moved to a value higher / lower than the limit and the external active power set point also have to be corrected by the operator.

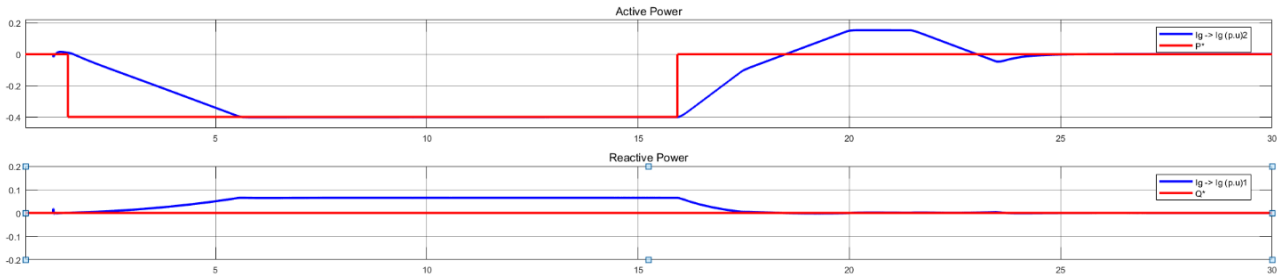


Figure D.28: Injected active and reactive power by AC side converter for active power external set point - Only Battery. Operation SoC limit reached

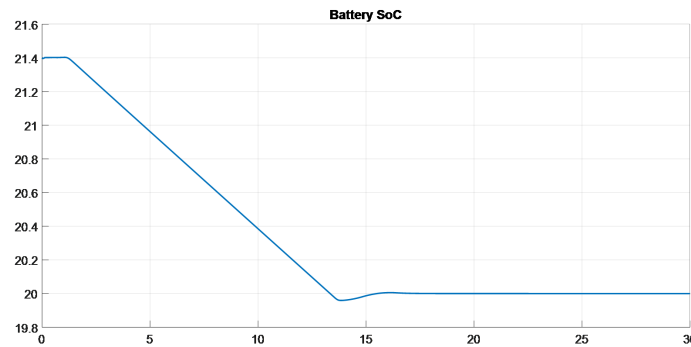


Figure D.29: Battery SoC evolution for active power external set point - Only Battery. Operation SoC limit reached.

External active power set point when the Soc limit is reached (hysteresis control). This case is exactly the same as in the HESS configuration. So, as illustrated in Fig. D.30 similar output power is observed. Figure D.31 shows the control signals during this event and the evolution of the SoC.

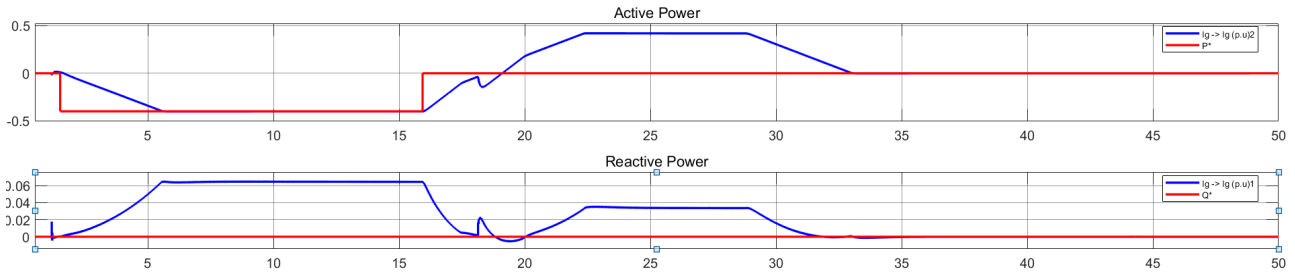
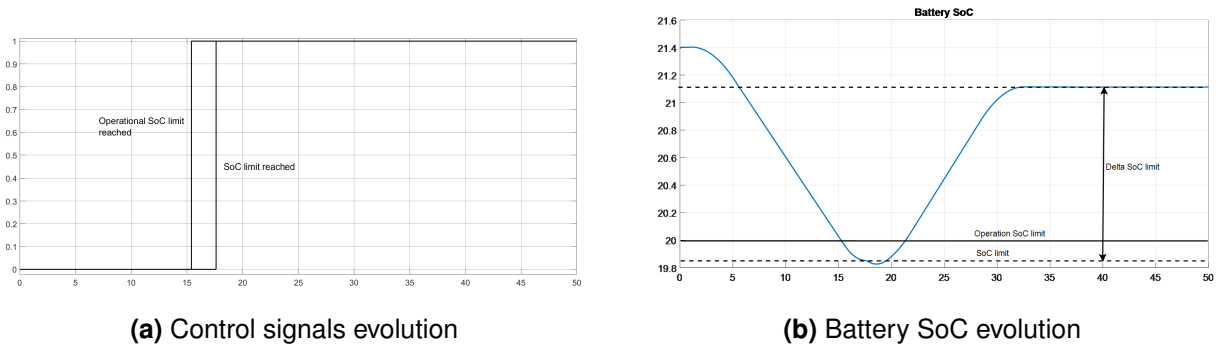


Figure D.30: Injected active and reactive power by AC side converter for active power external set point - Only Battery. Hysteresis SoC control limit reached



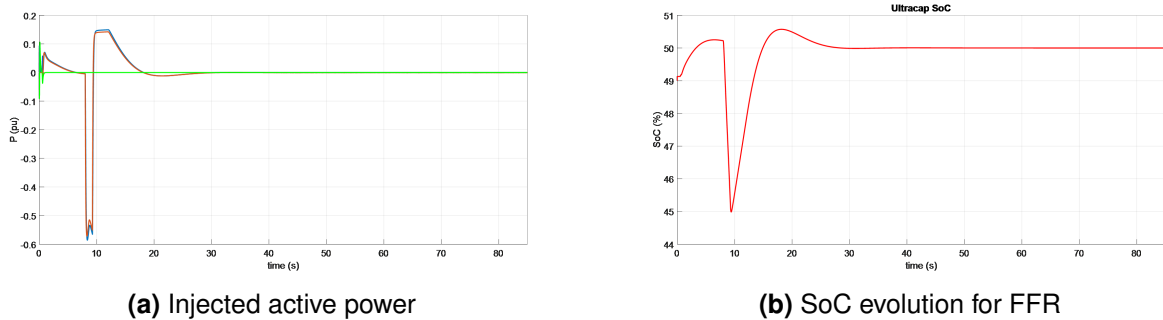
(a) Control signals evolution

(b) Battery SoC evolution

Figure D.31: Hysteresis SoC control limit reached for active power external set point - Only batteries

D.5.2.2. Only UCs

Long-period frequency downfall with transient grid forming. When the only energy storage system available at the DC side are the UCs, only the transient grid forming service can be activated. Other services require more active power consumption, so they are automatically disabled. As shown in Fig. D.32a, the active power injected by the grid forming converter has the same profile as before, but all the energy is now provided by the UCs. In this configuration the UCs are directly charged / discharged from the grid such that the output of the SoC regulation is directed to the grid forming converter (see Fig. D.32b).



(a) Injected active power

(b) SoC evolution for FFR

Figure D.32: Active power external set point only UCs ESS configuration

E. RTE-Ingeteam Demo: FAT test bench detailed description

E.1. Grid emulator capabilities

E.1.1. Rating

The rated capacity of the grid emulator is a 777 kVA and its output current is limited to 650A. Exceeding this value, even transiently during a fault test, leads to the grid emulator disconnection. Table E.1 (left) list its technical characteristics.

Base power calculation. When performing reduced power tests, special attention must be given to the impedance equivalency. We consider the values in Tab. E.1 (right):

Rated Power	735 kW	Sb	0.138 MVA
Max Current	650 A	Vb	220 V
Output voltage	690 V	Ib	363 A
DC bus voltage	1100 – 1500 Vdc	Zb	0.35 Ohm
Modulation	PWM 3L 2.1 kHz	Lb	1114 μ H
Cooling	Water	Cb	9094 μ F
Lc	130uH	Lc	70 μ H (6.3%) ¹
Cf	200uF		
Rc	0.1 Ohm		

Table E.1: (left) grid emulator characteristic - (right) Control bases

The virtual grid filter output impedance gives 11.6 %. Hence, the results are representative of the demonstrator connected to a system of SCR ≈ 20 ($\approx 5\%$, as we recall that the low voltage transformer reactance is 6.2%). In accordance with the nominal power reduction, the hardware limits are reduced. The hardware hard blocking current is estimated according to 3 terms:

$$I_{max_Hw} = I_{nom} + IZ_{virt} + I_{ripple}$$

While the rated current is reduced 40% the hardware hard blocking current is not reduced in the same percentile:

$$I_{max_Hw} = \frac{I_{nom_ant}}{2} + IZ_{virt} + I_{ripple}$$

E.1.2. User interface.

The interface between the virtual grid generator and the user is performed through a web client that links to the programmable logic controller (PLC). The latter is responsible for collecting and processing the data introduced by the user, and sending the voltage reference to the digital signal processor (DSP), in order to create the grid conditions specified by the user.

¹which is close to the filter impedance in nominal bases (6.41%)

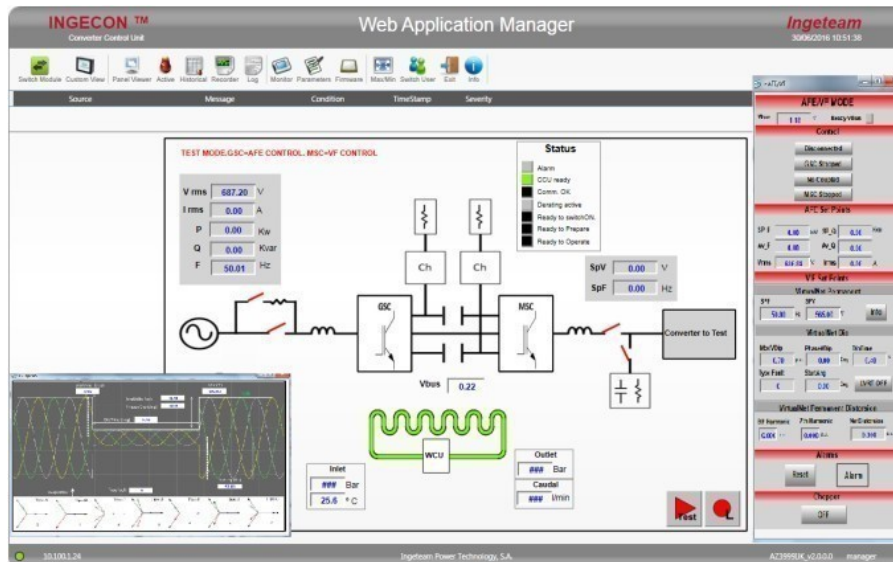


Figure E.1: Overview of the web client to command the grid emulator

E.1.3. Testing capabilities

To test the transient response on the device under test (DUT), the grid emulator converter control is capable of applying the disturbance in the instant of the wave as specified by the user (phase). For example, a one-phase voltage dip can be generated when the sinusoidal voltage is crossing zero or when it is in its maximum value. In addition, it can generate synthetic faults (for example type C) that represent the propagation of specific faults through different kinds of transformer connections. In short, as illustrated in the right-hand side of Fig.E.1, this platform is able to perform:

- Voltage dips with specific start phase-angle and phase-angle jumps.
- Grids with high negative sequence component in steady state.
- Frequency deviations.
- Grids with high harmonic components (5th and 7th).
- Symmetric and asymmetric voltage dips.
- OVRT up to 1.5 per unit.

E.2. Recorded signals

Due to limitations on the size of the register, we have basically two types of files, both of them include dq-axis voltages and currents (I_{sd} , I_{sq} , E_{gd} , E_{gq}) and the voltage references ($E_{gd,ref}$, $E_{gq,ref}$) as well as the internal converter frequency ω_{conv} , the measured positive sequence active and reactive power (denoted here P_{PS}) that is computed internally as the product of the $d-q$ axis voltages and currents after sequence separation is applied. However, we have:

- **Fault type record:** prioritize AC side and TVI signal including 2 phase-to-phase instantaneous voltages and the 3 phase currents, as well as the peak current estimation used for the activation of the TVI. In general we register 1.4 s length signals.
- **Ramp type record:** DC side signals including voltage and power of each DC-DC converter are included, but three-phase measurements were dropped to get a 2.6 s length signals.

E.3. Calculated signals

Some signals associated to the internal control variables are proprietary, hence the use of recalculated time-series from the terminal three-phase voltages and currents when available is preferred. The active and reactive, as well as positive and negative sequence components are computed according to [121] and [122]. In addition:

Instantaneous power. It is calculated as the sum of the power in each phase, knowing that the 3 currents are directly available but the phase-to-ground voltages have to be recalculated from the two measurements V_{grs} and V_{gst} as follows. By definition (experimental setting of the data acquisition system):

$$\begin{aligned} V_{grs} &= V_{gsn} - V_{grn} \\ V_{gst} &= V_{gtn} - V_{gsn}. \end{aligned} \quad (\text{E.1})$$

Then:

$$\begin{aligned} V_{grs} - V_{gst} &= 2V_{gsn} - V_{grn} - V_{gtn} \\ V_{gsn} &= \frac{V_{grs} - V_{gst}}{3}. \end{aligned} \quad (\text{E.2})$$

So:

$$\begin{aligned} V_{grn} &= -V_{grs} + V_{gsn}, \\ V_{gtn} &= V_{gst} + V_{gsn}. \end{aligned} \quad (\text{E.3})$$

And finally, the instantaneous power can be calculated by: $P_{inst} = V_{grn}I_{gr} + V_{gsn}I_{gs} + V_{gtn}I_{gt}$.

When available (fault type registers), it will always be shown in continuous line, while P_{PS} will be overlapped in dashed line. Ramp type register will only show P_{PS} .

AC voltage. For the moment we show the AC voltage amplitude computed as $E_g = \sqrt{E_{gd}^2 + E_{gq}^2}$ based on the internal dq -axis signals. The AC voltage references will be computed analogously.

AC current. The same principle is applied to the current. For the Ramp type registers, we have I_s and I_g but for the Fault type registers we only have I_s which will be more noisy.

E.4. Initial test matrices

E.4.1. Control settings

Default parameters are $\omega_c = 25$ rad/s and $m_p = 0.01$ p.u. for $H_e = 2$ s. H_e equal to 5 s can be obtained for $\omega_c = 20$ rad/s and $m_p = 0.005$ p.u. The steady state power is defined through P_{set} , which is set to zero to focus on the transient response. Nonetheless, an offset in the active power is observed in some tests due to the activation of the battery SoC control.

E.4.2. Scenarios

Table E.2 lists the study scenarios.

Table E.2: Scenarios

ID	Vc [V]	P [kW]	Q [kVar]	fc [Hz]	Vg [V]	fg [Hz]	Xcc [Ω]	Par
A	Nom	0	0	50	Nom	50	SCR max	default
B	Nom	Max	0	50	Nom	50	SCR max	default
C	Nom	Min	0	50	Nom	50	SCR max	default
D	Nom	0	Max	50	Nom	50	SCR min	default
E	Nom	0	Min	50	Nom	50	SCR min	default
F	Nom	0	0	50	Nom	50	SCR max	nq min
F (bis)	Nom	0	0	50	Nom	50	SCR max	nq max
G	Nom	0	0	50	Nom	50	SCR max	mp min
G (bis)	Nom	0	0	50	Nom	50	SCR max	mp max
H	Nom	0	0	50	Nom	50	SCR max	Tf min
H (bis)	Nom	0	0	50	Nom	50	SCR max	Tf max
J	Nom	0	0	50	Nom	50	SCR max	Battery only
K	Nom	0	0	50	Nom	50	SCR max	UC only

E.4.3. Events

Tables E.3, E.5 and E.6 list the study events.

Table E.3: Reference Tracking

Test ID	Description	Comments
1	$\Delta SpV = 0.05$ pu $Ramp = 1-2$ pu	Step amplitude depends on droop characteristic and system impedance
	Scenarios	A, E, F (bis)
	Expected results	Ramp tracking, max overshoot. If $SpV \approx Vg$, then $Qg = \frac{\Delta SpV - Qg \cdot nq}{X_{sys}}$
2	$\Delta SpV = -0.05$ pu $Ramp = 1-2$ pu	Step amplitude depends on droop characteristic and system impedance
	Scenarios	A, D, F
	Expected results	Ramp tracking, max overshoot. If $SpV \approx Vg$, then $Qg = \frac{\Delta SpV - Qg \cdot nq}{X_{sys}}$
3	$\Delta Spf = 0.01$ pu $Ramp = 0.02$ pu/s	Step amplitude depends on droop characteristic ($mp > 0.01$) Dynamic depends on LPF and ramp (inertia constant)
	Scenarios	A, C, G (bis)
	Expected results	If $SpF \approx Fg$: inertia response and stabilisation at $Pg = [(\Delta Spf/mp) - Ploss]$
4	$\Delta Spf = -0.01$ pu $Ramp = 0.02$ pu/s	Step amplitude depends on droop characteristic ($mp > 0.01$) Dynamic depends on LPF and ramp (inertia constant)
	Scenarios	A, B, G
	Expected results	If $SpF \approx Fg$: inertia response and stabilisation at $Pg = [(\Delta Spf/mp) - Ploss]$
5	$\Delta SpP = 0.5$ pu $Ramp = 2$ pu/s	Step amplitude depends on droop characteristic ($mp > 0.01$) Dynamic depends on $Ramp$, mp and LPF. Accuracy depends on losses and $Sp\omega \approx \omega_g$. Two measurements are needed to define accuracy
	Scenarios	A, H (bis)
	Expected results	settling time below 500ms
6	$\Delta SpP = -0.5$ pu $Ramp = 2$ pu/s	Step amplitude depends on droop characteristic ($mp > 0.01$) Dynamic depends on $Ramp$, mp and LPF. Accuracy depends on losses and $Sp\omega \approx \omega_g$. Two measurements are needed to define accuracy.
	Scenarios	A, H
	Expected results	settling time below 500ms
7	$\Delta SpQ = 0.5$ pu $Ramp = 1-2$ pu/s	Step amplitude depends on droop characteristic ($mp > 0.01$) Dynamic depends on $Ramp$, nq and $Tfnq$
	Scenarios	A, H (bis)
	Expected results	Steady State: $Qg = \frac{\Delta SpQ \cdot nq - Qg \cdot nq}{X_{sys}}$ Dynamics: no overshoot with low $Tfnq$ and settling time below 750ms
8	$\Delta SpQ = -0.5$ pu $Ramp = 1-2$ pu/s	Step amplitude depends on droop characteristic ($mp > 0.01$) Dynamic depends on $Ramp$, nq and $Tfnq$
	Scenarios	A
	Expected results	Steady State: $Qg = \frac{\Delta SpQ \cdot nq - Qg \cdot nq}{X_{sys}}$ Dynamics: no overshoot with low $Tfnq$ and settling time below 750ms

Table E.4: Grid disturbances

Test ID	Description	Comments
9	$\Delta V_g = 0.05$ pu $Ramp = 1-2$ pu	Step amplitude depends on droop characteristic and system impedance Ramp variation is preferred, step variations can be tested with faults
	Scenarios	A
	Expected results	Ramp tracking, max overshoot. $Q_g = \frac{\Delta V_g + Q_g \cdot nq}{X_{sys}}$
10	$\Delta V_g = -0.05$ pu $Ramp = 1-2$ pu	Step amplitude depends on droop characteristic and system impedance Ramp variation is preferred, step variations can be tested with faults
	Scenarios	A
	Expected results	Ramp tracking, max overshoot. $Q_g = \frac{\Delta V_g + Q_g \cdot nq}{X_{sys}}$
11	$\Delta f_g = 0.02$ pu $Ramp = 0.02$ pu/s	Step amplitude depends on droop characteristic ($mp > 0.02$) Dynamic depends on LPF and ramp (inertia constant)
	Scenarios	A
	Expected results	If $SpF \approx F_g$: Inertia response and stabilisation at $P_g = [(\Delta f_g / mp) - P_{loss}]$
12	$\Delta f_g = -0.02$ pu $Ramp = 0.02$ pu/s	Step amplitude depends on droop characteristic ($mp > 0.02$) Dynamic depends on LPF and ramp (inertia constant)
	Scenarios	A, B
	Expected results	If $SpF \approx F_g$: Inertia response and stabilisation at $P_g = [(\Delta f_g / mp) - P_{loss}]$
13	Symmetric fault $V_g=0.5$ $t=250$ ms	
	Scenarios	A, K
	Expected results	TVI correct activation, recovery time less than 250ms
14	Symmetric fault $V_g=0.1$ $t=250$ ms	
	Scenarios	A
	Expected results	TVI correct activation, recovery time less than 250ms
15	Asymmetric fault $V_g=0.5$ $t=250$ ms	
	Scenarios	A, K
	Expected results	TVI correct activation, recovery time less than 250ms
16	Asymmetric fault $V_g=0.1$ $t=250$ ms	
	Scenarios	A
	Expected results	TVI correct activation, recovery time less than 250ms
17	10 degrees phase jump	Initial current depends on phase jump (deg) and system impedance
	Scenarios	A, B, K
	Expected results	Not trip, inject active power smoothing frequency.
18	-10 degrees phase jump	Initial current depends on phase jump (deg) and system impedance
	Scenarios	A, C
	Expected results	Not trip, inject active power smoothing frequency

Table E.5: Grid distortion

Test ID	Description	Comments
19	10% unbalance voltage	Unbalance filtering may depend on Droop LPF
	Scenarios	A
	Expected results	Measured unbalance at converter terminals less than 2-3% (before power filter). Positive sequence voltage at converter terminals
20	5th harmonic	sensitivity evaluation
	Scenarios	A
	Expected results	Voltage source behaviour: absorb some current, do not amplify harmonics
21	7th harmonic	sensitivity evaluation
	Scenarios	A
	Expected results	Voltage source behaviour: absorb some current, do not amplify harmonics
22	5th, 7th harmonic	sensitivity evaluation
	Scenarios	A, K
	Expected results	Voltage source behaviour: absorb some current, do not amplify harmonics

Table E.6: DC side

Test ID	Description	Comments
23	$\Delta fg = 0.01$ pu $Ramp = 0.01$ pu/s	Step amplitude depends on droop characteristic ($mp > 0.01$) similar as event 12 but different measurements
	Scenarios	A, J, K
	Expected results	Correct load sharing between battery and UC, and SoC recovery
24	$\Delta SpP = 0.5$ pu $Ramp = 2$ pu/s	Same as event 5 but different measurements
	Scenarios	A, J, K
	Expected results	Correct load sharing between battery and UC, and SoC recovery
25	Symmetric fault $Vg=0.5$ $t=250$ ms	Same as event 13 but different measurements
	Scenarios	A, J, K
	Expected results	Correct load sharing between battery and UC, and SoC recovery

F. RTE-Ingteam Demo: model validation from FAT records

Model validation is a key step in order to use a model with confidence in any simulation analysis. The validation of the present model is intended to ensure that for each event, especially during severe transient disturbances, the response generated by the model matches as much as possible with the real equipment (FAT results presented in Chapter 4).

F.1. Model approximations with respect to the real equipment

Through the validation process the following modelling hypothesis must be kept in mind:

- Setpoint delay is not well modelled.
- It was not possible to set identical proportional gains for the inner control loops and the simulation model. The latter were set lower values as the simulation model is less damped than the real system and stability limits were tighter. Higher gains lead to instability in the simulation while the real equipment remained stable.

F.2. Validation method

To estimate the model accuracy, in this work we use the well-known German FGW TR4 code, which has been incorporated in simulations tools as DlgSILENT since 2016 [123]. The selected validation and certification approach is based on FRT-measurements at individual turbines, referred to as power generation units (PGUs). It compares the three-phase instantaneous measurements with the EMT model that provides equivalent quantities. Fault ride through transients are divided in three periods:

- **Period 1:** before the fault. A pre-fault measurement of the real equipment and simulation model to show that both are operating at the same stationary conditions.
- **Period 2:** from the beginning of the voltage dip to the voltage recovery.
- **Period 3:** From voltage recovery to the new stationary. The measurement and simulation should not end before all transients of active and reactive power have ended.

The average error values indicate how close the model matches real measurements. In addition to the average error, the TR4 FGW standard defines three different types of errors between two signals defined by the following equations:

- **Average Error**, representing the average error between all the analysed points.

$$X_{ME} = \frac{\sum_{i=K_{begin}}^{i=K_{end}} (K_{simulation.i} - K_{measure.i})}{K_{end} - K_{begin}} \quad (F.1)$$

- **Mean Absolute Error**, representing the mean of the absolute errors between all the analysed points.

$$X_{MAE} = \frac{\sum_{i=K_{begin}}^{i=K_{end}} |K_{simulation.i} - K_{measure.i}|}{K_{end} - K_{begin}} \quad (F.2)$$

- **Maximum Error**, representing the maximum deviation detected between all the analysed points.

$$X_{MXE} = \max_{i=K_{begin} \dots K_{end}} |K_{simulation.i} - K_{measure.i}| \quad (F.3)$$

Maximum error values for each type of error and period is clearly defined in the standard. The maximum values allowed are different for the defined two PGU types.

- Type 1 PGU: PGU, which contains for generating electrical energy only a direct grid-connected (only via generator transformer) synchronous generator.
- Type 2 PGU: PGU, which does not meet the conditions for Type 1.

F.3. Results

Periods 1 and 3 have been adjusted to measurements limits. Thus, results are not exactly the same as the specified on TR4 FGW standard. But the new periods have been selected to take into account the points with the maximum error.

Positive sequence error values of active power, reactive power, active current and reactive current are analysed in the present section for each simulated test case. Zero sequence components have been neglected due to transformer connection (Δ -Y). For most of the tests (balanced voltage events), negative sequence components have also been neglected. However, for unbalanced faults (type C fault), negative sequence components are estimated.

In addition to the standard standard criteria, visual inspection of the overlap of certain control signals will be analysed in order to provide a deeper understanding of mismatches between the simulation results and the measurements. In that case, modelling hypotheses listed in section F.1 must be kept in mind, in addition to the following points :

- Registered data is curtailed at the third decimal number.
- The faults generated in the test bench have some other harmonic components. At some faults high even order harmonics are detected. This harmonics are not present at simulation model. This may results on deviations.

F.3.1. Type A fault, 700ms 50%

From measured three phase currents (IRST) and two-phase line-line voltages (with Δ -Y transformer, VRST) obtained during FATs, we estimate positive sequence active and reactive current and power. Following the same procedure, the same components are estimated in the simulation scenario. Figure F.1 show the results obtained from the measurement and the simulation of a Type A fault (50%, 700ms). The error values according to FGW TR4 are summarised in Tab. F.2 and F.3.

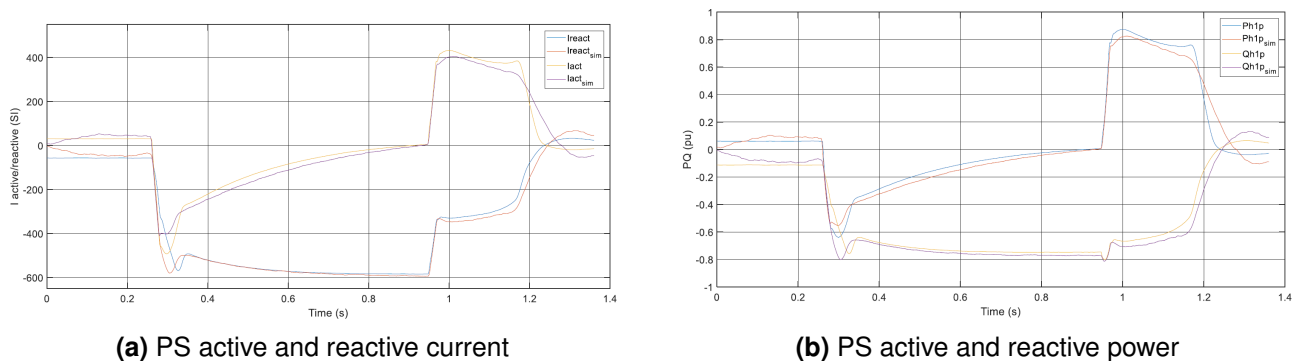


Figure F.1: Estimated quantities from measured three phase currents (IRST) and two-phase line-line voltage (VRST) for Type A fault (50%, 700ms).

Type 1 PGU		Positive sequence											
		P			Q			Ireact			Iactive		
		MXE	ME	MAE	MXE	ME	MAE	MXE	ME	MAE	MXE	ME	MAE
Pre	Max	0.15	±0.1	0.12	0.15	±0.1	0.12	0.15	±0.1	0.12	0.15	±0.1	0.12
	Meas	0.04	0.02	0.02	0.04	0.02	0.02	0.046	0.028	0.028	0.04	0.025	0.026
Fault	Max	0.5	±0.13	0.3	0.55	±0.28	0.38	0.7	±0.3	0.63	0.51	±0.29	0.35
	Meas	0.08	0.02	0.03	0.22	0.02	0.03	0.29	0.017	0.024	0.179	0.026	0.045
Post	Max	0.5	±0.15	0.17	0.79	±0.15	0.22	0.53	±0.15	0.17	0.76	±0.17	0.22
	Meas	0.13	0.11	0.11	0.1	0.09	0.09	0.088	0.059	0.06	0.11	0.15	0.15

Figure F.2: Maximum and measured positive sequence error values at a Type A fault (50%, 700ms) for each period according to TR4 FGW standard, limits for Type 1 PGU

Type 2 PGU		Positive sequence											
		P			Q			Ireact			Iactive		
		MXE	ME	MAE	MXE	ME	MAE	MXE	ME	MAE	MXE	ME	MAE
Pre	Max	0.15	±0.1	0.12	0.15	±0.1	0.12	0.15	±0.12	0.12	0.15	±0.1	0.12
	Meas	0.04	0.02	0.02	0.04	0.02	0.02	0.046	0.028	0.028	0.04	0.025	0.026
Fault	Max	0.17	±0.15	0.17	0.17	±0.15	0.17	0.5	±0.4	0.63	0.17	±0.15	0.17
	Meas	0.08	0.02	0.03	0.22	0.02	0.03	0.29	0.017	0.024	0.179	0.026	0.045
Post	Max	0.17	±0.15	0.17	0.17	±0.15	0.17	0.17	±0.17	0.17	0.17	±0.15	0.27
	Meas	0.13	0.11	0.11	0.1	0.09	0.09	0.088	0.059	0.06	0.11	0.15	0.15

Figure F.3: Maximum and measured positive sequence error values at a Type A fault (50%, 700ms) for each period according to TR4 FGW standard, limits for Type 2 PGU

In main lines, the estimated errors are below the TR4 FGW standard errors, nevertheless, the maximum error at the beginning in the fault is slightly higher than the standard for type 2 PGUs (see Fig. F.4).

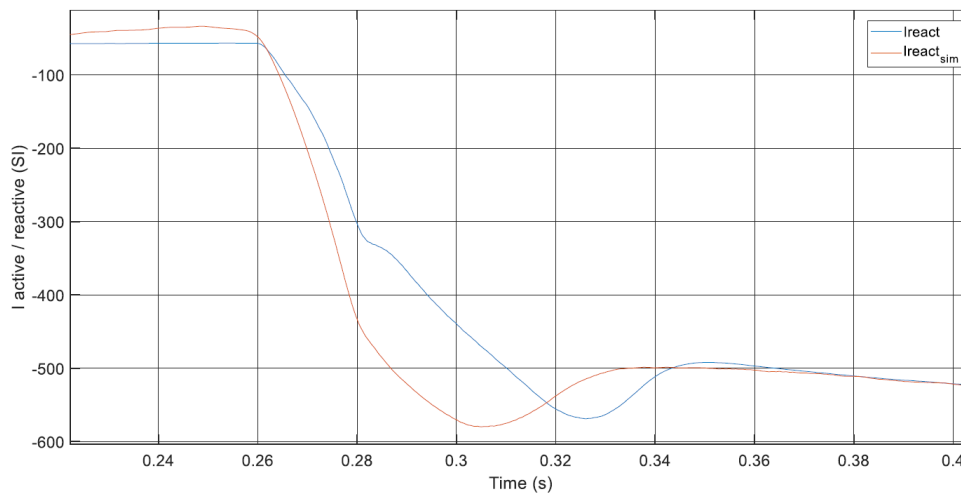
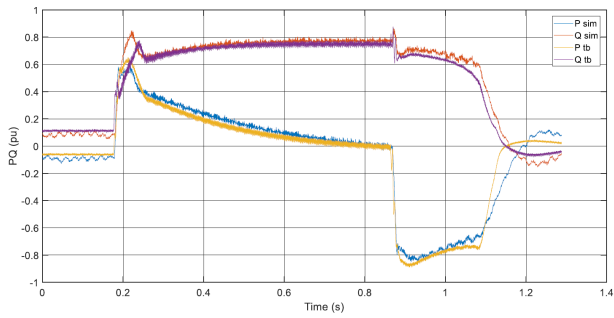
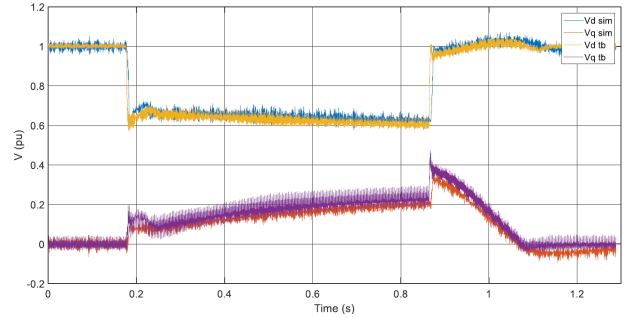


Figure F.4: Estimated reactive Power for Type A fault (50%, 700ms) simulation and measurements. Focus on the beginning of the fault

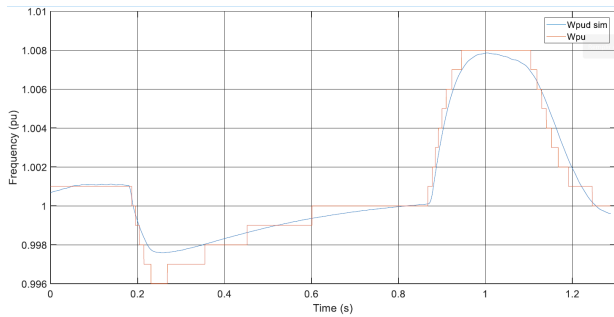
Regarding the comparison by overlapping the control signals of both systems, simulation and real equipment. Several internal key variables for the Type A fault (50%, 700ms) are shown in Fig. F.5



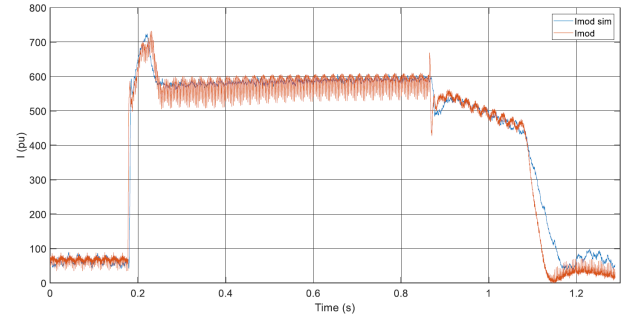
(a) PS active power



(b) Direct and quadrature axes voltages



(c) Grid forming internal frequency

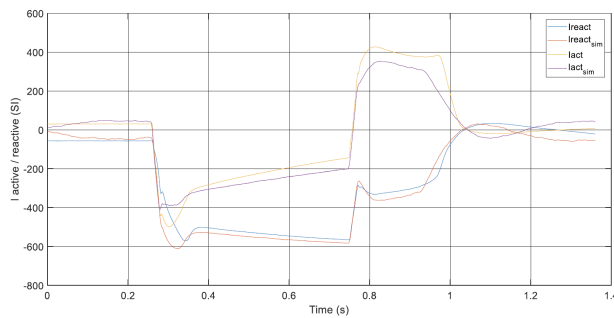


(d) Output current module

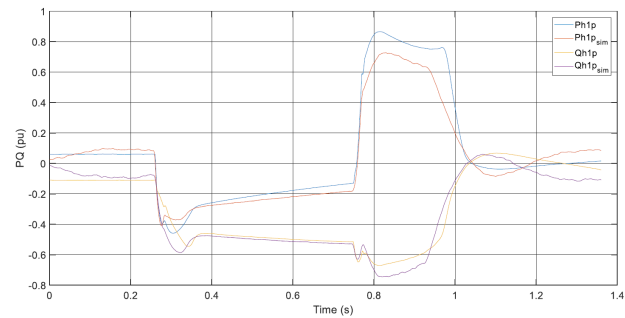
Figure F.5: Registered values at the CCU (converter control unit) and simulated internal control values for a Type A fault (50%, 700ms).

F.3.2. Type A fault, 500ms 70%

Following the same procedure of the previous section, from measured currents (IRST) and voltages at FATs, positive active and reactive current and power are estimated. For the Type A fault (70%, 500ms), overlapped simulation and real measurements are shown in Fig. F.6 and the error values according to FGW TR4 are summarised in Tab. F.7 and F.8.



(a) PS active and reactive current



(b) PS active and reactive power

Figure F.6: Estimated quantities from measured three phase currents (IRST) and two-phase line-line voltage (VRST) for Type A fault (70%, 500ms).

In this case the maximum error at the beginning in the fault is slightly higher than the standard for type 2 PGUs (Table 1-1). But the biggest source of error is the post fault period. The inertia and TVI have a different behaviour. The envelope of the signals is very similar, but the injected values to the grid have an offset. Also, after the re-synchronization with the grid, the behaviour is different, this case the difference is caused by the inner control loops different “Kp” value.

Type 1 PGU		Positive sequence											
		P			Q			Ireact			Iactive		
		MXE	ME	MAE	MXE	ME	MAE	MXE	ME	MAE	MXE	ME	MAE
Pre	Max	0.15	±0.1	0.12	0.15	±0.1	0.12	0.15	±0.1	0.12	0.15	±0.1	0.12
	Meas	0.05	0.02	0.02	0.04	0.02	0.02	0.04	0.02	0.02	0.05	0.02	0.02
Fault	Max	0.5	±0.13	0.3	0.55	±0.28	0.38	0.7	±0.3	0.63	0.51	±0.29	0.35
	Meas	0.09	0.01	0.03	0.18	0.02	0.03	0.37	0.06	0.07	0.21	0.04	0.08
Post	Max	0.5	±0.15	0.17	0.79	±0.15	0.22	0.53	±0.15	0.17	0.76	±0.17	0.22
	Meas	0.38	0.13	0.13	0.16	0.01	0.05	0.16	0.04	0.09	0.38	0.2	0.2

Figure F.7: Maximum and measured positive sequence error values at a Type A fault (70%, 500ms) for each period according to TR4 FGW standard, limits for Type 1 PGU

Type 2 PGU		Positive sequence											
		P			Q			Ireact			Iactive		
		MXE	ME	MAE	MXE	ME	MAE	MXE	ME	MAE	MXE	ME	MAE
Pre	Max	0.15	±0.1	0.12	0.15	±0.1	0.12	0.15	±0.12	0.12	0.15	±0.1	0.12
	Meas	0.05	0.02	0.02	0.04	0.02	0.02	0.04	0.02	0.02	0.05	0.02	0.02
Fault	Max	0.17	±0.15	0.17	0.17	±0.15	0.17	0.5	±0.4	0.63	0.17	±0.15	0.17
	Meas	0.09	0.01	0.03	0.18	0.02	0.03	0.37	0.06	0.07	0.21	0.04	0.08
Post	Max	0.17	±0.15	0.17	0.17	±0.15	0.17	0.17	±0.17	0.17	0.17	±0.15	0.27
	Meas	0.38	0.13	0.13	0.16	0.01	0.05	0.16	0.04	0.09	0.38	0.2	0.2

Figure F.8: Maximum and measured positive sequence error values at a Type A fault (70%, 500ms) for each period according to TR4 FGW standard, limits for Type 2 PGU

Regarding the comparison by overlapping the control signals of both systems, simulation and real equipment. Several internal key variables for the Type A fault (70%, 500ms) are shown in Fig. F.9

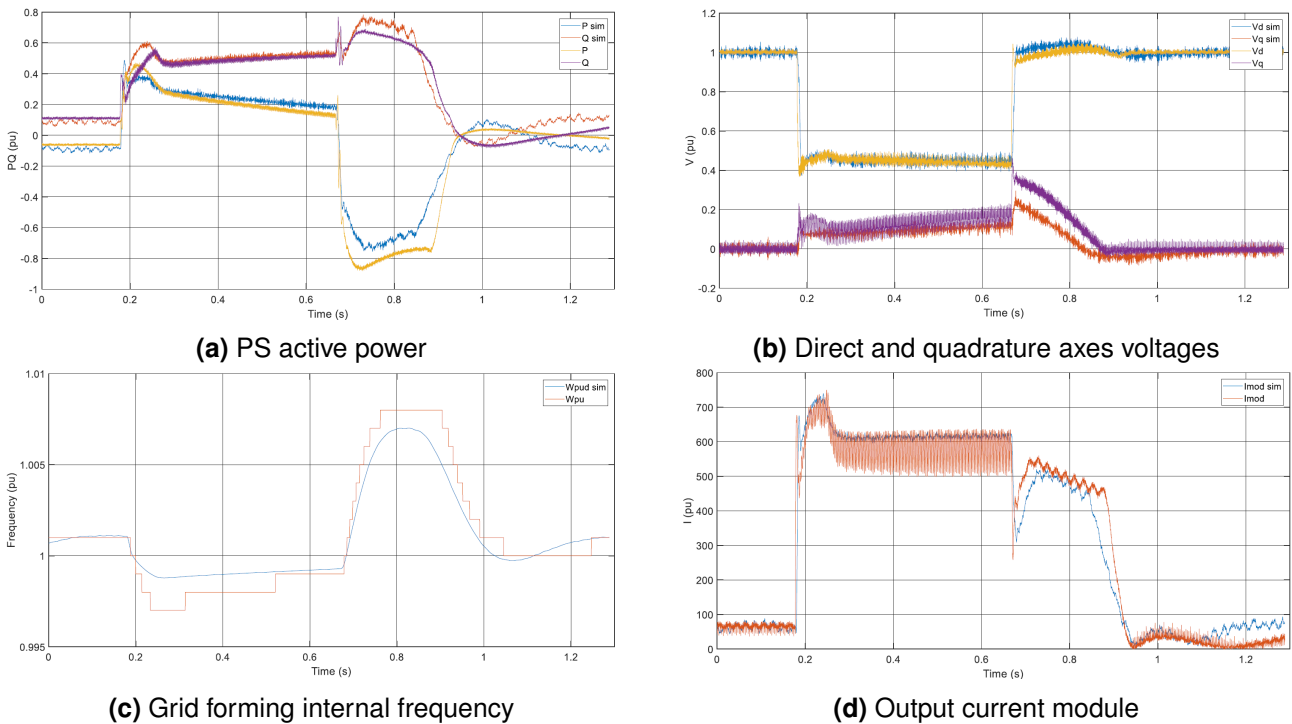


Figure F.9: Registered values at the CCU (converter control unit) and simulated internal control values for a Type A fault (70%, 500ms).

F.3.3. Type C fault, 400ms 50%

In this section an asymmetric fault is evaluated. Following the same procedure of the previous section, from measured currents (IRST) and voltages at FATs, positive and negative active and reactive current / Power are estimated. For the Type C fault (50%, 400ms), overlapped simulation and real measurements are shown in Figure Fig. F.10 (positive sequence) and in Figure Fig. F.13 (negative sequence). Error values according to FGW TR4 are summarised for positive sequence in Tab. F.11 and F.12. and for negative sequence in Tab. F.14 and F.15.

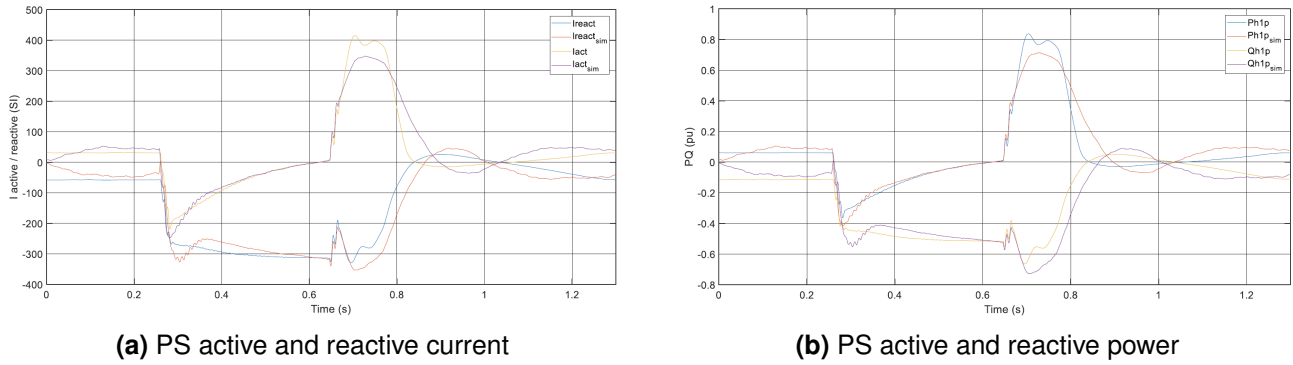


Figure F.10: Estimated PS quantities from measured three phase currents (IRST) and two-phase line-line voltage (VRST) for Type C fault (50%, 400ms).

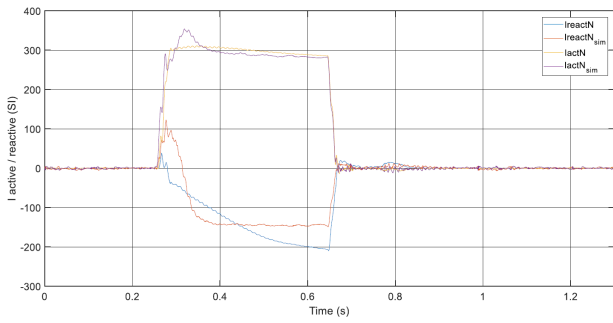
Type 1 PGU		Positive sequence											
		P			Q			Ireact			Iactive		
		MXE	ME	MAE	MXE	ME	MAE	MXE	ME	MAE	MXE	ME	MAE
Pre	Max	0.15	±0.1	0.12	0.15	±0.1	0.12	0.15	±0.1	0.12	0.15	±0.1	0.12
	Meas	0.03	0.04	0.04	0.04	0.02	0.02	0.04	0.02	0.02	0.03	0.03	0.03
Fault	Max	0.5	±0.13	0.3	0.55	±0.28	0.38	0.7	±0.3	0.63	0.51	±0.29	0.35
	Meas	0.14	0.003	0.01	0.27	0.03	0.04	0.31	0.03	0.05	0.14	0.002	0.02
Post	Max	0.5	±0.15	0.17	0.79	±0.15	0.22	0.53	±0.15	0.17	0.76	±0.17	0.22
	Meas	0.31	0.1	0.12	0.27	0.12	0.16	0.25	0.1	0.16	0.31	0.03	0.16

Figure F.11: Maximum and measured positive sequence error values at a Type C fault (50%, 400ms) for each period according to TR4 FGW standard, limits for Type 1 PGU

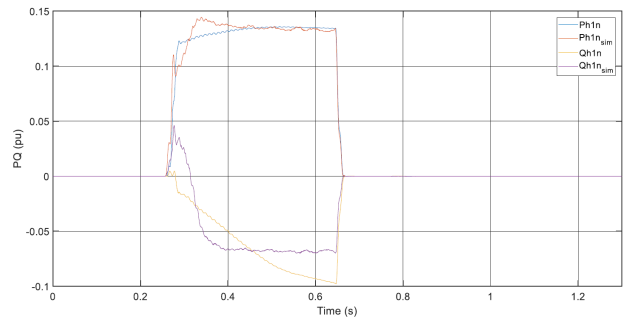
Type 2 PGU		Positive sequence											
		P			Q			Ireact			Iactive		
		MXE	ME	MAE	MXE	ME	MAE	MXE	ME	MAE	MXE	ME	MAE
Pre	Max	0.15	±0.1	0.12	0.15	±0.1	0.12	0.15	±0.12	0.12	0.15	±0.1	0.12
	Meas	0.03	0.04	0.04	0.04	0.02	0.02	0.04	0.02	0.02	0.03	0.03	0.03
Fault	Max	0.17	±0.15	0.17	0.17	±0.15	0.17	0.5	±0.4	0.63	0.17	±0.15	0.17
	Meas	0.14	0.003	0.01	0.27	0.03	0.04	0.31	0.03	0.05	0.14	0.002	0.02
Post	Max	0.17	±0.15	0.17	0.17	±0.15	0.17	0.17	±0.17	0.17	0.17	±0.15	0.27
	Meas	0.31	0.1	0.12	0.27	0.12	0.16	0.25	0.1	0.16	0.31	0.03	0.16

Figure F.12: Maximum and measured positive sequence error values at a Type C fault (50%, 400ms) for each period according to TR4 FGW standard, limits for Type 2 PGU

In this case, the source of the errors and the biggest errors are very similar of the previous case regarding the positive sequence (Type A fault, 70%, 500ms). All the estimated errors in negative sequence are below the TR4 FGW standard. The biggest absolute error is at the beginning of the fault and is caused by a fast oscillation (see Fig. F.16), and even that error is below the limits.



(a) NS active and reactive current



(b) NS active and reactive power

Figure F.13: Estimated NS quantities from measured three phase currents (IRST) and two-phase line-line voltage (VRST) for Type C fault (50%, 400ms).

Type 1 PGU		Negative sequence											
		P			Q			Ireact			Iactive		
		MXE	ME	MAE	MXE	ME	MAE	MXE	ME	MAE	MXE	ME	MAE
Pre	Max	0.15	±0.1	0.12	0.15	±0.1	0.12	0.15	±0.1	0.12	0.15	±0.1	0.12
	Meas	0	0	0	0	0	0	0	0	0	0	0	0.002
Fault	Max	0.5	±0.13	0.3	0.55	±0.28	0.38	0.7	±0.3	0.63	0.51	±0.29	0.35
	Meas	0.03	0	0.005	0.05	0.01	0.01	0.31	0.05	0.08	0.15	0.11	0.026
Post	Max	0.5	±0.15	0.17	0.79	±0.15	0.22	0.53	±0.15	0.17	0.76	±0.17	0.22
	Meas	0.003	0.001	0.001	0.02	0.01	0.01	0.12	0.06	0.07	0.02	0.12	0.018

Figure F.14: Maximum and measured negative sequence error values at a Type C fault (50%, 400ms) for each period according to TR4 FGW standard, limits for Type 1 PGU

Type 2 PGU		Negative sequence											
		P			Q			Ireact			Iactive		
		MXE	ME	MAE	MXE	ME	MAE	MXE	ME	MAE	MXE	ME	MAE
Pre	Max	0.15	±0.1	0.12	0.15	±0.1	0.12	0.15	±0.12	0.12	0.15	±0.1	0.12
	Meas	0	0	0	0	0	0	0	0	0	0	0	0.002
Fault	Max	0.17	±0.15	0.17	0.17	±0.15	0.17	0.5	±0.4	0.63	0.17	±0.15	0.17
	Meas	0.03	0	0.005	0.05	0.01	0.01	0.31	0.05	0.08	0.15	0.11	0.026
Post	Max	0.17	±0.15	0.17	0.17	±0.15	0.17	0.17	±0.17	0.17	0.17	±0.15	0.27
	Meas	0.003	0.001	0.001	0.02	0.01	0.01	0.12	0.06	0.07	0.02	0.12	0.018

Figure F.15: Maximum and measured negative sequence error values at a Type A fault (50%, 400ms) for each period according to TR4 FGW standard, limits for Type 2 PGU

Regarding the comparison by overlapping the control signals of both systems, simulation and real equipment. Several internal key variables for the Type C fault (50%, 400ms) are shown in Fig. F.17:

F.3.4. Type A fault, 300ms 100%

Some problems had arisen during this test, at low power and low voltage, the test bench wasn't capable to generate adequately the 100% voltage dip. Oscillations caused by a resonance also can be identify at the test bench results, In short, this test has several uncertainties. Due to this uncertainties, TR4 FGW maximum error quantities are not estimated, only simulation and test bench results are overlapped Figs. F.18 and F.19.

Regarding the comparison by overlapping the control signals of both systems, simulation and real equipment. Several internal key variables for the Type A fault (100%, 300ms) are shown in Fig. F.20.

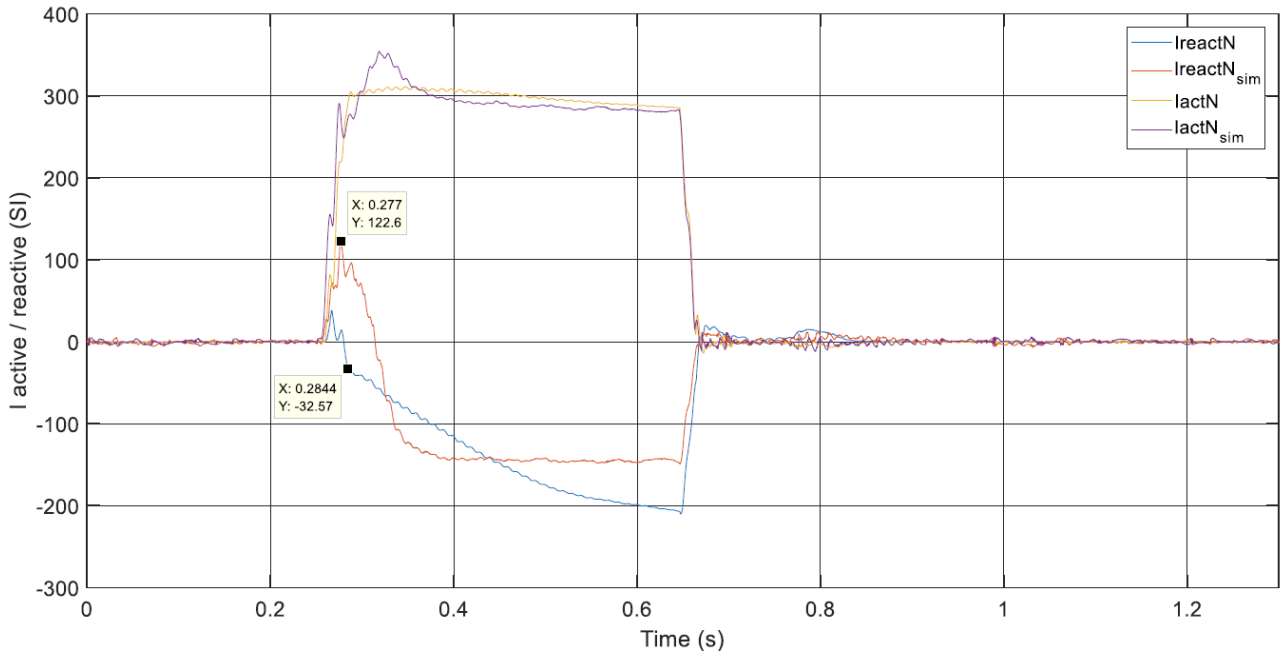
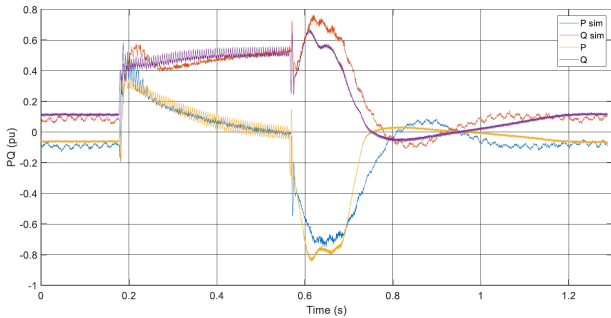
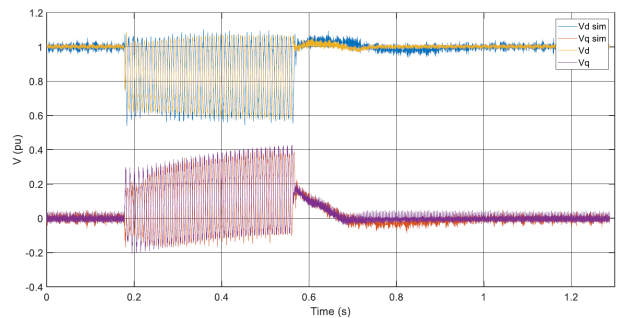


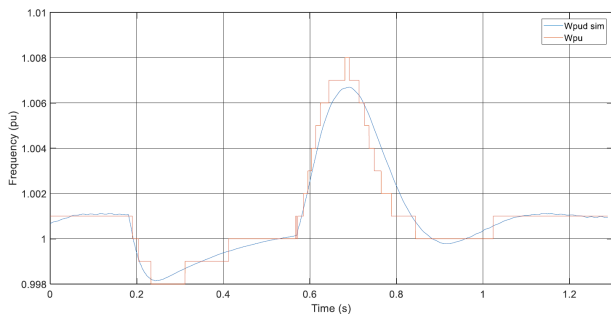
Figure F.16: Focus on the estimated active and reactive current for Type C fault (50%, 400ms) simulation and measurements.



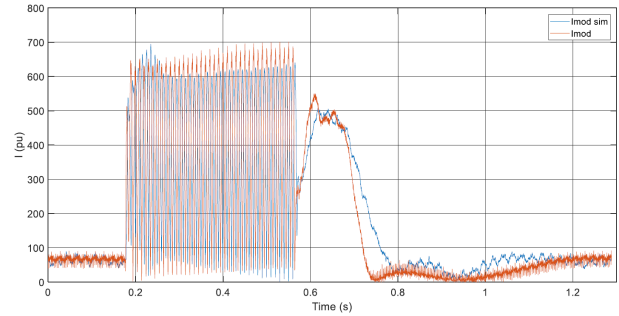
(a) PS active power



(b) Direct and quadrature axes voltages

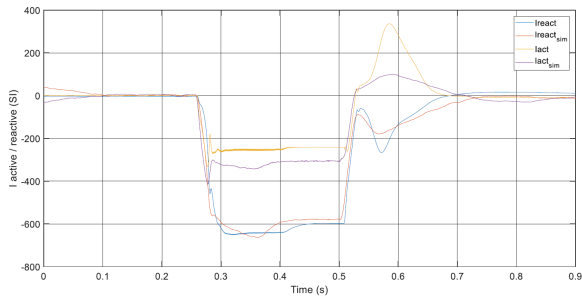


(c) Grid forming internal frequency

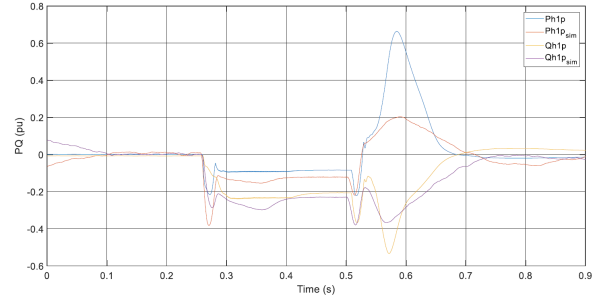


(d) Output current module

Figure F.17: Registered values at the CCU (converter control unit) and simulated internal control values for a Type C fault (50%, 400ms).

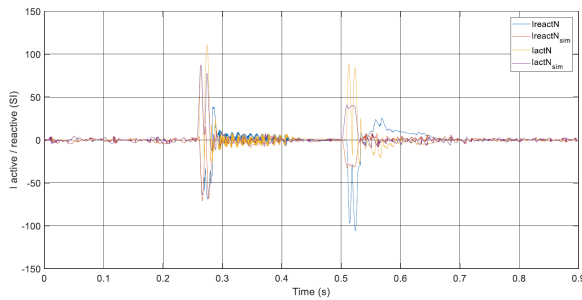


(a) PS active and reactive current

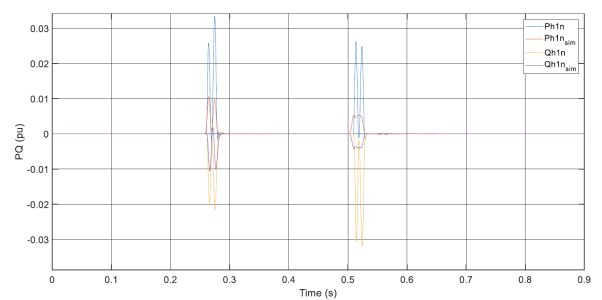


(b) PS active and reactive power

Figure F.18: Estimated PS quantities from measured three phase currents (IRST) and two-phase line-line voltage (VRST) for Type A fault (100%, 300ms).

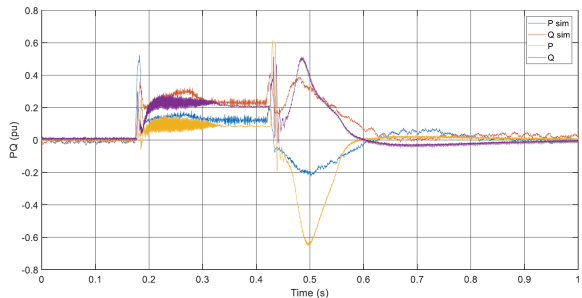


(a) NS active and reactive current

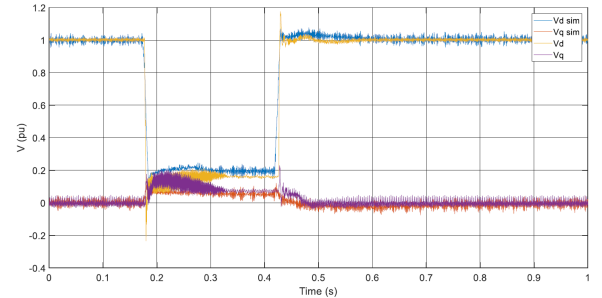


(b) NS active and reactive power

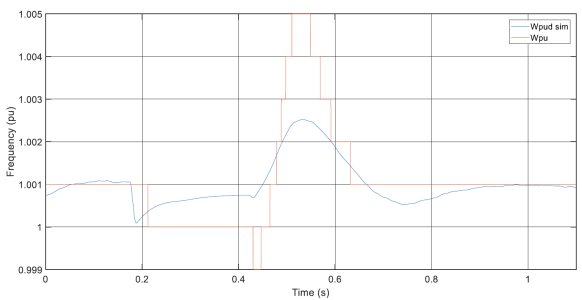
Figure F.19: Estimated NS quantities from measured three phase currents (IRST) and two-phase line-line voltage (VRST) for Type A fault (100%, 300ms).



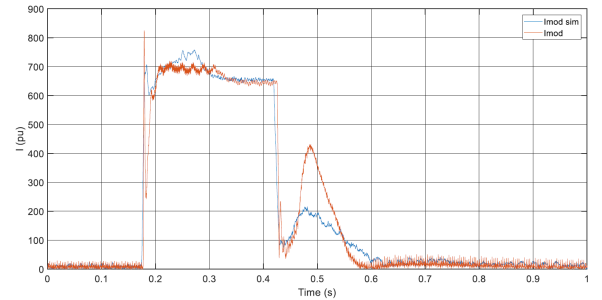
(a) PS active power



(b) Direct and quadrature axes voltages



(c) Grid forming internal frequency



(d) Output current module

Figure F.20: Registered values at the CCU (converter control unit) and simulated internal control values for a Type C fault (100%, 300ms).

F.3.5. Phase-jump 5°

Following the same procedure as for the faults, for the event of a grid voltage phase jump (5°), the TR4 FGW standard is applied. Thus, from measured currents (IRST) and voltages at FATs, positive active and reactive current / Power are estimated. Overlapped simulation and real measurements are shown in Fig. F.21 and the error values according to FGW TR4 are summarised in Tab. F.22 and F.22..

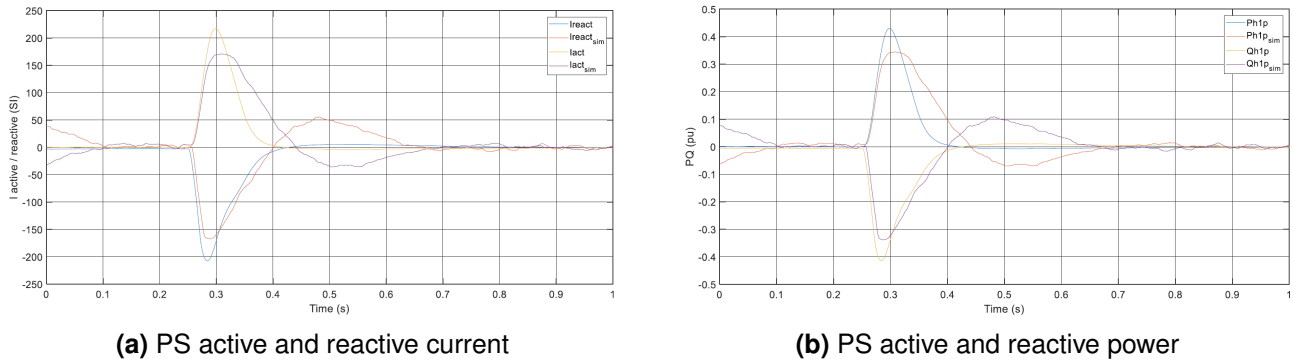


Figure F.21: Estimated quantities from measured three phase currents (IRST) and two-phase line-line voltage (VRST) for Type A fault (50%, 700ms).

Type 1 PGU		Positive sequence											
		P			Q			Ireact			Iactive		
		MXE	ME	MAE	MXE	ME	MAE	MXE	ME	MAE	MXE	ME	MAE
Pre	Max	0.15	±0.1	0.12	0.15	±0.1	0.12	0.15	±0.1	0.12	0.15	±0.1	0.12
	Meas	0.01	0	0	0.01	0	0	0.01	0	0	0.01	0.008	0
Fault	Max	0.5	±0.13	0.3	0.55	±0.28	0.38	0.7	±0.3	0.63	0.51	±0.29	0.35
	Meas	0.14	0.002	0.05	0.1	0.03	0.04	0.1	0.03	0.04	0.14	0.001	0.05
Post	Max	0.5	±0.15	0.17	0.79	±0.15	0.22	0.53	±0.15	0.17	0.76	±0.17	0.22
	Meas	0.06	0.03	0.04	0.1	0.04	0.06	0.1	0.04	0.06	0.06	0.03	0.04

Figure F.22: Maximum and measured positive sequence error values at a phase jump (5°) for each period according to TR4 FGW standard, limits for Type 1 PGU

		P			Q			Ireact			Iactive		
		MXE	ME	MAE	MXE	ME	MAE	MXE	ME	MAE	MXE	ME	MAE
Pre	Max	0.15	±0.1	0.12	0.15	±0.1	0.12	0.15	±0.12	0.12	0.15	±0.1	0.12
	Meas	0.01	0	0	0.01	0	0	0.01	0	0	0.01	0.008	0
Fault	Max	0.17	±0.15	0.17	0.17	±0.15	0.17	0.5	±0.4	0.63	0.17	±0.15	0.17
	Meas	0.14	0.002	0.05	0.1	0.03	0.04	0.1	0.03	0.04	0.14	0.001	0.05
Post	Max	0.17	±0.15	0.17	0.17	±0.15	0.17	0.17	±0.17	0.17	0.17	±0.15	0.27
	Meas	0.06	0.03	0.04	0.1	0.04	0.06	0.1	0.04	0.06	0.06	0.03	0.04

Figure F.23: Maximum and measured positive sequence error values at a phase jump (5°) for each period according to TR4 FGW standard, limits for Type 2 PGU

Even though all the estimated errors are below the standard limits, it is possible to notice some errors. The phase jump (5°) is not very big and the errors are low in absolute value but not that small in relative value.

The current loop Kp at real equipment is at its stability limits and the simulation model is unstable with the same value. It causes errors, especially at fault recovery.

It would be interesting to evaluate why the maximum K_p allowable at the real equipment is greater than the maximum K_p of the simulated equipment. The most probable cause is the filtering of the feedback signals.

Regarding the comparison by overlapping the control signals of both systems, simulation and real equipment. Several internal key variables for the phase-jump (5°) are shown in Fig. F.24

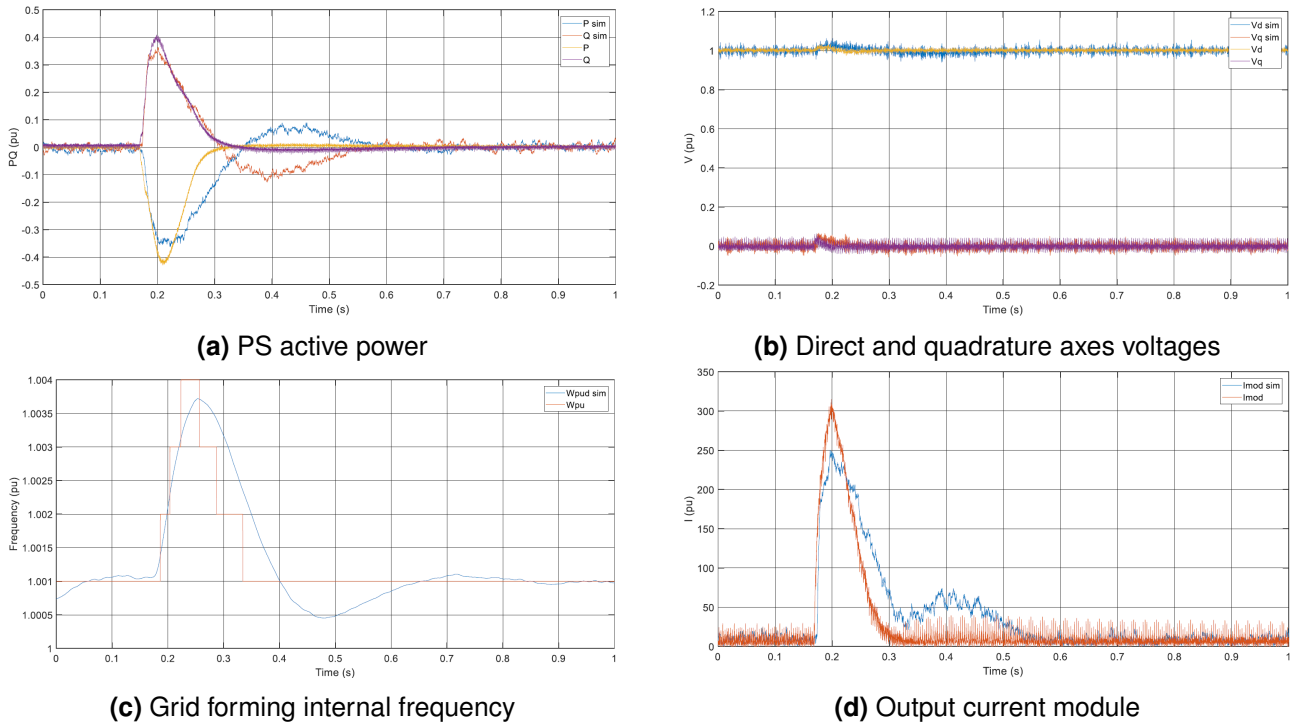


Figure F.24: Registered values at the CCU (converter control unit) and simulated internal control values for for a grid voltage phase-jump (5°).

F.3.6. Voltage step 5%

Besides faults, during FATs other events have also been tested. These events don't have the consideration of severe transient, so, the errors according to the TR4 FGW have not been estimated. Instead of that, a comparison by overlapping signals is performed.

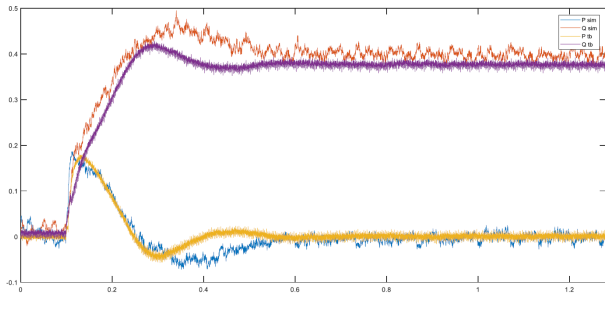
The comparison by overlapping the control signals of both systems, simulation and real equipment, for a 5% grid voltage step is shown in Fig. F.25.

F.3.7. Voltage step 10%

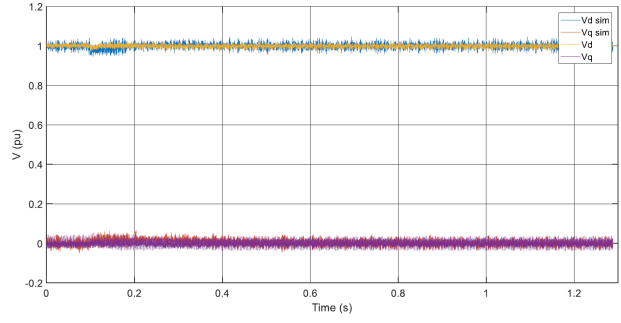
The comparison by overlapping the control signals of both systems, simulation and real equipment, for a 10% grid voltage step is shown in Fig. F.26.

F.3.8. Active power set point

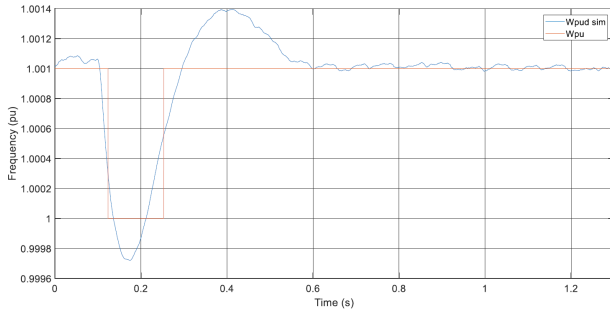
The comparison by overlapping the control signals of both systems, simulation and real equipment, for an active power set point ramp variation is shown in Fig. F.27.



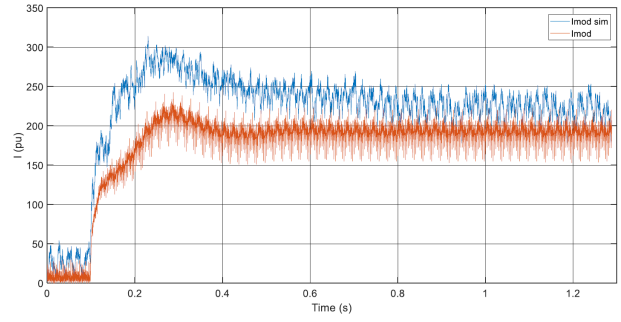
(a) PS active power



(b) Direct and quadrature axes voltages

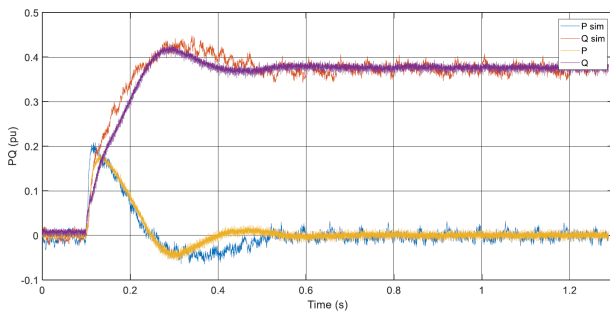


(c) Grid forming internal frequency

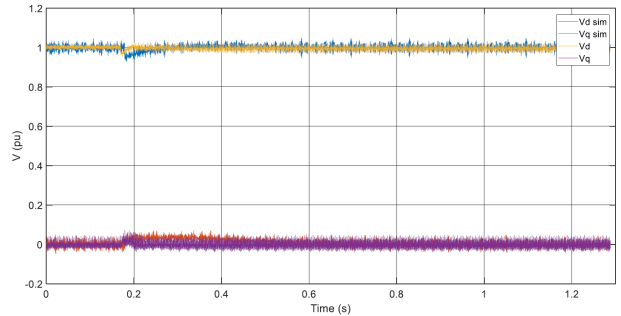


(d) Output current module

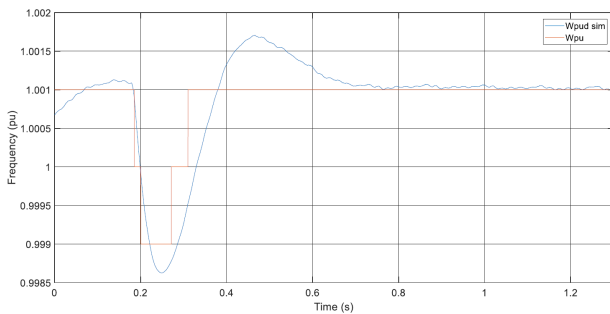
Figure F.25: Registered values at the CCU (converter control unit) and simulated internal control values for a grid voltage step (5%).



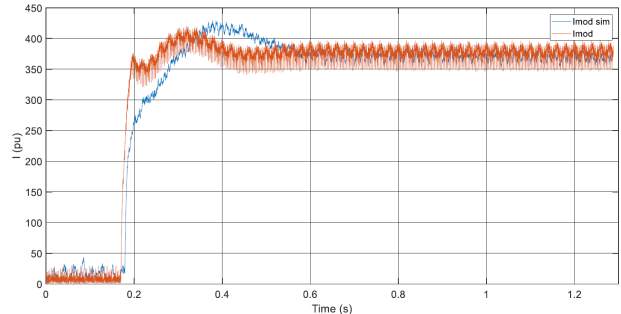
(a) PS active power



(b) Direct and quadrature axes voltages



(c) Grid forming internal frequency



(d) Output current module

Figure F.26: Registered values at the CCU (converter control unit) and simulated internal control values for a grid voltage step (10%).

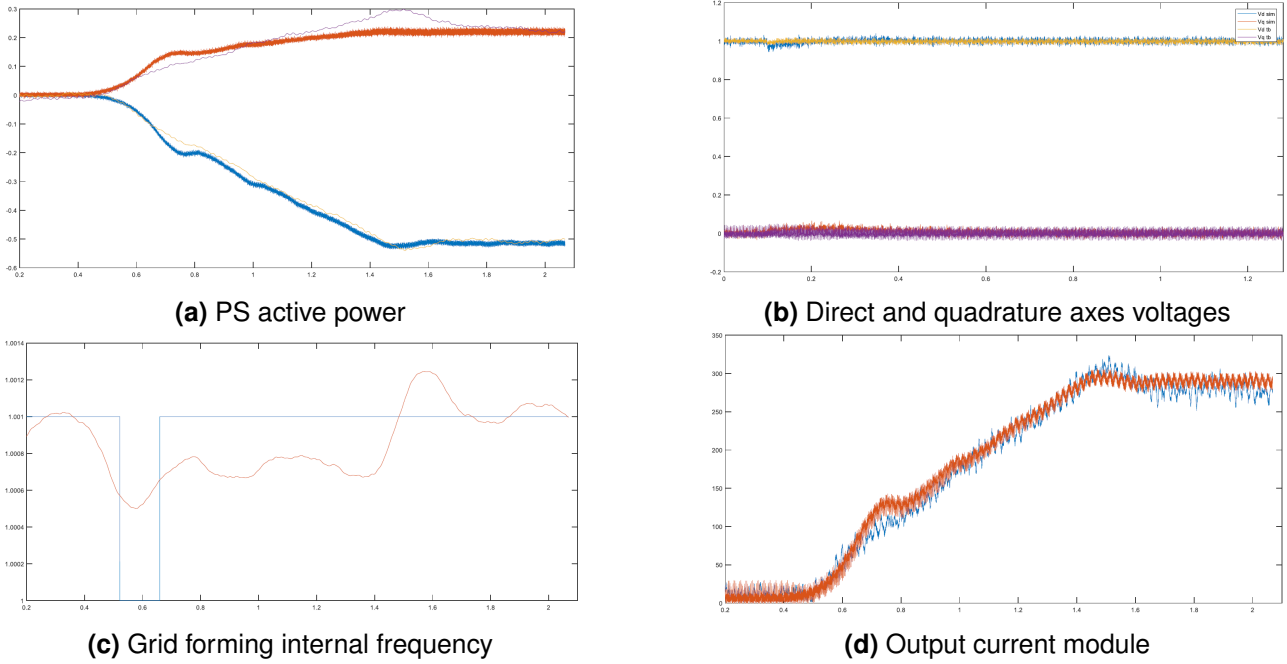


Figure F.27: Registered values at the CCU (converter control unit) and simulated internal control values for active power set point ramp variation.

F.3.9. DC side

Compared to the previous events, the DC side load sharing depends on more factors. A difference of the converter AC side is translated directly to the DC side and the final errors of the overlapped signals have the sum of both errors on AC and DC side. Furthermore, as the ESS have a SoC control, 3 different control systems are actuating on the DC side converters. The comparison by overlapping the control signals of both systems, simulation and real equipment, for an active power set point step variation and its effect on the DC side are shown in Fig. F.28a.

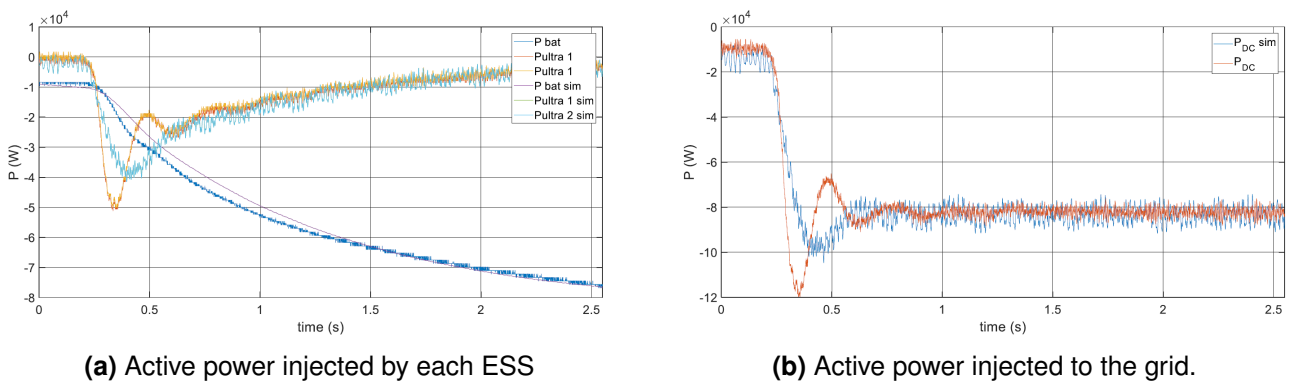
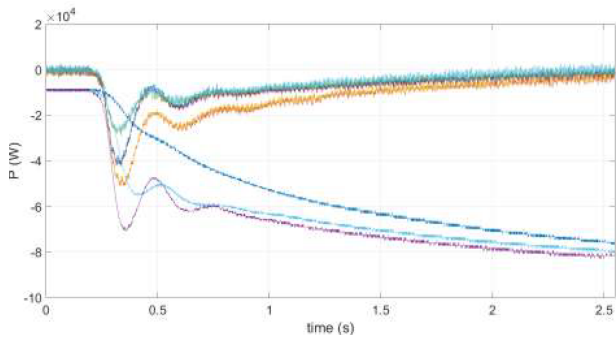


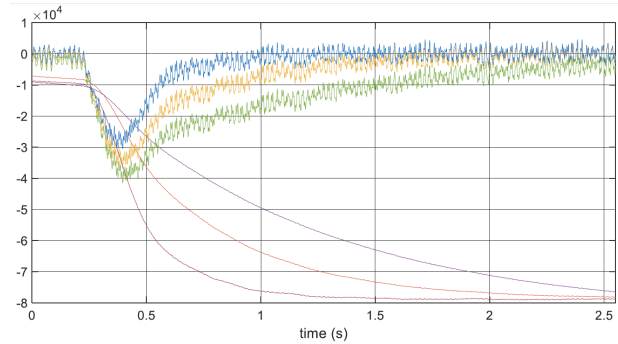
Figure F.28: DC side Registered values at the CCU (converter control unit) and simulated internal control values for active power set point.

The most important characteristic on the DC side is the load sharing between the energy storage systems. In Fig. F.28a a correct performance for the load sharing can be seen. The biggest difference between the simulation and FATs results is at the beginning of the step. The real equipment has a bigger overshoot and a more oscillated response. This error can be caused by the active power step response deviation at the AC side shown in Fig.F.28b.

At FATs besides the default configuration, two more ESS weighting configurations were also tested. The weighting is used to configure the Battery participation on events that require fast active power. The results recorded at FATs are shown in Fig. F.29. For the three configurations, the same performance and the same error (AC side overshoot related) can be seen.



(a) Registered values at the CCU (converter control unit)



(b) Simulation results

Figure F.29: Active power injected by each ESS for an active power step - Different weight factors.

G. RTE-Ingteam Demo incident: information and lessons learned

The RTE-Ingteam grid forming demonstrator associated to the OSMOSE WP3 project was delivered on site at the RTE substation in august 2020 and it was successfully connected to the RTE network in September 2020.

Unfortunately, on December 1st 2020, the container hosting the battery and supercapacitor modules of the hybrid energy storage system (HESS) went on fire and was completely destroyed. There were no injuries and no significant material damage. However, the experimentation could not be continued further as it was not possible to redesign, purchase the component and obtain authorization for a new installation within the year left of the project.

Besides the learnings about grid forming that could be gathered before the fire for the purpose of the OSMOSE project, this appendix aims at sharing information about the incident, with the hope to contribute to prevent similar events and improve system operators' and institutional response.

G.1. Course of events

After successfully performing Factory Acceptance Tests (FAT) in July 2020, the RTE/Ingteam demonstrator was installed in the Castelet substation according to the disposition showed in Fig. G.1 on August 18th 2020 and was supposed to run until the end of the OSMOSE project, initially planned for the end 2021 and extended to April 2022 due to the pandemic.

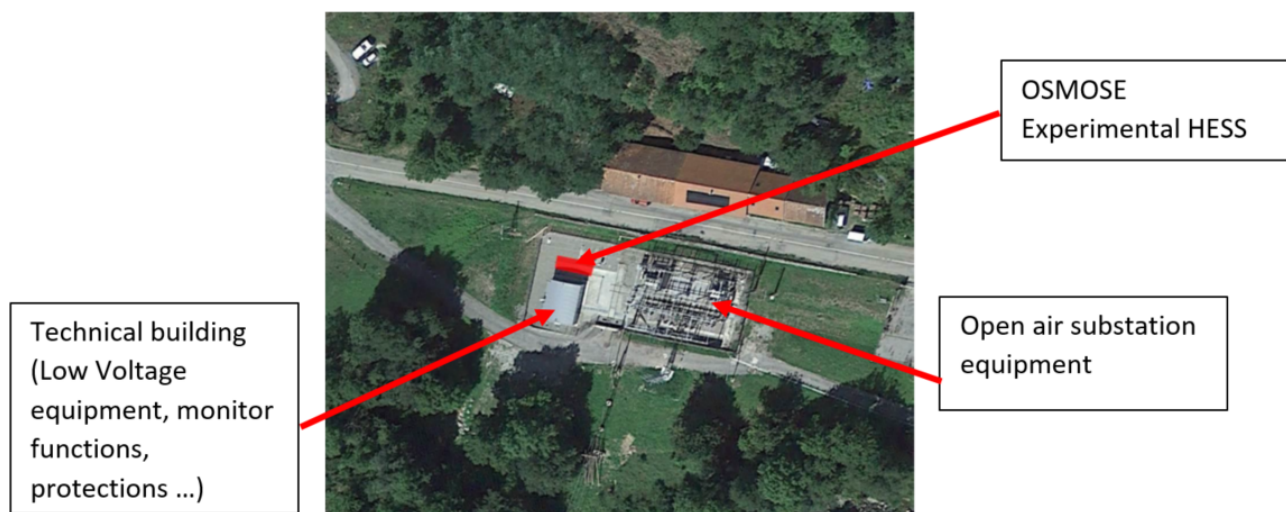


Figure G.1: Aerial view RTE Castelet substation

It was first connected to the grid on September 22th 2020 after performing subsystem tests which rely only on ancillary power, such as PCS energization (voltage and current mode), Ultracapacitors tests and Battery calibration tests, in order to proceed the full power Site Acceptance Tests (SAT). During all the tests carried out, the insulation of the batteries was monitored internally by their BMS. In addition to this, an insulation meter was installed to check the insulation of the system.

The 1st December 2020, during SATs, a fire occurred in the storage container leading to its full destruction. It is worth noticing that the lower container suffered limited damage (see Fig. G.2c)

The pre-fault conditions consisted in 2 racks connected to the battery bus, and the AC/DC converter normally operating on the supercapacitors. Table G.1 details further the event sequence before, during and after the event based in SCADA records.



Figure G.2: RTE–Ingteam demonstrator photos in the substation

Table G.1: Event log analysis

Hour	Nature of the operation
8:32	Connection of the storage system to the grid
8:39	Connection and load of supercapacitors
8:45	Start of the functional tests on supercapacitors
9:04:11	Connection order of DC-DC converter associated to the batteries. Failure notification of the battery racks connection to the DC bus.
9:04:24	Fire alarm and evacuation of the substation. RTE operators and firemen are contacted.
9:05:25	Opening of the 20kV breaker
9:48	Violent door opening of the upper container (that host the batteries), followed by heavy smoke and flames.
10:35	RTE switches the substation off-grid to allow firemen operation. 12h After analysis and preliminary measures, fire extinction operation start around 12h
18h	Flames are smothered by firemen
23h	A crane lifts down the upper container to allow complete access and water drenching by firemen.
01:30	on Dec. 2 The firemen declare the fire extinguished. A monitoring to check absence of re-ignition will be held 72 hours further.

G.2. Direct consequence and incident management

- Health and human safety concerns. First of all, the three people on site at the moment of the incident were completely unharmed. They were in the substation technical building next to container where the installation was remotely operated. They evacuated the premises following the fire alarm activation in order to place themselves within a safe distance according to safety and evacuation procedure.
- Operation of RTE substation and impact to consumers. In order to enable the safe operation of firefighters, RTE switched the substation off-grid at 10:35 until next day 15:10 (so for 28 hours and 40 minutes). No household was deprived from electricity, but a 2 MW hydro power plant remained disconnected and an industrial customer could only be partially supplied through an alternative distribution feeder until the substation was put back into service.

- **Fire control.** Fire extinction operation started around 12h, once the substation was put out of service, all equipment was grounded, the transformer oil pit was sealed to serve as polluted water collection system, and the local firefighters team (SDIS09, Service départemental d'incendie et de secours Ariège) prepared the manoeuvres. The cooling process started with water after opening the container back door as shown in Fig. 3 G.3a to limit the impact on the rest of the substation. The flames were mastered after 3 hours and dry chemical extinguishers were the privileged to stop the remaining combustion during the next 3 hours. Afterwards, around 6 pm, SDIS requested to lower the container. The procedure was initiated at 23:30 when a suitable crane was found available and arrived on site (see Fig. G.3b). Finally, the temperature was monitored for 72 h but it was already below 30° the next morning as showed in Tig. G.3c and did not reignite.

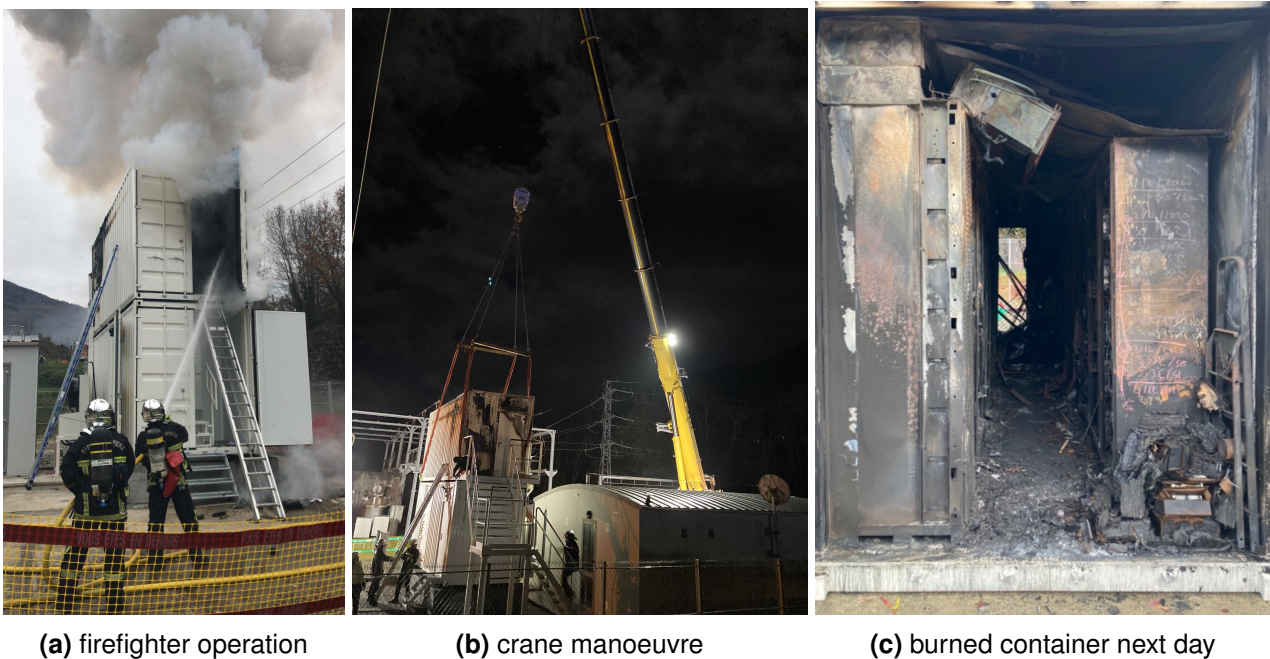


Figure G.3: Firefighter operation (left), crane manoeuvre (centre), burned container next day (right)

- **For the OSMOSE project.** Project deadline did not allow to redesign, replace and retest a new storage system. Therefore, this deliverable D3.3 does not include on-field and on-the-run measurement for grid-forming and multi-services connected to the RTE grid as initially planned. Resources for the last year of the WP3 were reduced. However, as demonstrated in this deliverable, results from Power Hardware in the Loop (PHIL) FAT are still concluding on grid forming control feasibility on commercial products. Finally, the independent EPFL demo remained unaffected and extended the duration and scope of the trials in order to secure relevant contributions of WP 3 to the OSMOSE project.

G.3. Subsequent actions

The local and national administrations initiated and followed up several actions, related to law, regulation and government bodies' missions.

- **Prefecture.** A decree was published by the local authority on December 3th requesting RTE to deploy a set of emergency actions including in particular : 1) prevent access to any person to the zone and, 2) monitor the temperature of the storage container within one day, 3) assessment

of the extent of any pollution by analysis soils, plants and extinction water samples collected within one week, 4) respond to the inquiries from the authorities 5) perform waste management according to polluted effluents regulation, as burnt batteries are considered as such.

- Work administration. RTE was also submitted to an investigation to verify compliance with labour regulations concerning employees and in particular the employer obligations in terms of prevention of occupational risks in the work place. No deficiencies were found.
- Environment, Risk and Regulation administration. These three administrations worked in cooperation as follows:
 1. DREAL (Direction Régionale et Interdépartementale de l'Environnement et de l'Energie) as the reference entity with respect to pollution risk provided support in the specification of the environmental studies and was in charge of their approval.
 2. BEA-RI (Bureau d'enquêtes et d'analyses sur les risques industriels) is the national authority in charge of conducting technical investigations following industrial accidents in order to improve safety and prevent risk through recommendations. Together with INERIS (Institut national de l'environnement industriel et des risques) they performed an independent audit.
 3. BEA-RI and INERIS will use their learnings for contribution to the improvement of regulation, in particular the regulation regarding the design, installation and operation of classified installations (ICPE, installation classée pour la protection de l'environnement) under the heading 2925-2, which was initially conceived for storage associated to electrical vehicle and might be submitted to different interpretation when applied to stationary equipment and does not consider fire risk.
 4. BEA-RI and INERIS will also share within the International Electrotechnic Commission (IEC) Technical Committee 120 for Electrical Energy Storage (EES) Systems.
- Environmental impact analyses were carried out upon the request expressed by the Prefecture. No specific contamination attributable to the BESS fire was identified.
- Disposal of the burn container. The remaining of the burnt BESS will be dismantled and recycled according to the regulation for environmentally dangerous materials. At the date when this document is issued, due mainly to the saturation of treatment capacities of the few industrial sites handling Li-Ion batteries residues, the BESS is still waiting in line for recycling.

G.4. Technical analysis

At the date when this document is issued, technical investigations and analyses are still ongoing, and no technical conclusion can be drawn yet.

We hereafter only share some facts assessed at date. A post-incident analysis of the converter Supervisory Control and Data Acquisition (SCADA) system recovered from the lower container showed that at 9h04min11s, the connection order of the DC-DC 1 (associated to the battery) failed. This last action is illustrated in Fig. G.4.

More precisely, at 9:04:11, the control and protection system of the DC-DC 1 converter measured a voltage at the battery side below the minimum battery voltage threshold and stops the connection order of the battery string to the DC bus. The DC-DC 1 contactor stays open accordingly during the whole event. Then a large current over 250 A (which is the highest value which can be measured by the sensors) is observed between the two battery racks. No power is exchanged between the battery and the DC-DC converter, which rules out the possibility of DC-AC (grid forming) controls, which are the main object of the experimentation, taking part in the origin of the incident.

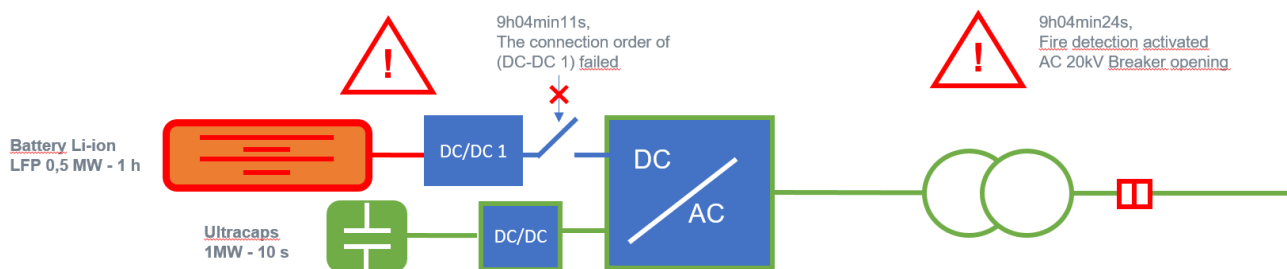


Figure G.4: Initial state of the system and last action before alarms triggering

Some seconds later, at 9h04min24s, the fire detection system was activated in the storage (upper) container, which starts a 1 minute countdown (safety delay) to trigger the extinction procedure (an aerosol released by the system) and command an emergency stop (opening of the 20kV breaker). At this time, several battery alarms are generated by the 2 battery racks (BMU fatal error, over discharge current alarm and under cell voltage alarm).

G.5. Some other learnings on BESS security as critical factor

BESS security is of major importance. Several BESS fire incidents have been reported worldwide and safety improvement regarding BESS fire system is an ongoing process. Authors hope that this fire incident faced during demonstrator Site Acceptance Tests will benefit for the BESS community to improve BESS safety and related standards.

While the technical investigation about origin is in the hand of specialists and while no conclusions have been drawn at the time when the present report is edited, it is nevertheless possible to issue some operational recommendations to either reduce the risk that a fire occurs, or to mitigate the effects in case the fire starts.

At the specification and design stage, special attention should be paid to i) the electrical protection within modules and to the speed of reaction of components and alarm and safeguarding systems; ii) assessing the performance of the fire extinguishing systems. This is in particular to prevent the risk of thermal runaway.

During the test phase, it is important to test all modules with full charge. If the storage system is connected to a network delivering other services during the test phase, make sure that it can be disconnected without nuisance to the other services at all test stages, including the possibility of fault.

For the onsite installation, do consider the specifics of battery system fires in view of accidents that have occurred. Considering your own specific environment, take into consideration: fire duration when the thermal runaway could not be contained; distances considering heat propagation; access for firefighters; possible environmental issues. All this is particularly true as regulation is not stable and is learning from each new case.

When all conclusions have been gathered, the French Agency for Industrial Risks will publish a final report. This report will contribute to the evolution of the regulation for storage batteries at French level. Findings will also be shared within the IEC International Electrotechnic Commission) Technical Committee 120 for Electrical Energy Storage (EES) Systems.

H. EPFL RTS model: Battery pack model parameters

The battery pack is simulated with a three-time-constant equivalent circuit model with SOC-dependant parameters, reported in Table H.1. The arrows in the table imply that the values vary linearly with the SoC in the indicated ranges. We use the model proposed in [124, 125] for a Lithium-Titanate-Oxide battery, assuming a 2s156p (¹) configuration of the battery packs (with identical parameters) feeding a single DC bus. The power converter is modelled in detail at the level of the switching devices.

Table H.1: Parameters of the BESS connected to the HV transmission grid

SOC[%]	10→30	30→50	50→70	70→90
E [V]	1184.4 → 1250.0	1250.0 → 1305.8	1305.8 → 1360.4	1360.4 → 1466.4
R_s [Ω]	0.052 → 0.042	0.042 → 0.030	0.030 → 0.028	0.028 → 0.026
R_1 [Ω]	0.190 → 0.150	0.150 → 0.180	0.180 → 0.158	0.158 → 0.398
C_1 [F]	4465.0 → 4904.5	4904.5 → 6998.0	6998.0 → 6000.0	6000.0 → 5617.0
R_2 [Ω]	0.080 → 0.018	0.018 → 0.018	0.018 → 0.018	0.018 → 0.020
C_2 [F]	454.50 → 1069.5	1069.5 → 1241.0	1241.0 → 1245.0	1245.0 → 1252.5
R_3 [Ω]	5.0e-3 → 9.8e-5	9.8e-5 → 4.8e-4	4.80e-4 → 13.6e-4	13.6e-4 → 12.0e-4
C_3 [F]	272.10 → 394.50	394.50 → 1479.8	1479.8 → 2250.0	2250.0 → 3088.7

¹Two battery packs in series, and 156 series in parallel.